Acoustical Physics, Vol. 49, No. 1, 2003, p. 1. Translated from Akusticheskiĭ Zhurnal, Vol. 49, No. 1, 2003, p. 5.

To the Readers of *Acoustical Physics*

Dear readers,

This issue is devoted to the memory of the eminent scientist and specialist in acoustics Leonid Mikhaĭlovich Lyamshev. His contribution to contemporary science can hardly be overestimated. He is the author of pioneering works that initiated several new fields of research: fractal acoustics, radiation acoustics, acoustics of elastic shells, etc. Today, these fields of research are rapidly progressing owing to the efforts of numerous scientists and engineers all over the world, including the former students of Professor Lyamshev.

The scientific and organizational activities of Lyamshev were varied: he headed a research department at the Acoustics Institute, chaired the Scientific Council on Acoustics of the Russian Academy of Sciences, and took part in the work of the International Commission on Acoustics and other international and Russian organizations. His work in *Akusticheskiĭ Zhurnal* (*Acoustical Physics*) was of special importance. Since 1963, he was Deputy Editor-in-Chief and since 1987, Editor-in-Chief of this journal. Under Lyamshev's supervision, *Akusticheskiĭ Zhurnal* (*Acoustical Physics*) has become one of the leading journals on acoustics in the worldwide scientific literature.

This issue of the journal contains the papers whose authors, from both Russia and other countries, work on the problems closely related to those investigated by Lyamshev. Some of these papers were even written on Lyamshev's initiative. The number of scientists who would like to present their papers—colleagues, successors, and students of Lyamshev—exceeds the limits of one issue. Therefore, the publication of papers devoted to the memory of Leonid Mikhaĭlovich Lyamshev will be continued in the second issue of *Acoustical Physics* of this year and, possibly, in the following issues as well.

F.V. Bunkin,
Deputy Editor-in-Chief

1063-7710/03/4901-0001$24.00

Acoustical Physics, Vol. 49, No. 1, 2003, pp. 10–18. Translated from Akusticheskiĭ Zhurnal, Vol. 49, No. 1, 2003, pp. 14–23.

Reciprocity in the Wave Reflection and Transmission Problem: Part 1. Symmetry of the Matrices of Reflection Coefficients

Yu. I. Bobrovnitskiĭ

Institute of Mechanical Engineering, Russian Academy of Sciences, Malyĭ Khariton'evskiĭ per. 4, Moscow, 101990 Russia
e-mail: bobrovni@orc.ru

Received March 28, 2002

Abstract—The reciprocity theorem in Lyamshev's formulation is used to derive a general symmetry relationship for the matrices of reflection coefficients in homogeneous media and one-dimensional waveguides. This relationship is shown to be equivalent to the normalization of the amplitudes by the cross power flux of the forward and backward waves. The relationship is valid for both propagating and evanescent waves, and all the symmetry relationships known from the literature represent its particular cases. © *2003 MAIK "Nauka/Interperiodica".*

In acoustics, the classical reciprocity principle states that the response remains unchanged when a point source and a receiver exchange places, which is equivalent to the symmetry of the Green's function with respect to the coordinates of the source and the observation point. Reciprocity is inherent in a wide class of linear media and structures and is often used in solving applied problems [1–3].

In this paper, we focus on the reciprocity in the problem of wave reflection and transmission (see also [4–7]). In this problem, the source is a wave incident on an obstacle and the response is represented by the reflected and transmitted waves. Reciprocity means that the reflection (transmission) coefficient remains unchanged when the incident and reflected (transmitted) waves exchange places. Mathematically, reciprocity is equivalent to the symmetry of the matrix of reflection and transmission coefficients about its principal diagonal.

It is known from the literature (see, e.g., [8]) that, in the general case, the reflection and transmission coefficients do not exhibit reciprocity. However, if the wave amplitudes are normalized by the time-averaged power flux (such a normalization means that the wave amplitude is considered as unity if the wave intensity normal to the boundary is unity), the reflection (transmission) becomes reciprocal [5, 8–12]. Unfortunately, this result is valid only for homogeneous waves, which propagate without attenuation. It is inapplicable to evanescent waves, which decay exponentially with increasing distance, because their power flux is identically equal to zero. Particular relationships between the symmetric reflection and transmission coefficients were derived for the evanescent waves in a few simple structures (a rod or a plate) [7, 10, 11]. However, no general reciprocity relationship was obtained.

This paper shows that, if a waveguide (a medium) and an obstacle exhibit reciprocity in its classical sense, reciprocity also takes place in the wave reflection and transmission problem. Below, we use the classical reciprocity theorem to derive a new symmetry relationship for the reflection coefficient, which generalizes all relationships known from the literature and is valid for both propagating and evanescent waves. The most significant result of this work is that this relationship is equivalent to the amplitude normalization by the alternating component of the cross power flux of the forward and backward waves rather than by the direct component of the power flux, as is common in the literature. In other words, if all the waves taken into account in the problem are normalized by the alternating component of the cross power flux, the complete matrix of reflection and transmission coefficients becomes symmetric. This alternating component is nonzero for waves of all types and, for a propagating wave, is equal to the direct component of its power flux.

Below, we derive and analyze the symmetry relationship for the wave reflection problem. We also establish a number of new properties of the wave matrices, on which the theory is based. The general wave reflection and transmission problem will be considered later, and general energy relationships for the waves (including evanescent waves) that take part in the process will be presented.

Consider the problem of wave reflection from an obstacle in a homogeneous continuous structure in which all the field quantities depend on one spatial coordinate x. Assume that, at each frequency ω, the structure can support $2n$ independent waves of the form

$$u(\pm k_j)\exp(\pm ik_j x - i\omega t), \tag{1}$$

where k_j is, in general, the complex propagation constant of the jth wave in the x direction;

$$u = [u_1, u_2, \ldots, u_n]^{\mathrm{T}} \tag{2}$$

1063-7710/03/4901-0010$24.00

is the n-dimensional vector of the generalized displacement in the cross section of the structure; $j = 1, 2, \ldots, n$; and the superscript "T" means transposition. Real propagation constants correspond to the propagating waves or waves homogeneous in x. The imaginary and complex k_j refer to the evanescent waves. Half of waves (1) that have the plus sign before k_j are the forward waves; i.e., they propagate or decay in the positive x direction. The remaining n waves (with the minus sign) are the backward waves; i.e., they propagate or decay in the negative x direction.

The term *structure* primarily refers in this paper to one-dimensional solid and fluid waveguides, in which, unlike two-dimensional and three-dimensional waveguides, a finite number of modes can exist. A typical example of such a waveguide is a thin straight rod. It allows the propagation of $n = 6$ waves of form (1): a longitudinal wave, a torsional wave, and two flexural waves in each of the two orthogonal planes [13], while the components of the vector u are the displacements along the three orthogonal axes and the rotation angles about them. In the general case, the number of independent waves in a one-dimensional waveguide is equal to the number of degrees of freedom in its cross section [14].

The structures of interest also include uniform three-dimensional media if the waves are plane and are reflected from uniform planar boundaries. In this case, the projection of all reflected waves on the boundary is fixed, because it is dictated by the incident wave (Snell's law [8]) and the reflection problem is actually one-dimensional: all the field quantities depend on only the x coordinate, which is perpendicular to the boundary. The number of waves (1) is limited and equal to the number of different types of plane waves in this medium. For instance, in a fluid or gaseous medium, it is only the longitudinal wave ($n = 1$). In an elastic medium, two wave types exist: the longitudinal wave and the shear wave ($n = 2$). In porous media, composite materials, and microstructured media, the number of waves can be equal to three or more [15].

The theory reported below also covers homogeneous two-dimensional media in which waves with a linear front are reflected from uniform linear obstacles. In this case, the trace of the waves on the linear boundary is also given, and the problem is one-dimensional with the number n of waves (1) being equal to the number of plane waves in the medium. For example, in a thin uniform plate, there are four waves: two flexural waves (one propagating and one evanescent) and the longitudinal and shear waves, which propagate across the plate without attenuation [13].

Let one of the above structures occupy the negative x region and its right boundary $x = 0$ be connected with the obstacle z (Fig. 1). Assume that the interval $[-l, 0]$ of the structure, adjacent to the obstacle, is free from the external action and n forward (incident on the obstacle) waves (1) with the complex displacement amplitudes $a_1, \ldots, a_n$ and n backward (reflected from the obstacle) waves (1) with the complex displacement amplitudes $b_1, \ldots, b_n$ are excited in it. The amplitudes of the reflected waves are uniquely determined by the amplitudes of the incident waves and by the parameters of the structure and obstacle. This relationship is commonly written in matrix form as

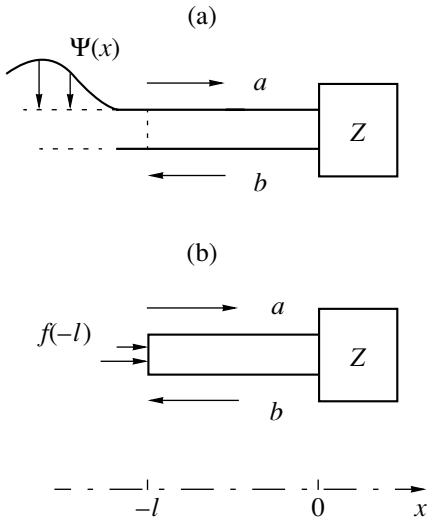

Fig. 1. Homogeneous structure (waveguide) with the obstacle Z at its end $x = 0$: (a) incident waves with the amplitudes a excited by the external load $\Psi(x)$ are reflected from the obstacle with the amplitudes b; (b) the same incident and reflected waves excited by the force $f(-l)$ applied at the cross section $x = -l$.

$$b = Ra, \tag{3}$$

where a and b are the amplitudes of the incident and reflected waves written as the n-dimensional vectors

$$a = [a_1, \ldots, a_n]^{\mathrm{T}}, \quad b = [b_1, \ldots, b_n]^{\mathrm{T}}, \tag{4}$$

and R is the $n \times n$ matrix of reflection coefficients. An element R_{jm} of this matrix is equal to the displacement amplitude of the jth reflected wave when a unit-amplitude mth wave is incident on the obstacle.

The problem is to calculate the matrix of reflection coefficients and establish a symmetry relationship between its symmetrically positioned elements R_{jm} and R_{mj} or, what is the same, the relationship of matrix R to its transposed matrix R^{T}.

Following [13, 16], consider the wave matrices, which describe the main characteristics of the medium that are necessary for solving the reflection problem. Since the cross section of the structure that supports n types of waves has n degrees of freedom [14], its vibrations are characterized not only by n generalized displacements (2), but also by n generalized forces $f = [f_1, f_2, \ldots, f_n]^{\mathrm{T}}$ associated with them. Each of the n forward (incident) waves, say, the one with the number m, has its individual cross-sectional mode of vibration charac-

terized by n-dimensional generalized displacement and force vectors

$$u^{(m)} = [u_1^{(m)}, \ldots, u_n^{(m)}]^{\mathrm{T}}, \quad f^{(m)} = [f_1^{(m)}, \ldots, f_n^{(m)}]^{\mathrm{T}}, \quad (5)$$

this mode of vibration being independent of the longitudinal coordinate x; $m = 1, \ldots, n$. Let us use column vectors (5) to construct two $n \times n$ matrices: the displacement matrix D_{i} and the force matrix F_{i},

$$D_{\mathrm{i}} = [u^{(1)}, \ldots, u^{(n)}], \quad F_{\mathrm{i}} = [f^{(1)}, \ldots, f^{(n)}]. \quad (6)$$

Let us also construct two similar matrices D_{r} and F_{r} of vectors (5) that refer to the backward (reflected) waves. Clearly, matrices D_{r} and F_{r} can be obtained from matrices D_{i} and F_{i} by changing the sign of all propagation constants.

The x dependence of the displacement and force in the normal wave is determined by its amplitude, which is an exponential function of x according to Eq. (1). If the amplitudes of the incident and reflected waves in Eqs. (4) refer to the cross section $x = 0$, then, in an arbitrary cross section x, they can be written in matrix form as

$$a(x) = \Phi_{\mathrm{i}}(x)a, \quad b(x) = \Phi_{\mathrm{r}}(x)b, \quad (7)$$

where the amplitude matrices

$$\begin{aligned} \Phi_{\mathrm{i}}(x) &= \mathrm{diag}[\exp(ik_1x), \ldots, \exp(ik_nx)], \\ \Phi_{\mathrm{r}}(x) &= \mathrm{diag}[\exp(-ik_1x), \ldots, \exp(-ik_nx)] \end{aligned} \quad (8)$$

determine the phase advance and the amplitude decay within the interval $[0, x]$.

Using matrices (6) and (8) and amplitudes (7), in the most general case when all incident and reflected waves are present, the displacement and stress (force) in any cross section of the structure can be written in the following compact form:

$$\begin{aligned} u(x) &= D_{\mathrm{i}}a(x) + D_{\mathrm{r}}b(x) = D_{\mathrm{i}}\Phi_{\mathrm{i}}(x)a + D_{\mathrm{r}}\Phi_{\mathrm{r}}(x)b, \\ f(x) &= F_{\mathrm{i}}a(x) + F_{\mathrm{r}}b(x) = F_{\mathrm{i}}\Phi_{\mathrm{i}}(x)a + F_{\mathrm{r}}\Phi_{\mathrm{r}}(x)b. \end{aligned} \quad (9)$$

These relationships completely describe an arbitrary harmonic motion of the structure and are the starting point for the further analysis. They contain six $n \times n$ matrices, which we will refer to as the *wave matrices*. The latter completely characterize the structure as a carrier of the wave field. The elements of the wave matrices are complex-valued and depend on the frequency and the parameters of the structure, in particular, on the propagation constants k_j.

As an example, let us calculate the wave matrices for a thin homogeneous beam that experiences flexural vibrations. The general solution to the Bernoulli–Euler equation [13] $Bd^4w(x)/dx^4 - \rho\omega^2 Aw(x) = 0$ for the transverse displacement w can be written as

$$w(x) = a_1e^{ikx} + a_2e^{-kx} + b_1e^{-ikx} + b_2e^{kx}, \quad (10)$$

where the propagation constants of the two normal waves are $k_1 = k$ and $k_2 = ik$; $k^4 = \rho\omega^2 A/B$, ρ is the density of the material, A is the cross section area, and B is the flexural stiffness of the beam. We calculate the generalized displacements $u_1(x) = w(x)$ and $u_2(x) = -w'(x)$ and the generalized forces associated with them, the shear force $f_1(x) = Bw'''(x)$ and bending moment $f_2(x) = Bw''(x)$, from Eq. (10). Then, after reducing the results to the form of Eqs. (9), it can easily be shown that the wave matrices for the forward waves are

$$\begin{aligned} D_{\mathrm{i}} &= \begin{bmatrix} 1 & 1 \\ -ik & k \end{bmatrix}, \quad F_{\mathrm{i}} = -Bk^2 \begin{bmatrix} ik & k \\ 1 & -1 \end{bmatrix}, \\ \Phi_{\mathrm{i}}(x) &= \begin{bmatrix} e^{ikx} & 0 \\ 0 & e^{-kx} \end{bmatrix}, \end{aligned} \quad (11)$$

while, for the backward waves, they can be obtained by replacing k with $-k$; $a = [a_1, a_2]^{\mathrm{T}}$ and $b = [b_1, b_2]^{\mathrm{T}}$.

Now, we present some general properties of the wave matrices, which will be necessary below. These properties were never considered in the literature. First of all, note that the wave matrices are nonsingular. For diagonal amplitude matrices (8), this property is evident. For the displacement matrices D_{i} and D_{r} and the force matrices F_{i} and F_{r}, this property is a consequence of the fact that their columns, which are the eigenvectors of a certain normal matrix [14], are linearly independent [see Eqs. (5) and (6)]. The nonsingularity means, in particular, that all the wave matrices have inverse ones. The following evident equalities are also valid for amplitude matrices (8):

$$\Phi_{\mathrm{r}}(x) = \Phi_{\mathrm{i}}^{-1}(x), \quad \Phi_{\mathrm{i}}(0) = \Phi_{\mathrm{r}}(0) = I, \quad (12)$$

where I is an $n \times n$ identity matrix.

In deriving the symmetry relationships, the following *power matrices*, which determine various power characteristics of the wave field in the structure, are of importance:

$$P_{\mathrm{i}} = D_{\mathrm{i}}^* F_{\mathrm{i}}, \quad P_{\mathrm{r}} = D_{\mathrm{r}}^* F_{\mathrm{r}}, \quad (13)$$

$$S_{\mathrm{i}} = D_{\mathrm{i}}^{\mathrm{T}} F_{\mathrm{i}}, \quad S_{\mathrm{r}} = D_{\mathrm{r}}^{\mathrm{T}} F_{\mathrm{r}}, \quad (14)$$

$$S = \frac{1}{2}(D_{\mathrm{i}}^{\mathrm{T}} F_{\mathrm{r}} - F_{\mathrm{i}}^{\mathrm{T}} D_{\mathrm{r}}), \quad Q = D_{\mathrm{i}}^{\mathrm{T}} F_{\mathrm{r}}, \quad (15)$$

where the asterisk symbol means Hermitian conjugation. Matrices (13) represent the time-average power fluxes of the forward and backward waves. For instance,

$$W_{\mathrm{i}}^{=} = \frac{i\omega}{2} a^* P_{\mathrm{i}} a$$

is the time-independent complex-valued power flux of the incident waves. Matrices (14) represent the alternating component of the instantaneous power flux (see Appendix 1 for details). Matrices (15) are closely con-

nected with the alternating component of the cross power flux.

Matrices (13)–(15) satisfy the following relationships:

$$P_i + P_r = 0, \quad S_i + S_r = 0, \tag{16}$$

$$S_i^T = S_i, \quad S_r^T = S_r, \tag{17}$$

$$S = \frac{1}{2}(Q + Q^T) = \mathrm{diag}[Q_{11}, Q_{22}, \ldots, Q_{nn}]. \tag{18}$$

Relationships (16) mean that, for the direct, as well as for the alternating component, the power fluxes of the forward and backward waves have equal magnitudes and opposite signs. Relationships (17) express the symmetry property of the power matrices. Relationship (18) means that the matrix S of Eqs. (15) is diagonal. A rigorous proof of relationships (16)–(18) is given in Appendix 2, where properties (17) and (18) are also shown to follow from the classical reciprocity theorem.

To obtain a general solution to the wave reflection problem, the obstacle and the waveguide must be described in the same terms. Since the obstacle is acted upon by n generalized forces $g = [g_1, \ldots, g_n]^T$ from the side of the waveguide and the response is represented by n generalized displacements (2), it is most natural to characterize the motion of the obstacle by its $n \times n$ matrix Z of input impedances with respect to the interaction forces or by its $n \times n$ input admittance matrix Y, which are defined as

$$g = Zu, \quad u = Yg. \tag{19}$$

Matrices Z and Y are complex valued and symmetric. Their symmetry is a consequence of the reciprocity theorem, which is assumed to be also valid for the obstacle. (Strictly speaking, equalities (19) define the dynamic stiffness and compliance matrices, which differ from the impedance and admittance matrices in the factor $-i\omega$. In the framework of this paper, this difference is of no importance.)

Consider now a structure with an obstacle at its end $x = 0$ (Fig. 1). Let g and $f(-0)$ be the generalized force vectors that act upon the obstacle and structure, respectively, and u and $u(0)$ be the corresponding generalized displacements at $x = 0$. Then, we use the condition of rigid connection between the obstacle and the structure

$$g + f(-0) = 0, \quad u = u(0) \tag{20}$$

and substitute relationships (9) and (19) into them. After some algebra, we obtain the following expression for the $n \times n$ reflection coefficient matrix (3):

$$R = -(F_r - ZD_r)^{-1}(F_i - ZD_i). \tag{21}$$

If, instead of the impedance matrix Z, we use the admittance matrix Y, then, instead of Eq. (21), we obtain the formula

$$R = -(YF_r - D_r)^{-1}(YF_i - D_i). \tag{22}$$

The matrix R relates the amplitudes a of the incident waves to the amplitudes b of the reflected waves in the cross section $x = 0$. It depends on the physical and geometrical parameters of the structure (to be more precise, on its wave matrices) and on the input impedance matrix Z or input admittance matrix Y of the obstacle.

Consider several particular cases of formulas (21) and (22).

Free end. The reflection coefficient matrix for the free end of the structure is obtained from Eq. (21) with the impedance matrix of the obstacle being set equal to the zero matrix:

$$R_0 = -F_r^{-1} F_i. \tag{23}$$

Fixed end. The reflection coefficient matrix for the fixed end of the structure is

$$R_\infty = -D_r^{-1} D_i. \tag{24}$$

It can be obtained from Eq. (22) by setting the admittance matrix Y equal to the zero matrix.

Transparent obstacle. All the reflection coefficients are zero (R is the zero matrix) if the obstacle's impedance matrix is

$$Z = Z_i = F_i D_i^{-1}. \tag{25}$$

Matrix Z_i is the *matrix of characteristic impedances* of the structure. It is equal to the matrix of input impedances in the cross section $x = 0$ of the semi-infinite structure that occupies the region $x \geq 0$. [Indeed, in this case, we have $f(0) = F_i a$ and $u(0) = D_i a$. Eliminating a from these expressions yields $f(0) = F_i D_i^{-1} u(0)$.] Note that the input impedance matrix for a semi-infinite structure that occupies the region $0 \geq x$ is $Z_r = -F_r D_r^{-1}$. It differs from Z_i in the sign of some off-diagonal elements. In terms of the characteristic impedance matrices Z_i and Z_r, formula (21) can be written as

$$R = D_r^{-1}(Z_r + Z)^{-1}(Z_i - Z)D_i. \tag{26}$$

Similarly, if admittances are used instead of impedances, we have

$$R = F_r^{-1}(Y_r + Y)^{-1}(Y_i - Y)F_i, \tag{27}$$

where $Y_i = Z_i^{-1}$ and $Y_r = Z_r^{-1}$. Matrix expressions (21), (22), (26), and (27) for the reflection coefficients extend the familiar Fresnel formulas [8] to waveguides and media with several normal modes. Some of these formulas can be found in the literature, e.g., in [13].

To derive the symmetry relationship for the reflection coefficient matrix R, we use the classical reciprocity theory [2]. To this end, consider the region $[-l, 0]$ of the waveguide, which is free from external actions, and replace the action of the region $x < -l$ with the generalized reaction force $f(-l)$, which is applied to the cross section $x = -l$ as shown in Fig. 1b. This force creates the

same set of forward and backward waves in the region under consideration as that created by the external action $\Psi(x)$ in the original structure (Fig. 1a). With Eqs. (3) and (9), the forces and displacements in the $x = -l$ cross section can be written as

$$\begin{aligned} u(-l) &= [D_i\Phi_i(-l) + D_r\Phi_r(-l)R]a, \\ f(-l) &= [F_i\Phi_i(-l) + F_r\Phi_r(-l)R]a. \end{aligned} \tag{28}$$

Let there be two different sets of incident wave amplitudes $a^{(1)}$ and $a^{(2)}$ and the corresponding force and displacement vectors (28): $f^{(1)}(-l)$, $u^{(1)}(-l)$ and $f^{(2)}(-l)$, and $u^{(2)}(-l)$. Then, according to the classical reciprocity theorem, the following equality is valid:

$$[f^{(1)}(-l)]^T u^{(2)}(-l) - [u^{(1)}(-l)]^T f^{(2)}(-l) = 0. \tag{29}$$

Substitution of Eqs. (28) into Eq. (29) after some algebra yields

$$[a^{(1)}]^T[\Phi_i(-l)(S_i - S_i^T)\Phi_i(-l)$$

$$+ R^T\Phi_r(-l)(S_r - S_r^T)\Phi_r(-l)R + 2\Phi_i(-l)S\Phi_r(-l)R$$

$$- 2R^T\Phi_r(-l)S^T\Phi_i(-l)]a^{(2)} = 0,$$

where the power matrices S_i, S_r, and S are defined by formulas (13)–(15). Using the fact that the matrices S_i and S_r are symmetric and that the matrix S is diagonal [see Eqs. (17) and (18)], as well as the relationship $\Phi_i(-l)S\Phi_r(-l) = S$, which can easily be proved, the above equality can be reduced to

$$[a^{(1)}]^T(SR - R^TS^T)a^{(2)} = 0.$$

Since the amplitudes of the incident waves are arbitrary, this relationship means that the SR matrix is symmetric:

$$SR = (SR)^T. \tag{30}$$

This is the desired symmetry relationship: the reflection coefficient matrix R defined in terms of the displacement amplitudes, being originally nonsymmetric ($R^T \neq R$), becomes symmetric after being premultiplied by the matrix $S = (D_i^T F_r - F_i^T D_r)/2$. The matrix S depends only on the waveguide (medium) parameters, and it is nonsingular $|S| \neq 0$ and diagonal.

Property (30) can be written as a relationship between the symmetric elements of the matrix R:

$$S_{jj}R_{jm} = S_{mm}R_{mj}, \tag{31}$$

where S_{jj} and S_{mm} are the jth and mth diagonal elements of the matrix S, $j \neq m$.

We can also show that symmetry property (30), (31) is equivalent to a certain normalization of the normal wave amplitudes. Indeed, if, instead of the displacement amplitudes a and b, we use the amplitudes α and β defined as

$$a = S^{-1/2}\alpha, \quad b = S^{-1/2}\beta, \tag{32}$$

the reflection coefficient matrix R_1 that relates the new amplitudes is symmetric. By substituting Eqs. (32) into Eq. (3), we obtain

$$\beta = R_1\alpha, \quad R_1 = S^{1/2}RS^{-1/2}. \tag{33}$$

The matrix R_1 can be represented as

$$R_1 = S^{1/2}RS^{-1/2} = S^{-1/2}(SR)S^{-1/2}.$$

Since the normalization matrix $S^{1/2}$ is a diagonal matrix and, therefore, symmetric, the symmetry of the new reflection coefficient matrix becomes evident, $R_1^T = R_1$. Thus, if the displacement amplitudes of the normal waves are normalized by the elements of the diagonal matrix $S^{1/2}$, the reflection becomes reciprocal (symmetric): the amplitude β_m of the mth reflected wave produced by the jth unit wave ($\alpha_j = 1$) incident on an obstacle is equal to the amplitude β_j of the jth reflected wave produced by the mth unit wave ($\alpha_m = 1$) incident on the obstacle. Note that this property is valid for all types of waves, both propagating and evanescent.

Consider the physical meaning of this symmetry relationship. As can be seen from Eq. (18), the matrix S is composed of diagonal elements of the matrix $Q = D_i^T F_r$. According to formula (A5) of Appendix 1, its mth element $S_{mm} = Q_{mm}$ gives the alternating component of the cross power flux of the mth forward and backward normal waves: if a_m and b_m are the displacement amplitudes of these waves, the quantity

$$-\frac{i\omega}{2}S_{mm}a_mb_m = -\frac{i\omega}{2}(u_i)_m(f_r)_m \tag{34}$$

is the complex amplitude of the alternating component of the work done by the generalized force $(f_r)_m$ of the mth backward wave over the displacement $(u_i)_m$ of the mth forward wave per unit time. Let $\tilde{W}_{im}$ be the quantity given by Eq. (34) and calculated for the forward normal wave at $b_m = a_m$, and $\tilde{W}_{rm}$ be the quantity of Eq. (34) calculated for the backward wave at $a_m = b_m$. Then, if, instead of the displacement amplitudes a_m and b_m, we use the power amplitudes

$$\begin{aligned} \alpha_m &= (\tilde{W}_{im})^{1/2} = (-i\omega S_{mm}/2)^{1/2}a_m, \\ \beta_m &= (\tilde{W}_{rm})^{1/2} = (-i\omega S_{mm}/2)^{1/2}b_m, \end{aligned} \tag{35}$$

which differ from those of Eqs. (32) in the constant factor $(-i\omega/2)^{1/2}$, the physical meaning of symmetry relationships (30)–(33) becomes quite clear: for the reflection coefficient matrix to be symmetric, the amplitudes of the normal waves must be defined as square roots of the alternating components of the cross power fluxes.

Let us show that, for a homogeneous wave with a real propagation constant k_m, alternating component (34) of the cross power flux is equal to the direct component of the power flux of the mth wave. Indeed,

according to property (A6) of the force matrix F_r (see Appendix 2), the force $(f_r)_m$ in the mth backward wave with a real amplitude is equal to the complex conjugate of the force $(f_i)_m$ in the mth forward wave, which shows that the quantity of Eq. (34) is equal to the time-average complex power flux of the mth forward wave. For the propagating waves, the normalization defined by formulas (32) and (35) is thus equivalent to the power normalization known from the literature.

The power flux of an evanescent wave is zero. However, the cross power fluxes of the forward and backward waves are nonzero [17]. Therefore, normalization of Eqs. (32), (35) by the cross fluxes is presumably the only normalization leading to symmetric reflection coefficient matrices that exhibit reciprocity for waveguides and media with normal waves of any type. Also note that the relationships between symmetric reflection coefficients for evanescent waves in some particular waveguides and media described in the literature [7–12] follow from the normalization to the cross power flux as particular cases.

Consider two simple examples that illustrate the symmetry relationship obtained above. Let us begin with the Bernoulli–Euler beam, which supports two normal waves: one propagating wave and one evanescent wave. The wave matrices for this waveguide are given by formulas (11). They can be used to calculate the power matrices, the characteristic impedance matrices, and the reflection coefficient matrices. In particular, the diagonal matrix of Eqs. (15) has the following nonzero elements:

$$S_{11} = 2iBk^3, \quad S_{22} = 2Bk^3. \tag{36}$$

Symmetry relationship (31) for the reflection coefficient matrix takes the form

$$R_{21} = R_{12}(S_{11}/S_{22}) = iR_{12}, \tag{37}$$

which coincides with the result reported in [7]. For example, for the free and fixed ends, the reflection coefficient matrices calculated from Eqs. (23) and (24) are

$$R_0 = \begin{bmatrix} i & 1-i \\ 1+i & -i \end{bmatrix}, \quad R_\infty = \begin{bmatrix} i & -1+i \\ -1-i & -i \end{bmatrix}.$$

It can easily be shown that these matrices satisfy relationship (37). The validity of the latter was directly (analytically) verified by the author of this paper for the case of reflection from an obstacle with an arbitrary symmetric impedance matrix Z. The complex amplitudes of the alternating component of the cross power flux of Eq. (34) are in this case equal to (they differ from Eq. (36) in the factor $-i\omega/2$)

$$W_1^{\sim} = Bk^3\omega a_1^2, \quad W_2^{\sim} = -iBk^3\omega a_2^2. \tag{38}$$

For the propagating wave, $W^{\sim}$ is real (if a_1 is real) and is equal to the time-average power flux of this wave. For the evanescent wave, its own power flux is identically zero. The cross flux is however a nonzero, purely imaginary quantity, as can be seen from Eqs. (38).

Consider now an example of the wave reflection in a two-dimensional structure, namely, in a semi-infinite ($x < 0$) uniform plate with a linear boundary $x = 0$. Assume that the plate has a small wave thickness h, so that its flexural vibrations comply with the classical Germin–Lagrange equation [13]; $\Delta^2 w(x, y) - k_0^4 w(x, y) = 0$, where $k_0 = (\rho\omega^2/D)^{1/4}$ is the wavelength, D is the flexural stiffness, ρ is the density, and Δ is the two-dimensional Laplacian operator. Let two incident flexural waves with the amplitudes a_1 and a_2 be excited (for example, by external forces applied at a certain distance from the boundary $x = 0$) in the plate, whose trace on the boundary $x = 0$ is an exponential function $\exp(iky)$ with a given y component k of the wave vector. Two flexural waves with the amplitudes b_1 and b_2 are reflected from the boundary, and these waves have the same trace on the boundary due to Snell's law. The total transverse displacement field of the plate can be represented as the superposition of displacements of all these waves:

$$\begin{aligned} w(x, y) = [&a_1\exp(ik_1x) + a_2\exp(ik_2x) \\ &+ b_1\exp(-ik_1x) + b_2\exp(-ik_2x)]e^{iky}, \end{aligned} \tag{39}$$

where the complex-valued x components of the propagation constants

$$k_1^2 = k_0^2 - k^2, \quad k_2^2 = -k_0^2 - k^2 \tag{40}$$

are obtained after substituting Eq. (39) into the Germin–Lagrange equation. Choosing the coordinates of the vector u as the displacement $u_1 = w$ and the rotation angle $u_2 = -\partial w/\partial x$ and taking the coordinates of the vector f as the shear force $f_1 = D[\partial^3 w/\partial x^3 + (2 - \nu)\partial^3 w/\partial x\partial y^2]$ and bending moment $f_2 = D(\partial^2 w/\partial x^2 + \nu\partial^2 w/\partial y^2)$, where ν is Poisson's ratio, we represent these vectors in the form of Eq. (9) to obtain the following expressions for the wave matrices:

$$D_i = \begin{bmatrix} 1 & 1 \\ -ik_1 & -ik_2 \end{bmatrix}, \quad F_i = D\begin{bmatrix} -ik_1p_1 & ik_2p_2 \\ -p_2 & p_1 \end{bmatrix}. \tag{41}$$

Here, $p_1 = k_0^2 + k^2(1 - \nu)$ and $p_2 = k_0^2 - k^2(1 - \nu)$. The diagonal elements of the matrix of Eqs. (15) calculated from Eqs. (41) are

$$S_{11} = i2Dk_0^2k_1, \quad S_{22} = -i2Dk_0^2k_2. \tag{42}$$

Therefore, symmetry relationship (31) for an arbitrary obstacle placed on the plate on the line $x = 0$ can be written as

$$R_{21} = R_{12}(S_{11}/S_{22}) = R_{12}(-k_1/k_2), \tag{43}$$

where $k_{1,2}$ are given by Eqs. (40). For the normal incidence on the boundary ($k = 0$), we have $k_1 = k_0$ and $k_2 =$

ik_0, and relationship (43) coincides with symmetry relationship (37) for the beam. According to Eq. (34), the quantities of Eqs. (42) multiplied by $-i\omega/2$ are equal to the complex amplitude of the alternating component of the cross power flux. If the trace of the incident waves is characterized by a real ($k < k_0$) or purely imaginary k, the first flexural wave in the plate is homogeneous and the quantity $-i\omega S_{11}/2$ is its real positive power flux in the x direction. For an arbitrary trace of the incident waves (complex-valued k), all waves, both incident and reflected, are inhomogeneous, and quantities (42) and, consequently, the cross power fluxes are complex valued.

APPENDIX 1. INSTANTANEOUS POWER FLUX AND ITS COMPONENTS

All calculations in this paper are performed for time-harmonic signals using the complex representation. Actual signals are always real valued. Therefore, to reveal the physical meaning of second-degree complex quantities, for instance, of a product of the complex amplitudes of the displacement and force, one should know the relationships between the real and complex representations of the corresponding functions. Below, we present the relationships used in this paper [18].

Let

$$\begin{aligned} u(t) &= u_c\cos(\omega t) + u_s\sin(\omega t), \\ f(t) &= f_c\cos(\omega t) + f_s\sin(\omega t) \end{aligned} \tag{A1}$$

be n-dimensional displacement and force vectors of Eqs. (2) and (5) written as real functions of time, where the components of the vectors $u_{c,s}$ and $f_{c,s}$ are real. The complex representation of signals (A1) has the form

$$u(t) = \mathrm{Re}(ue^{-i\omega t}), \quad f(t) = \mathrm{Re}(fe^{-i\omega t}),$$

where

$$u = u_c + iu_s, \quad f = f_c + if_s \tag{A2}$$

are the n-dimensional vectors of complex amplitudes. The instantaneous flux of the oscillatory power through the waveguide cross section is defined as

$$\begin{aligned} W(t) &= f(t)du(t)/dt \\ &= W_0 + W_c\cos(2\omega t) + W_s\sin(2\omega t), \end{aligned} \tag{A3}$$

where W_0 is the direct (i.e., time-average) flux component and $W^{\sim} = W_c + iW_s$ is the complex amplitude of the alternating power flux component with the frequency 2ω. By direct calculations, one can verify that the following relationships are valid:

$$W_0 = \mathrm{Re}\left(\frac{i\omega}{2}u^* f\right), \tag{A4}$$

$$W^{\sim} = -\frac{i\omega}{2}u^{\mathrm{T}} f. \tag{A5}$$

By replacing the vectors u and f with their representations in terms of the wave matrices [see Eqs. (9)], we obtain that the direct power flux component of Eq. (A4) can be expressed in terms of the power matrix of Eqs. (13); alternating component (A5), in terms of the matrix of Eqs. (14); and the matrix of Eqs. (15) determines the alternating component of the cross power flux [see also Eq. (34)].

APPENDIX 2. PROPERTIES OF THE POWER MATRICES

Below, we derive relationships (16)–(18) for power matrices (13)–(15).

To prove relationships (16), we first consider the wave matrices as a function of propagation constants k_j of the normal waves. Let $j_1, j_2, \ldots, j_m$ be the ordinal numbers of those components of the generalized displacement vector of Eqs. (2), (5) that are odd functions of k_j, i.e., change their sign when the signs of all propagation constants are changed. Conversely, since the displacement and force are interrelated quantities and their product is proportional to the power flux, which is an odd function of k_j, the force components with ordinal numbers $j_1, j_2, \ldots, j_m$ are even functions and the remaining components are odd functions of k_j. Let us introduce two diagonal matrices of order n: the matrix J_d, whose diagonal elements with the numbers $j_1, j_2, \ldots, j_m$ are equal to –1 and other elements are equal to unity, and the matrix J_f, whose diagonal elements with the numbers $j_1, j_2, \ldots, j_m$ are equal to unity and other elements, to –1. Then, the relationships between the wave matrices of the forward and backward normal waves can be written as

$$D_r = J_d D_i, \quad F_r = J_f F_i, \tag{A6}$$

where J_d is the $n \times n$ diagonal matrix, whose elements of numbers $j_1, j_2, \ldots, j_m$ are equal to –1 and the remaining elements are equal to 1, and J_f is the diagonal matrix, whose elements of numbers $j_1, j_2, \ldots, j_m$ are equal to 1 and the remaining elements are equal to –1. Clearly, these diagonal matrices satisfy the following equalities:

$$J_d + J_f = 0, \quad J_d J_f = J_f J_d = -I, \tag{A7}$$

where I is the identity matrix. In addition, they are also nilpotent matrices:

$$J_d^2 = J_f^2 = I. \tag{A8}$$

Using properties (A6)–(A8), Eqs. (16) can easily be proved. In particular, for the matrix P_r, we have

$$P_r = D_r^* F_r = (J_d D_i)^* J_f F_i = D_i^* J_d J_f F_i = -P_i,$$

which is equivalent to the first equality of Eqs. (16). The second equality can be proved in a similar way. Also, (A6)–(A8) yield a relationship between two

terms of the matrix S [see Eqs. (15), (18)]. Indeed, the second term proves to be equal to

$$F_i^T D_r = F_i^T J_d D_i = F_i^T J_f^2 J_d D_i$$

$$= -F_i^T J_f D_i = -(D_i^T F_r)^T = -Q^T,$$

so that the matrix of Eqs. (15) can be written as $S = (Q + Q^T)/2$, which proves the first equality in Eqs. (18).

Symmetry property (17) of the matrices S_i and S_r and the property of the matrix S of being diagonal are closely connected to the classical reciprocity theorem. To prove these properties, consider a uniform region of the structure between $x = 0$ and l. Let the field in it be characterized by forward normal waves with the amplitudes a and backward waves with the amplitudes b. Then, due to Eqs. (9), the generalized forces at the structure ends, which excite this set of normal waves, must be equal to

$$f(0) = F_i a + F_r b, \quad f(l) = -F_i \Phi_i(l) a - F_r \Phi_r(l) b, \quad \text{(A9)}$$

and the generalized displacements at the ends will be written as

$$u(0) = D_i a + D_r b, \quad u(l) = D_i \Phi_i(l) a + D_r \Phi_r(l) b. \quad \text{(A10)}$$

Now, let us use the reciprocity theorem [2]. Let there be two sets of forces of Eqs. (A9): $f^{(1)}(0)$, $f^{(1)}(l)$ and $f^{(2)}(0)$, $f^{(2)}(l)$. These forces excite two sets of normal waves with the amplitudes $a^{(1)}$, $b^{(1)}$ and $a^{(2)}$, $b^{(2)}$ and the displacements $u^{(1)}(0)$, $u^{(1)}(l)$ and $u^{(2)}(0)$, $u^{(2)}(l)$. Due to the reciprocity theorem, we have

$$[f^{(1)}(0)]^T u^{(2)}(0) + [f^{(1)}(l)]^T u^{(2)}(l) = [u^{(1)}(0)]^T f^{(2)}(0) + [u^{(1)}(l)]^T f^{(2)}(l). \quad \text{(A11)}$$

Substitution of Eqs. (A9) and (A10) into Eq. (A11) yields an equality, which we omit here for reasons of space. We will instead consider its particular cases that are sufficient for proving relationships (17) and (18).

Assume that all the backward wave amplitudes in (A9)–(A11) are equal to zero: $b^{(1)} = b^{(2)} = 0$. Then, the reciprocity relationship is reduced to

$$[a^{(1)}]^T[(S_i - S_i^T) - \Phi_i(l)(S_i - S_i^T)\Phi_r(l)]a^{(2)} = 0.$$

Since the vectors $a^{(1)}$ and $a^{(2)}$ are arbitrary, each jmth element in the brackets must be equal to zero:

$$(S_i - S_i^T)_{jm}[1 - \exp i(k_j + k_m)l] = 0.$$

Since the propagation constants are nonzero and the length l of the structure region is arbitrary, the symmetric elements of the matrix S_i: $(S_i)_{jm} = (S_i)_{mj}$ are equal, which means that the matrix is symmetric: $S_i^T = S_i$. The second equality in Eqs. (17), i.e., the symmetry of the matrix S_r, is proved in a similar way by assuming that the forward wave amplitudes in Eqs. (A.9)–(A11) are equal to zero, $a^{(1)} = a^{(2)} = 0$, and only the backward waves are excited.

The property that the matrix of Eqs. (15) is diagonal can be proved in a similar manner by setting $b^{(1)} = a^{(2)} = 0$ in Eqs. (A9)–(A11). In this case, reciprocity relationship (A11) can be reduced to

$$[a^{(1)}]^T[S - \Phi_i(l)S\Phi_r(l)]b^{(2)} = 0.$$

Clearly, since the amplitudes $a^{(1)}$ and $b^{(2)}$ are arbitrary, the matrix in the brackets must be zero. Consider its arbitrary, say, the jmth, element:

$$(S)_{jm}[1 - \exp i(k_j - k_m)l] = 0.$$

For off-diagonal elements $j \neq m$, the expression in the brackets is nonzero, because $k_j \neq k_m$ and l is arbitrary. Hence, the jmth off-diagonal element of the matrix S must be zero. Conversely, for the diagonal elements $j = m$, the expression in the brackets is identically zero and the elements of the matrix are nonzero, which proves that S is a diagonal matrix and, thereby, proves the second equality in Eqs. (18).

It should be noted that the proof used the assumption that the propagation constants of all waves are different. This assumption is valid for all fluid and solid waveguides and media at all frequencies, except for a countable number of critical frequencies, at which the dispersion relationships have multiple roots. If the roots are multiple, the set of waves given by Eq. (1) is mathematically incomplete and must be complemented by the so-called adjoined waves [19]. As far as is known, for the adjoined waves, the reflection and transmission theory has not yet been developed and the problem of the symmetry of their reflection and transmission matrices has not therefore been formulated. However, in our opinion, the notion of the adjoined waves is too strong a mathematical idealization and these waves do not exist in real media. It has been shown [20] that the presence of even a negligibly small loss in the waveguide or in the medium removes the root multiplicity of the dispersion relationship. This makes all the roots different, and the results of this paper become valid for all frequencies.

REFERENCES

1. Lord Rayleigh, *Theory of Sound* (reprinted) (Dover, New York, 1945; GITTL, Moscow, 1955).
2. L. M. Lyamshev, Dokl. Akad. Nauk SSSR **125**, 1231 (1959) [Sov. Phys. Dokl. **4**, 406 (1959)].
3. L. M. Lyamshev, in *Proceedings of International Noise and Vibration Control Conference NOISE-93* (St. Petersburg, 1993), Vol. 5, p. 41.
4. V. V. Tyutekin, Akust. Zh. **43**, 570 (1997) [Acoust. Phys. **43**, 492 (1997)].
5. B. R. Mace, J. Sound Vibr. **155** (2), 375 (1992).
6. G. Caviglia and A. Morro, J. Acoust. Soc. Am. **106**, 1666 (1999).
7. H. K. Milne, J. Sound Vibr. **114** (1), 149 (1987).

8. L. M. Brekhovskikh, *Waves in Layered Media* (Akad. Nauk SSSR, Moscow, 1957; Academic, New York, 1960).
9. G. J. Kuhn, J. Acoust. Soc. Am. **36**, 423 (1964).
10. B. L. N. Kennett, N. J. Kerry, and J. H. Woodhouse, Geophys. J. R. Astron. Soc. **52** (2), 215 (1978).
11. B. M. Gibbs and J. D. Tattersall, Trans. ASME, J. Vib. Acoust. Stress **109** (4), 348 (1987).
12. D. P. Kouzov and T. S. Kravtsova, Akust. Zh. **29**, 204 (1983) [Sov. Phys. Acoust. **29**, 118 (1983)].
13. I. I. Artobolevskiĭ, Yu. I. Bobrovnitskiĭ, and M. D. Genkin, *Introduction to Acoustic Dynamics of Machines* (Nauka, Moscow, 1979).
14. P. E. Krasnushkin, Zh. Tekh. Fiz. **17** (6), 705 (1947).
15. I. A. Kunin, *Theory of Elastic Media with Microstructure* (Nauka, Moscow, 1975).
16. D. W. Miller and A. von Flotow, J. Sound Vibr. **128** (1), 145 (1989).
17. Yu. I. Bobrovnitskiĭ, J. Sound Vibr. **152** (2), 175 (1992).
18. Yu. I. Bobrovnitskiĭ, Akust. Zh. **42**, 267 (1996) [Acoust. Phys. **42**, 234 (1996)].
19. P. E. Krasnushkin and E. N. Fedorov, Radiotekh. Élektron. (Moscow) **17**, 1129 (1972).
20. Yu. I. Bobrovnitskiĭ, Akust. Zh. **23**, 34 (1977) [Sov. Phys. Acoust. **23**, 18 (1977)].

Translated by A. Khzmalyan

Acoustical Physics, Vol. 49, No. 1, 2003, pp. 109–112. Translated from Akusticheskiĭ Zhurnal, Vol. 49, No. 1, 2003, pp. 123–126.

SHORT COMMUNICATIONS

Experimental Study of the Elements of Acoustic Screens Made of Rubber with Cylindrical Voids

A. I. Boĭko*, V. E. Glazanov, A. V. Mikhaĭlov**, and V. V. Tyutekin***

** Andreev Acoustics Institute, Russian Academy of Sciences, ul. Shvernika 4, Moscow, 117036 Russia*

*** Morfizpribor Central Research Institute, Chkalovskiĭ pr. 46, St. Petersburg, 197376 Russia*

e-mail: eugenia@dg3409.spb.edu

Received May 14, 2001

Abstract—For samples of screens made in the form of a steel layer with an overlying stack of rubber layers with cylindrical voids, the reflection and transmission coefficients are measured using the Low-Frequency Acoustic Pipe system. The experimental data are shown to agree well with the calculations performed on the basis of the theory of large deformations of rubber with cylindrical voids. *© 2003 MAIK "Nauka/Interperiodica".*

In designing acoustic screens for broadband receiving antennas that must meet a wide spectrum of requirements including the ability to operate under high hydrostatic pressures, it is advantageous to use a layered mass-elasticity system [1], in which a metal plate serves as a mass and a set of plane layers made of rubber with cylindrical voids (RCV) and bonded together with thin metal pads of the same area provides the elasticity. The theory for calculating the acoustic and elastic characteristics of a medium with cylindrical voids was first described in [2] and then considered in many publications, the results of which are generalized in [1, 3]. The application of screens made of elastomers is studied in [4]. In the present paper, the results of the experimental investigation of samples made of RCV are presented. The reflection and transmission coefficients of the samples were measured at the Andreev Acoustics Institute in the Low-Frequency Acoustic Pipe (LFAP) system [5, 6] under hydrostatic pressures of up to 6×10^6 Pa.

Sample no. 1 contained the following four elements: (a) a steel layer of thickness $d = 7$ cm; (b) two elements, each consisting of four RCV layers with outer titanium straps of thickness $\Delta_1 = 0.5$ cm and intermediate titanium plates of thickness $\Delta_2 = 0.1$ cm; and (c) one element consisting of three RCV layers with plates as described above (Δ_1 and Δ_2). The total number of RCV layers was $N = 11$, the diameter of a cylindrical void was $2a = 1.1$ cm, the number of voids in a layer was $n = 55$, and the diameter of the sample was $D = 14.8$ cm. In determining the perforation coefficient of RCV, one should take into consideration that, when the outer titanium plates are sufficiently stiff, the longitudinal static compression of a layer of rubber with cylindrical voids, as well as the impedance of the sample of diameter limited by the pipe walls for a plane wave, is determined by the average perforation coefficient, which is defined by the ratio of the total area of cross sections of all cylindrical voids to the area of the sample placed in the pipe. When determined in this way, the perforation coefficient is equal to $\varepsilon^2 = \dfrac{n\pi a^2}{\pi D^2/4} = 0.29$. The height of a single RCV layer is $h_0 = 1.3$ cm, and $h_0/b = 1.6$, where b is the outer radius of the tube representing the model of the medium with cylindrical voids. The total thickness of the stack of RCV layers is $L_0 = 18$ cm, and the total thickness of the sample is $L_0 + d = 25$ cm.

Sample no. 2 contained the following five elements: (a) a layer of steel of thickness $d = 7$ cm; (b) three elements, each consisting of three layers of RCV with outer titanium plates of thickness $\Delta_1 = 0.4$ cm and intermediate titanium plates of thickness $\Delta_2 = 0.1$ cm; and (c) one element consisted of two RCV layers with the same outer plates Δ_1 and the inner plate Δ_2 as specified above. The total number of RCV layers was $N = 11$. The cylindrical voids were of two types: (1) $2a_1 = 1.6$ cm, $n_1 = 31$ and (2) $2a_2 = 1.0$ cm, $n_2 = 10$. The perforation coefficient averaged over the area was $\varepsilon^2 = \dfrac{n_1\pi a_1^2 + n_2\pi a_2^2}{\pi D^2/4} = 0.39$; $h_0 = 1.6$ cm, $h_0/b = 1.5$, $L_0 = 21$ cm, and $L_0 + d = 28$ cm. The straps and the intermediate plates of the samples were attached to the RCV layers by vulcanization.

The measurements were carried out separately in the frequency ranges (300–1000) Hz and (1000–4000) Hz under hydrostatic pressures P from 1×10^6 to 6×10^6 Pa. The accuracy of the LFAP system was determined by measuring the coefficients of reflection r and transmission t of a steel sample 14.8 cm in diameter and 7 cm in

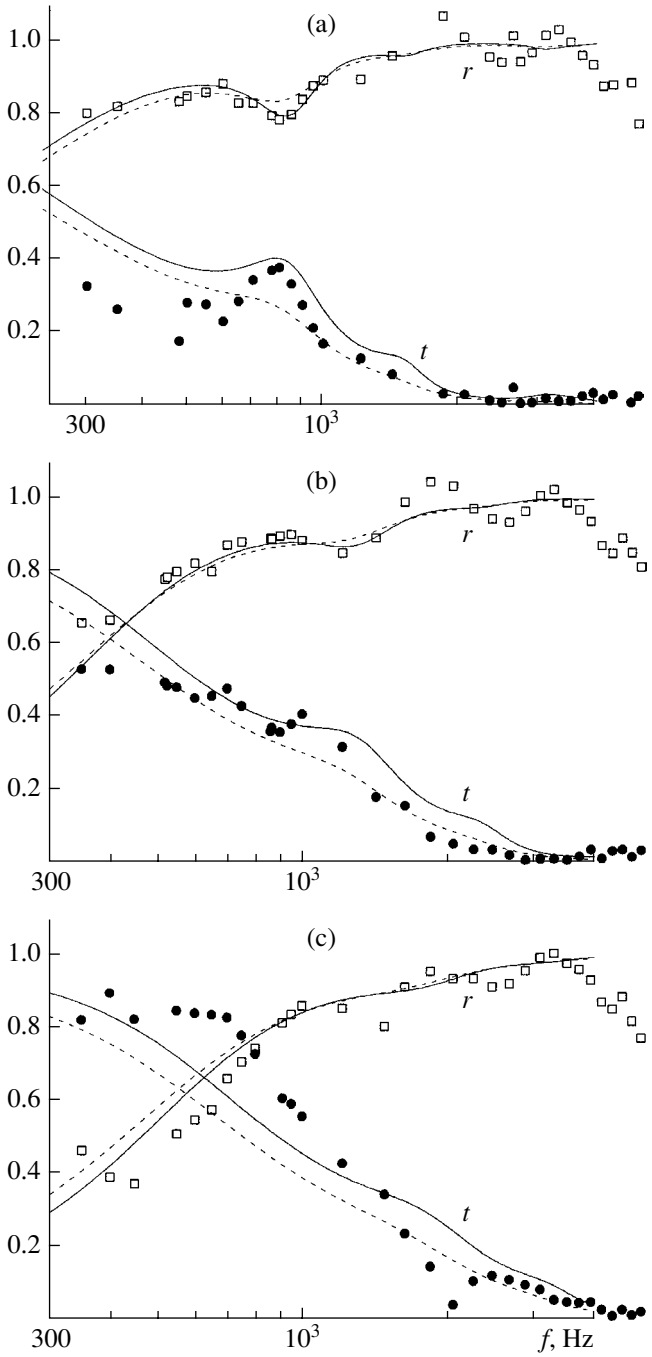

Fig. 1. Frequency dependences of the absolute values of the reflection r and transmission t coefficients for sample no. 1: $\eta_c = 0.1$ (solid line) and 0.2 (dashed line); P = (a) 2×10^6, (b) 4×10^6, and (c) 6×10^6 Pa.

thickness. From these measurements and subsequent statistical processing, it was found that the random errors in measuring r and t did not exceed 1.5 dB.

The results of measurements for samples nos. 1 and 2 for three values of hydrostatic pressure are presented in Figs. 1 and 2. The same figures show the theoretical dependences of the absolute values of the reflection r and transmission t coefficients on frequency that were calculated by using the layer theory [7] for several values of the loss factor ($\eta_c = 0.1$ refers to the solid lines and $\eta_c = 0.2$, to the dashed lines). In the calculation program, the multilayer system is represented as a cascade connection of four-terminal networks. The parameters of RCV for the samples under study were calculated from relations given in paper [1], which were derived for the case of large deformations of rubber layers with cylindrical voids. (Note that the calculation was performed without allowance for the dynamic correction similar to the Rayleigh correction for rubber with cylindrical voids [8], because, at frequencies below 1000 Hz, its effect on the velocity of elastic waves is insignificant, and at frequencies above 1000 Hz, it practically does not manifest itself owing to the high degree of sound insulation of the massive steel plate.) The elastic characteristics of the base rubber were assumed in calculations as follows: the static shear modulus measured in a static press by the technique given in [9] was $\mu_{\tilde{n}0}$ = 15 kg/cm^2; the velocity of shear waves determined by using a Bruel and Kjaer 3930 instrument for measuring the complex Young's modulus $\bar{E} = E_0(1 - i\eta_E)$ [10] was $c_t = \sqrt{E_0/3\rho} = 0.7 \times 10^4$ cm/s.

The analysis of the results of measuring the reflection r and transmission t coefficients leads to the following conclusions:

(1) In the frequency range (300–1000) Hz, the experimental values of r under hydrostatic pressures up to $P = 6 \times 10^6$ Pa practically coincide with the calculated characteristics. Due to the special features of the measuring system, for the sample with a high degree of sound insulation (at pressures up to $P \le 4 \times 10^6$ Pa), the measured values of t noticeably differ from the calculated ones. However, for $P = 6.0 \times 10^6$ Pa, when the transmission coefficient of the samples increases owing to the compression of the RCV layers, i.e., due to the growth of the relative wave impedance m and the decrease in the thickness h_P, the calculation again approaches the experiment.

(2) In the frequency range above 1000 Hz, the measured values of r, regardless of the value of the hydrostatic pressure, oscillate near the calculated characteristics with a practically constant period. This points to the presence of a systematic error introduced by the measuring system, which, however, does not exceed the random error.

(3) In the frequency range below 1000 Hz, it is preferable to assume the value of the loss factor in rubber as $\eta_c = 0.1$. With an increase in frequency, the value η_c = 0.2 gives the best agreement with the experiment, especially for the quantity t, which is most sensitive to this parameter.

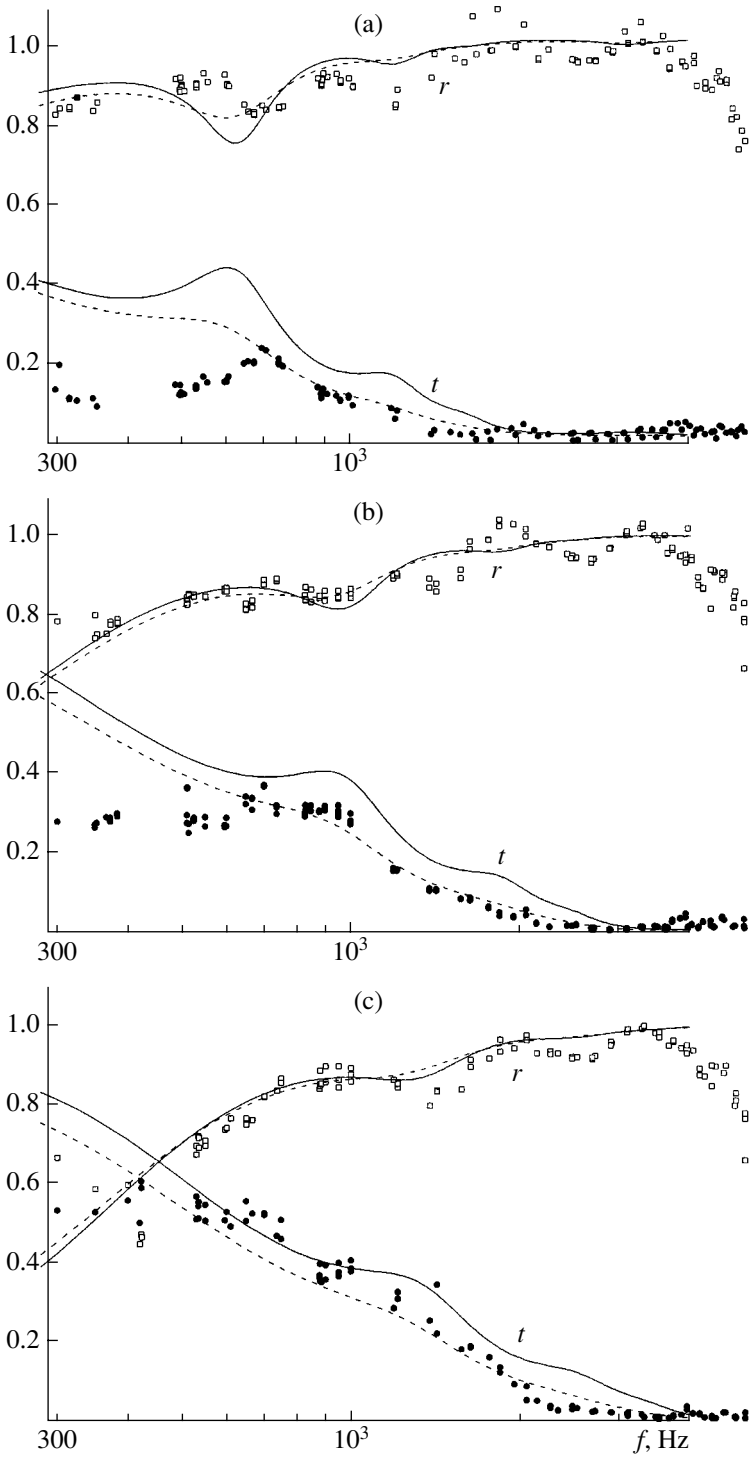

Fig. 2. Frequency dependences of the absolute values of the reflection r and transmission t coefficients for sample no. 2. The notation is the same as in Fig. 1.

(4) For sample no. 2, unlike sample no. 1, a series of measurements were carried out at different times, withdrawing the sample from the pipe and then remounting it. The good agreement between the results of these measurements testifies to their reliability.

ACKNOWLEDGMENTS

We are grateful to É.V. Labetskiĭ for the metrological certification of the measuring system and to N.S. Isaev and I.I. Andreev for providing the tuning and efficient operation of the Low-Frequency

Acoustic Pipe and for participation in the measurements.

REFERENCES

1. V. E. Glazanov, *Screening of Hydroacoustic Antennas* (Sudostroenie, Leningrad, 1986).
2. V. V. Tyutekin, Akust. Zh. **2**, 291 (1956) [Sov. Phys. Acoust. **2**, 307 (1956)].
3. V. T. Lyapunov, É. É. Lavendel, and S. A. Shlyapochnikov, *Rubber Vibration Insulators* (Sudostroenie, Leningrad, 1988).
4. H. Ko. Sung, J. Acoust. Soc. Am. **101**, 3306 (1997).
5. A. V. Vovk, S. P. Klimov, and V. V. Tyutekin, Izmer. Tekh., No. 7, 76 (1975).
6. V. V. Tyutekin, Akust. Zh. **47**, 843 (2001) [Acoust. Phys. **47**, 741 (2001)].
7. L. M. Brekhovskikh, *Waves in Layered Media*, 2nd ed. (Nauka, Moscow, 1973; Academic, New York, 1960).
8. V. E. Glazanov and A. V. Mikhaĭlov, Akust. Zh. **47**, 835 (2001) [Acoust. Phys. **47**, 671 (2001)].
9. L. A. Tarasov and V. V. Tyutekin, Kauch. Rezina, No. 9, 38 (1960).
10. *Catalog of Instruments for Analyzing Sound and Vibration and Data Processing* (Bruel and Kjaer, Denmark, 1978–1981).

Translated by A. Svechnikov

Acoustical Physics, Vol. 49, No. 1, 2003, pp. 113–115. Translated from Akusticheskiĭ Zhurnal, Vol. 49, No. 1, 2003, pp. 127–129.

SHORT COMMUNICATIONS

Correlation of Pressure Fluctuations with Tangential Stresses in a Turbulent Boundary Layer

B. M. Efimtsov*, V. V. Zosimov, A. V. Romashov***, and S. A. Rybak*****

** State Research Center Zhukovskiĭ Central Aerohydrodynamics Institute, Moscow, Russia*

*** Research Institute of Applied Acoustics, Dubna, Russia*

**** Andreev Acoustics Institute, Russian Academy of Sciences, ul. Shvernika 4, Moscow, 117036 Russia*

e-mail: rybak@akin.ru

Received February 7, 2002

The study of pressure fluctuations in a turbulent boundary layer was one of the outstanding areas of research among the variety of investigations carried out by L.M. Lyamshev [1, 2]. The studies initiated by L.M. Lyamshev are continued in this paper.

Previous publication [3] presents the experimentally measured cross spectra for the fluctuations of the longitudinal tangential stresses σ_{xz} (the x axis is directed along the flow) that occur at the boundary of a turbulent boundary layer at points separated along the flow direction; the same paper presents the cross spectra for the fluctuations of tangential stresses and the pressure fluctuations:

$$\varphi_\tau = \langle \sigma^*_{xz}(\omega, 0, y)\sigma_{xz}(\omega, 0, y+\eta)\rangle / \langle |\sigma|^2\rangle,$$
$$\varphi_{p\sigma} = \langle p^*(\omega, 0, y)\sigma_{xz}(\omega, 0, y+\eta)\rangle / \sqrt{\langle |p|^2\rangle \langle |\sigma|^2\rangle}, \quad (1)$$

where ω is the frequency and y and η are the coordinate and displacement of the observation points across the flow. The results of measurements for different frequencies are shown in Fig. 1.

The following publication [4] determines the relation of the pressure fluctuation spectra obtained for sound and pseudosound to the spectrum of the fluctuations of tangential stresses at the wall:

$$p(\omega, \mathbf{k}) = \frac{1}{q_z}\frac{c^2}{c_1^2}(k_x\sigma_{xz}(\omega, \mathbf{k}) + k_y\sigma_{yz}(\omega, \mathbf{k})), \quad (2)$$

where $\mathbf{k} = (k_x, k_y)$ is the wave vector; c is the velocity of sound; $c_1^2 = c^2 + i\left(\varsigma + \frac{4}{3}\mu\right)\omega/\rho$; and ς, μ, and ρ are the bulk viscosity, the shear viscosity, and the density of the medium, respectively.

This result allows a comparison with the aforementioned experimental data and also makes it possible to obtain the spatial spectrum of pressure fluctuations, which is the aim of the present study.

Let us introduce some assumptions. First, we assume that the transverse component of the tangential forces is negligibly small in comparison with the longitudinal component:

$$\sigma_{yz}(\omega, \mathbf{k}) \ll \sigma_{xz}(\omega, \mathbf{k}).$$

Second, the cross spectrum of the longitudinal (σ_{xz}) tangential stresses is representable in factorized form:

$$\langle \sigma^*_{xz}(\omega, 0, y)\sigma_{xz}(\omega, 0, y+\eta)\rangle = \Phi_0(\omega)\phi(\xi, \eta, \omega), \quad (3)$$
$$\phi(\xi, \eta, \omega) = \phi(\zeta, 0, \omega)\phi(0, \eta, \omega).$$

The expression for the dimensional factor $\Phi_0(\omega)$ and the form of the longitudinal cross spectrum of tangential stress fluctuations $\phi(\xi, 0, \omega)$ were obtained from the analysis of experimental data in [5]:

$$\Phi_0(\omega) = \rho^2 U_\tau^2 \nu F(\omega\nu/U_\tau^2),$$
$$\phi(\xi, 0, \omega) = \exp(-\xi/\Lambda_1(\mathrm{Sh}) - i\omega\xi/U_\mathrm{f}), \quad \xi > 0,$$

where $U_\tau = 1.26$ m/s is the friction speed and the quantities U_f, Λ_1, and F for different Strouhal numbers $\mathrm{Sh} = \omega\nu/U_\tau^2$ are given in the table.

Table

Sh 10^3	2	4	8	15	30
U_f, m/s	25	24.4	23.9	23.5	22.8
Λ_1, mm	75	68.5	62.0	57.7	31.0
F	0.63	0.63	0.525	0.38	0.263

The function $\phi(0, \eta, \omega)$ used for calculations in this paper can be obtained by the interpolation of the experimental data [3].

The factorization of the cross spectrum yields a complete representation of the correlation of tangential stresses $\langle \sigma_{xz}(\omega, x, y)\sigma_{xz}(\omega, x+\xi, y+\eta)\rangle$ from the experimental data, which allows us to obtain the spatial spectrum of tangential stresses $\sigma_{xz}(\omega, \mathbf{k})$ through the two-

1063-7710/03/4901-0113$24.00

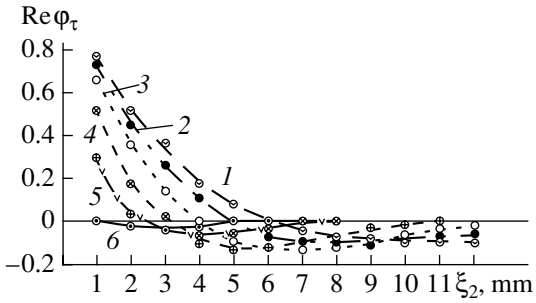

Fig. 1. Real part of the transverse cross spectrum (of turbulent fluctuations of the tangential stresses at the wall) for different Strouhal numbers: Sh = (*1*) 2×10^{-3}, (*2*) 4×10^{-3}, (*3*) 8×10^{-3}, (*4*) 15×10^{-3}, and (*5*) 30×10^{-3}.

dimensional Fourier transform with respect to the coordinates ξ and η.

After the spatial spectrum of tangential stresses is obtained using Eqs. (1) and (2), one can calculate any of the second moments of the tangential stresses and pressure at the surface about which the flow moves. In particular, it is possible to obtain the cross spectrum of pressure and tangential stresses:

$$\phi_{p\sigma}(\rho) = \frac{\langle p(\varpi, r)\sigma(\omega, r+\rho)\rangle}{\sqrt{\langle |p|^2\rangle \langle |\sigma|^2\rangle}}.$$

This spectrum can be compared with the experimental data presented in [3].

However, the following fact should be taken into account in this case. In the experiment in [3], the pressure was measured by a pressure sensor with a finite spatial aperture, namely, by a 4138 Bruel & Kjer microphone with a membrane 1/8 in. in diameter. The spatial spectrum of the quantity measured in this way is related to the spatial spectrum of tangential stresses by a formula that differs from Eq. (2):

$$p(\omega, \mathbf{k}) \propto \frac{J_1(kR)}{k}\frac{1}{q_z}\frac{c^2}{c_1^2}k_x\sigma_{xz}(\omega, \mathbf{k}),$$

where J_1 is the Bessel function of the first kind. Indeed, the pressure experimentally measured at a point r can be represented as an integral of the true pressure over the sensitive surface of the sensor with the center at the point r. Assuming that the sensitive surface is a circle of radius R, we obtain

$$p_m(r) = \int \Pi(\rho - r)p(\rho)d^2\rho,$$

where p_m is the measured pressure and the function Π is equal to unity when its argument does not exceed R in magnitude and is equal to zero in the opposite case. The expression for the measured pressure is a convolution in the coordinate space. The spatial spectrum of the measured pressure is the product of the spatial spectrum of the true pressure by the spatial spectrum of the function Π:

$$\int_R \Pi(r)\exp(-ikr)d^2r = 2\pi\int_0 rJ_0(kr)dr = 2\pi R\frac{J_1(kR)}{k},$$

which yields the expression given above for the spatial spectrum of the measured pressure.

The average square of the pressure magnitude is obtained by the integration of the squared magnitude of the spatial spectrum of pressure with respect to the wave numbers:

$$|p(\omega, k)|^2 = \left|\frac{J_1(kR)}{k}\frac{1}{q_z}\frac{c^2}{c_1^2}k_x\right|^2 |\sigma_{xz}(\omega, k)|^2. \qquad (4)$$

For the normalized correlation of pressure and tangential stresses, we derive the expression

$$\phi_{\sigma p}(\omega, \xi, \eta) = \frac{\mathrm{IFFT}\left(\frac{J_1(kR)}{k}\frac{1}{q_z}\frac{c^2}{c_1^2}k_x|\sigma_{xz}(\omega, k)|^2\right)}{\sqrt{|p|^2|\sigma|^2}}, \qquad (5)$$

where IFFT means the inverse two-dimensional Fourier transform.

The calculations by Eqs. (4) and (5) were performed numerically in the MATLAB medium. The initial experimental data for the correlation of tangential stresses were represented on a square grid with a pitch of 2.3 mm and a size of 300 mm by means of factorization. The longitudinal part of the correlation was calculated by Eq. (3), and the transverse part was obtained by the interpolation of the experimental data in the measurement interval 0–12 mm; beyond this interval, the correlation was assumed to be zero. The calculations were performed using the fast two-dimensional Fourier transform.

Figure 2 shows the calculated transverse correlation $R_{\sigma p}(\omega, 0, \eta)$ between pressure and tangential stresses in comparison with the experimentally measured correlation values for different Strouhal numbers.

Note that it is precisely this allowance made for the finite aperture of the pressure sensor that provides the coincidence with the experiment for the minima and zeros of the function $\phi_{\sigma p}(\omega, 0, \eta)$ and, hence, a good agreement with the experimental curve from the cited paper [3].

The main conclusion drawn from the above analysis is that, in the case of subsonic flow velocities, tangential stresses make a considerable contribution to

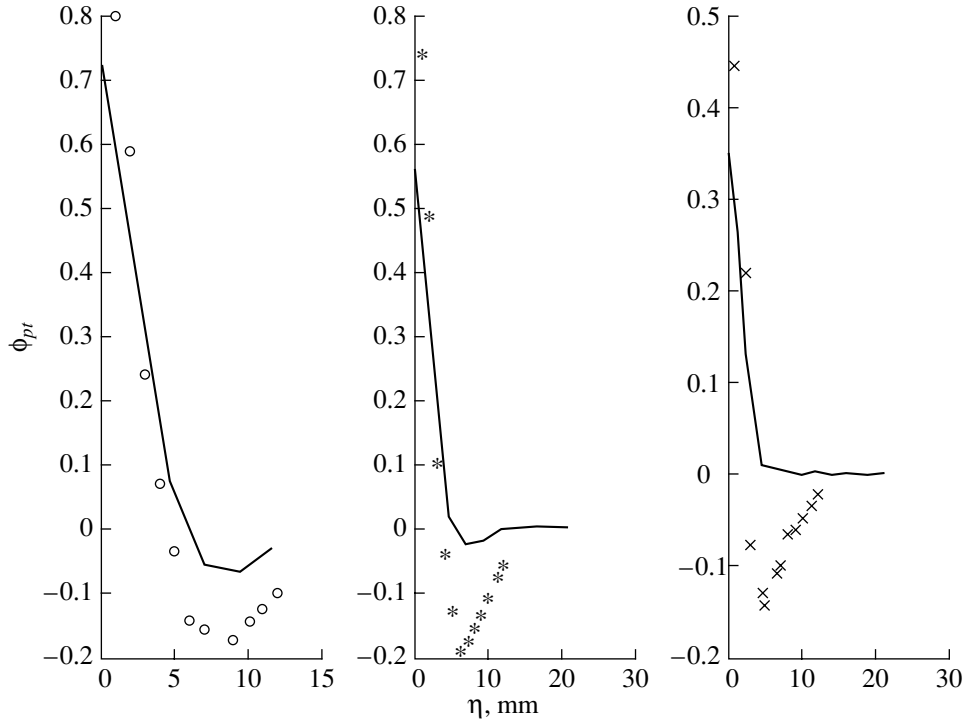

Fig. 2. Calculated transverse correlation between pressure and tangential stresses in comparison with the experimentally measured correlation of tangential stresses for the Strouhal numbers (from left to right) Sh = 8×10^{-3}, 15×10^{-3}, and 30×10^{-3}.

the formation of the wall pressure fluctuations. This conclusion agrees well with the results of the previous study [6].

ACKNOWLEDGMENTS

This work was supported in part by the Russian Foundation for Basic Research (project no. 99-02-16161a), the Support Program for Scientific Schools (project no. 00-15-96678), and INTAS (project no. 99-0088).

REFERENCES

1. L. M. Lyamshev, Vestn. Akad. Nauk SSSR, No. 6, 22 (1973).
2. L. M. Lyamshev, Dokl. Akad. Nauk SSSR **213**, 544 (1973) [Sov. Phys. Dokl. **18**, 695 (1973)].
3. B. M. Efimtsov and V. A. Sysoev, Akust. Zh. **43**, 358 (1997) [Acoust. Phys. **43**, 307 (1997)].
4. S. A. Rybak, Akust. Zh. **47**, 717 (2001) [Acoust. Phys. **47**, 629 (2001)].
5. B. M. Efimtsov, V. B. Kuznetsov, and V. A. Sysoev, Uch. Zap. TsAGI **14** (2), 67 (1983).
6. K. A. Naugol'nykh and S. A. Rybak, Tr. Akust. Inst. Akad. Nauk SSSR, issue 16, 129 (1971); Akust. Zh. **26**, 890 (1980) [Sov. Phys. Acoust. **26**, 502 (1980)].

Translated by E. Golyamina

Acoustical Physics, Vol. 49, No. 1, 2003, pp. 116–118. Translated from Akusticheskiĭ Zhurnal, Vol. 49, No. 1, 2003, pp. 130–132.

SHORT COMMUNICATIONS

The Output Power of an Acoustic Source in the Presence of Elastic Scatterers

T. M. Tomilina

Institute of Mechanical Engineering, Russian Academy of Sciences, Malyĭ Khariton'evskiĭ per. 4, Moscow, 101990 Russia

e-mail: tatiana@imash.ac.ru

Received September 10, 2002

This paper studies the problems in which a finite source interacts with an elastic structure through a medium. New results are presented that demonstrate the effect of elastic scatterers on the power emitted by the source. Conditions are discussed under which the emitted power increases by several orders of magnitude over that emitted by the source in free space. This study was inspired by the research of L.M. Lyamshev [1–3], who experimentally and theoretically investigated the interaction between acoustic fields and elastic structures (plates and shells) and discovered a considerable amplification of the scattered sound due to resonance properties of such a coupled system. This paper addresses the problem with an active source and a passive finite scatterer, and the solutions are found with allowance for the multiple reflection between them. The problem was brought up by the necessity to describe an acoustic model for such mechanical acoustic sources as vibrating elements of machines and structures that interact with each other and with other elastic structures through a medium and generate sound. The consideration of a more complex model of such sources (instead of a point source), namely, a model with an extended surface (even one of compact geometry) revealed new effects, which we managed to describe quantitatively.

The effect of increasing (or decreasing) the acoustic power of a source operating near reflectors or scatterers has long been known qualitatively. The first quantitative estimates were obtained for a point source. For instance, the problem of a monopole operating near a rigid boundary in a dihedral angle and in a trihedral angle is considered in [4]; in a waveguide with two rigid parallel walls, in [5]. Since the rigid walls can be replaced by imaginary sources located in free space, solutions to all these problems can be represented as a superposition of fields produced by a group of point sources, and the only physical mechanism (which is far from efficient) for increasing the power is wave interference. In particular, the power produced by a monopole near a rigid wall may become two times that of the power in free space; in a trihedral angle, eight times as great (by the number of imaginary sources).

The first results for the output power of a finite source reported in [6], where the sound produced by a thin disk vibrating near a rigid wall was studied, have shown that the output of an extended source may vary within much wider limits, reaching an order of magnitude at certain frequencies, and that the physical mechanism responsible for this effect is cavity resonance (the resonance of the space between the disk and the wall). Investigation of this effect in another model, a sphere vibrating near rigid surfaces (a sphere, a dihedral angle, and a trihedral angle), has shown that, even for a source of compact geometry, the amplification may be as high as 20-fold, depending on the oscillation mode [7].

In this work, to study the effect of resonance properties of an elastic scatterer on the source output power, we considered the acoustic field emitted by an infinite cylinder (of radius a) with a given vibration velocity distribution over its surface located near a simply supported elastic slab (with the width l and thickness h). In this problem, flexural vibrations were excited by the acoustic pressure produced on the surface of the slab by an active source. Figure 1a plots the dimensionless ratio of the full power flow of the source in the presence of the slab to that in free space, PR, versus the frequency for the slab material with a loss factor of 0.01. As can be seen from the plot, a considerable power amplification is observed near the first resonance frequency ka = 0.3 of the slab's flexural vibrations.

The effect of the resonance scattering from the slab essentially depended on the azimuthal vibration mode of the cylinder (the azimuthal distribution of the vibration velocity v was taken to be $v = v_0\cos(m\varphi)$ or $v = v_0\sin(m\varphi)$). With the slab vibrating at the first resonance frequency of its flexural vibrations and the cylinder pulsating (m = 0) and oscillating (m = 1 or 2), the emitted power increased by a factor of 1.7, 4.8, and approximately 180, respectively. In order to isolate the resonance scattering effect, Fig. 1b presents the ratio of the power emitted by the source near the elastic slab to that near a perfectly rigid slab versus frequency.

The power amplification at resonances of the space between the source and the scatterer is also observed in

1063-7710/03/4901-0116$24.00

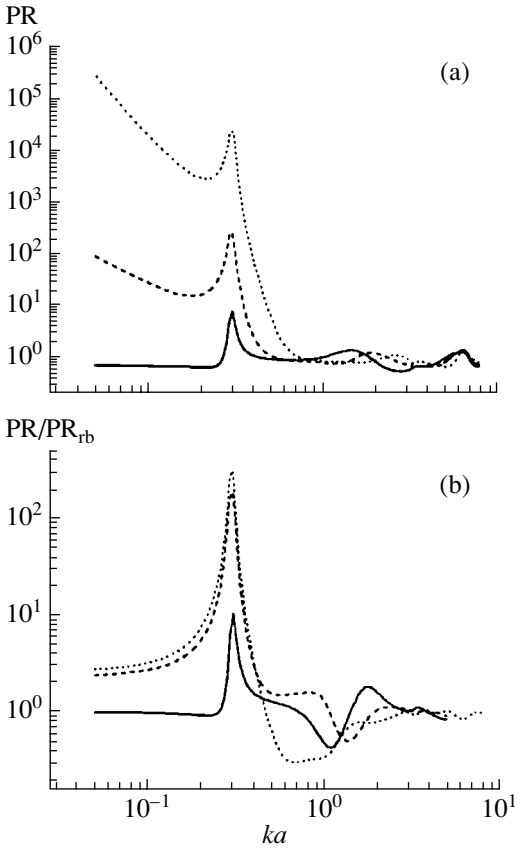

Fig. 1. (a) Power gain versus frequency for a cylinder of radius a vibrating at a distance $H = 0.5a$ from a thin elastic slab of width $l = 2a$; (b) the normalized characteristics of the radial vibration velocity distribution over the cylinder circumference: $v_0(\varphi) = v_0\sin(\varphi)$ (solid line), $v_0 = v_0\cos(2\varphi)$ (dashed line), and $v_0(\varphi) = v_0\sin(3\varphi)$ (dotted line).

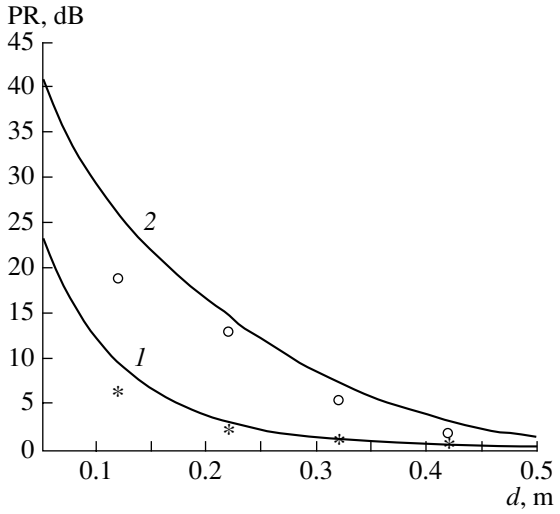

Fig. 2. Power gain for a dipole-type source [(*1*) theory and (∗) experiment] and a quadrupole-type source [(*2*) theory and (o) experiment] versus the distance from the scatterer.

this geometry, but this effect is not as significant as in the case of a vibrating disk. The amplification is only by a factor of 2.7 due to the compact geometry of the source. As the source moves away from the scatterer, the effect vanishes.

We have also established an interesting effect, which is observed at low frequencies in sources operating in high-order vibration modes. The effect was called the source order reduction effect: near a boundary, the power of a source operating in a higher vibration mode corresponds to that of a lower order source in free space. For example, near a rigid or an elastic boundary, a finite quadrupole source emits as a monopole, etc. The acoustic power increases by several orders of magnitude due to the oscillations of the medium near the source. The higher the vibration mode of the source surface, the stronger the effect is. This result is clearly seen in Fig. 1a.

To make sure that the power amplification in the presence of a scatterer is observed in real conditions, we performed a laboratory experiment. A rectangular wooden plate with two built-in dynamic loudspeakers was used as the source. The loudspeakers could be operated in phase or in antiphase, simulating the dipole or quadrupole source. As the scatterer, a metal pipe was used, whose open end was placed near the source. The experimental setup was installed in a large room. The radiated power was measured by an intensitimeter at 162 points over a 2-m-diameter hemisphere enclosing the source and the scatterer. The main results of the experiment were as follows.

At the first resonance frequency of the pipe ($f_1 = 92$ Hz), the full power of the source increases by two orders of magnitude compared to that without the scatterer. For the quadrupole-type source (the loudspeakers operate in antiphase), the power gain is higher than that for the dipole-type source. The reason is that the quadrupole has a stronger near field, which excites the resonance vibrations of the pipe stronger and the pipe reradiates the sound more efficiently, thus transforming part of the near-field reactive energy into the active far-field energy. Figure 2 shows the power gain at the resonance frequency f_1 in decibels versus the distance d between the source and the scatterer. As we see from Fig. 2, the power gain increases as the distance decreases and the near field grows.

Similar results were also obtained in other geometries, in particular, in the three-dimensional situation with a spherical source near a circular plate executing flexural vibrations. The validity of the quantitative results in these computationally complex problems is largely due to the use of the efficient numerical solution technique with a controlled accuracy [9, 10].

The results of studying the effect of elastic scatterers on the power emitted by an acoustic source reported in this paper are important for the correct evaluation of the energy characteristics of real sources used, for example, in the SEA method. They are also important for

designing sources with desired acoustic properties by way of affecting the acoustic environment in which they operate, by increasing or decreasing their output power due to the elastic properties and relative position of the scatterers. The results can be useful for understanding the physical mechanisms of sound generation by complex industrial noise sources.

ACKNOWLEDGMENTS

This work was carried out under the State Support Program for Scientific Schools (project no. 00-15-96004, K.V. Frolov).

The author thanks Yu.I. Bobrovnitskiĭ for discussing the results in the course of the study.

REFERENCES

1. L. M. Lyamshev, *Sound Reflection by Thin Plates and Shells in Liquid* (Akad. Nauk SSSR, Moscow, 1955).
2. L. M. Lyamshev, Akust. Zh. **15**, 303 (1969) [Sov. Phys. Acoust. **15**, 264 (1969)].
3. L. M. Lyamshev, Akust. Zh. **45**, 693 (1999) [Acoust. Phys. **45**, 619 (1999)].
4. R. V. Waterhouse, J. Acoust. Soc. Am. **30**, 4 (1958).
5. P. M. Morse and K. V. Ingard, *Theoretical Acoustics* (McGraw-Hill, Princeton, 1968).
6. T. M. Tomilina, in *Proceedings of INTER-NOISE96* (Liverpool, UK, 1996), p. 3149.
7. V. B. Yashkin, Akust. Zh. **44**, 689 (1998) [Acoust. Phys. **44**, 598 (1998)].
8. T. M. Tomilina, Yu. I. Bobrovnitskiĭ, V. B. Yuashkin, and A. A. Kochkin, J. Sound Vibr. **226**, 285 (1999).
9. T. M. Tomilina, Rev. Fr. Mech., Special Issue 538 (1991).
10. Yu. I. Bobrovnitskiĭ and T. M. Tomilina, Akust. Zh. **41**, 737 (1995) [Acoust. Phys. **41**, 649 (1995)].

Translated by A. Khzmalyan

Acoustical Physics, Vol. 49, No. 1, 2003, pp. 19–23. Translated from Akusticheskiĭ Zhurnal, Vol. 49, No. 1, 2003, pp. 24–29.

Parametric Phase Conjugation for the Second Harmonic of a Nonlinear Ultrasonic Beam

A. P. Brysev*, F. V. Bunkin*, M. F. Hamilton, R. V. Klopotov*, L. M. Krutyanskiĭ*, and K. Yan****

** Wave Research Center, General Physics Institute, Russian Academy of Sciences, ul. Vavilova 38, Moscow, 119991 Russia*

e-mail: brysev@orc.ru

*** Department of Mechanical Engineering, Texas University, Austin, Texas, 78712-1063 USA*

e-mail: hamilton@mail.utexas.edu

Received March 18, 2002

Abstract—The effect of phase conjugation for the second harmonic of a focused ultrasonic beam was investigated experimentally and by numerical simulation. An ultrasonic pulse with the carrier frequency f = 3 MHz was emitted into water and focused at a point between the source and the phase conjugating system. The phase conjugation for the second harmonic of the incident wave ($2f$ = 6 MHz) was performed in a magnetostrictive ceramic as a result of the parametric interaction of the incident wave with the pumping magnetic field (the pumping frequency was $f_p = 4f$ = 12 MHz). The axial and focal distributions of sound pressure in the incident and conjugated beams were measured using a broadband PVDF membrane hydrophone. The corresponding calculations were performed by solving numerically the Khokhlov–Zabolotskaya–Kuznetsov (KZK) equation allowing for the nonlinearity, diffraction, and thermoviscous absorption. The results of measurements agreed well with the calculations and showed that the field of a conjugate wave adequately reproduces the field of the second harmonic of the incident wave. A certain advantage of focusing with the phase conjugation for the second harmonic was demonstrated in comparison with the operation at the doubled frequency of the incident wave. The results of this study can serve as a basis for the utilization of the phase conjugation of harmonics in ultrasonic tomography and nondestructive testing. *© 2003 MAIK "Nauka/Interperiodica".*

The problem of phase conjugation in acoustics has attracted the attention of researchers for a long time. L.M. Lyamshev, to whose memory this issue of the journal is dedicated, was also interested in it. He worked in this field himself [1] and took a keen interest in the research performed by other teams, including ours.

Traditionally, in the case of phase conjugation in acoustics, the sources are passive scatterers or common ultrasonic radiators [2]. In this case, a phase conjugate wave reproducing all stages of propagation of an incident wave in the inverse sequence comes back to a localized source. This property of phase conjugation is the basis for the technique of self-targeting of ultrasonic energy to scattering objects in liquids [3, 4] and for the method of compensation of phase distortions in the reconstruction of ultrasonic images in a phase-inhomogeneous medium [5, 6].

At the same time, another physical situation is possible, when the source of a conjugate wave is distributed and does not have a definite localization. An example can be the harmonics arising in the course of the propagation of intense sound waves in a nonlinear medium. It is not quite clear *a priori* what the wave resulting from the phase conjugation of one of the harmonics of an incident wave is like. The investigation of such waves is also necessary and interesting from the point of view of the application of phase conjugation for the compensation of phase distortions in nonlinear techniques of acoustic imaging [7]. As a rule, these techniques utilize the second harmonic of the probing radiation, which is focused better than the first harmonic, has a lower level of side peaks, and is less subjected to the effect of reverberation.

One can get a certain qualitative idea of the expected results of phase conjugation of harmonics on the basis of the Khokhlov–Zabolotskaya–Kuznetsov (KZK) equation using its analytical solution for the case of an axisymmetric source with a Gaussian amplitude distribution. The second harmonic generated in an incident wave can be written as $p_{2\text{in}}(r, z, t) = q_{2\text{in}}(r, z)e^{i2(\omega t - kz)}$, where r and z are the transverse and longitudinal cylindrical coordinates, respectively; $k = \omega/c$; $\omega = 2\pi f$ is the circular frequency; c is the sound velocity; and the expression for $q_{2\text{in}}$ is known (see, e.g., [8]). Then, the conjugate wave should have the form $p_{2c}(r, z, t) = q_{2c}(r, z)e^{i2(\omega t + kz)}$. Assuming for simplicity that the amplification in the case of phase conjugation is equal to one and that the propagation of a conjugate wave is linear, we

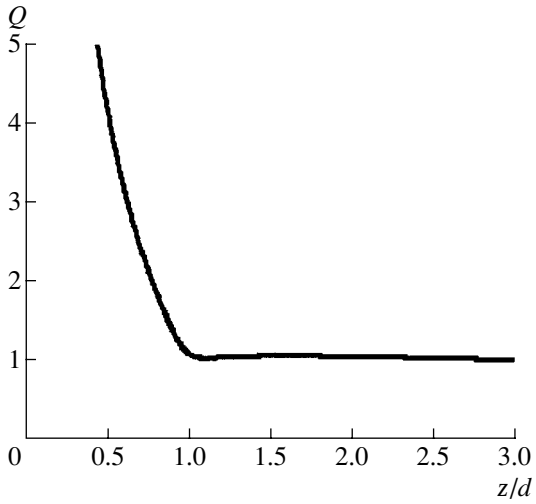

Fig. 1. Axial distribution of the ratio of the amplitudes of the conjugate wave and the second harmonic of the incident wave ($Q = |q_{2c}/q_{2i}^*|$) in a focused Gaussian beam.

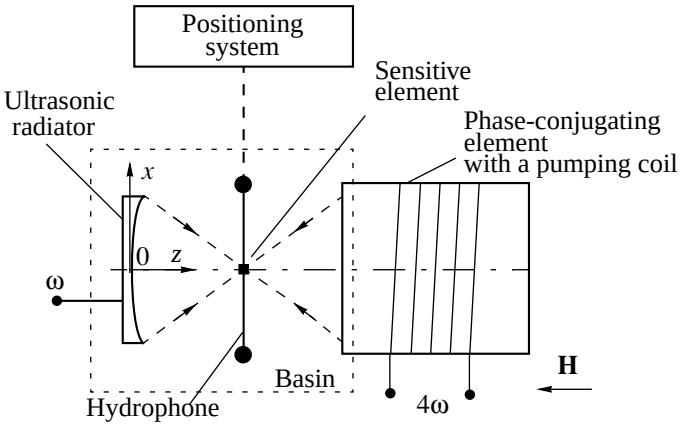

Fig. 2. Experimental setup: **H** is the constant bias magnetic field and *x* and *z* are the coordinate axes. The dashed arrows indicate the propagation of the sound beams.

ignore the absorption to obtain the following expression for the case of a focused incident beam:

$$\frac{q_{2c}}{q_{2i}^*} = \frac{\ln[1-(1+1/iG)h/d]}{\ln[1-(1+1/iG)z/d]}. \qquad (1)$$

Here, the asterisk denotes complex conjugation, $G = ka^2/2d$ is the focusing coefficient, a is the source radius, d is the focal distance, and h is the distance from the source to the plane of phase conjugation. It is interesting that the transverse distributions of the incident and conjugate beams coincide and the differences manifest themselves only along the propagation direction. Figure 1 shows the dependence of $Q = |q_{2c}/q_{2i}^*|$ on the dimensionless longitudinal coordinate z/d for the case $G = 10$ and $h/d = 3$. Between the focus and the phase-conjugating system, where generation of the second harmonic in the incident wave is weak, the amplitudes of both waves are almost equal ($Q \approx 1$). The value of Q increases monotonically in the direction from the focus to the source, since the amplitude of the second harmonic generated in the incident beam tends to zero as the source is approached, while the conjugate wave propagates linearly along z.

The subject of this study is the experimental realization and investigation of the parametric phase conjugation of the second harmonic of a focused ultrasonic beam generated by a real source. It is quite easy to perform the phase conjugation of individual harmonic components of incident ultrasonic radiation in the framework of the method of parametric phase conjugation [9]. The necessary conditions are provided by the resonance nature of the sound wave interaction and the parametric electromagnetic pumping in an active conjugating medium. To select the necessary harmonic, it is sufficient to set the relationship between the pumping frequency f_p and the chosen frequency component f of the conjugate wave that is common to the parametric method: $f_p = 2f$. We measured and numerically simulated the axial and focal distributions of sound pressure in both incident and conjugate beams. A good agreement of the calculated and experimental data is obtained, and the reconstruction of the field of the second harmonic of the incident wave in the conjugate wave is demonstrated. It is shown that, in the case of phase conjugation of the second harmonic of a focused beam, it is possible to reduce to a certain extent the level of side peaks in the phase-conjugation focusing, as compared to the case of using a double-frequency incident wave.

A simplified experimental scheme is given in Fig. 2. A Panametrics M307 focusing transducer with a diameter of 27 mm and a focusing distance of 84 mm generated an ultrasonic pulse with a duration of 30 μs and a carrier frequency $f = 3$ MHz into the water filling a basin.[1] The wave excited by the source was sufficiently intense, and the generation of higher harmonics ($2f$, $3f$, etc.) occurred in the course of its propagation. A special filter was used in the generation circuit to minimize spurious emission by the transducer of the second harmonic. The level of the second harmonic at the distances 20–25 mm from the source did not exceed –35 dB of the first harmonic level, which agrees well with calculations for the case of a purely monochromatic radiation. A phase-conjugating element made of a special magnetostrictive ceramic in the form of a cylinder with a diameter of 36 mm and a length of 150 mm was fixed in a hole in the basin wall coaxially with the source at a

[1] Here, the focusing distance is understood as the so-called geometric-optical focusing distance. The real point of the maximal pressure amplitude is more shifted towards the source, the lower the radiation frequency is.

distance of 206 mm from it.[2] The design and operation of the utilized phase-conjugating system were described earlier (e.g., in [2, 3]). A system of concentric grooves was made on the working surface of the active element to extend the angular operation range of the system and to improve the quality of phase conjugation (see [10, 11]). The phase conjugation for the second harmonic of the incident wave was performed with the help of parametric pumping. It was a pulse of alternating magnetic field with a duration of 50 μs and with the carrier frequency $2 \times 2f = 12$ MHz. The field was produced by a special coil in the direction along the axis of the phase-conjugating element at the moment when the pulse of the incident wave arrived at the element. The amplitude of the resulting conjugate wave (with the frequency $2f = 6$ MHz) was in its turn sufficient for an intense generation of harmonics ($4f$, $6f$, $8f$, …) in the course of propagation, which is of interest for many practical applications. The acoustic fields of the incident and conjugate beams were measured by a broadband PVDF membrane hydrophone, which was moved both along the beam axis and across it. The diameter of the sensitive element of the hydrophone was 0.5 mm. In the course of the measurements, a given part of the wave packet was monitored along the axis with the help of the corresponding delay of the analysis interval. The signal from the hydrophone was amplified and measured by a "Tektronix" TDS 340A digital oscilloscope, where the averaging over 32 samples and the fast Fourier transformation were performed. After that, the data arrays were fed to a computer.

The simulation was conducted on the basis of the numerical solution of the KZK equation in the time domain [12]. The nonlinear propagation of the incident wave to the phase-conjugating element was calculated on the assumption of piston radiation. The second harmonic of the frequency spectrum ($2f$) was separated in the operating plane of the element with the help of the Fourier transformation, and the values of the Fourier components beyond the system aperture were assumed to be equal to zero. The complex conjugate field of the second harmonic was transformed back into the time domain taking into account the system gain obtained in the experiments. Then, the nonlinear propagation of the inverted and amplified wave toward the source was calculated.

The results of the measurements and the corresponding calculations are shown in Figs. 3–6. Figure 3 presents (a) the axial and (b) the transverse distributions of pressure in the incident beam. A transverse scanning was performed at the point $z = 82$ mm, where the maximum of the second harmonic of interest was located. The measurements agree with calculations rather well, and the dependences are typical of a focused beam with a finite amplitude. The generation of higher harmonics

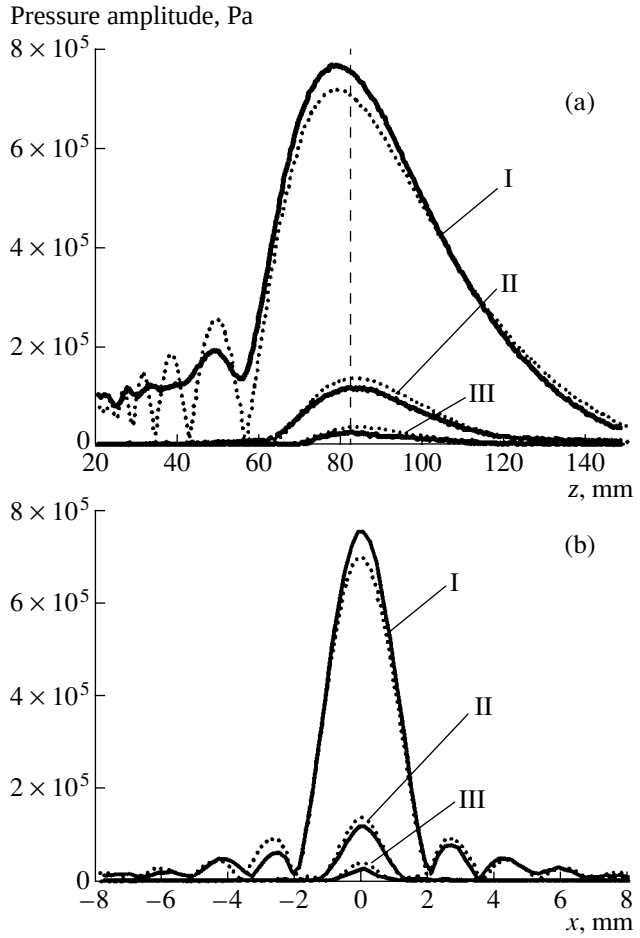

Fig. 3. Distribution of pressure amplitudes for the first three harmonics in the incident beam (a) along the axis and (b) across the beam, at the focus of the second harmonic; z is the distance from the source and x is the distance from the beam axis. The solid lines correspond to the experiment and the dotted lines, to the calculation. The numbers I–III are those of harmonics with the frequencies $f = 3$ MHz, $2f = 6$ MHz, and $3f = 9$ MHz, respectively. The dashed line indicates the position of the transverse scanning plane.

is observed, and their amplitudes increase with the distance and reach their maximum near the focus. The width of the principal maximum in the focal plane and the relative level of side components decrease as the harmonic index grows. The time profile of the incident wave at the focal point had characteristic nonlinear distortions, and the amplitudes of the harmonics $2f$, $3f$, and $4f$ were 15.6, 3.5, and 2.8%, respectively, of the amplitude of the first harmonic.

Figure 4 shows the measured distributions of the fundamental harmonic of the conjugate wave (the frequency $2f$) in comparison with the incident wave component to be conjugated (the second harmonic). One can see that, on the whole, the conjugate wave reproduces the field of the second harmonic of the incident wave. The conjugate beam is focused. The width of the focal maximum of the fundamental component of the

[2] The distance was selected in such a way that the incident beam completely falls within the aperture of the conjugating element in the geometric approximation.

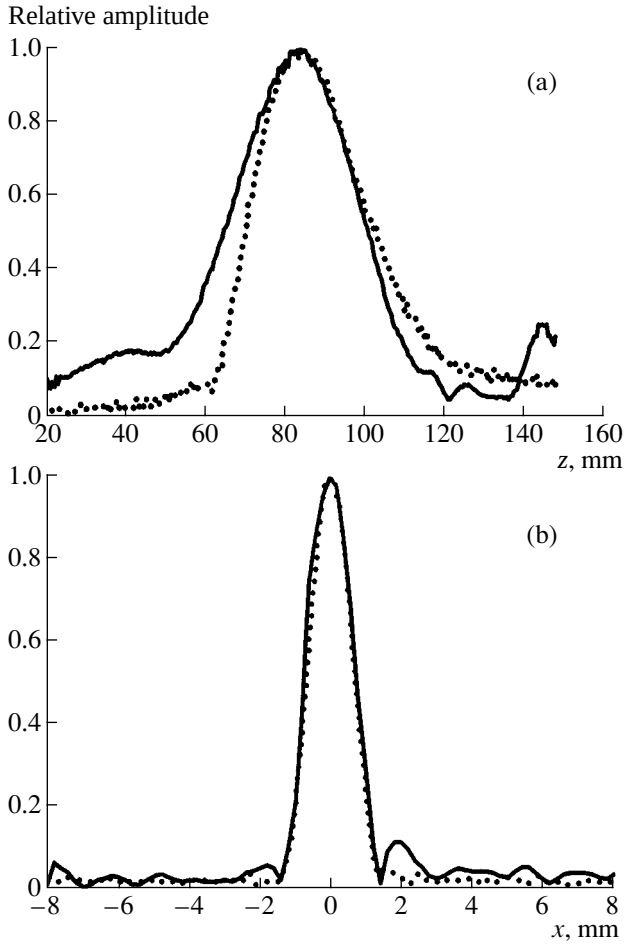

Fig. 4. Comparison of the fields of the fundamental harmonic of the conjugate wave and the second harmonic of the incident wave (a) along the beam axis and (b) across the axis at the point $z = 82$ mm. The solid line corresponds to the conjugate wave and the dashed line, to the second harmonic of the incident wave.

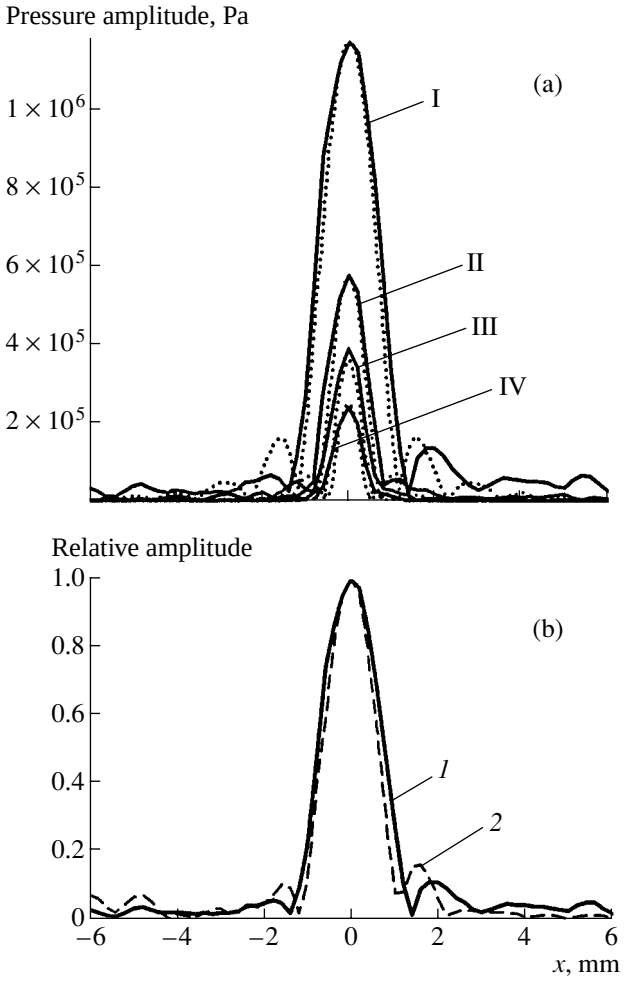

Fig. 5. Transverse pressure distribution in the conjugate beam at $z = 82$ mm. (a) Harmonic amplitudes. The solid lines correspond to the experiment and the dashed lines, to the calculation. The numbers I–IV are those of harmonics with the frequencies $2f = 6$ MHz, $4f = 12$ MHz, $6f = 18$ MHz, and $8f = 24$ MHz, respectively. (b) Comparison of the experimental data on the phase-conjugation focusing with the use of conjugation of the first and second harmonics: (*1*) the second harmonic of the incident wave is conjugated ($2f = 6$ MHz) and (*2*) the fundamental harmonic of the linear incident wave with a frequency of 6 MHz is conjugated.

conjugate beam and its axial position almost do not differ from those for the second harmonic of the incident beam. Note that the resulting dependences qualitatively correspond to the analytical estimate for the Gaussian beam (Fig. 1). Figures 5 and 6 present the pressure distributions for the first four harmonics of the conjugate beam ($2f$, $4f$, $6f$, and $8f$) in the plane $z = 82$ mm and along the beam axis, respectively. One can see that the data of the focal measurements of harmonics (Fig. 5a) agree well with the numerical model. The calculated and experimental curves for the axial distributions are given separately in Figs. 6a and 6b to make it easier to see them. Being similar in general, they have certain differences, namely, the shifts of the measured maxima of the harmonics towards the source from their calculated positions. The reason for this phenomenon can be the presence of multiple internal reflections of an ultrasonic pulse in the phase-conjugating element, which are not taken into account in the model. These reflections lead to the rise of waves, including those not coupled with pumping. The indicated nonideal character of real phase-conjugating systems needs further investigation.

Figure 5b additionally presents the comparison of the focal distribution measured in the case of phase conjugation of the second harmonic ($2f = 6$ MHz) with the case when a wave with a frequency of 6 MHz is generated directly by the source. Although the curves are generally similar, the first version gives a slightly wider principal maximum with a simultaneous small reduction of the side peaks.

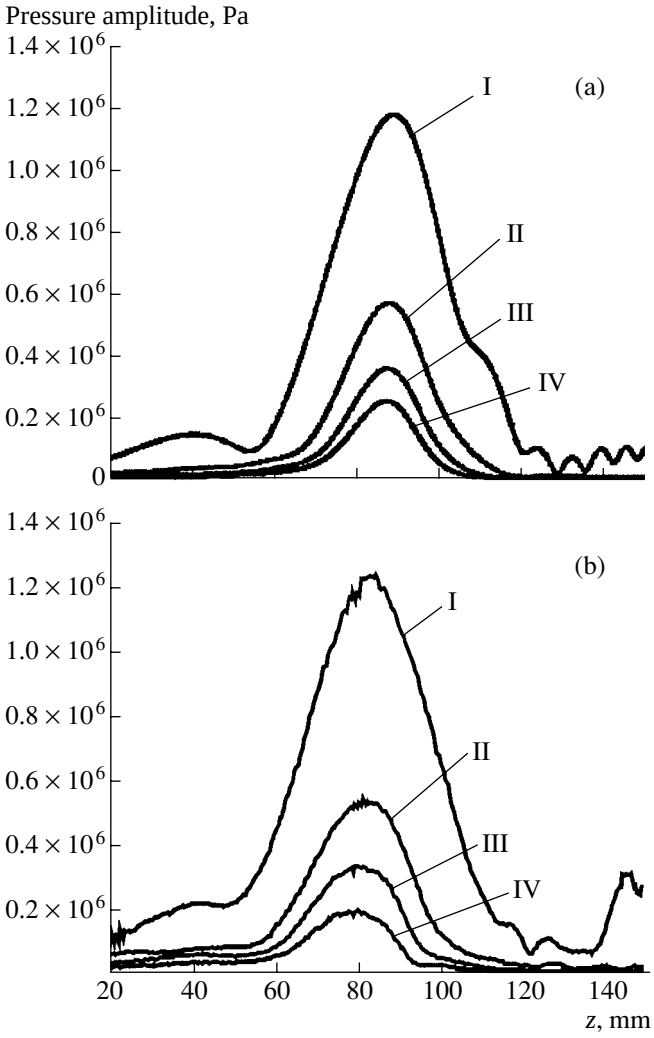

Fig. 6. Dependences of the pressure amplitudes of the first four harmonics of the conjugate beam on the longitudinal coordinate: (a) the calculation and (b) the experiment; z is the distance from the source. The numbers I–IV are those of harmonics with the frequencies $2f$ = 6 MHz, $4f$ = 12 MHz, $6f$ = 18 MHz, and $8f$ = 24 MHz, respectively.

Thus we investigated numerically and experimentally the parametric phase conjugation of the second harmonic of a focused ultrasonic beam. It was demonstrated that the field of the conjugate wave is also focused and, on the whole, adequately reproduces the field of the second harmonic of the incident wave. The data of measurements agree rather well with the results of the numerical simulation. Using phase conjugation of harmonics, it is possible to design high-resolution phase-conjugating systems for acoustic imaging. With the same frequency of the conjugate wave, the systems utilizing phase conjugation of the second harmonic can be advantageous in comparison with the utilization of the phase conjugation of the fundamental component owing to the reduction of reverberation in the course of propagation and because of the reduced relative level of side peaks in the second harmonic of the incident wave and their attenuation in the conjugate wave. In the case of a sufficient amplification of the conjugate wave that provides its nonlinear propagation back to the source, it is possible to obtain an acoustic image with a correspondingly increased resolution by using the harmonics of this wave, for example, at the fourfold frequency of the incident wave.

ACKNOWLEDGMENTS

This work was supported by the US Civilian Research and Development Foundation (CRDF, project no. RP2-2367-MO-02). The work of the Russian authors was supported in part by the Russian Foundation for Basic Research (project nos. 00-15-96636 and 02-02-16916), the French Foundation for International Programs of Scientific Cooperation (PICS 1573), and the Russian-French program PAI-RUSSIER (Dossier no. 04585TK). The work of the US authors was also supported by the US Office of Naval Research.

REFERENCES

1. L. M. Lyamshev and P. V. Sakov, Akust. Zh. **34**, 127 (1988) [Sov. Phys. Acoust. **34**, 68 (1988)].
2. A. P. Brysev, L. M. Krutyanskiĭ, and V. L. Preobrazhenskiĭ, Usp. Fiz. Nauk **168**, 877 (1998) [Phys.–Usp. **41**, 793 (1998)].
3. A. P. Brysev, F. V. Bunkin, L. M. Krutyanskiĭ, *et al.*, Pis'ma Zh. Éksp. Teor. Fiz. **61**, 454 (1995) [JETP Lett. **61**, 464 (1995)].
4. A. P. Brysev, F. V. Bunkin, A. D. Stakhovsky, *et al.*, Suppl. Phys. Vibr. **59** (1), 40 (1995).
5. K. Yamamoto, M. Ohno, A. Kokubo, *et al.*, J. Acoust. Soc. Am. **106**, 1339 (1999).
6. A. Brysev, L. Krutyansky, P. Pernod, and V. Preobrazhensky, Appl. Phys. Lett. **76**, 3133 (2000).
7. M. A. Averkiou, D. N. Roundhill, and J. E. Powers, in *Proceedings of the 1997 IEEE Ultrasonics Symposium*, Ed. by S. C. Schneider *et al.* (1997), Vol. 2, p. 1561.
8. *Nonlinear Acoustics*, Ed. by M. F. Hamilton and D. T. Blackstock, (Academic, Boston, 1998), p. 245.
9. F. V. Bunkin, D. V. Vlasov, and Yu. A. Kravtsov, Kvantovaya Élektron. (Moscow) **8**, 1144 (1981).
10. A. P. Brysev, F. V. Bunkin, L. M. Krutyanskiĭ, *et al.*, Akust. Zh. **43**, 244 (1997) [Acoust. Phys. **43**, 207 (1997)].
11. A. P. Brysev and L. M. Krutyanskiĭ, Akust. Zh. **46**, 447 (2000) [Acoust. Phys. **46**, 382 (2000)].
12. K. B. Cunningham, M. F. Hamilton, A. P. Brysev, and L. M. Krutyansky, J. Acoust. Soc. Am. **109**, 2668 (2001).

Translated by M. Lyamshev

Acoustical Physics, Vol. 49, No. 1, 2003, pp. 2–9. Translated from Akusticheskiĭ Zhurnal, Vol. 49, No. 1, 2003, pp. 6–13.

A Brief Review of L.M. Lyamshev's Work in Science (August 30, 1928–March 28, 2002)

Among the researchers working in acoustics all over the world, Leonid Mikhaĭlovich Lyamshev occupies a special place owing to his great and many-sided contribution to the development of this field of science. He is the founder of a number of areas of research that determine the state of the art in modern acoustics. Many of the results obtained by Lyamshev have become classical and were included in textbooks. His scientific career coincided with the period of global rapid progress in acoustics, and his life was interesting and full of remarkable events—the life of a scientist whose works gained worldwide recognition.

The beginning of Lyamshev's work in science dates back to 1951, when, after graduating from the Radio Faculty of Moscow Electrotechnical Institute of Communication, he became a postgraduate student of the Lebedev Physical Institute of the Academy of Sciences of the USSR. Yu.M. Sukharevskiĭ, who supervised Lyamshev's postgraduate studies, proposed that the first research project of Lyamshev be the reflection of sound from submerged shells. At that time, after World War II, work aimed at the enhancement of the defense potential of the country, including the development of the underwater fleet, was among the top priorities (not only in the USSR). The problem of protecting submarines from being detected by sonars or by way of receiving their noise was set as one of the burning problems before scientists and engineers. However, the results of the first experiments carried out by Lyamshev with shell models at the Acoustics Laboratory of the Lebedev Physical Institute proved to be rather complicated and could not be explained in terms of the acoustical concepts available at that time. Then, Lyamshev turned to the simplest models of elastic bodies in the form of rectangular plates. In this case, the experimental results also proved to be unexpected: at certain angles of sound wave incidence, a strong reflection of sound in the backward (nonspecular) direction was observed. Some time elapsed before this result was recognized as a discovery, the role of the flexural and longitudinal vibrations of plates in this effect was understood, and the whole picture of sound scattering by a plate was described mathematically. The first publication by Lyamshev [4] summarized the results of thorough research and was rather informative: it described the new physical phenomenon of nonspecular reflection and presented a complete mathematical description of it with an adequate physical interpretation. In the subsequent works by Lyamshev (see the list of his publications given below), these results were generalized to more complex elastic structures. Finally, the complicated picture of sound scattering by shells was fully understood, the physical mechanism of the spatial wave coincidence underlying this phenomenon was revealed, and a strict theory of the sound scattering by cylindrical and spherical shells was developed. Today, the scattering of sound by elastic bodies is a large and important part of structural acoustics. It is represented by several thousands of publications including several monographs. Lyamshev is deservedly considered the founder of this field of research.

The next major contribution to science made by Lyamshev is related to the proof of the reciprocity theorem. The necessity to study the specific features of sound radiation by shells (in connection with the development of passive methods of acoustic detection) drew Lyamshev's attention to the reciprocity principle. This principle could serve to relate the radiation field to the scattering field and, hence, be a handy instrument for studying sound radiation from shells by using the scattering properties studied before. However, no strict mathematical proof of the reciprocity principle existed at that time. In 1958, Lyamshev gave a new formulation of this principle and provided its strict proof on the basis of the theory of self-conjugated operators [16]. Thus, the reciprocity principle has become the reciprocity theorem. Until today, Lyamshev's formulation of this theorem is used as the most general one in the literature. Lyamshev and his students used it for studying the radiation of sound by plates and shells and generalized the results to the boundary-value problems for the fields of different nature (not only acoustic fields).

Studying the acoustic interaction of elastic bodies with a fluid, Lyamshev turned his attention to the problem of radiation and scattering of sound by shells in a moving medium. A moving medium is described by non-self-conjugate equations, and the classical reciprocity principle does not hold in this case. However, by applying the previously developed approach, Lyamshev managed to derive new integral equations relating the solutions to two conjugate problems. Later on, these equations were called the modified reciprocity theorem or the acoustic theorem of flow reversal [22]. They were used by Lyamshev to study the radiation and scattering

1063-7710/03/4901-0002$24.00

of sound by shells in a moving medium. In addition, Lyamshev generalized the notion of impedance for a moving medium [112], which allowed him to extend many results obtained for the acoustics of stationary media, e.g., the Fresnel reflection/transmission formulas, to the acoustics of moving media. These results were summarized in Lyamshev's doctoral dissertation, "Some Problems of the Scattering and Radiation of Sound in Moving Media" (Acoustics Institute, Moscow, 1964).

In parallel with the aforementioned investigations, Lyamshev studied the hydrodynamic sources of sound, i.e., the flow noise of elastic shells, which, at high speeds, is often predominant in the sound field. On the basis of the equations of the continuum mechanics, Lyamshev developed the approximate theory of a turbulent boundary layer [66] in terms of the small perturbation method. This theory explained a number of experimental results, such as the effect of the shell vibrations on the properties of the turbulent layer, the effect of the shell inhomogeneities (stiffening ribs) on the sound radiation, and other effects. These studies were performed with the aim of answering the question of whether it is possible to efficiently reduce the flow noise by controlling the boundary layer, i.e., by eliminating the fluid through gaps or pores, or, conversely, by introducing aqueous solutions of, e.g., polymers into the boundary layer. Finally, a general answer to this question was obtained. The series of comprehensive experimental and theoretical studies performed by Lyamshev together with his students in this area of research provided a substantial contribution not only to the theory of hydrodynamic sources of sound but also to the practical design of low-noise moving sea objects.

In the early 1970s, on Lyamshev's initiative and with his participation, systematic investigations of sound generation by laser radiation in liquid were started [111]. The operation principle of a laser source is based on the sound generation as a result of the interaction of optical radiation with a medium (water or some solid). Such sources have some advantages over conventional acoustic radiators (the absence of the contact with the medium, the possibility to move with any speed, etc.) and, therefore, extend the capabilities of experimental acoustics. Together with his colleagues, Lyamshev developed the theory of sound excitation by a laser beam and proposed new schemes for practical applications of such sources. At that time, he also continued the search for new applications of optical methods in acoustics. He studied the possibilities offered by the fiber-optic sound detectors and took active part in the development of laser-acoustic technologies (photoacoustic sounding of a medium, laser-acoustic microscopy, and diagnostics of deep defects) and optical systems of data processing. All this allowed Lyamshev to create a new promising direction of research—laser acoustics [2, 144].

The problem studied by Lyamshev and his colleagues in the 1980s was close to the aforementioned area of research: sound generation by penetrating radiation [167]. The studies of the radiation-acoustic effects accompanying the interaction of individual particles or particle fluxes with matter opened up new wide possibilities for the visualization and control of the internal areas of opaque materials in biology (radiation-acoustic microscopy), geology (neutrino-acoustic sounding of the Earth), astrophysics (detection of cosmic neutrinos), etc. The monograph *Radiation Acoustics* [3] written by Lyamshev summarizes the results obtained in this area of research before 1995.

The end of the cold war changed the tendencies of the development of acoustics in the world [which is confirmed by the statistics of the acoustic publications during the last 30 years: see J. Acoust. Soc. Am. **109** (5) 1779 (2001), Part 2]. In line with these changes, Lyamshev's scientific interests were shifted in the 1990s toward the basic and general physical problems of acoustics. In addition to radiation acoustics, he developed another new direction of research: fractal acoustics. He was the first to realize the important role of fractals in acoustics and showed that many experimental facts can be explained by the fractal properties of media and wave processes [175]. For example, the fractal structure of such media as various grounds, porous materials, amorphous bodies, etc., determines the velocity and attenuation of waves propagating in them, the oscillation spectra, the localization of modes, and other properties. The fractal dimension of a wind-agitated sea surface proves to be responsible for the character of the frequency–angular dependences of the scattered fields. The sound fields themselves can also exhibit fractal properties as a result of, e.g., nonlinear interaction of waves. These and related problems were the major preoccupation of Lyamshev during the last years of his life. Unfortunately, his investigations were terminated by his unexpected death. However, the work carried out by him together with his students and colleagues has made this area of research one of the most promising fields of modern acoustics.

The list of the main scientific publications by Lyamshev is presented below. It includes papers that appeared in refereed journals, such as *Doklady Rossiĭskoĭ Akademii Nauk* (Doklady Physics), *Uspekhi Fizicheskikh Nauk*, *Zhurnal Tekhnicheskoĭ Fiziki* (Technical Physics), and, naturally, *Akusticheskiĭ Zhurnal* (Acoustical Physics). The list does not contain numerous abstracts of talks given at various conferences, book reviews, reports on conferences, inventions, and popular scientific papers and books. However, the list gives a rather comprehensive idea of the fruitful scientific work of Leonid Mikhaĭlovich Lyamshev.

MAIN SCIENTIFIC PUBLICATIONS BY L.M. LYAMSHEV

Monographs

1. L. M. Lyamshev, *Reflection of Sound from Thin Plates and Shells in Liquid* (Akad. Nauk SSSR, Moscow, 1955).
2. L. M. Lyamshev, *Laser Thermooptic Excitation of Sound* (Nauka, Moscow, 1989).
3. L. M. Lyamshev, *Radiation Acoustics* (Fizmatlit–Nauka, Moscow, 1996).

Papers

4. "Reflection of Sound from a Thin Plate in Water," Dokl. Akad. Nauk SSSR **99** (5), 719 (1954).
5. "Diffraction of Sound by a Thin Bounded Plate," Akust. Zh. **1** (2), 138 (1955).
6. "Reflection of Sound from a Thin Rod in Water," Dokl. Akad. Nauk SSSR **110** (1) 48 (1956); coauthor: S. N. Rudakov.
7. "On Investigating the Field of Diverging Ultrasonic Lenses in Liquid," Akust. Zh. **2** (1), 103 (1956).
8. "Nonspecular Reflection of Sound from a Thin Cylindrical Shell," Akust. Zh. **2** (2), 188 (1956).
9. "Reflection of Sound from Thick Bounded Plates in Water," Akust. Zh. **2** (3), 281 (1956); coauthor: S. N. Rudakov.
10. "On the Theory of Sound Scattering by a Thin Rod," Akust. Zh. **2** (4), 358 (1956).
11. "Nonspecular Reflection of Sound from Thin Bounded Plates in Liquid," Acta Phys. Acad. Sci. Hung. **6** (1), 56 (1956).
12. "Diffraction of Sound by a Thin Bounded Elastic Cylindrical Shell," Dokl. Akad. Nauk SSSR **115** (2), 271 (1957).
13. "Scattering of Sound by a Thin Bounded Rod," Akust. Zh. **4** (1), 51 (1958).
14. "Diffraction of Sound by an Unbounded Thin Elastic Cylindrical Shell," Akust. Zh. **4** (2), 161 (1958).
15. "Experimental Study of the Nonspecular Reflection of Sound," Akust. Zh. **4** (3), 283 (1958); coauthor: S. N. Rudakov.
16. "On the Problem of the Reciprocity Principle in Acoustics," Dokl. Akad. Nauk SSSR **125** (6), 1231 (1959).
17. "Sound Scattering by Elastic Cylinders," Akust. Zh. **5** (1), 58 (1959).
18. "A Method for Solving the Problem of Sound Radiation by Thin Elastic Shells and Plates," Akust. Zh. **5** (4), 501 (1959).
19. "On the Theory of Sound Radiation by Thin Elastic Shells and Plates," Akust. Zh. **5** (4), 420 (1959)
20. "Calculation of the Acoustic Radiation of a Turbulent Aerodynamic Flow," Akust. Zh. **6** (4), 472 (1960).
21. "Reflection of Sound from a Moving Thin Plate," Akust. Zh. **6** (4), 505 (1960).
22. "Some Integral Relations in Acoustics of Moving Media," Dokl. Akad. Nauk **138** (3), 575 (1961).
23. "Acoustic Radiation of a Turbulent Flow in the Presence of Elastic Boundaries," Dokl. Akad. Nauk SSSR **137** (6), 1343 (1961).
24. "Sound Radiation from Elastic Shells Excited by a Turbulent Aerodynamic Flow," Akust. Zh. **7** (1), 59 (1961).
25. "Sound Radiation from Plates and Shells in Water," Akust. Zh. **7** (3), 380 (1961); coauthor: S. N. Rudakov.
26. "On Aeolian Tones," Akust. Zh. **8** (1), 91 (1962).
27. "Diffraction Theory of Noise Generated by Turbulent Flows and Boundary Layers," in Proceedings of IV International Congress on Acoustics (Copenhagen, 1962).
28. "Scattering of Sound by a Cylindrical Shell in a Moving Medium," Dokl. Akad. Nauk SSSR **152** (6), 1339 (1963).
29. "Reflection of Sound from a Cylindrical Shell in a Moving Medium," Akust. Zh. **9** (3), 329 (1963).
30. "Reflection of Sound from a Moving Elastic Rod," Akust. Zh. **9** (4), 488 (1963).
31. "On the Theory of Oscillations of Inhomogeneous Elastic Plates," Akust. Zh. **10** (1), 81 (1964).
32. "An Integral Representation of the Field of a Point Source in a Moving Medium," Akust. Zh. **10** (1), 124 (1964).
33. "Sound Reflection from an Interface between Moving Media," Akust. Zh. **10** (2), 247 (1964).
34. "Exact Theory of Sound Radiation by a Semi-Infinite Tube in a Moving Medium," in Proceedings of V International Congress on Acoustics (Liege, 1965).
35. "Effect of the Receiver Dimensions on the Results of Measuring the Spectrum of Wall Pressure Fluctuations in a Boundary Layer," Akust. Zh. **12** (2), 261 (1966); coauthor: S. A. Salosina.
36. "Diffraction of Sound by a Semi-Infinite Elastic Plate in a Moving Medium," Akust. Zh. **12** (3), 340 (1966).
37. "Scattering of Sound by a Semi-Infinite Cylindrical Shell in a Moving Medium," Akust. Zh. **13** (1), 90 (1967).
38. "Measurement of Wall Pressure Fluctuations in the Boundary Layer on a Surfacing Object," Akust. Zh. **13** (4) 591 (1967); coauthor: S. N. Rudakov.
39. "Calculation of the Sound Radiation by a Cylindrical Shell in a Flow," Akust. Zh. **14** (1), 131 (1968).
40. "The Field of a Point Source Over an Elastic Plate in a Moving Homogeneous Medium," Akust. Zh. **14** (2), 241 (1968).
41. "Calculation of the Sound Radiation at a Boundary Layer Drawoff," Akust. Zh. **14** (3), 416 (1968).
42. "Sound Transmission Through a Piezoelectric Semiconducting Plate in Liquid," Akust. Zh. **14** (3), 474 (1968).
43. "Sound Scattering by a Thin Piezoelectric Semiconducting Rod," Akust. Zh. **14** (4), 615 (1968); coauthor: V. A. Chernova.
44. "On the Theory of Sound Radiation from a Turbulent Flow Near an Inhomogeneous Elastic Plane," in Proceedings of VI International Congress on Acoustics (Tokyo, 1968).
45. "On the Spectrum of Wall Pressure Fluctuations in a Flow About a Rough Wall," in Proceedings of IV All-

Union Acoustical Conference (Moscow, 1968); coauthor: E. M. Greshilov.

46. "Spectral Characteristics of Wall Pressure Fluctuations at the Separation of the Boundary Layer Behind a Ledge on a Smooth Wall," Akust. Zh. **15** (1), 33 (1969); coauthors: E. M. Greshilov and A. V. Evtushenko.
47. "On the Spectrum and the Correlation of Wall Pressure Fluctuations in a Flow About a Rough Wall," Akust. Zh. **15** (1), 126 (1969); coauthor: E. M. Greshilov.
48. "Amplification of a Nonspecularly Reflected Wave," Akust. Zh. **15** (2), 303 (1969).
49. "Amplification of Ultrasonic Vibrations in a Nonconducting Fluid at the Interaction with a Thin Elastic Piezoelectric Semiconducting Layer," Akust. Zh. **15** (3), 460 (1969).
50. "On the Theory of Cavitation Hydrodynamic Noise," Akust. Zh. **15** (4), 572 (1969).
51. "Amplification and Absorption of Acoustic Waves at Their Reflection from a CdSe Crystal in Water," Dokl. Akad. Nauk SSSR, **194** (5), 1049 (1970).
52. "Effect of Polymer Additives on the Pressure Fluctuations in a Boundary Layer," **16** (1), 75 (1970); coauthor: I. F. Kadykov.
53. "On the Problem of Evaluating Acoustic Radiation at a Slot Drawoff of a Boundary Layer," Akust. Zh. **16** (1), 158 (1970).
54. "On the Amplification of Surface Waves," Akust. Zh. **16** (2), 319 (1970).
55. "Amplification of Acoustic Waves in a Nonconducting Ideal Fluid at Their Interaction with Piezoelectric Semiconducting Plates and Shells," in Proceedings of Acoustics Institute, issue 10, 149 (1970).
56. "Reflection of Ultrasonic Waves from a CdSe Crystal in Water," Akust. Zh. **17** (1), 74 (1971); coauthor: Yu. V. Kurilkin.
57. "Acoustics of a Controlled Boundary Layer," in Proceedings of VII International Congress on Acoustics (Budapest, 1971).
58. "On the Approximate Theory of the Cavitation Hydrodynamic Noise," in Proceedings of VII International Congress on Acoustics (Budapest, 1971).
59. "Noise of a Controlled Boundary Layer at a Drawoff and an Injection of the Fluid," in Proceedings of VII All-Union Acoustical Conference (Leningrad, 1971).
60. "Effect of Polymer Additives on the Boundary Layer Noise," in Proceedings of VII All-Union Acoustical Conference (Leningrad, 1971).
61. "Pressure Fluctuations in the Flows of Dilute Polymer Solutions Along Rough Boundaries," Dokl. Akad. Nauk SSSR, **207** (6) 1288 (1972); coauthors: E. M. Greshilov and A. V. Evtushenko.
62. "On the Methods of Evaluating the Efficiency of Ultrasonic Cleaning Systems (A Review)," Akust. Zh. **18** (3), 337 (1972); coauthors: V. A. Agranat and L. B. Gutnova.
63. "On the Choice of the Reference Contamination for Evaluating the Efficiency of Ultrasonic Cleaning Systems," Akust. Zh. **18** (3), 464 (1972); coauthors: V. A. Agranat and L. B. Gutnova.
64. "Noise of a Controlled Boundary Layer," Morskoe Priborostroenie (Akustika), No. 1 (1972).
65. "Correlation and Spectral Characteristics of Flow Pressure Fluctuations Under a Distributed Drawoff of a Turbulent Boundary Layer," Dokl. Akad. Nauk SSSR **213** (3), 544 (1973); coauthors: M. G. Puzino and S. A. Salosina.
66. "Acoustics of a Controlled Boundary Layer," Vestn. Akad. Nauk SSSR, No. 7, 22 (1973).
67. "Some Features of the Effect of Polymer Additives on the Pressure Fluctuations in a Boundary Layer," Inzh.-Fiz. Zh. **25** (6), 999 (1973); coauthors: E. M. Greshilov, A. V. Evtushenko, and N. L. Shirokova.
68. "A Possibility of an Amplification of Elastic Waves at their Reflection from the Free Boundaries of Piezoelectric Crystals," Akust. Zh. **19** (6), 618 (1973); coauthor: N. S. Shevyakhov.
69. "Effect of a Distributed Drawoff on the Wall Pressure Fluctuations at Different Flow Regimes in the Boundary Layer," in Proceedings of VIII All-Union Acoustical Conference (Moscow, 1973); coauthors: M. G. Puzino, S. A. Salosina, and A. G. Shustikov.
70. "Reflection of Shear Waves from Flat Boundaries of Piezoelectric Semiconducting Crystals," in Proceedings of VIII All-Union Acoustical Conference (Moscow, 1973); coauthors: O. A. Kosolapova and N. S. Shevyakhov.
71. "Effect of Discrete Drawoff of the Fluid on the Pressure Fluctuations in a Turbulent Boundary Layer," Dokl. Akad. Nauk SSSR **217** (1), 44 (1974); coauthors: S. A. Salosina and A. G. Shustikov.
72. "Wall Pressure Fluctuations in the Transition Zone at a Drawoff of the Boundary Layer," Akust. Zh. **19** (2), 325 (1974); coauthors: S. A. Salosina and A. G. Shustikov.
73. "Pressure Fluctuations in a Turbulent Boundary Layer at a Discrete Drawoff of the Fluid," Akust. Zh. **19** (3), 435 (1974); coauthors: S. A. Salosina and A. G. Shustikov.
74. "Characteristics of the Pressure Fluctuations in a Turbulent Boundary Layer at a Distributed Drawoff of the Fluid," Akust. Zh. **20** (5), 733 (1974); coauthors: S. A. Salosina and M. G. Puzino.
75. "On the Theory of Sound Radiation by Plates and Shells," in Proceedings of VIII International Congress on Acoustics (London, 1974).
76. "Correlation of Pressure Fluctuations in the Flows of Polymer Solutions along Rough Boundaries," Dokl. Akad. Nauk SSSR **220** (2), 308 (1975); coauthors: E. M. Greshilov and A. V. Evtushenko.
77. "Acoustics and Protection of the Environment," Vestn. Akad. Nauk SSSR, No. 2, 78 (1975); coauthor: L. M. Brekhovskikh.
78. "Scattering of an Axial Shear Wave by a Piezoelectric Semiconducting Circular Cylinder," Akust. Zh. **21** (1), 140 (1975); coauthor: N. S. Shevyakhov.
79. "Hydrodynamic Noise and the Thoms Effect," Akust. Zh. **21** (3), 396 (1975); coauthors: E. M. Greshilov and A. V. Evtushenko.
80. "A Mechanism of Sound Radiation by a Controlled Boundary Layer," Akust. Zh. **21** (5), 805 (1975).
81. "Phenomenon of a Negative Displacement of an Ultrasonic Beam at the Reflection from a Free Boundary of a Piezoelectric Crystal," Akust. Zh. **21** (6), 951 (1975); coauthor: N. S. Shevyakhov.

82. “Sound Generation by a Vortex Moving Over an Inhomogeneous Elastic Surface,” in Proceedings of VI International Symposium on Nonlinear Acoustics (Mosk. Gos. Univ., Moscow, 1975), p. 135; coauthor: S. G. Kasoev.

83. “Sound Generation by Heat Sources,” Akust. Zh. **22** (4), 625 (1976).

84. “Sound Generation by a Turbulent Boundary Layer in a Weakly Compressible Medium at the Interaction with an Inhomogeneous Boundary,” in Proceedings of VII International Symposium on Nonlinear Acoustics (Blacksburg, 1976); coauthor: S. G. Kasoev.

85. “On the Theory of Optical Sound Generation in a Moving Medium,” Dokl. Akad. Nauk SSSR **234** (4), 814 (1977).

86. “On the Theory of Sound Generation Due to the Absorption of Laser Radiation with a Modulated Intensity in a Fluid Waveguide,” Akust. Zh. **23** (1), 91 (1977); coauthor: L. V. Sedov.

87. “Scattering of a Plane Axial Shear Wave by a Piezoelectric Semiconducting Circular Cylinder,” Akust. Zh. **23** (1), 96 (1977); coauthor: N. S. Shevyakhov.

88. “On the Theory of Optical Sound Generation in Liquids and Solids,” Akust. Zh. **23** (1), 169 (1977).

89. “Sound Generation Due to the Absorption of Modulated Laser Radiation in a Liquid Half-Space with Large-Scale Inhomogeneities of the Boundary,” Akust. Zh. **23** (2), 265 (1977); coauthor: S. G. Kasoev.

90. “On the Theory of Sound Generation in a Liquid Half-Space with a Rough Boundary Absorbing a Laser Radiation with a Modulated Intensity,” Akust. Zh. **23** (3), 411 (1977); coauthor: L. V. Sedov.

91. “Sound Generation in a Liquid by a Laser Beam Whose Intensity is Modulated by a Frequency-Modulated Signal,” Akust. Zh. **23** (4), 608 (1977); coauthor: S. G. Kasoev.

92. “On the Optical Generation of Sound in a Liquid Half-Space in the Presence of a Layer of Another Liquid at Its Boundary,” Akust. Zh. **23** (5), 788 (1977); coauthor: L. V. Sedov.

93. “On the Theory of Sound Generation by Laser Pulses in a Fluid,” Akust. Zh. **23** (6), 890 (1977); coauthor: S. G. Kasoev.

94. “Pulse Acoustic Optic Phenomena,” in Proceedings of IX International Congress on Acoustics (Madrid, 1977); coauthor: K. A. Naugol’nykh.

95. “Optical Generation of Sound In Liquid,” in Collection of Plenary Papers of IX All-Union Acoustical Conference (Moscow, 1977); coauthor: S. G. Kasoev.

96. “Reflection of Shear Waves and Beams from the Boundary of a Cubic Ferrite with a Vacuum,” in Proceedings of IX All-Union Acoustical Conference (Moscow, 1977), Vol. 8; coauthors: I. V. Barabanshchikov and N. S. Shevyakhov.

97. “Sound Generation by Laser Pulses of Arbitrary Form,” Akust. Zh. **24** (4), 534 (1978); coauthor: S. G. Kasoev.

98. “Optical Sound Generation in a Liquid Half-Space with an Inhomogeneous Surface Layer,” Akust. Zh. **24** (6), 906 (1978); coauthor: L. V. Sedov.

99. “Sound Generation by Laser Pulses,” Vopr. Sudostr., Ser. Akust., No. 10 (1978); coauthor: K. A. Naugol’nykh.

100. “Optic–Acoustic Sounding of an Inhomogeneous Condensed Medium,” Dokl. Akad. Nauk SSSR **246** (5), 1099 (1979).

101. “Study of the Thermooptic Sound Generation by Nanosecond Laser Pulses,” Pis’ma Zh. Tekh. Fiz. **5** (16), 986 (1979); coauthors: T. A. Dunina, S. V. Egerev, and K. A. Naugol’nykh.

102. “The Near Field of a Pulsed Thermoacoustic Antenna,” Akust. Zh. **25** (1), 60 (1979); coauthors: T. A. Dunina, S. V. Egerev, and K. A. Naugol’nykh.

103. “Sound Generation by Long Laser Pulses,” Akust. Zh. **25** (2), 220 (1979); coauthors: S. V. Egerev, I. B. Esipov, and K. A. Naugol’nykh.

104. “Sound Generation by Laser Radiation in a Liquid Half-Space with Two Types of Boundary Roughness,” Akust. Zh. **25** (3), 401 (1979); coauthors: S. G. Kasoev, M. G. Lisovskaya, and L. V. Sedov.

105. “Fundamentals of the Design of Acoustic Blood Flow Meters,” Akust. Zh. **25** (3), 469 (1979); coauthors: E. M. Greshilov, V. E. Mogorovskiĭ, and Ya. G. Shverida.

106. “Optical Sound Generation in a Liquid Half-Space Bordering a Solid Layer,” Akust. Zh. **25** (4), 566 (1979).

107. “On the Nonlinear Theory of the Thermal Mechanism of Sound Generation by Laser Radiation,” Akust. Zh. **25** (4), 622 (1979); coauthors: T. A. Dunina, S. V. Egerev, and K. A. Naugol’nykh.

108. “Sound Generation by a Moving Pulsed Optoacoustic Source,” Akust. Zh. **25** (6), 906 (1979); coauthor: L. V. Sedov.

109. “Optical Sound Generation,” Akust. Zh. **26** (4), 625 (1980); coauthor: K. A. Naugol’nykh.

110. “Optoacoustic Sound Sources,” in Proceedings of X International Congress on Acoustics (Plenary Lectures) (Sydney, 1980).

111. “Optoacoustic Sound Sources,” Usp. Fiz. Nauk **135** (4), 637 (1981).

112. “On the Determination of the Impedance in Acoustics of Moving Media,” Dokl. Akad. Nauk SSSR **261** (1), 74 (1981).

113. Optical Sound Generation in Liquid: The Thermal Mechanism (A Review),” Akust. Zh. **27** (1), 5 (1981); coauthor: L. V. Sedov.

114. “Optical Sound Generation: Nonlinear Effects (A Review),” Akust. Zh. **27** (6), 541 (1981); coauthor: K. A. Naugol’nykh.

115. “Some Features of Sound Generation by a Penetrating Radiation in a Solid,” Pis’ma Zh. Tekh. Fiz. **8** (19), 1189 (1982); coauthor: B. I. Chelnokov.

116. “Rayleigh Wave Generation on the Free Surface of a Homogeneous Isotropic Solid Half-Space by Pulses of Penetrating Radiation,” Pis’ma Zh. Tekh. Fiz. **8** (22), 1361 (1982); coauthor: B. I. Chelnokov.

117. “Hydrodynamic Effects at an Optical Breakdown in a Liquid,” Akust. Zh. **28** (2), 192 (1982); coauthors: T. A. Dunina, S. V. Egerev, K. A. Naugol’nykh, and A. E. Pashin.

118. "On the Theory of Sound Wave Propagation in a Moving Layered Inhomogeneous Medium," **28** (3), 367 (1982).
119. "Structure of High-Frequency Pressure Fluctuations in Water and Polymer Solution Flows," Akust. Zh. **28** (4), 474 (1982); coauthors: E. M. Greshilov, V. G. Tkachenko, and N. L. Shirokova.
120. "Sound Scattering by a Periodically Moving Plate," Dokl. Akad. Nauk SSSR **269** (2), 346 (1983).
121. "Effect of the Absorption Features of Penetrating Radiation in a Condensed Medium on the Sound Generation," Zh. Tekh. Fiz. **53** (11), 2238 (1983); coauthor: B. I. Chelnokov.
122. "The Sound Field of a Turbulent Wake," Pis'ma Zh. Tekh. Fiz. **9** (24), 1506 (1983); coauthor: A. G. Skvortsov.
123. "Fiber-Optic Sound Detectors (A Review)," Akust. Zh. **29** (3), 289 (1983); coauthor: Yu. Yu. Smirnov.
124. "Sound Generation in a Solid by Penetrating Radiation," Akust. Zh. **29** (3), 372 (1983); coauthor: B. I. Chelnokov.
125. "On the Theory of Sound Generation Due to the Absorption of a Penetrating Radiation with Modulated Intensity in a Solid Waveguide," Akust. Zh. **29** (4), 505 (1983); coauthor: B. I. Chelnokov.
126. "Study of the Erosion Activity of Acoustic Cavitation in Organic Solvents," Akust. Zh. **29** (5), 577 (1983); coauthors: B. A. Agranat, V. L. Dokuchaeva, I. A. Tulaev, and A. P. Chernov.
127. "Pressure Fluctuations in the Turbulent Boundary Layer of a Water Flow with a Gas Injection," Akust. Zh. **29** (6), 806 (1983); coauthors: B. I. Chelnokov and A. G. Shustikov.
128. "Lasers in Acoustics," in Proceedings of X All-Union Acoustical Conference: Plenary Lectures (Moscow, 1983).
129. "Some Features of Sound Generation in Liquid by Pulses of Arbitrary Shape," in Proceedings of X All-Union Acoustical Conference (Moscow, 1983); coauthor: B. I. Chelnokov.
130. "Lasers in Acoustics," Vestn. Akad. Nauk SSSR, No. 8, 97 (1984).
131. "Characteristic Features of the Dynamic Self-Diffraction of Modulated Wave Beams," Zh. Tekh. Fiz., No. 1, 341 (1984); coauthor: V. V. Zosimov.
132. "Sound Radiation by Vorticity Solitons," Pis'ma Zh. Tekh. Fiz. **10** (16), 988 (1984); coauthor: A. T. Skvortsov.
133. "Radiation-Acoustothermal Microscopy of Condensed Media," Akust. Zh. **30** (4), 563 (1984); coauthor: B. I. Chelnokov.
134. "Pressure Fluctuations in a Turbulent Boundary Layer Under the Conditions of a Continuous Medium Supply Through a Permeable Boundary," Akust. Zh. **30** (5), 668 (1984); coauthors: B. I. Chelnokov and A. G. Shustikov.
135. "Sound Radiation by Three-Dimensional Vortex Singularities (Vortons)," Akust. Zh. **30** (6), 843 (1984); coauthor: A. T. Skvortsov.
136. "Sound Radiation by the Wall Turbulence," Pis'ma Zh. Tekh. Fiz. **11** (8), 686 (1985); coauthor: A. T. Skvortsov.
137. "Fiber-Optic Measuring Hydrophone," Akust. Zh. **31** (1), 140 (1985); coauthor: Yu. Yu. Smirnov.
138. "Thermooptic Sound Generation Under a Fully Developed Surface Evaporation," Akust. Zh. **31** (2), 277 (1985); coauthors: S. V. Egerev, K. A. Naugol'nykh, A. E. Pashin, and V. N. Uchastnov.
139. "The Use of Active Media in Measuring Sound Fields and Quantum Noise," Akust. Zh. **31** (3), 409 (1985); coauthor: V. V. Zosimov.
140. "A Mechanism of Underwater Acoustic Noise Generation in a Calm Ocean," Akust. Zh. **31** (5), 709 (1985); coauthors: A. V. Furduev, B. I. Chelnokov, and V. I. Yakovlev.
141. "Study of Small Ultrasonic Vibrations by the Methods of Optical Dynamic Holography," Dokl. Akad. Nauk SSSR **290** (5), 1095 (1986); coauthors: Yu. S. Barmenkov, V. V. Zosimov, N. M. Kozhevnikov, and S. A. Sergushchenko.
142. "Reflection of a Transverse Wave from a Piezoelectric–Semiconductor Interface Under the Conditions of an Acoustic Contact," Akust. Zh. **32** (2), 198 (1986); coauthor: N. S. Shevyakhov.
143. "Study of Acoustic Fields by the Methods of Holography and Nonlinear Optics (A Review)," Akust. Zh. **32** (6), 721 (1986); coauthor: V. V. Zosimov.
144. "Lasers in Acoustics," Usp. Fiz. Nauk **151** (3), 479 (1987).
145. "Detection of the Phase Modulation Signal of a Fiber-Optic Interferometer With the Help of a Dynamic Hologram in Bacteriorhodopsin," Akust. Zh. **33** (3), 569 (1987); coauthors: Yu. O. Barmenkov, V. V. Zosimov, N. M. Kozhevnikov, O. I. Kotov, and V. M. Nikolaev.
146. "Wave Conjugation in the Sound Scattering by a Pulsating Cylinder," Akust. Zh. **33** (4), 716 (1987); coauthor: P. V. Sakov.
147. "On the Problem of Sound Generation in a Solid by a Moving Thermoacoustic Source of Radiation Origin," Akust. Zh. **33** (6), 1083 (1987); coauthor: B. I. Chelnokov.
148. "Wave Conjugation in the Nonlinear Sound Scattering by a Pulsating Cylinder," Dokl. Akad. Nauk SSSR **299** (6), 1382 (1988); coauthor: P. V. Sakov.
149. "Photorefractive Sensitivity of Polymer Films Containing Bacteriorhodopsin," Zh. Tekh. Fiz., No. 4, 833 (1988); coauthors: N. G. Abdulaev, Yu. O. Barmenkov, S. Yu. Zaitsev, *et al.*
150. "Wave Conjugation in the Nonlinear Scattering of Sound by a Pulsating Sphere," Akust. Zh. **34** (1), 127 (1988); coauthor: P. V. Sakov.
151. "Boundary Condition for the Problems of Nonlinear Sound Scattering from an Acoustically Stiff Surface," Akust. Zh. **34** (2), 355 (1988); coauthor: P. V. Sakov.
152. "Nonlinear Interaction of Plane and Spherical Waves," Akust. Zh. **34** (3), 485 (1988); coauthor: P. V. Sakov.
153. "Sound Radiation by Localized Vortices in a Weakly Compressible Medium (A Review)," Akust. Zh. **34** (5), 769 (1988); coauthor: A. T. Skvortsov.
154. "Propagation of Acoustic Pulses under Their Forced Acoustic Interaction on the Way through Fiber Light Guides," Izv. Akad. Nauk SSSR **53** (8), 1520 (1989).

155. “Sound Scattering by a Vortex Soliton in an Axially Symmetric Flow with a Velocity Shift,” Akust. Zh. **35** (3), 477 (1989); coauthor: A. T. Skvortsov.

156. “Sound Scattering by Three-Dimensional Point Vortices,” Akust. Zh. **35** (5), 805 (1989); coauthors: A. E. Golovchanskaya and A. T. Skvortsov.

157. “Fiber-Optic Intensity Meter,” Akust. Zh. **35** (6), 1087 (1989); coauthor: Yu. Yu. Smirnov.

158. “Laser Pulse Optoacoustics of Condensed Nonhomogeneous Matter,” in Proceedings of XIII International Congress on Acoustics (Belgrade, 1989), Vol. 4, p. 229; coauthors: S. V. Egerev, K. A. Naugol’nykh, and O. V. Puchenkov.

159. “Laser Dynamic Optoacoustic Diagnostics of Condensed Media,” Usp. Fiz. Nauk **160** (9), 111 (1990); coauthors: S. V. Egerev and O. V. Puchenkov.

160. “Sound Radiation Due to the Collapse of a Localized Density Disturbance in a Stratified Liquid,” Akust. Zh. **36** (1), 36 (1990); coauthors: A. N. Kopysov and A. T. Skvortsov.

161. “Sound Scattering by Potential Flows,” Akust. Zh. **36** (2), 368 (1990); coauthors: A. E. Golovchanskaya and A. T. Skvortsov.

162. “Scattering of Sound Waves by a Localized Inhomogeneity of Magnetic Field,” Akust. Zh. **36** (3), 503 (1990); coauthor: A. T. Skvortsov.

163. “Fiber-Optic Polarization Detector of Sound Pressure Gradient,” Akust. Zh. **36** (3), 563 (1990); coauthor: Yu. Yu. Smirnov.

164. “Optoacoustic Sources in an Oceanic Experiment,” Akust. Zh. **36** (5), 807 (1990); coauthors: S. V. Egerev and K. A. Naugol’nykh.

165. “Wave Field Structure of a Transverse Wave at a Moving Domain Boundary in a Ferroelectric and a Ferrite,” Akust. Zh. **37** (6), 1170 (1991); coauthor: N. S. Shevyakhov.

166. “Transverse Waves Associated with a Moving Domain in a Ferroelectric Crystal,” Pis’ma Zh. Tekh. Fiz. **17** (17), 13 (1991); coauthor: N. S. Shevyakhov.

167. “Radiation Acoustics,” Usp. Fiz. Nauk **162** (4), 43 (1992).

168. “Nonlinear Scattering of Sound by a Pulsating Sphere,” Akust. Zh. **38** (1), 100 (1992); coauthor: P. V. Sakov.

169. “Radiation Acoustics and Its Applications (A Review),” Akust. Zh. **38** (2), 197 (1992).

170. “Amplification of the Backscattering of a Sound Wave at an Arbitrarily Oriented Thin Plate in Liquid,” Akust. Zh. **38** (5), 874 (1992); coauthors: F. M. Ismagilov and Yu. A. Kravtsov.

171. “Reciprocity Principle and Its Applications in Underwater Acoustics,” in Proceedings of XIV International Congress on Acoustics (Beijing, 1992), Vol. 1 (Plenary Lectures), p. 5.

172. “Chaotic and Fractal Dynamics,” Usp. Fiz. Nauk **164** (2), 239 (1994).

173. “Fractals and Scaling in Acoustics (A Review),” Akust. Zh. **40** (5), 709 (1994) [Acoust. Phys. **40**, 627 (1994)]; coauthor: V. V. Zosimov.

174. “Fractals in the Problem of Noise and Vibration,” in Proceedings of II International Symposium on Noise and Vibration Control in Transportation (St. Petersburg, 1994), Vol. 1, p. 75.

175. “Fractals in Wave Processes,” Usp. Fiz. Nauk **165** (5), 361 (1995); coauthor: V. V. Zosimov.

176. “Distributed Fiber-Optic Acoustic Detectors (A Review),” Akust. Zh. **41** (4), 533 (1995) [Acoust. Phys. **41**, 467 (1995)]; coauthor: Yu. Yu. Smirnov.

177. “Fractals in Acoustics,” in Proceedings of XV International Congress on Acoustics (Trondheim, 1995), Vol. 1 (Plenary Lectures), p. 129.

178. “Optoacoustics and Acoustooptics of Penetrating Radiation,” J. Acoust. Soc. Am. **100** (4), 2625 (1996), Part 2; coauthor: M. L. Lyamshev.

179. “A Laser Thermooptical Sound Source at a Fractal Surface,” Akust. Zh. **42** (5), 667 (1996) [Acoust. Phys. **42**, 588 (1996)]; coauthor: M. L. Lyamshev.

180. “Sound Emission by Plane Layered Elastic Structures,” Akust. Zh. **42** (6), 819 (1996) [Acoust. Phys. **42**, 723 (1996)].

181. “Optoacoustic Remote Control Channel for Underwater Oceanological Instruments,” Okeanologiya **36** (2), 314 (1996); coauthors: S. V. Egerev, A. K. Morozov, and A. E. Pashin.

182. “Radiation Acoustics: Photoacoustics of Penetrating Radiation (Plenary Lecture),” in Proceedings of 9th International Conference on Photoacoustics and Photothermal Phenomena (Nanjing, 1996), p. 4.

183. “Laser Acoustic Sound Source at a Fractal Rough Large-scale Surface,” Dokl. Ross. Akad. Nauk **356** (6), 755 (1997); coauthor: M. L. Lyamshev.

184. “Sound Radiation by Flat Layered Structures,” J. Acoust. Soc. Am. **101** (5), 3132 (1997).

185. “Laser Thermooptic Excitation of Sound in a Fractal Medium Loaded Waveguide,” Akust. Zh. **43** (6), 821 (1997) [Acoust. Phys. **43** 716 (1997)]; coauthor: M. L. Lyamshev.

186. “Fractals in Underwater Acoustics (Plenary Lecture),” in Proceedings of International Symposium on Hydroacoustic and Ultrasonics (Gdansk–Yurata, 1997), p. 251.

187. “Search for Charged Massive Particles of Dark Matter Using Sattelite-Based Acoustic Detectors,” Akust. Zh. **44** (1), 76 (1998) [Acoust. Phys. **44**, 61 (1998)]; coauthors: K. A. Kotel’nikov, G. I. Merzon, N. G. Polukhina, T. Saito, H. Sasaki, N. I. Starkov, and V. A. Tsarev.

188. “Sound Scattering by Random Volume Inhomogeneities with a Fractal Spectrum,” Akust. Zh. **44** (4), 506 (1998) [Acoust. Phys. **44**, 434 (1998)]; coauthor: Yu. P. Lysanov.

189. “An Optoacoustic Channel for Remote Control of Underwater Instrumentation Acoustics,” Acustica **3** (4), 631 (1998); coauthors: S. V. Egerev, A. K. Morozov, and A. E. Pashin.

190. “Radiation Acoustics: Photoacoustics and Acoustooptics of Penetrating Radiation,” in Proceedings of XVI International Congress on Acoustics (Seattle, 1998), Vol. 2, p. 2595.

191. “On the Fractal Nature of Low-Frequency Attenuation in the Ocean,” in Proceedings of IV European Conference on Underwater Acoustics (Roma, 1998), Vol. 1, p. 801; coauthor: Yu. P. Lysanov.

192. "On the Fractal Nature of Low-Frequency Sound Attenuation in the Ocean," Dokl. Ross. Akad. Nauk **366** (1), 36 (1999); coauthor: Yu. P. Lysanov.

193. "Nonspecular Reflection, Resonance Scattering and Radiation of Sound by Plates and Shells in Water," Akust. Zh. **45** (5), 693 (1999) [Acoust. Phys. **45**, 619 (1999)].

194. "Radiation Acoustics," Soros Educational Journal, No. 5, 98 (1999).

195. "Reflection of Transverse Waves in a Structure 'Dielectric–Piezoelectric Semiconductor with Current'," Akust. Zh. **46** (3), 373 (2000) [Acoust. Phys. **46**, 317 (2000)]; coauthor: N. S. Shevyakhov.

196. "Fractals, Chaos, and Wavelets in Underwater Acoustics," in Proceedings of X Session of the Russian Acoustical Society (Moscow, 2000), Vol. 1, p. 7.

197. "Excitation of Sound by Laser Pulses in a Liquid in the Process of Optical Breakdown," in Proceedings of XV International Symposium on Nonlinear Acoustics (Göttingen, 2000).

198. "Fractal Nature of the Sea Surface Reverberation," Dokl. Ross. Akad. Nauk **378** (5), 610 (2001).

199. "Electromagnetic-Acoustic Evaluation of the Permeability of Porous Media," Akust. Zh. **47** (1), 62 (2001) [Acoust. Phys. **47**, 50 (2001)]; coauthor: A. A. Davydov.

200. "On the Fractal Nature of Sea Surface Reverberation," Akust. Zh. **47** (2), 283 (2001) [Acoust. Phys. **47**, 236 (2001)].

201. "Fractal Laws of Sound Backscattering by Sea Surface and Bottom," Hydroacoustics **4**, 143 (2001); coauthor: A. Stepnowski.

202. "Thermooptical Excitation of Sound in Liquids by Modulated Radiation of an Unstable Cavity Laser," J. Sound Vibr. **239** (4), 885 (2001); coauthor: M. L. Lyamshev.

203. "Lasers and Accelerators in Acoustics. Radiation Acoustics: Photoacoustics and Acoustooptics of Penetrating Radiation," in Proceedings of XI Session of the Russian Acoustical Society (Moscow, 2001), Vol. 1, p. 3.

Compiled by Yu.J. Bobrovnitskiĭ
Translated by E. Golyamina

Acoustical Physics, Vol. 49, No. 1, 2003, pp. 24–30. Translated from Akusticheskiĭ Zhurnal, Vol. 49, No. 1, 2003, pp. 30–37.

Features of Underwater Acoustics from Aristotle to Our Time[1]

Leif Bjørnø

Stendiget 19, Taastrup, DK-2630 Denmark

Received August 3, 2002

Abstract—Underwater acoustics has been one of the fastest growing fields of research in acoustics. In particular, the 20th Century has taken our understanding of underwater acoustics phenomena a great step forward. The two World Wars contributed to the recognition of the importance of research in underwater acoustics, and the momentum in research and development gained during World War II did not reduce in the years after the war. The so-called cold war and the development in computer technology both contributed substantially to the development in underwater acoustics over the second half of the 20th Century. However, the very widespread field of underwater acoustic activities started nearly 2300 years ago with human curiosity about the fundamental nature of sound in the sea. From primitive philosophical and experimental studies of the velocity of sound in the sea and through centuries of successes and failures, the knowledge about underwater acoustics has developed into its high-technological status of today. In particular the development through the period from Aristotle (384–322 BC) to 1960 formed the basis for the tremendous research and development efforts we have witnessed in our time. In this paper most emphasis will be put on the development in underwater acoustics through this period of nearly 2300 years duration, and only the main trends in later research will be mentioned. © *2003 MAIK "Nauka/Interperiodica".*

Dedicated to the memory of my friend and colleague Professor L.M. Lyamshev

After my plenary lecture held at the 2nd EAA International Symposium on Hydroacoustics in Gdansk in May 1999, Professor L.M. Lyamshev asked me to write this lecture as a paper to be published in the international journal *Acoustical Physics*, for which he was editor-in-chief. I promised to do it when time allowed. Now having been asked to contribute a paper to a special memory issue of *Acoustical Physics* for Professor L.M. Lyamshev, I found that this paper, which he encouraged me to write, would be the best contribution I could give to the memory of a great acoustician, an internationally recognized scientist, and a good friend and colleague whose modest and friendly personality we shall miss in the years to come.

Underwater acoustics is one of the fastest growing fields of research in acoustics, which is reflected in the increasing number of publications per year in international journals. Underwater acoustics' relation to other fields of importance to science and technology like oceanography, meteorology, seismology, and fishery is becoming closer. Every year billions of dollars are spent on the use of underwater acoustics by the mineral industry (oil and solid mineral exploration in the sea), the communication and energy sector (cable and tube laying, survey and maintenance), the food industry (fishing), the transportation and recreation industries (navigation and safety devices), and the worlds' navies (undersea warfare). A great number of industrial companies are developing, manufacturing, and selling instruments and devices for underwater acoustics, including, for instance, instruments for the inspection and mapping of the seabed, underwater communication, control of processes in offshore activities, search and recovery missions, etc.

STUDIES OF UNDERWATER ACOUSTICS BEFORE WORLD WAR I

This comprehensive activity in underwater acoustics is based on research and development over more than two millennia, spawned by the human curiosity in the sea and its ability to carry sound waves. As far as we know today, it started with the Greek philosopher Aristotle (384–322 BC), who was the first to note that sound could be heard in water as well as in air. In 1490 the Italian scientist and artist Leonardo da Vinci (1452–1519) wrote in his notebook, "If you cause your ship to stop and place the head of a long tube in the water and place the other extremity to your ear, you will hear ships at great distances." Of course, the ambient noise level in lakes and seas was much lower during his days than today, when all kinds of ships and offshore activities pollute the seas with noise. About one hundred years later, the English philosopher Francis Bacon (1551–1626) in his work *Historia Naturalis et Experimentalis* supported the idea that water is the principal medium by which sounds originating therein reach a human observer standing nearby.

[1] This article was submitted by the author in English.

In the 18th and early 19th centuries, a few scientists became interested in sound transmitted in water. They measured the speed of sound in fresh and salt water, comparing these with the speed of sound in air, already measured by then. Their sound sources included bells, gunpowder, hunting horns, and human voices. Their own ears usually served as receivers. In 1743, J.A. Nollet conducted a series of experiments in order to prove that water is compressible. With his head underwater, he heard a pistol shot, a bell, a whistle and loud shouts. He noted that the intensity of the sound decreased little with the depth, thus indicating that the loss mostly occurred at the water surface. In 1780, Alexander Monro (1733–1817) tested his ability to hear sounds underwater. He used a large and a small bell, which he sounded both in air and in water. The bells could be heard in water, but he found that the pitch sounded lower in water than in air. He also attempted to compare the speed of sound in air and in water, and he concluded that the two sound speeds seemed to be the same.

The breakthrough in sound speed measurement came in September 1826, when the Swiss physicist J.D. Colladon (1802–1893) and the French mathematician J.K.F. Sturm (1803–1855) on Lake Geneva at a water temperature of 8°C made the first widely known measurement of the speed of sound in water. A bell hanging down from a boat was used as transmitter, and when striking the bell a flash of light was made by igniting some gunpowder. This flash could be seen by Colladon in a boat situated at a distance of about 10 miles from the transmitter. He started his watch when he saw the flash and stopped it when he heard the sound signal in the water about 10 s later. His receiver was a trumpet design with one end in the water and the other in his ear. By means of this rather primitive setup they measured the speed of sound in water at 8°C to 1435 m/s, only about 3 m/s less than accepted today [1].

During the years 1830–1860 scientists started thinking over some applications of underwater sound. Questions like “Can the echo of a sound pulse in water be used for determination of the water depth or the distance between ships?” or “Can the communication between ships be improved by underwater transmission of sound?” were posed. The frustration in relation to the use of underwater sound for depth measurements is obvious from M.F. Maury’s (1806–1873) words in chapter 12 of his book *Physical Geography of the Sea*, 6th ed. 1859, where he says, “Attempts to fathom the ocean, by both sound and pressure, had been made, but out in blue water every trial was only a failure repeated. The most ingenious and beautiful contrivances for deep-sea sounding were resorted to. By exploding petards, or ringing bells in the deep sea, when the winds were hushed and all was still, the echo or reverberation from the bottom might, it be held, be heard, and the depth determined from the rate at which sound travels through water. But though the concussion took place many feet below the surface, echo was silent, and no answer was received from the bottom.”

During the last half of the 19th Century, when the maritime world changed from sail to engine driven ships and wood was replaced by steel for ship constructions, concern was expressed about the safety of navigation in fog and the danger of collision with other ships or with icebergs. John Tyndall (1820–1893) in England and Joseph Henry (1797–1878) in the USA—in spite of the fact that they both in separate investigations found sound propagation in air to be unreliable—recommended in 1876 to the lighthouse authorities in both countries that they should adopt high-power siren warning installations for use in air at all major lighthouses. From 1873 joint experiments took place and a large-scale steam-driven siren was built at the South Foreland lighthouse in England using frequencies from 100 to 400 Hz [2]. Sound transmission conditions, however, gave rise to problems. Gradients in wind speed and in temperature over the path of sound propagation caused strong variations in the sound detection distance. This blow to underwater acoustics, therefore, did not have any serious consequences. The possible advantages of signaling by sound in water were taken up again in the late 1880s by Lucien Blake and Thomas Alva Edison (1847–1931) in the USA. Edison invented an underwater device for communication between ships, but for some unknown reasons the US government lost interest in his invention.

Submerged bells on lightships were introduced to a large extent during the last years of the 19th century. The sound from these bells could be detected at a great distance through a stethoscope or by means of simple microphones mounted on a ships hull. Moreover, when the ship was outfitted with two detecting devices, one on each side of the hull, it became possible to determine the possible bearing of the lightship by transmitting the sounds separately to the right and the left ears of the observer. Elisha Gray, working with Edison on improving the telephone, recognized that the carbon-button microphone in a suitable waterproof container could be used as a hydrophone to receive underwater bell signals (see Fig. 1).

In 1899, Gray and A.J. Mundy were granted a patent on an electrically operated bell for underwater signalling (see Fig. 2).

The commercial market now started to motivate efforts. The work by Gray and Mundy led in 1901 to the establishment of the Submarine Signal Company in Boston, USA (now part of the Raytheon Company), but the rapid development in radio communication and direction finding technology threatened the commercial market of undersea acoustic navigation devices.

In 1912, the Submarine Signal Company hired the Canadian R.A. Fessenden (see Fig. 3) to develop a sound source more efficient than the pneumatically or electrically operated bells.

Fessenden designed and built a moving coil transducer for the emission of underwater sound. The Fessenden oscillator, which was designed somewhat like

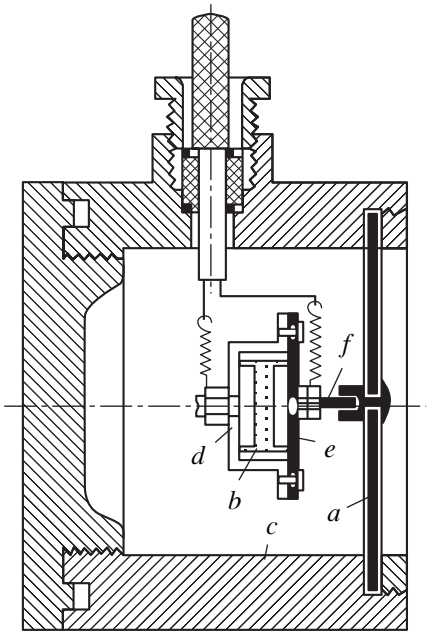

Fig. 1. Carbon-button microphone in a watertight housing.

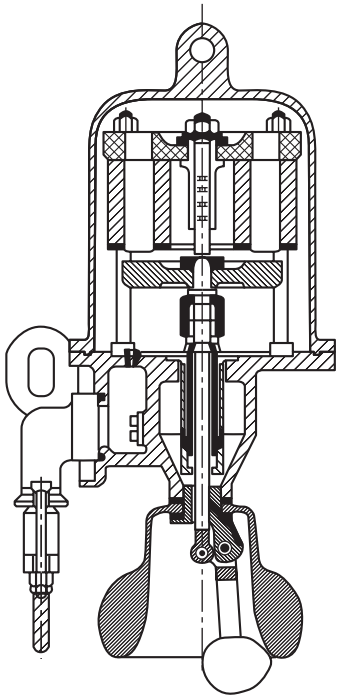

Fig. 2. Electrically driven underwater bell.

an electrodynamic loudspeaker (see Fig. 4), allowed ships to both communicate with each other by use of Morse code or to detect echoes from underwater objects. The acoustic power transmitted into the water was about 2 kW at a resonance frequency of 540 Hz, and the electroacoustic efficiency was 40–50%.

In 1914, the echo location process known as echo ranging was far enough developed to locate an iceberg at a distance of 3.2 km. This development, unfortunately, came too late to avoid the Titanic disaster.

UNDERWATER ACOUSTICS DURING WORLD WAR I

The outbreak of World War I and the later introduced unrestricted submarine warfare from the German side were the impetus for the development of a number of military applications of underwater sound. In France the Russian electrical engineer Constantin Chilowsky collaborated with the physicist Paul Langevin (1872–1946) on a project involving a condenser (electrostatic) projector and a carbon-button microphone situated at the focus of a concave acoustic mirror. In 1916 they filed an application for a patent comprising the principle of their method and their equipment. The same year they had been able to transmit an underwater signal over a distance of 3 km and to detect echoes from reflection by an iron plate at a distance of 100 m. As Chilowsky left the project after filing the patent, Paul Langevin in 1917 turned his interest to the piezoelectric effect—originally discovered by Jacques and Pierre Curie in 1880—in order to develop transmitters and receivers for undersea use. The newly developed vacuum tube amplifier was used by Langevin for his quartz receiver, and in 1918 he completed the development of his sandwich-type, steel–quartz–steel transmitter (see Fig. 5). By means of this transmitter, the range for one-way transmission was increased to more than 8 km, and clear submarine echoes were heard.

A slab of quartz was sent to Robert W. Boyle in England, who in 1916 had organized a research group

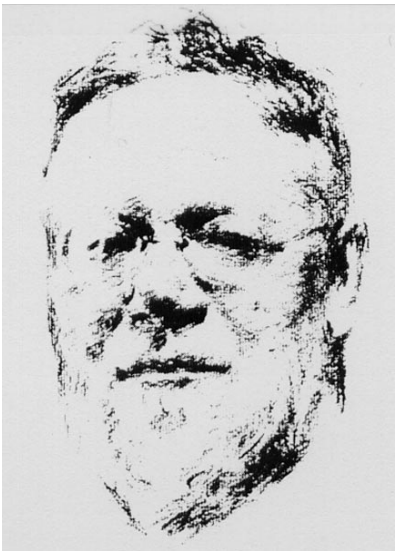

Fig. 3. Reginald A. Fessenden [3].

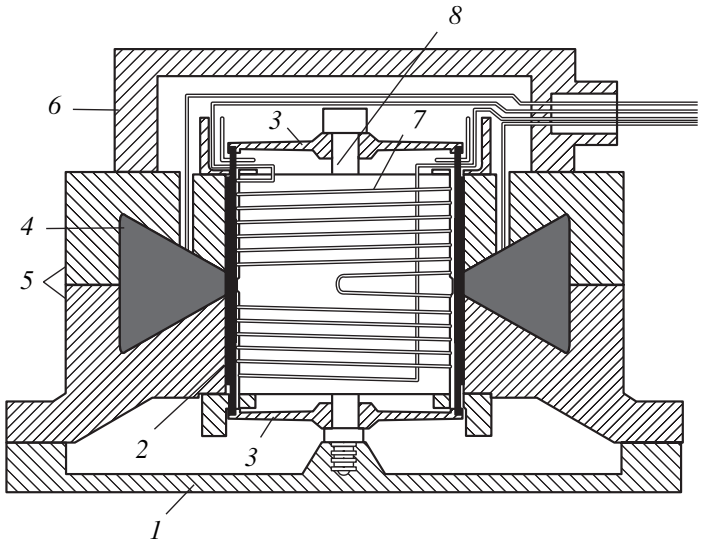

Fig. 4. A cross section of the working parts of the Fessenden oscillator. (*1*) The diaphragm is about 60 cm in diameter, (*2*) moveable copper-tube conductor, (*3*) flexible discs, (*4*) the coil, (*5*) the electromagnet, (*6*) the iron core, (*7*) turns of wire, and (*8*) steel bolt [3].

to study underwater ultrasound. His experiments with a quartz receiver were as successful as Langevin's. The name ASDIC (Anti-Submarine Detection Investigation Committee) for the underwater detection system was coined during these days. The magnitude and importance of the submarine war during World War I is reflected in the number and types of ships the British admiral Jellicoe had gathered in November 1917 when the German navy had 137 submarines. To protect convoys against German submarines a fleet consisting of the following ships was necessary: 277 destroyers, 44 P-boats, 65 submarines, 50 airships, 194 airplanes, 849 armed trawlers, 867 drifters, 338 motor launches, 68 coastal motorboats, 30 sloops, 77 decoy ships, 24 paddle minesweepers, and 49 yachts. However, submarines sunk more than 4800 merchant ships during World War I.

In the USA, Dr. Harvey Hayes had gathered a group of specialists at the Naval Experimental Station, New London, with the term of reference "to devise as quickly as possible the best of available technology to defeat a U-boat." Hayes and his group developed the towed hydrophone assembly called the Eel, and a passive sonar installation using 48 hydrophones—hull mounted and towed—was tested. This installation was the most advanced passive sonar system produced during World War I. Some US inventions made during World War I are shown in Figs. 6 and 7.

In Germany, Heinrich Hecht in Kiel developed a hydrodynamic source for underwater sound (see Fig. 8), and an electromagnetic membrane transmitter, which during the war was built into several hundred surface ships and submarines. Moreover, the German engineer Hugo Lichte (1891–1963) performed rather extensive underwater acoustic studies in which he correctly deduced the effects of temperature, salinity, and pressure on the speed of sound, and he predicted in 1919 that in deep water the upward refraction produced by pressure should produce extraordinarily long sound listening ranges. This fact was verified only many years later.

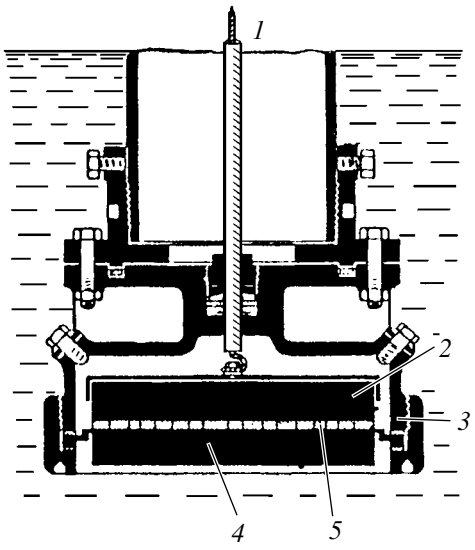

Fig. 5. Paul Langevin's piezoelectric quartz based transmitter/receiver. In spite of random variation of the quartz in the *Y* direction, but by exploiting the vacuum tube amplifier, Langevin was able in the active mode to detect submarines at distances exceeding 8 km. The transducers beam angle was 20° at a driving frequency of 38 kHz [4]. (*1*) To the a.c. oscillator and receiver; (*2*) circular steel inner electrode; (*3*) watertight container; (*4*) circular steel outer electrode; (*5*) layer of thin slices of quartz.

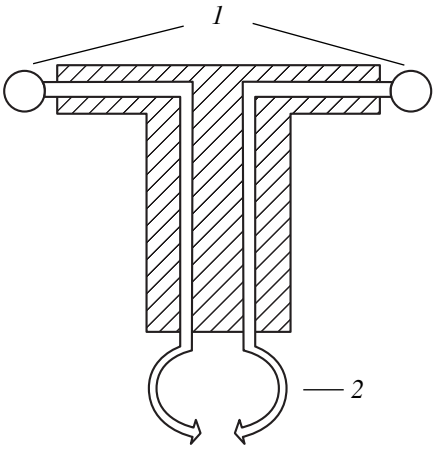

Fig. 6. A simple mechanically rotated rubber bulb stethoscope for direct listening. This device was able to record an underwater explosion at a distance of 120 km and it was mounted on patrol boats and on submarines. (*1*) Rubber bulbs; (*2*) stethoscope.

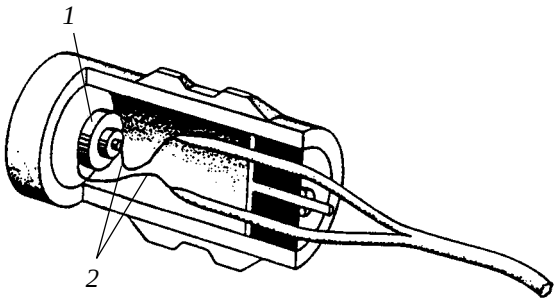

Fig. 7. A US invention from World War I was the so-called "Rat" (due to its rodentlike appearance) consisting of a rubber diaphragm and a housing forming the watertight space for a carbon-granules microphone and its electrical leads. The nonresonant diaphragm gave a broadband hydrophone, particular applicable for operation in the frequency range of 500–1500 Hz. (*1*) Carbon microphone; (*2*) electric leads.

UNDERWATER ACOUSTICS 1918–1940

During the period 1918–1940, three uses of underwater acoustics based on wartime experiences were developed extensively but slowly. They were echo sounding, sound ranging in the ocean, and seismic prospecting. A great practical impetus was received from advances in electronics, which made available new methods and devices for amplification, processing, and displaying of received underwater signals. M. Marti had in 1919 patented a recorder to be used for echo sounding. This recorder, which turned out to be of extreme importance to ocean studies using sound, consisted of a sheet of paper constrained to move slowly beneath a pen writing on the paper while traversing the paper from one side to the other in a direction perpendicular to the motion of the paper. The pen was driven laterally to the paper motion by an electric signal the amplitude of which was proportional to the output from the underwater sound receiver. Viewing side by side the successive echoes, with passage of time, a profile of the seabed could be produced. In 1922 the first long echo-sounding depth profiles were made while exploring a cable route between France and Algeria.

The need for improved and more robust high-power underwater sound sources instead of the Langevin type transducers based on quartz or Rochelle salt crystals, led G.W. Pierce in the USA, in 1925, to develop a magnetostrictive oscillator operating at 25 kHz with an emitted sound power of a few kilowatts, without the danger of fracture of the oscillating element, as frequently found by crystal based transducers.

During the same period, the US Coast and Geodetic Survey in their attempt to establish geodetic control by horizontal sound ranging was experiencing a strong variability in sound intensity and speed in the sea. Also the Naval Research Laboratory, established in 1923 on a suggestion from Edison, when seeking to improve submarine hunting, working at 20–30 kHz, found the same variability. Some of this variability appeared to show a diurnal cycle, where the equipment in the morning was working according to the specifications while in the afternoon it did not produce any echoes from submarines, except at very short ranges. The same "afternoon effect" was found in several regions of the ocean. Dr. Harvey Hayes and scientists from the newly established oceanographic institution at Woods Hole, includ-

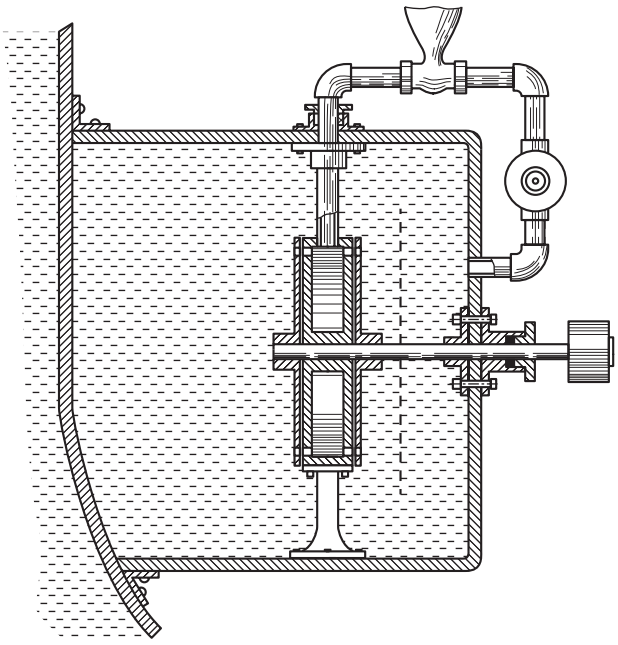

Fig. 8. The hydrodynamic siren for generation of underwater sound at frequencies around 1 kHz and with an acoustical power of up to 600 W [5].

ing the institutions head, Columbus Iselin, decided to study these phenomena in more depth.

It soon became clear that the upper parts of the ocean were heated during the day by the sun, thus leaving a layer 4.5–9 m thick with a temperature 1–2°C warmer than the more uniform water layer beneath and with a gradual decrease in temperature with distance from the surface of the sea. As the appearance of the temperature layer coincided with the deterioration of the signal reception, the scientists concluded that the warm layer caused sound entering the water to bend downward, thus producing an acoustic shadow zone in which a submarine could hide. This discovery in 1937, achieved through cooperation between acousticians and oceanographers, led to the start of a new field of research called acoustical oceanography. The same year Athelstan Spilhaus from MIT invented and build the first bathythermograph, a small torpedo-shaped device that held a temperature sensor and an element to detect changes in static water pressure. By the beginning of World War II, all US naval vessels engaged in antisubmarine work was equipped with the Spilhaus device.

The SONAR (SOund NAvigation and Ranging) developments in the years before World War II was based on exploitation of the crystals quartz, Rochelle salt, and tourmaline, along with magnetostrictive Ni–Fe alloys. Single hydrophones, as well as linear and planar arrays, were developed and tested and found their way into the major navies. A Rochelle salt-based hydrophone developed in Germany in 1935 for use onboard warships is shown in Fig. 9.

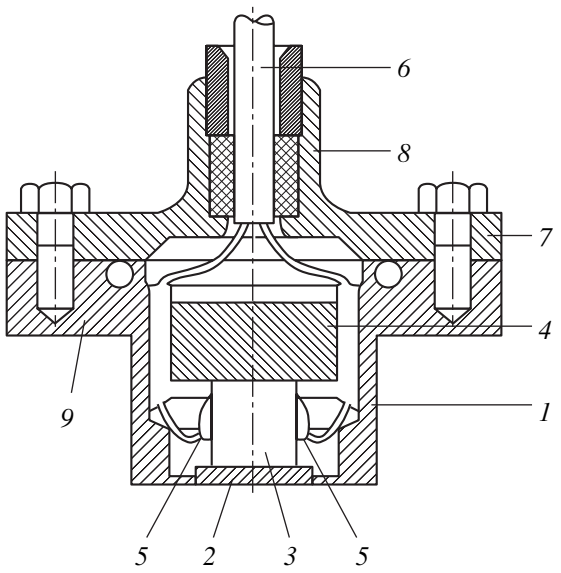

Fig. 9. The German developed Rochelle salt based Gruppen Horch Gerat GHG hydrophone used as an element in receiving arrays. (*1*) Housing, (*2*) membrane, (*3*) Rochelle salt element, (*4*) back mass, (*5*) electric connectors, and (*6*) cable. These hydrophones were carefully vibration isolated, and they were flush mounted to a ship's hull with close tolerances.

UNDERWATER ACOUSTICS DURING WORLD WAR II

The outbreak of World War II launched great activity in underwater acoustics research in Europe, USA, and the Far East. The hunt for submarines received high priority. The combination of convoys, aircraft patrols, and ASDIC gear effectively held off conventional daylight attacks by the original small number of German submarines. However, the Germans soon learned to launch night attacks on convoys using so-called "wolf-pack" techniques. The development of airborne radar, and in particular the Allied's monopoly on the 10 cm radar, became a great help in hunting down German submarines, of which Germany during the war lost 781.

Apart from the development of underwater arms like the acoustic homing torpedo, the acoustic mine, and the scanning sonar, a much better understanding of underwater factors influencing sound propagation was established. Concepts like target strength, self-noise of ships, reverberation of the underwater environment, scattering of sound and sound absorption in seawater, were established and studied. Sound propagation under the influence of vertical variation in sound speed was investigated and modeled using the "ray theory" borrowed from the theory of light. Most of the achievements in underwater acoustics during World War II were published in the USA just after the war in 23 reports called "National Defence Research Committee Division 6, Summary Technical Reports." One of these reports—entitled "Physics of Sound in the Sea"—comprises chapters on deep- and shallow-water acoustic transmission, on intensity fluctuations, and on the explosion as a source of underwater sound.

UNDERWATER ACOUSTICS FROM WORLD WAR II TO 1960

Maurice Ewing, professor of physics at Lehigh University, had during the war studied the characteristics of low frequency sound propagation in the sea, and he was convinced that it would be possible to propagate sound over hundreds—possibly thousands—of kilometers through the ocean if both source and receiver were appropriately placed. In 1945 he propagated sound from a small explosion over a distance of more than 3000 km from Eleuthera in the Bahamas to Dakar in West Africa. The sound propagation took place in a ubiquitous permanent sound channel of the deep ocean. The channel was called by Ewing the SOFAR (SOund Fixing And Ranging) channel. The first application of this discovery was aimed at providing a rescue system for downed-at-sea airmen. From his inflated rubber boat, the airman should drop small cartridges over the side set to explode on the axis of the SOFAR channel situated at some 1200 m depth in the North Atlantic.

Sound from the explosion would be refracted back to the channel axis and the propagation would only be influenced by cylindrical spreading. The signals would then be picked up by hydrophones positioned on the channel axis at various positions off the continental shelves, making it possible by comparing arrival times for the signals to find the position of the source. Not only Maurice Ewing in the USA, but also Academician L.M. Brekhovskikh in the USSR was studying the undersea sound channel, and in the years just after the war he discovered the existence of the sound channel in the Pacific Ocean by analyzing signals received from underwater explosions in the Sea of Japan.

Ewing, together with J.L. Worzel and several other colleagues at Woods Hole Oceanographic Institute, also studied long-distance sound propagation in shallow water. Based on their data, Chaim Pekeris constructed his normal mode propagation theory. The concept of elastic wave propagation has allowed underwater acousticians to model and understand the complex acoustics of shallow water. Ewing and Worzel's research also formed the basis of a series of seabed geologic structure studies performed mostly in shallow water off the East Coast of the USA. The cooperation established between Ewing's group at Columbia University and the scientists at Woods Hole Oceanographic Institute turned out to be most fruitful for underwater seismology investigations. The "refraction method" and the "continuous seismic profiler" were results of this cooperation.

A group around C.F. Eyring in San Diego, USA, had observed that diffuse echoes were received from the volume of the water column. These echoes were arranged roughly in horizontal layers whose depths were of the order of 400 m at noon, but they migrated to the surface during the twilight and the early evening. At dawn, they migrated downward to complete a daily cycle. Based on help from marine biologists it was possible to show that the responsible scatterers were small planktonic fish that have a swim bladder and living in the deep water regions of the oceans. The research into the "deep scattering layers" peaked during the period 1949–1957. Important contributions to marine bioacoustics were produced during the subsequent years.

These years also brought important research results related to sound absorption mechanisms in the sea and related to sources and spectra of ambient noise.

The comprehensive research and development efforts in underwater acoustics up to 1960 and the development in computer technology after 1960 formed the basis for the nearly explosive development in underwater acoustics from 1960 until today. Among the main trends in underwater acoustics research and development are underwater sound propagation modeling involving mode theory, parabolic equations, and finite element methods to include realistic range dependence and surface and bottom effects, reverberation studies, and ambient noise directivity studies; underwater acoustical tomography including the international Acoustic Thermometry of the Ocean Climate (ATOC) studies; and the coupling between acoustics, oceanography, and meteorology to lead to long term reliable weather forecasts, acoustical studies of biomass in the sea, and extensive bottom and subbottom studies for the exploitation of minerals, oil, and gas, as well as for cable and tube laying.

CONCLUSIONS

The development over 2300 years in underwater acoustics has shown an exponential trend. The importance of the impact of underwater warfare and military applications on the development in underwater acoustics is obvious, and this close relationship has frequently given underwater acoustics a heavy military element, which has sometimes overshadowed the many important civilian applications of underwater acoustics research results. However, the substantial civilian research and development efforts funded by the EU through several Marine Science and Technology (MAST) programs and by science foundations in many countries outside the EU have contributed to the development of large-scale research in underwater acoustics and to meeting the grand challenges of the world's oceans. The use of autonomous underwater vehicles for underwater acoustic studies of long term ocean effects and for operations in difficult accessible and hostile environments of the deep seas is only in its starting-up phase, broadband transducer technology and intelligent sensors will bring us new knowledge in the future, and the interest among scientists to use sound for investigations of the sea has never been higher. All this points to increasing research and development activity in underwater acoustics in the time to come, exploiting the valuable broad basis of knowledge in underwater acoustics created over more than two millennia.

REFERENCES

1. R. B. Lindsay, *Acoustics—Historical and Philosophical Development* (Dowden, Hutchinson, and Ross, Stroudsburg, PA, 1973).
2. J. Tyndall, *On Sound*, 3rd ed. (Appeton, New York, 1876).
3. J. B. Hersey, Oceanus **20** (2), 8 (1977).
4. M. Lasky, J. Acoust. Soc. Am. **61**, 283 (1977).
5. G. H. Ziehm, Deutsche Hydrographische Zeitschrift B, No. 20 (1988), Ergänzungsheft.
6. C. S. Clay and H. Medwin, *Acoustical Oceanography: Principles and Applications* (Wiley, New York, 1977).
7. L. M. Brekhovskikh and Yu. P. Lysanov, *Fundamentals of Ocean Acoustics* (Gidrometeoizdat, Leningrad, 1982; Springer, 1982).
8. R. J. Urick, *Principles of Underwater Sound*, 3rd ed. (McGraw-Hill, New York, 1983).
9. J. R. Apel, *Principles of Ocean Physics* (Academic, London, 1987).

Acoustical Physics, Vol. 49, No. 1, 2003, pp. 31–35. Translated from Akusticheskiĭ Zhurnal, Vol. 49, No. 1, 2003, pp. 38–42.

Resonances of the Rayleigh Waves in an Elastic Semi-Infinite Strip

M. V. Wilde* and Yu. D. Kaplunov**

** Chernyshevsky State University, ul. Astrakhanskaya 83, Saratov, 410026 Russia*
e-mail: KossovichLU@info.sgu.ru
*** Institute of Problems of Mechanics, Russian Academy of Sciences,*
pr. Vernadskogo 101-1, Moscow, 117526 Russia
e-mail: kaplunov@ma.man.ac.uk

Received December 28, 2001

Abstract—Kirchhoff's theory of plates is used to study forced harmonic vibrations of a semi-infinite strip when the latter is in the generalized stressed state or experiences flexural deformation. The forced vibrations are excited by a load applied to the strip end. Cross-boundary conditions are imposed on the strip's sides, which allows one to obtain a closed solution. The presence of an infinite real frequency spectrum corresponding to the edge resonances is revealed. The relation of these resonances to the Rayleigh planar and flexural waves is established. © *2003 MAIK "Nauka/Interperiodica".*

The edge resonance effect was first discovered in experimental studies of vibrations of a circular disk [1]. Paper [1] initiated a series of publications on the edge resonance in a semi-infinite strip with free edges [2, 3, etc.]. These works indicated that the edge resonance in a semi-infinite strip is damped by the propagating modes. A resonance with an amplitude tending to infinity was described in [4], where it was shown that, in a material with a zero Poisson ratio, coupling between propagating and evanescent waves vanishes and, in the framework of the model of a perfectly elastic body, the amplitude of vibrations tends to infinity at the frequency of the first edge resonance if the strip is excited at its end by a self-balanced load.

We assume that cross-boundary conditions are satisfied at the strip sides, which allows the separation of variables. In this case, there is no damping of the edge resonance of any index by the propagating modes, whatever value the Poisson ratio takes. We use Kirchhoff's theory of plates to study the planar vibrations of a semi-infinite strip in a generalized planar stressed state, as well as its flexural vibrations. For each of these problems, equations for the resonance frequencies are derived and shown to correspond to the dispersion relations for the Rayleigh surface waves. In the first case, this is the classical Rayleigh wave extended to the case of the generalized planar stressed state; in the second case, the flexural Rayleigh wave first obtained in [5]. It is established that the above edge resonances are caused by the accumulation of the energy of surface waves. Each of these cases is illustrated by a numerical example.

Free oscillations of a semi-infinite strip with cross-boundary conditions imposed on its sides were first considered in [6]. The eigenfrequencies obtained there coincide with those obtained by us. The problem considered in [6] played an important part in the asymptotic study of free edge vibrations of shells [7, 8].

1. GENERALIZED PLANAR STRESSED STATE

Consider a thin plate of thickness $2h$ whose middle surface lies in the xy plane in the region ($0 \le x < \infty$, $|y| \le b$) (Fig. 1). Vibrations are excited in the plate by a load applied to its end. Assume that the plate is in a generalized planar stressed state. Vibrations of a plate are then described by the following equations in the dimensionless coordinates $x_1 = \pi x/b$ and $y_1 = \pi y/b$:

$$\begin{aligned} &\frac{\partial^2 u_1}{\partial x_1^2} + \frac{1-\nu}{2}\frac{\partial^2 u_1}{\partial y_1^2} + \frac{1+\nu}{2}\frac{\partial^2 v_1}{\partial x_1 \partial y_1} + \nu_2 \lambda u_1 = 0, \\ &\frac{1+\nu}{2}\frac{\partial^2 u_1}{\partial x_1 \partial y_1} + \frac{1-\nu}{2}\frac{\partial^2 v_1}{\partial x_1^2} + \frac{\partial^2 v_1}{\partial y_1^2} + \nu_2 \lambda v_1 = 0, \end{aligned} \tag{1.1}$$

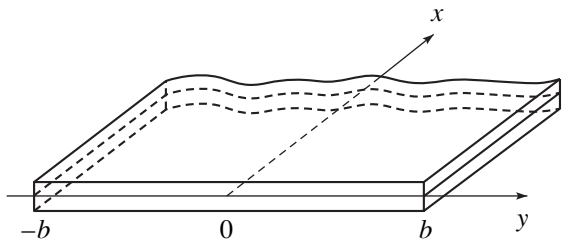

Fig. 1.

1063-7710/03/4901-0031$24.00 © 2003 MAIK "Nauka/Interperiodica"

Table 1. Resonance frequencies of planar vibrations of the plate

n	1	2	3	4	5
ω_0	0.568	1.136	1.705	2.273	2.841

where

$$\lambda = \frac{\rho\omega^2 b^2}{E\pi^2}, \quad \nu_2 = 1-\nu^2, \quad u_1 = \frac{u}{b}, \quad v_1 = \frac{v}{b},$$

λ is the dimensionless frequency parameter, ω is the circular frequency, E is the Young modulus, ν is the Poisson ratio, and u_1 and v_1 are the dimensionless displacements. The time dependence of vibrations is taken to obey the law $\exp(i\omega t)$.

Assume that the load is applied normally to the plate end and is described by the following boundary conditions at $x_1 = 0$:

$$\frac{\partial u_1}{\partial x_1} + \nu\frac{\partial v_1}{\partial y_1} = f(y_1), \quad \frac{\partial u_1}{\partial y_1} + \frac{\partial v_1}{\partial x_1} = 0. \tag{1.2}$$

At the strip sides $y_1 = \pm\pi$, the cross-boundary conditions are imposed:

$$v_1 = \frac{\partial u_1}{\partial y_1} = 0. \tag{1.3}$$

Consider the case when the load is symmetric about $y_1 = 0$. Let us represent the boundary values of the normal stress as the Fourier series

$$f(y_1) = \sum_{n=0}^{\infty} a_n \cos n y_1 \tag{1.4}$$

and seek the displacements u_1 and v_1 in the form

$$\begin{aligned} u_1 &= \sum_{n=0}^{\infty} u_n(x_1)\cos n y_1, \\ v_1 &= \sum_{n=1}^{\infty} v_n(x_1)\sin n y_1. \end{aligned} \tag{1.5}$$

It can easily be seen that representations (1.5) satisfy boundary conditions (1.3). By substituting Eqs. (1.5) into Eqs. (1.1), we obtain the system of ordinary differential equations for the functions $u_n(x_1)$ and $v_n(x_1)$:

$$\begin{aligned} &\frac{d^2 u_n}{dx_1^2} - \frac{1-\nu}{2}n^2 u_n + \frac{1+\nu}{2}n\frac{dv_n}{dx_1} + \nu_2\lambda u_n = 0, \\ &-\frac{1+\nu}{2}\frac{du_n}{dx_1} + \frac{1-\nu}{2}\frac{d^2 v_n}{dx_1^2} - n^2 v_n + \nu_2\lambda v_n = 0 \end{aligned} \tag{1.6}$$

with the boundary conditions imposed at $x_1 = 0$:

$$\frac{du_n}{dx_1} + \nu n v_n = a_n, \quad -nu_n + \frac{dv_n}{dx_1} = 0. \tag{1.7}$$

The general solution to system (1.6) can be represented as

$$\begin{aligned} u_n(x_1) &= C_1 n\exp(-r_1 x_1) + C_2 r_2 \exp(-r_2 x_1), \\ v_n(x_1) &= C_1 r_1 \exp(-r_1 x_1) + C_2 n\exp(-r_2 x_1), \end{aligned} \tag{1.8}$$

where

$$\begin{aligned} r_1 = \sqrt{n^2 - \nu_1\lambda}, \quad r_2 = \sqrt{n^2 - \nu_2\lambda}, \\ \nu_1 = 2(1+\nu). \end{aligned} \tag{1.9}$$

By satisfying boundary conditions (1.7), we obtain

$$C_1 = a_n\frac{2nr_2}{D}, \quad C_2 = -a_n\frac{r_1^2 + n^2}{D}, \tag{1.10}$$

where

$$D = 2(1-\nu)[(n^2 - (1+\nu)\lambda)^2 - n^2 r_1 r_2]. \tag{1.11}$$

Thus, the solution to the problem has the form

$$\begin{aligned} u_1 &= a_0 p_2^{-1} i\exp(-ip_2 x_1) \\ &+ \sum_{n=1}^{\infty} a_n\frac{r_2}{D}(2n^2\exp(-r_1 x_1) \\ &- (r_1^2 + n^2)\exp(-r_2 x_1))\cos n y_1, \\ v_1 &= \sum_{n=1}^{\infty} a_n\frac{n}{D}(2r_1 r_2\exp(-r_1 x_1) \\ &- (r_1^2 + n^2)\exp(-r_2 x_1))\sin n y_1, \\ p_2 &= \sqrt{\nu_2\lambda}. \end{aligned} \tag{1.12}$$

Clearly, the resonance frequencies of the problem correspond to zero values of the function D. The equation

$$D = 0 \tag{1.13}$$

can be reduced to an equation for the phase velocity of the Rayleigh waves for the case of the general planar stressed state. Dividing it by $n^4/4$ and using the notations

$$\frac{\omega b}{n\pi} = c_R, \quad \frac{E}{\nu_2\rho} = c_1^2, \quad \frac{E}{\nu_1\rho} = c_2^2,$$

we arrive at the equation

$$\left(2 - \frac{c_R^2}{c_2^2}\right)^2 - 4\sqrt{1 - \frac{c_R^2}{c_1^2}}\sqrt{1 - \frac{c_R^2}{c_2^2}} = 0, \tag{1.14}$$

which coincides with the equation for the phase velocity of the Rayleigh wave accurate to the value of the longitudinal wave velocity c_1. The first five resonance frequencies at $\nu = 0.3$ are listed in Table 1, where $\omega_0 = \sqrt{\lambda}$.

As an example, consider vibrations of the semi-infinite strip excited by the load

$$f(y_1) = \sigma_0\left(1 - \frac{y_1^2}{\pi^2}\right), \tag{1.15}$$

where σ_0 is a dimensionless constant factor. For function (1.15), the coefficients of expansion (1.4) have the form

$$a_0 = \frac{2}{3}\sigma_0, \quad a_n = \frac{4\sigma_0(-1)^{n+1}}{\pi^2 n^2}. \tag{1.16}$$

Figure 2 shows the displacement amplitude u_1 at the point (0, 0) versus frequency at $\sigma_0 = 1$. Figures 3 and 4 illustrate the energy distribution in the planar Rayleigh wave. The solid line in Fig. 3 shows the displacement u_1 versus x_1 at $y_1 = 0$ in the vicinity of the third resonance frequency ($\omega_0 = 1.703$). The dashed line shows the zero-order term of series (1.12); the dot-and-dash line represents the third-order term. Figure 4 shows the same quantities at $\omega_0 = 1.673$.

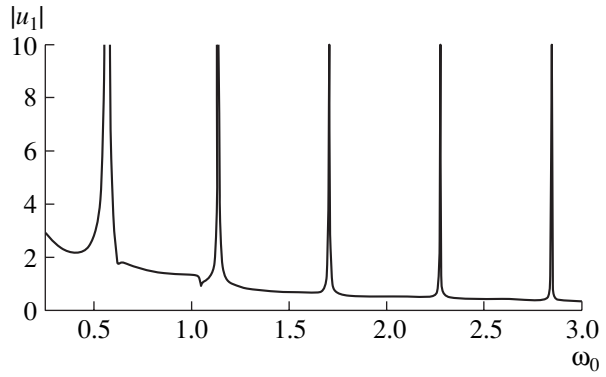

Fig. 2. Displacement amplitude u_1 versus frequency.

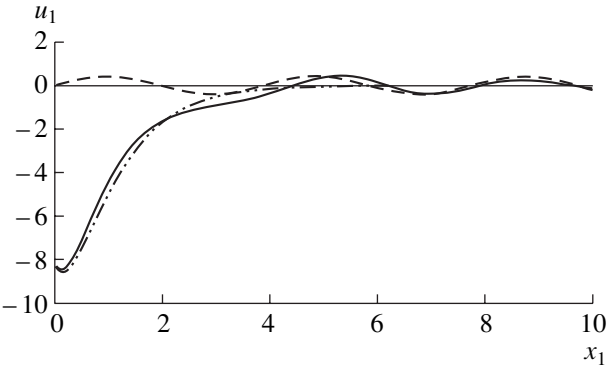

Fig. 3. Displacement u_1 in the vicinity of the third resonance frequency.

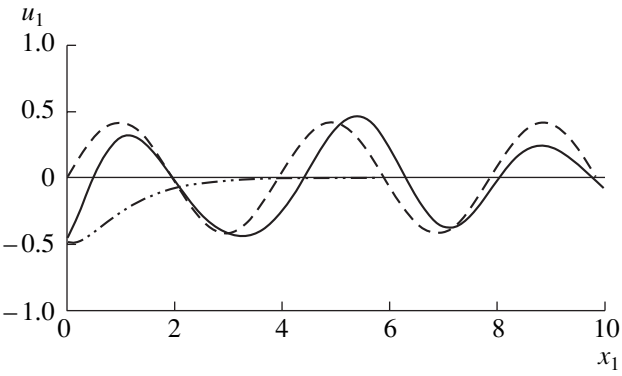

Fig. 4. Displacement u_1 far from the third resonance frequency.

2. FLEXURAL VIBRATIONS

Consider forced flexural vibrations of the semi-infinite strip illustrated in Fig. 1. Introduce the dimensionless parameter

$$\eta = \frac{h\pi}{b}. \tag{2.1}$$

Then, in the framework of the theory of Kichhoff's plates, the equation of motion (Germin's equation) takes the form

$$\frac{1}{3}\eta^2\Delta^2 w_1 - \nu_2\lambda w_1 = 0, \tag{2.2}$$

where

$$w_1 = \frac{w}{b}, \quad \Delta = \frac{\partial^2}{\partial x_1^2} + \frac{\partial^2}{\partial y_1^2},$$

w_1 is the dimensionless deflection, and Δ is the Laplacian operator. Let the vibrations be excited by the bending moment

$$\frac{\partial^2 w_1}{\partial x_1^2} + \nu\frac{\partial^2 w_1}{\partial y_1^2} = f(y_1),$$
$$\frac{\partial^3 w_1}{\partial x_1^3} + (2-\nu)\frac{\partial^3 w_1}{\partial x_1 \partial y_1^2} = 0 \tag{2.3}$$

at the strip's end $x_1 = 0$, and let the hinge-support boundary conditions

$$w_1 = \frac{\partial^2 w_1}{\partial y_1^2} = 0 \tag{2.4}$$

be imposed at its sides $y_1 = \pm\pi$. We expand the load into

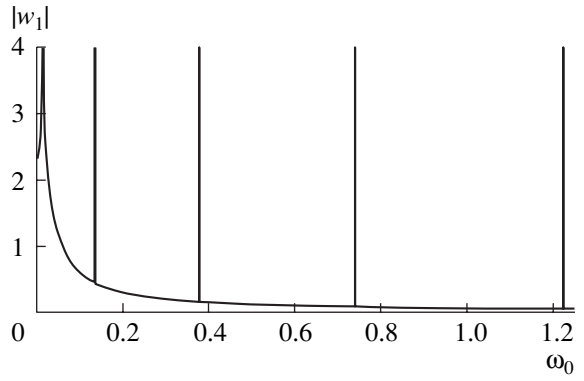

Fig. 5. Deflection amplitude versus frequency.

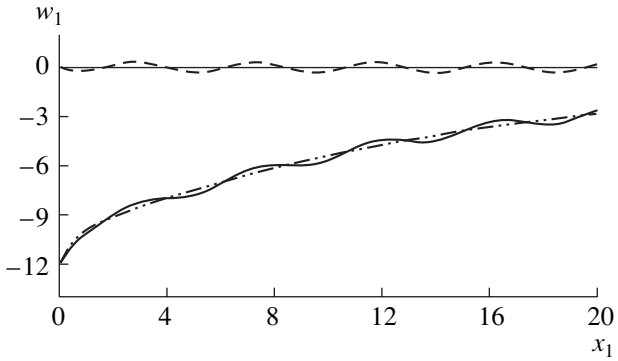

Fig. 6. Deflection in the vicinity of the second resonance frequency.

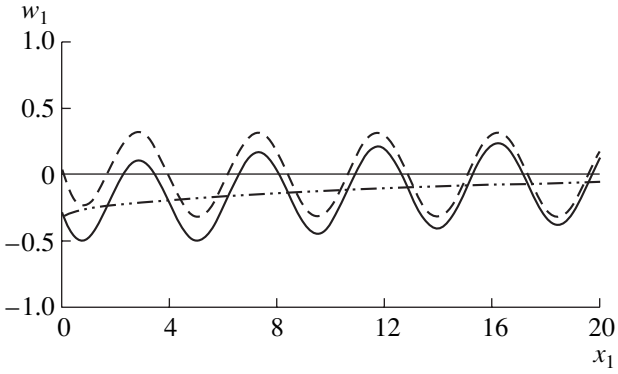

Fig. 7. Deflection far from the second resonance frequency.

a trigonometric series assuming that the function $f(y_1)$ is symmetric about $y_1 = 0$:

$$f(y_1) = \sum_{n=1}^{\infty} a_n \cos\gamma_n y_1, \quad \gamma_n = \frac{2n-1}{2}. \tag{2.5}$$

Table 2. Resonance frequencies of flexural vibrations of the plate

n	1	2	3	4	5
ω_0	0.015102	0.135918	0.377549	0.739997	1.223260

Represent the deflection as

$$w_1 = \sum_{n=1}^{\infty} w_n(x_1)\cos\gamma_n y_1, \tag{2.6}$$

and impose boundary conditions (2.4).

The differential equation and the boundary conditions for the function $w_n(x_1)$ have the form

$$\frac{1}{3}\eta^2\left(\frac{d^4 w_n}{dx_1^4} - 2\gamma_n^2\frac{d^2 w_n}{dx_1^2} + \gamma_n^4 w_n\right) - \nu_2\lambda w_n = 0, \tag{2.7}$$

$$\frac{d^2 w_n}{dx_1^2} - \nu\gamma_n^2 w_n = a_n, \quad \frac{d^3 w_n}{dx_1^3} - (2-\nu)\gamma_n^2\frac{dw_n}{dx_1} = 0. \tag{2.8}$$

Let us write the general solution to Eq. (2.7):

$$\begin{aligned} w_n(x_1) &= C_1\exp(-r_1 x_1) + C_2\exp(-r_2 x_1), \\ r_{1,2} &= \sqrt{\gamma_n^2 \mp \lambda^{1/2}\eta_1^{-1}}, \quad \eta_1 = \eta/\sqrt{3\nu_2}. \end{aligned} \tag{2.9}$$

From boundary conditions (2.8), we obtain

$$C_1 = -a_n\frac{r_2 s_1}{D}, \quad C_2 = a_n\frac{r_1 s_2}{D}, \tag{2.10}$$

where

$$D = r_1 s_2^2 - r_2 s_1^2, \quad s_{1,2} = (1-\nu)\gamma_n^2 \mp \lambda^{1/2}\eta_1^{-1}. \tag{2.11}$$

The solution to the problem has the form

$$\begin{aligned} w_1 = \sum_{n=1}^{\infty}\frac{a_n}{D}&(-r_2 s_1\exp(-r_1 x_1) \\ &+ r_1 s_2\exp(-r_2 x_1))\cos\gamma_n y_1. \end{aligned} \tag{2.12}$$

The resonance frequencies of the problem correspond to the roots of the equation $D = 0$, which can be expressed explicitly as

$$\lambda_n = \eta_1^2\gamma_n^4(1-\nu)(3\nu - 1 + 2\sqrt{(1-\nu)^2 + \nu^2}). \tag{2.13}$$

It can be shown that relationship (2.13) corresponds to the dispersion relation of the flexural Rayleigh wave [5]. Table 2 lists the first five resonance frequencies at $\nu = 0.3$ and $h/b = 0.1\pi^{-1}$.

Let the bending moment applied at the end vary as

$$f(y_1) = M_0\left(1 - \frac{y_1^2}{\pi^2}\right). \tag{2.14}$$

Then, the expansion coefficients in series (2.5) take the form

$$a_n = \frac{4M_0(-1)^{n+1}}{\pi^3}\frac{}{\gamma_n^3}. \tag{2.15}$$

Figure 5 presents the deflection amplitude at the point with the coordinates (0, 0) versus the frequency at

$M_0 = 1$. Figure 6 shows the deflection (the solid line) versus the coordinate x_1 at $y_1 = 0$ in the vicinity of the second resonance frequency $\omega_0 = 0.135915$. The dashed line represents the first-order term of series (1.12), and the dot-and-dash line, the second-order term of this series. Figure 7 shows the same quantities for $\omega_0 = 0.1358$.

Note that the resonance phenomena considered above should also be observed in anisotropic plates, because they support similar surface waves (see, e.g., [9, 10]).

ACKNOWLEDGMENTS

This work was supported by INTAS (grant no. YSF 2001/1-7) and the Russian Foundation for Basic Research (project no. 02-01-00843).

The authors are grateful to professor Yu.I. Bobrovnitskiĭ for interesting discussions that led to the idea of extending their results to forced vibrations.

REFERENCES

1. E. A. G. Shaw, J. Acoust. Soc. Am. **28**, 38 (1956).
2. P. J. Torvik, J. Acoust. Soc. Am. **41**, 346 (1967).
3. P. J. Torvik and J. J. McClatchey, J. Acoust. Soc. Am. **44**, 59 (1968).
4. V. T. Grinchenko and V. V. Meleshko, Prikl. Mekh. **16**, 58 (1980).
5. Yu. K. Konenkov, Akust. Zh. **6**, 124 (1960) [Sov. Phys. Acoust. **6**, 122 (1960)].
6. M. V. Wilde, in *Mechanics of Deformed Media* (Sarat. Gos. Univ., Saratov, 1997), issue 13, pp. 8–11.
7. J. D. Kaplunov, L. Yu. Kossovich, and M. V. Wilde, J. Acoust. Soc. Am. **107**, 1383 (2000).
8. J. D. Kaplunov and M. V. Wilde, ZAMP **51** (4), 530 (2000).
9. A. N. Norris, V. V. Krylov, and I. D. Abrahams, J. Acoust. Soc. Am. **107**, 1781 (2000).
10. M. Destrade, J. Acoust. Soc. Am. **110**, 837 (2001).

Translated by A. Khzmalyan

Acoustical Physics, Vol. 49, No. 1, 2003, pp. 36–42. Translated from Akusticheskiĭ Zhurnal, Vol. 49, No. 1, 2003, pp. 43–50.

Sound Scattering by Spatially Localized Inhomogeneities in a Shallow-Water Waveguide in the Presence of Internal Waves

V. A. Grigor'ev*, B. G. Katsnel'son*, S. A. Pereselkov*, and V. G. Petnikov**

** Voronezh State University, Universitetskaya pl. 1, Voronezh 394693 Russia*
e-mail: katz@mph.vsu.ru
*** Wave Research Center, General Physics Institute, Russian Academy of Sciences, ul. Vavilova 38, Moscow, 117333 Russia*
e-mail: petniko@kapella.gpi.ru

Received April 3, 2002

Abstract—A method is developed for solving the problem of sound scattering by concentrated inhomogeneities in a waveguide of small depth in the presence of internal waves (IW) typical of an oceanic shelf. The sound field fluctuations related to the motion of a model scatterer (a soft spheroid) and to the propagation of the IW are calculated and analyzed. It is shown that the field of internal waves considerably affects the scattered sound field even when the source–receiver and source–scatterer distances are relatively small (about several kilometers). This effect depends not only on the amplitude of the IW, but on their propagation direction as well. © *2003 MAIK "Nauka/Interperiodica".*

In view of its applied significance, the investigation of the small-angle scattering (diffraction) of sound waves in plane-layered waveguides is one of the urgent areas of development of wave theory. Some approaches to the solution of this problem are presented in a series of publications [1–7]. In particular, the expansion of the incident and scattered fields in the waveguide modes for a waveguide without a scatterer is used in [3, 5, 6]. The possibility of obtaining analytically closed expressions in the framework of this approach is related to the assumption that a scatterer is small compared with typical scales of medium variability. This allows one to consider separately the sound propagation in the waveguide and the scattering by the object. In its turn, such an approach allows one to obtain expressions for the scattered field by using the data on the scattering by the object located in a homogeneous boundless space. Although the basic results obtained in papers [5, 6] are presented for regular channels, they evidently can be generalized to the case of a smooth (adiabatic) variation of the waveguide parameters. In others words, in the framework of this approach, the single reason for sound scattering (in a waveguide, this is equivalent to mode transformations) is a scatterer (a localized inhomogeneity). However, to take into account the real properties of the medium, one has to consider other mechanisms of mode transformation in addition to the sound scattering by localized inhomogeneities. It is clear that this fact complicates the pattern of the sound diffraction in a waveguide, which imposes certain limitations on the field calculations. In particular, the problem of sound scattering by a body in a randomly inhomogeneous oceanic waveguide was considered in [7]. The combined effect of a randomly inhomogeneous medium and a scatterer on the sound field was considered in the framework of the small-angle transfer equation for the propagation and the Kirchhoff approximation for the diffraction of sound. This approach made it possible to determine the statistical characteristics of the scattered sound field.

However, in the cited paper [7], the statistical characteristics were analyzed only for the scattered field P_s but not for the total field $P_1 = P_0 + P_s$ at the point of reception, where P_0 is the incident field. In reality, we always observe the total field and, in this case, temporal fluctuations of the field P_1 are caused by the variations of P_s due to the motion of the scatterer and by the changes in the direct and scattered fields because of the fluctuations of the parameters of the medium. This paper is devoted to the analysis of the total field with consideration of the effect of the fluctuations of the parameters of the medium on the direct and scattered fields.

The fluctuations of the medium in oceanic waveguides with typical times comparable with the variations of P_s are mainly related to the presence of internal waves. However, the realizations of the internal waves described by the Garrett–Munk model (considered in [7]) are not the only possible ones for such waveguides. Such realizations are typical only for the deep ocean. In this paper, we consider examples of solving the diffraction problems in the presence of the internal waves typical of shallow water areas [8]. In this

1063-7710/03/4901-0036$24.00 © 2003 MAIK "Nauka/Interperiodica"

case, the deterministic approach is quite admissible for describing the waveguide perturbations [6]. Note also that the method used below for solving the diffraction problems allows one to analyze the fluctuations of the sound field P_1 for scatterers with small wave dimensions (compared to the sound wavelength). Such scatterers are, e.g., large sea animals of the whale family [9].

Let a waveguide be formed by a water layer with the squared refractive index $n^2(\vec{r}, z, t) = n_0^2(\vec{r}, z) + \mu(\vec{r}, z, t)$, where $\vec{r}$ is the horizontal radius vector of a point with the coordinates (x, y); t is time; and $n_0^2(\vec{r}, z)$ corresponds to an average layer stratification described by the sound velocity $c(\vec{r}, z)$, the density $\rho(z)$, and the perturbation $\mu(\vec{r}, z, t)$ of the acoustic properties of the layer due to the internal wave packet. The problem is solved in the coordinate system related to the waveguide (the xy plane coincides with the sea surface and the z axis is directed vertically downward). The water layer is bounded in depth by the free surface $z = 0$ and by a homogeneous absorbing half-space representing the bottom at $z = H(\vec{r})$. The half-space is characterized by the density ρ_1 and the squared refractive index $n_1^2 = n_d^2(1 + i\alpha)$, where α is determined by the absorbing properties of the bottom.

The spatial and temporal variations of $\mu(\vec{r}, z, t)$ are determined by the relationship [10]

$$\mu(\vec{r}, z, t) = -\frac{2\delta c(\vec{r}, z, t)}{c(\vec{r}, z)} = 2QN^2(z)\zeta(\vec{r}, z, t). \quad (1)$$

Here, $N(z) = \{(g/\rho)(d\rho/dz)\}^{1/2}$ is the frequency of buoyancy, g is the gravitational acceleration, $Q \approx 2.4$ s^2/m is a constant determined by the physical properties of water, and ζ represents the vertical displacements of the water layers. The latter quantity is expressed as

$$\zeta(\vec{r}, z, t) = \bar{\Phi}(z)\zeta_0(\vec{r} - \vec{u}t), \quad (2)$$

where $\bar{\Phi}(z)$ is the amplitude of the first gravitation mode of internal waves (IW) normalized by its maximal value, $\vec{u}$ is the speed of motion of the IW packet, and $\zeta_0(\vec{r} - \vec{u}t)$ represents the vertical displacements of the surface of the constant density at a depth where the function $\bar{\Phi}(z)$ is maximal. (The predominance of the first gravitational mode in the modal expansion of IWs is typical of shallow water.) Figure 1 shows the average equilibrium depth dependences of the sound velocity profile $c(z)$, the frequency of buoyancy $N(z)$, and the function $\bar{\Phi}(z)$ obtained from the experimental data [8] that are used in our calculations. According to Eq. (2),

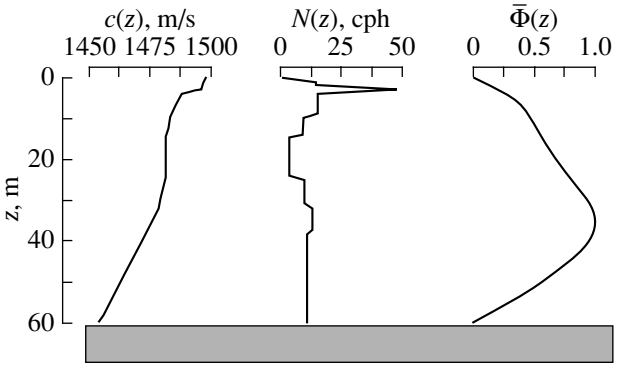

Fig. 1. Average depth dependences of the sound velocity $c(z)$, the frequency of buoyancy $N(z)$, and the first gravitational mode $\bar{\Phi}(z)$.

the wave fronts of the IW packet are assumed to be plane, which adequately describes the real IWs (the length of an almost plane IW front can be 20 to 30 km). In others words, Eq. (2) reflects the well known experimental fact that the sound velocity field in the presence of IWs in a shallow sea is anisotropic. This leads to the dependence of the sound velocity fluctuations (the refractive index) and, hence, acoustic fluctuations on the orientation of the sound propagation track, or, more precisely, on the angle between the track and the direction of the speed $\vec{u}$ in the framework of our assumption about the rectilinear character of the wave fronts. It is clear that the changes in the refractive index are most sharp when the acoustic track is directed almost at right angle to the wave fronts of the IWs. The typical scales of the spatial variability in this case can be ~200–400 m. At such distances, the sound velocity in the thermocline region can vary by 20–30 m/s. In this case, the mode interactions at distances of the order of several kilometers can be significant and must be taken into account together with the sound scattering by a localized inhomogeneity. However, our analysis will be carried out on the assumption that we may separate the processes of the sound propagation in the waveguide (even with allowance for the mode transformations) and the scattering by the object. In our case, it is possible, because the typical scales of the mode transformation (i.e., the distance at which a change in the modal composition becomes noticeable) are of several kilometers, which far exceeds the size of the scatterer.

Let us assume that the source is at the point $(\vec{r}_0, z_0)$, where $\vec{r}_0 = (0, 0)$. In this case, the field $P_0(\vec{r}, z)$ at an arbitrary point $(\vec{r}, z)$ in the sound channel that is irregular due to the presence of internal waves can be represented as the superposition of the interacting local modes (normal waves) of the channel [10]:

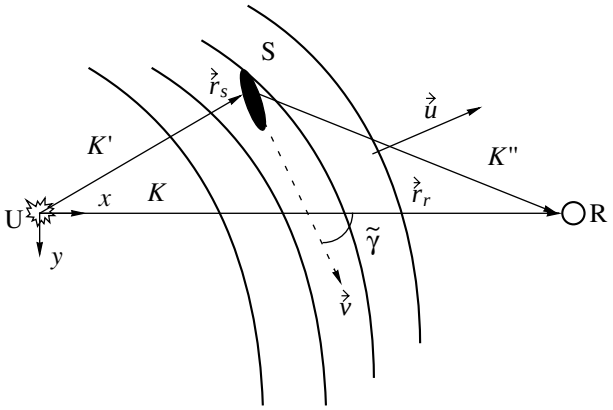

Fig. 2. Geometry of scattering: U is the source, R is the receiver, and S is the model scatterer.

$$P_0(\vec{r}, z) = \sqrt{\frac{i}{8\pi}} \sum_m^M \frac{C_m(\vec{r}_0, \vec{r})\psi_m(\vec{r}; z)}{\sqrt{q_m r}} \times \exp\left(i \int\limits_{(K_m)} q_m(s) ds \right). \quad (3)$$

Here, $\psi_l(\vec{r}; z)$ and $\xi_m = q_m + i\gamma_m/2$ are the local eigenfunctions and the eigenvalues of the unperturbed Sturm–Liouville boundary-value problem (note that the Sturm–Liouville problem is formulated differently, depending on the orientation of the sound propagation track), M is the number of the energy modes in the channel, and $C_m(\vec{r}_0, \vec{r})$ are the modal amplitudes varied in the course of the propagation. Generally speaking, the integration in Eq. (3) is performed along a horizontal curvilinear (due to the horizontal refraction) ray K_m connecting the source and the point where the field is calculated. This ray corresponds to the vertical mode of number m. The time dependence in Eq. (3) and in further expressions for the field is omitted. In connection with relatively slow variations of the medium and the scatterer position (as compared to the times of the sound wave propagation), the problem is solved on the assumption of a frozen time; in other words, the time t is a parameter that is not involved explicitly in the calculations.

The variation of the modal amplitudes $C_m(\vec{r}_0, \vec{r})$ along such a ray characterized by the current coordinate s is determined by the equation of the interacting modes:

$$\frac{dC_m}{ds} = -\frac{\gamma_m}{2} C_m + i \sum_{l=1}^M C_l V_{ml}(\vec{r}) \times \exp\left(i \int\limits_{K_m} (q_m(s') - q_l(s')) ds' \right), \quad (4)$$

with the initial conditions for $C_m(\vec{r}_0, \vec{r}_0)$ that are determined by source type. In particular, for a point sound source of the power W, the initial conditions have the form

$$C_m(\vec{r}_0, \vec{r}_0) = \sqrt{8\pi c(z_0)\rho(z_0) W}\psi_m(0; z_0). \quad (5)$$

The interaction coefficients in these equations are determined by the decomposition of the problem into an unperturbed part and a perturbation. In particular, when analyzing the sound propagation almost at right angles to the wave fronts of the IWs, the local modes are determined by the Sturm–Liouville problem

$$\frac{d^2\psi_l(\vec{r}; z)}{dz^2} + [k^2 n_0^2(\vec{r}, z) - \xi_l^2(\vec{r})]\psi_l(\vec{r}; z) = 0,$$
$$\psi_l(\vec{r}; z)\big|_{z=0} = 0,$$
$$\left[\psi_l(\vec{r}; z) + g(\vec{r}; \xi_l) \frac{d\psi_l(\vec{r}; z)}{dz} \right]_{z=H} = 0, \quad (6)$$
$$g(\xi) = \frac{\rho_1/\rho}{\sqrt{\xi^2 - k^2 n_1^2}},$$

where $k = 2\pi f/c$ is the wave vector corresponding to the sound velocity c at a certain depth and f is the sound frequency.

The perturbation responsible for the mode interactions in the case of the given direction of propagation is described by the variation of the refractive index (1). Then, the mode interaction coefficients in Eq. (4) have the form

$$V_{ml}(\vec{r}) = \frac{k^2}{2\sqrt{q_l q_m}} \int_0^\infty \frac{\rho}{\rho(z)} \psi_m(\vec{r}; z)\mu(\vec{r}; z)\psi_l(\vec{r}; z) dz. \quad (7)$$

In general, in calculating the sound field at an arbitrary point, the equations of interacting modes (4) are numerically integrated from the source to the given point along the corresponding horizontal ray. In this paper, we consider only the cases when the changes of the vertical displacements that are caused by the IWs propagating at right angles to the vector $\vec{r}$ are small and the horizontal refraction may be ignored. This means that the integration in Eq. (3) can be performed along this vector also in the case of the numerical solution of Eq. (4).

Consider next the solution of the diffraction problem (see Fig. 2). Assume that a scattering body moves in a waveguide with the constant speed $\vec{v}$ along a direct line at a constant depth. The position of the body at the instant t is determined by a conditional point connected with the body and called "the center of the body" ($\vec{r}_s(t)$, z_s). The acoustic track (the direct line connecting the source and the receiver) coincides with the x axis. Let this body cross the acoustic track under the angle $\tilde{\gamma}$. To

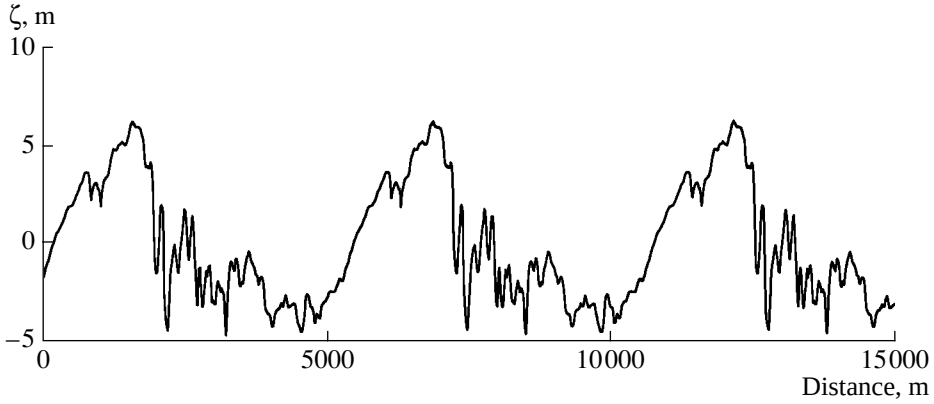

Fig. 3. Vertical displacements of liquid particles due to the internal waves.

calculate the sound field $P_0(\vec{r}_r, z_r)$ arriving at the point of reception without scattering, the field $P_i(\vec{r}_s, z_s)$ incident on the body, and the scattered field $P_s(\vec{r}_r, z_r)$ at the point of reception, we use expressions similar to Eq. (3):

$$P_0(\vec{r}_r, z_r) = \sqrt{\frac{i}{8\pi}}\sum_m^M \frac{C_m^0(\vec{r}_0, \vec{r}_r)\psi_m(\vec{r}_r; z_r)}{\sqrt{q_m r_r}} \times \exp\left(i\int\limits_{(K)} q_m(s)ds\right), \quad (8)$$

$$P_i(\vec{r}_s, z_s) = \sqrt{\frac{i}{8\pi}}\sum_m^M \frac{C_m^i(\vec{r}_0, \vec{r}_s)\psi_m(\vec{r}_s; z_s)}{\sqrt{q_m r_s}} \times \exp\left(i\int\limits_{(K')} q_m(s)ds\right), \quad (9)$$

$$P_s(\vec{r}_r, z_r) = \sqrt{\frac{i}{8\pi}}\sum_\mu^M \frac{C_\mu(\vec{r}_s, \vec{r}_r)\psi_\mu(\vec{r}_r; z_r)}{\sqrt{q_\mu|\vec{r}_r - \vec{r}_s|}} \times \exp\left(i\int\limits_{(K'')} q_\mu(s)ds\right), \quad (10)$$

where the integration is carried out along the corresponding direct lines: K between the source $(0, z_0)$ and the reception point $(\vec{r}_r, z_r)$, K' connecting the points with the coordinates $(\vec{r}_0, z_0)$ and $(\vec{r}_s, z_s)$, and K'' connecting the points $(\vec{r}_s, z_s)$ and $(\vec{r}_r, z_r)$. The modal amplitudes $C_m^0(\vec{r}_0, \vec{r}_r)$, $C_m^i(\vec{r}_0, \vec{r}_s)$, and $C_\mu(\vec{r}_s, \vec{r}_r)$ are also found from the solution to the system of equations (4), and these equations are integrated along the same direct lines K, K', and K'', respectively.

The initial conditions for the modal amplitudes $C_m^0(\vec{r}_0, \vec{r}_r)$ and $C_m^i(\vec{r}_0, \vec{r}_s)$ in Eqs. (8) and (9) are determined from Eq. (5). To write the initial conditions for the amplitudes $C_\mu(\vec{r}_s, \vec{r}_r)$, we use the results of our previous paper [6], where the expression for the matrix $S_{\mu m}$ is obtained. The latter determines the scattering of the mth normal wave of the incident field into the μth normal wave of the scattered field:

$$C_\mu(\vec{r}_s, \vec{r}_s) = \sum_m^M S_{\mu m}\frac{C_m^i(\vec{r}_0, \vec{r}_s)}{\sqrt{q_m r_s}}\exp\left(i\int\limits_{K'} q_m(s)ds\right), \quad (11)$$

where

$$S_{\mu m} = 4\pi[a_m^+ a_\mu^+ F(\vec{k}_m^+, \vec{k}_\mu^-) + a_m^+ a_\mu^- F(\vec{k}_m^+, \vec{k}_\mu^+) + a_m^- a_\mu^+ F(\vec{k}_m^- \vec{k}_\mu^-) + a_m^- a_\mu^- F(\vec{k}_m^-, \vec{k}_\mu^+)]. \quad (12)$$

Here, $a_m^\pm = \frac{1}{2}\left[\psi_m(z) \pm \frac{d\psi_m/dz}{i\sigma_m}\right]_{z=z_s}$, $\sigma_m = \sqrt{k^2 - q_m^2}$, k is the wave number, $F(\vec{k}_m^\pm, \vec{k}_\mu^\pm)$ is the scattering amplitude of the body in free space, and $\vec{k}_m^\pm$ and $\vec{k}_\mu^\pm$ are the wave vectors of the incident and scattered plane waves corresponding to the waveguide modes.

Consider now some numerical examples of the solutions of the diffraction problem using the above-mentioned relationships for the direct P_0 and scattered P_s sound fields at the point of reception. Assume that a model waveguide has the average depth dependences $c(z)$ and $N(z)$ shown in Fig. 1, its depth being $H = 60$ m, and the bottom parameters being $n_g = 0.829$, $\rho_1 = 2$ g/cm^3, and $\alpha = 0.02$. Assume also that the IW packets propagate in such a waveguide with the speed $u = 0.2$ m/s. These packets generate vertical oscillations of liquid particles at a depth of 33.5 m (Fig. 3). (The model packets of IWs were formed on the basis of the experimental data given in [8].) In the numerical experiments, we used a soft spheroid of length $L = 10$ m and

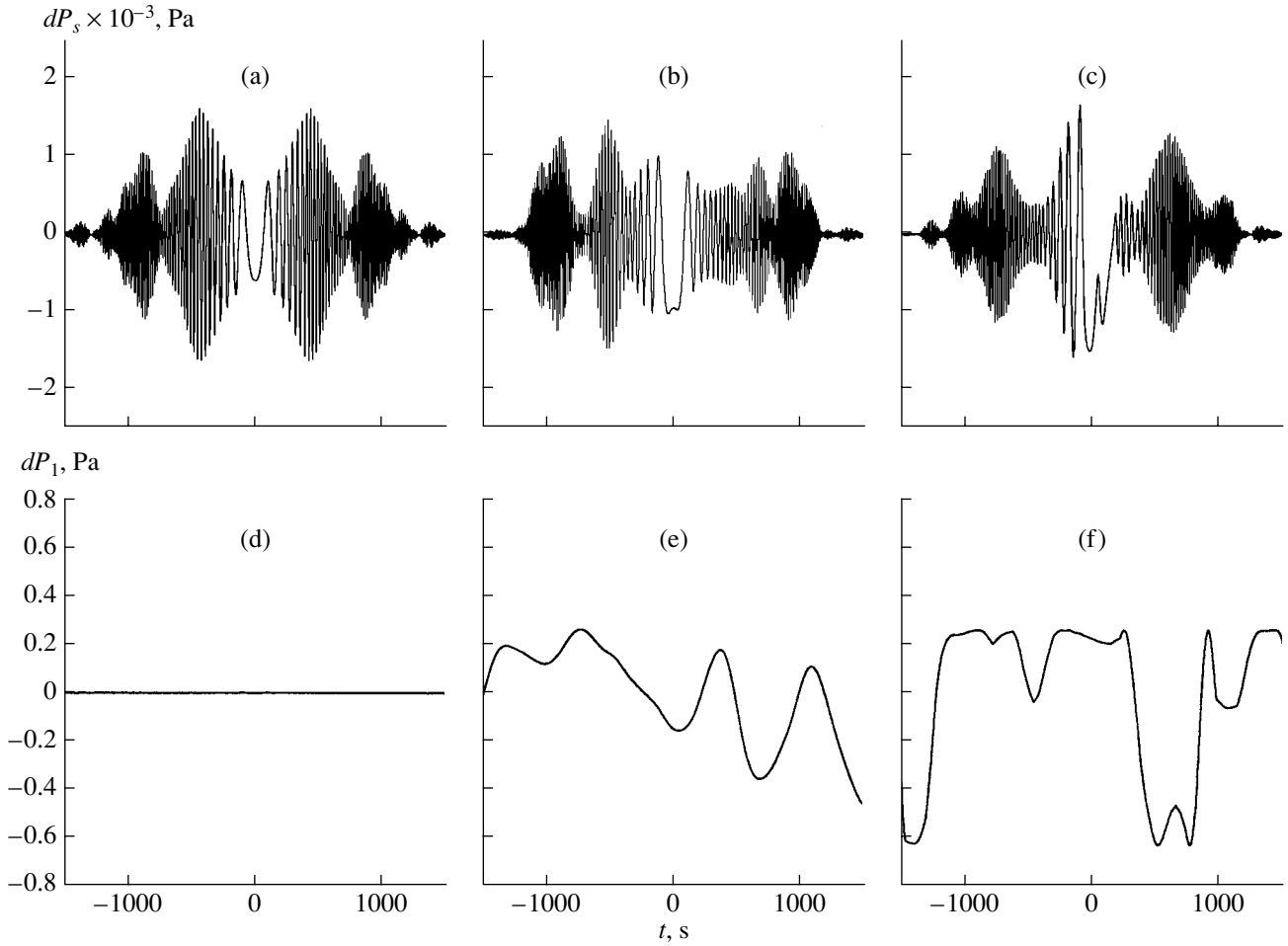

Fig. 4. Sound field variations due to scattering by a moving soft spheroid: (a, d) in the absence of internal waves, (b, e) in the case of the longitudinal propagation of internal waves, and (c, f) in the case of the transverse propagation of internal waves.

diameter $D = 3$ m as a scattering body. The sound velocity in the spheroid body was $c_s = 1540$ m/s and the density of the spheroid was $\rho_s = 1.05$ g/cm^3 (the spheroid with such dimensions and acoustic properties models a grey whale [9]). It was assumed that the spheroid moves with the speed $v = 1$ m/s at the depth $z_s = 20$ m and crosses the acoustic track between the stationary sound source and the vertical chain of receivers at a right angle ($\tilde{\gamma} = 90°$). The length of the stationary track was $r = 10$ km. A source of power of 20 W generated a cw signal with the frequency $f = 300$ Hz. In the calculations of the field scattered by the soft spheroid, the scattered field amplitude was chosen in the following form [11]:

$$F(\vec{k}_m^{\pm}, \vec{k}_\mu^{\pm}) = \frac{2i}{k}\sum_{n=0}^{\infty}\sum_{l=n}^{\infty}\varepsilon_n S_{nl}(\chi, \cos\theta_m^{\pm}) S_{nl}(\chi, \cos\theta_\mu^{\pm}) \times \frac{m_s^{-1} R_{nl}^{(1)}(\chi, \vartheta) R_{nl}^{(1)'}(\chi_s, \vartheta) - R_{nl}^{(1)'}(\chi, \vartheta) R_{nl}^{(1)}(\chi_s, \vartheta)}{m_s^{-1} R_{nl}^{(1)'}(\chi, \vartheta) R_{nl}^{(3)}(\chi_s, \vartheta) - R_{nl}^{(3)'}(\chi, \vartheta) R_{nl}^{(1)}(\chi_s, \vartheta)} \times \cos[n(\varphi_m^{\pm} - \varphi_\mu^{\pm})], \quad (13)$$

where $\theta_m^{\pm}$, $\varphi_m^{\pm}$, $\theta_\mu^{\pm}$ and $\varphi_\mu^{\pm}$ are the angles in the spherical system of coordinates, which determine the directions of the wave vectors $\vec{k}_m^{\pm}$ and $\vec{k}_\mu^{\pm}$; $\varepsilon_n = \begin{cases} 1, n = 0 \\ 2, n \neq 0 \end{cases}$ is the Neumann symbol; S_{nl}, $R_{nl}^{(1)}$, $R_{nl}^{(3)}$ are the prolate angular and radial spheroidal functions of the first and third kinds (the primed radial functions mean the derivatives with respect to ϑ); $\chi_s = \frac{k_s}{2}\sqrt{L^2 - D^2}$ ($k_s = 2\pi f/c_s$); $m_s = \rho_s/\rho(z_s)$, $\chi = (k/2)\sqrt{L^2 - D^2}$ ($k = 2\pi f/c(z_s)$); and $\vartheta = L/\sqrt{L^2 - D^2}$.

Taking into account the strong horizontal anisotropy of the IWs in shallow water and the characteristics of the sound fields connected with this anisotropy [8, 10], two possible situations of the internal wave propagation were analyzed in the numerical modeling: along and across the stationary track. When the internal wave moves from the receiver to the source, we assumed that the distribution $\zeta(x)$ along the track at the initial instant

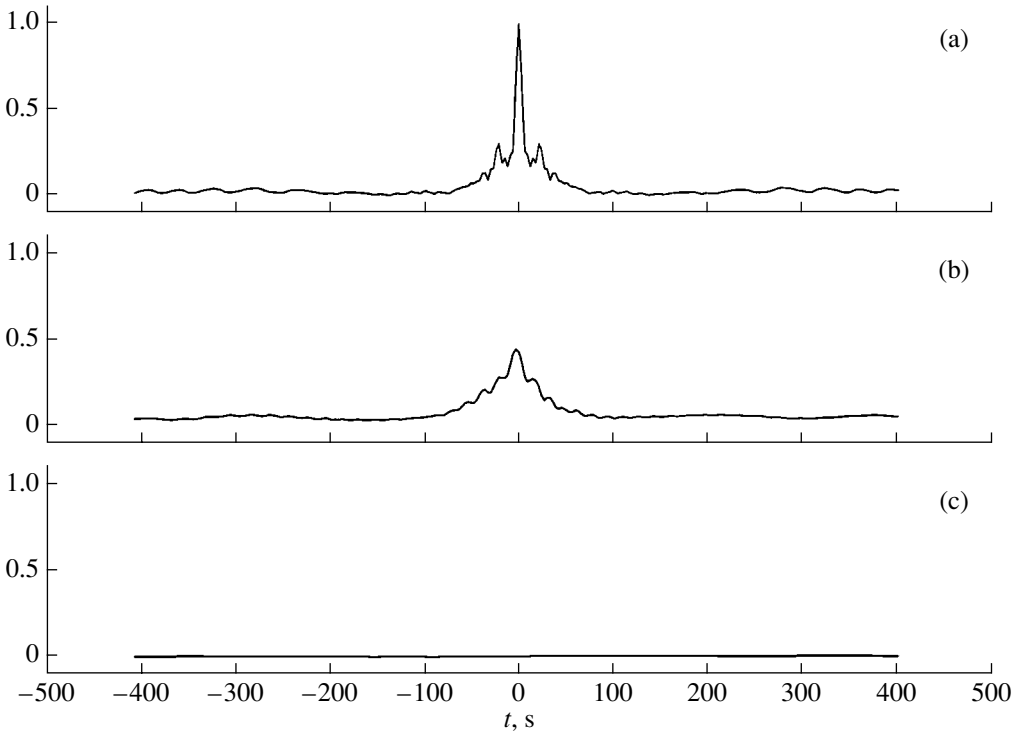

Fig. 5. (a) Autocorrelation coefficient of the signal $K_0(\tau) = B_1(\tau)/B_1(0)$ and the cross-correlation coefficient $K(\tau)$ of the signals in the cases of the (b) longitudinal and (c) transverse propagation of the internal waves.

of time corresponds to that shown in Fig. 3 (the interval 0–10 km). When integrating system (4), we took into account the dependence of the coefficients of mode interactions on the angle between the direct lines K' and K'' and the acoustic track, which vary as the scatterer moves. When the internal waves propagate across the stationary track, the IW front is assumed to be plane over the whole track length; i.e., the oscillations of the particles of liquid occur synchronously along the whole track. The displacement $\zeta(y)$ across the track at the initial instant of time was chosen so as to correspond to that within the track part from 3740 to 5250 m (Fig. 3). Note also that, for such a model of transverse perturbations of the waveguide, the calculation technique was simpler, because the eigenfunctions $\psi_l(\vec{r}; z)$ were constructed with allowance for perturbation (1) caused by the IWs. This perturbation was also included in Eq. (6). (Instead of the average refractive index $n_0(\vec{r}, z)$, Eq. (6) is now written for $n(\vec{r}, z, t)$ depending on time as a parameter.) In this case, the coefficients V_{ml} for such modes in Eq. (4) are equal to zero.

The results of the numerical experiments for the depth of reception z_r = 25 m are shown in Fig. 4. Figures 4a–4c present the time dependence of the quantity $dP_s = |P_s + \bar{P}_0| - |\bar{P}_0|$, where $\bar{P}_0$ is the average value of the direct field within the numerical experiment. Figures 4d–4f demonstrate the variations of $dP_1 = |P_s + P_0| - |\bar{P}_0|$. Figures 4a and 4d correspond to the situation when the internal waves are absent (in fact, these figures show the same dependence but on different scales along the vertical axis). Figures 4b and 4e refer to the longitudinal propagation of the IWs, and Figs. 4c and 4f, to the transverse propagation. As illustrated, the internal waves noticeably affect the fluctuations of the direct and scattered sound fields, and for the transverse propagation this effect is much greater, despite the fact that, in modeling the transverse propagation, we chose a piece of the IW realization (Fig. 3) with relatively small amplitudes. It is also significant that, in the case of the transverse propagation, the frequency of fluctuations is higher, which agrees with the previous results [8]. In general, it is important to note that the fluctuations of the direct field are so large that the received field variations related to the motion of the scatterer are almost invisible against their background (see Figs. 4e and 4f). This situation takes place despite the evident differences in the characteristic frequencies of the sound field variation. As seen in Fig. 4, the model scatterer causes variations of higher frequency.

Analyzing only high-frequency[1] (above 0.0067 Hz; at higher frequencies, the fluctuations of the direct field in the longitudinal propagation of the IWs are almost absent) variations of the sound field at the point of

[1] For high-frequency filtering of the dependence $dP_1(t)$, we used the Batterworth filter of the eighth order.

reception, we compare them with and without the internal waves by using the correlation criterion:

$$K(\tau) = 2\frac{\langle B(\tau)\rangle}{\langle B_1(0)\rangle + \langle B_2(0)\rangle}. \quad (14)$$

Here, $B(\tau)$ is the envelope of the cross-correlation function of filtered signals $dP_1(t)$ with and without IWs (the technique for selecting the envelope of the cross-correlation function using the quadrature components of the signals is described, e.g., in the monograph [12]), and $B_1(\tau)$ and $B_2(\tau)$ are the autocorrelation functions of the filtered signals in the absence and presence of IWs, respectively. The angular brackets mean the averaging over the depth of reception. Here in the calculations, the receivers were assumed to be located at depths from 5 to 55 m at a step of 5 m. The dependences $K(\tau)$ for the different cases are presented in Fig. 5. As seen from this figure, for the longitudinal propagation of internal waves, an appreciable correlation exist between the signals in the presence of the IWs and without them. For the transverse propagation, the internal waves almost totally destroy the abovementioned correlation.

In closing, we emphasize that the results obtained testify to the significant effect of the field of internal waves on the scattered sound field even for relatively small (several kilometers) distances between the source and the receiver and between the source and the scatterer. In a shallow-water sound channel, this effect depends not only on the amplitudes of the IWs but also on the direction of their propagation.

ACKNOWLEDGMENTS

This work was supported by the Russian Foundation for Basic Research, project nos. 99-02-17671, 00-05-64752, and 02-02-16509.

REFERENCES

1. L. M. Lyamshev, Akust. Zh. **45**, 693 (1999) [Acoust. Phys. **45**, 619 (1999)].
2. S. M. Gorskiĭ, V. A. Zverev, and A. I. Khil'ko, in *Formation of Acoustic Fields in Oceanic Waveguides*, Ed. by V. A. Zverev (Inst. Prikl. Fiz., Akad. Nauk SSSR, Nizhni Novgorod, 1991), pp. 82–114.
3. F. Ingenito, J. Acoust. Soc. Am. **82**, 2051 (1987).
4. V. A. Eliseevnin and Yu. I. Tuzhilkin, Akust. Zh. **41**, 249 (1995) [Acoust. Phys. **41**, 214 (1995)].
5. A. Sarkissian, J. Acoust. Soc. Am. **102**, 825 (1997).
6. V. A. Grigor'ev, B. G. Katsnel'son, V. M. Kuz'kin, and V. G. Petnikov, Akust. Zh. **47**, 44 (2001) [Acoust. Phys. **47**, 35 (2001)].
7. N. K. Vdovicheva, A. G. Sazontov, and A. I. Khil'ko, Akust. Zh. **44**, 181 (1998) [Acoust. Phys. **44**, 143 (1998)].
8. B. G. Katsnel'son, S. A. Pereselkov, V. G. Petnikov, *et al.*, Akust. Zh. **47**, 494 (2001) [Acoust. Phys. **47**, 424 (2001)].
9. V. M. Bel'kovich, V. A. Grigor'ev, B. G. Katsnel'son, and V. G. Petnikov, Akust. Zh. **48**, 162 (2002) [Acoust. Phys. **48**, 133 (2002)].
10. B. G. Katsnel'son and V. G. Petnikov, *Acoustics of a Shallow Sea* (Nauka, Moscow, 1997).
11. É. P. Babaĭlov and V. A. Kanevskiĭ, Akust. Zh. **34**, 19 (1988) [Sov. Phys. Acoust. **34**, 11 (1988)].
12. I. S. Gonorovskiĭ, *Radio Engineering Circuits and Signals* (Sovetskoe Radio, Moscow, 1977).

Translated by Yu. Lysanov

Acoustical Physics, Vol. 49, No. 1, 2003, pp. 43–50. Translated from Akusticheskiĭ Zhurnal, Vol. 49, No. 1, 2003, pp. 51–58.

Efficient Method for Solving the Problems of Wave Diffraction by Scatterers with Broken Boundaries

Do Dyk Tkhang and A. G. Kyurkchan

Moscow Technical University of Communication and Information Science, ul. Aviamotornaya 8a, Moscow, 111024 Russia

e-mail: kyurkchan@mtuci2.ru

Received August 22, 2001

Abstract—The pattern equations method is extended to solving the problems of wave scattering by bodies with piecewise smooth boundaries. The method is based on the reduction of the initial boundary-value problem to an integro-operator equation of the second kind in the scattering pattern of a body. With the use of the series expansion of the scattering pattern in angular spherical harmonics, the problem is ultimately reduced to solving an infinite algebraic system of equations in the expansion coefficients of the scattering pattern. The conditions at which this system can be solved by the method of reduction are formulated. Examples of solving the problems of wave scattering by bodies with impedance boundaries are considered. Essential advantages of the proposed method over other known methods are demonstrated. *© 2003 MAIK "Nauka/Interperiodica".*

The three-dimensional problem of wave scattering by a body of limited size is categorized as a classical problem of the theory of diffraction [1, 2]. Its solution in the region of resonance frequencies, in which case the size of the body is about the wavelength of the incident field, encounters severe computational difficulties [3]. If the boundary of the scatterer is broken, the difficulties become still greater. For example, in the strict sense, the widely used method of auxiliary (or discrete) sources [4], which is very convenient from the computational standpoint, is inapplicable to this kind of problem, because, by the theorem of existence [5], the carrier of auxiliary currents must encompass the singularities of the diffraction field, while, in the situation under consideration, some singularities will exist at the boundary of the scatterer. It is clear that rounding off the edges will not change the situation fundamentally.

When the problems of wave scattering are solved with the use of such a universal method as the method of integral equations for the field at the body boundary [6], the corresponding algebraic systems, even in the two-dimensional case, have orders of about 10–20 *kd*, where *d* is the characteristic size of the body [6]. In the three-dimensional case, the order of the system will obviously be proportional to the square of the above order, and the presence of breaks of the boundaries will undoubtedly make the algorithm more difficult.

The pattern equations method (PEM) suggested in [7, 8] is characterized by a much higher degree of convergence, and this degree only slightly depends on the geometry of the scatterers. For example, the use of this method for solving the problem of scattering by an oblate spheroid [9] showed that, even for a spheroid with an axis ratio of 40 : 1, the degree of convergence of the computational algorithm was nearly the same as in the problem of scattering by a sphere of the same diameter. In our opinion, this occurs, because, when solving the scattering problems with the use of the PEM, one directly considers the scattering pattern [i.e., some (stationary) functional of the field distributed over the scatterer's surface] as the desired quantity. As a result, the fast field components, whose correct approximation requires the use of higher harmonics, are smoothed out by the integration, which finally results in a considerable reduction in the amount of calculation required for a fixed accuracy.

This paper extends the approach suggested in paper [8] to the case of impedance boundary conditions. In addition, we show that the method remains highly efficient even in the case when the scatterer has a broken boundary.

PROBLEM FORMULATION AND SOLUTION

Consider the following boundary-value problem:

$$\Delta u^1 + k^2 u^1 = 0, \tag{1}$$

$$u|_S = \frac{W}{k}\frac{\partial u}{\partial n}\bigg|_S, \tag{2}$$

where u^1 is the velocity potential of the scattered sound field; $u = u^0 + u^1$ is the velocity potential of the total field; u^0 is the velocity potential of the primary, or incident, field; $k = \frac{\omega}{c}$, $W = \frac{Z}{ic\rho}$; c is the sound velocity; ρ is the density of the medium; Z is the local acoustic impedance that is constant at the boundary S of the scat-

terer; and $\frac{\partial}{\partial n}$ denotes the differentiation in the direction of the external normal to surface S.

In addition to Eqs. (1) and (2), the function u^1 must satisfy the radiation condition [2]

$$\lim_{r\to\infty} r\left(\frac{\partial u^1}{\partial r} + iku^1\right) = 0. \tag{3}$$

For brevity, in what follows we will call the function u^1 simply the wave field or the diffraction field.

In accordance with condition (3), the following asymptotic equality holds in the so-called wave zone (i.e., in the region $r \gg d$):

$$u^1(r, \theta, \varphi) = \frac{e^{-ikr}}{kr} g(\theta, \varphi) + O\left(\frac{1}{(kr)^2}\right). \tag{4}$$

Here, $g(\theta, \varphi)$ is the scattering pattern. Taking into account boundary condition (2), the following representation for the function g in the spherical coordinate system may be obtained:

$$g(\alpha, \beta) = \int_0^{2\pi}\int_0^{\pi} v(\theta, \varphi)\left\{1 - i\frac{W}{\chi}\left[R(\theta, \varphi)\cos\gamma\sin\theta - R'_\theta(\theta, \varphi)\frac{\partial\cos\gamma}{\partial\theta}\sin\theta\right.\right. \tag{5}$$

$$\left.\left. - R'_\varphi(\theta, \varphi)\frac{\partial\cos\gamma}{\partial\varphi}\frac{1}{\sin\theta}\right]\right\}\exp[ikR(\theta, \varphi)\cos\gamma]d\theta d\varphi,$$

where

$$v(\theta, \varphi) = -\frac{k}{4\pi}\chi R(\theta, \varphi)\frac{\partial u}{\partial n} = -\frac{k}{4\pi}\left[R^2(\theta, \varphi)\sin\theta\frac{\partial u}{\partial r} - R'_\theta\frac{\partial u}{\partial\theta}\sin\theta - \frac{R'_\varphi}{\sin\theta}\frac{\partial u}{\partial\varphi}\right]\Bigg|_{r = R(\theta, \varphi)},$$

$$\chi = \sqrt{[R^2(\theta, \varphi) + R'^2_\theta(\theta, \varphi)]\sin^2\theta + R'^2_\varphi(\theta, \varphi)}, \tag{6}$$

$$dS = \chi R d\theta d\varphi,$$

$$\cos\gamma = [\sin\theta\sin\alpha\cos(\varphi - \beta) + \cos\theta\cos\alpha]$$

and $r = R(\theta, \varphi)$ is the equation of the surface S.

The wave field is representable in the following form [10]:

$$u^1(r, \theta, \varphi) = \frac{1}{2\pi i}\int_0^{2\pi}\int_0^{\pi/2 + i\infty} \exp(-ikr\cos\alpha) \times \hat{g}(\alpha, \beta; \theta, \varphi)\sin\alpha d\alpha d\beta, \tag{7}$$

where $\hat{g}(\alpha, \beta; \theta, \varphi)$ is determined as

$$\hat{g}(\alpha, \beta; \theta, \varphi) = \int_0^{2\pi}\int_0^{\pi} v(\theta', \varphi')\left\{1 - i\frac{W}{\chi}\left[R(\theta', \varphi')\cos\hat{\gamma}\sin\theta' - R'_{\theta'}(\theta', \varphi')\frac{\partial\cos\hat{\gamma}}{\partial\theta'}\sin\theta' - R'_{\varphi'}(\theta', \varphi')\frac{\partial\cos\hat{\gamma}}{\partial\varphi'}\frac{1}{\sin\theta'}\right]\right\} \tag{8}$$

$$\times \exp[ikR(\theta', \varphi')\cos\hat{\gamma}]d\theta' d\varphi'.$$

Here,

$$\cos\hat{\gamma} = \{\sin\theta'\sin(\varphi' - \varphi)\sin\alpha\cos\beta + [\sin\theta\cos\theta' - \cos\theta\sin\theta'\cos(\varphi' - \varphi)]\sin\alpha\sin\beta + [\cos\theta\cos\theta' + \sin\theta\sin\theta'\cos(\varphi' - \varphi)]\cos\alpha\} = \vec{p}^T A\vec{i}_{r'},$$

where

$$\vec{p}^T = (\sin\alpha\cos\beta, \sin\alpha\sin\beta, \cos\alpha), \quad \vec{i}_{r'} = \vec{r}'/|\vec{r}'|$$

and

$$A = \begin{pmatrix} -\sin\varphi & \cos\varphi & 0 \\ -\cos\varphi\cos\theta & -\sin\varphi\cos\theta & \sin\theta \\ \cos\varphi\sin\theta & \sin\varphi\sin\theta & \cos\theta \end{pmatrix}$$

is the rotation matrix that brings the z axis of the coordinate system in coincidence with the direction toward the observation point.

Representation (7) makes it possible to determine the function u^1 everywhere in $R^3\setminus\bar{E}$, where $\bar{E}$ is the convex envelope of singularities of the wave field $u^1(r, \theta, \varphi)$. Using Eqs. (5)–(7), we can obtain, by analogy with [8], the following integro-operator equation of the second kind for the scattering pattern:

$$g(\alpha, \beta) = g^0(\alpha, \beta) + \frac{1}{8\pi^2}\int_0^{2\pi}\int_0^{\pi}\int_0^{2\pi}\int_0^{\pi/2 + i\infty} \left\{1 - i\frac{W}{\chi}\left[R(\theta, \varphi)\cos\gamma\sin\theta - R'_\theta\frac{\partial\cos\gamma}{\partial\theta}\sin\theta - \frac{R'_\varphi}{\sin\theta}\frac{\partial\cos\gamma}{\partial\varphi}\right]\right\} \tag{9}$$

$$\times\left[ik^2R^2(\theta, \varphi)\cos\alpha'\hat{g}(\alpha', \beta'; \theta, \varphi)\sin\theta + \hat{g}'_\theta(\alpha', \beta'; \theta, \varphi)kR'_\theta\sin\theta + \hat{g}'_\varphi(\alpha', \beta'; \theta, \varphi)\frac{kR'_\varphi}{\sin\theta}\right]$$

$$\times \exp[ikR(\theta, \varphi)(\cos\gamma - \cos\alpha')]\sin\alpha' d\alpha' d\beta' d\theta d\varphi.$$

In this equation, $g^0(\alpha, \beta)$ is the known function determined by Eq. (5), in which the function $v(\theta, \varphi)$ should be replaced with

$$v^0(\theta, \varphi) = -\frac{k}{4\pi}\chi R(\theta, \varphi)\frac{\partial u^0}{\partial n}.$$

Equation (8) is solvable under the condition that

$$\bar{E} \subseteq \bar{D},$$

where $\bar{D}$ is the region occupied by the scatterer, including the boundary.

In the particular case of a spherical scatterer ($R(\theta, \varphi) = a \equiv \text{const}$), Eq. (9) takes the form

$$\begin{aligned} g(\alpha, \beta) &= g^0(\alpha, \beta) \\ &+ \frac{(ka)^2}{2(2\pi)^2}\int_0^{2\pi}\int_0^{\pi}\int_0^{2\pi}\int_0^{\pi/2+i\infty} (1 - iW\cos\gamma)\cos\alpha' \\ &\times \exp[ika(\cos\gamma - \cos\psi)] \\ &\times \hat{g}(\alpha', \beta'; \theta, \varphi)\sin\alpha' d\alpha' d\beta' \sin\theta d\theta d\varphi. \end{aligned} \tag{10}$$

Equation (10) can be solved, in particular, with the use of an iterative method. Carrying out simple but cumbersome calculations, we obtain

$$\begin{aligned} &g(\alpha, \beta) \\ &= -i\sum_{n=0}^{\infty}(2n+1)\frac{j_n(ka) - Wj_n'(ka)}{h_n^{(2)}(ka) - Wh_n^{(2)\prime}(ka)}P_n(\cos\alpha). \end{aligned} \tag{11}$$

Expression (11) coincides with the known solution for an impedance sphere. Series (11) converges absolutely for any value of the parameter ka; therefore, it can be used for constructing asymptotic solutions (for $ka \gg 1$) [7].

In the general case of a nonspherical scatterer, one can also solve Eq. (9) using an iterative method; however, in this case, the solution cannot be represented in closed analytical form. For this reason, we consider another way of solving Eq. (9); namely, we reduce it to a system of algebraic equations. For this purpose, we use a generalized Fourier series expansion of the pattern

$$g(\theta, \varphi) = \sum_{n=0}^{\infty}\sum_{m=-n}^{n} a_{nm}P_n^m(\cos\theta)e^{im\varphi}. \tag{12}$$

From Eq. (8), we have

$$\hat{g}(\alpha, \beta; \theta, \varphi) = \sum_{n=0}^{\infty}\sum_{m=-n}^{n} \hat{a}_{nm}(\theta, \varphi)P_n^m(\cos\alpha)e^{im\beta}, \tag{13}$$

where

$$\begin{aligned} &\hat{a}_{nm}(\theta, \varphi) \\ &= \sqrt{\frac{(n-m)!}{(n+m)!}}\sum_{s=-n}^{n}\sqrt{\frac{(n+s)!}{(n-s)!}}a_{ns}i^s P_{ms}^n(\cos\theta)e^{is\varphi} \end{aligned}$$

and $P_{ms}^n(\cos\theta)$ are the generalized Legendre functions [10].

Substituting Eqs. (12) and (13) into Eq. (9) and using the relationship [11]

$$P_{0s}^n(z) = (-i)^s\sqrt{\frac{(n-s)!}{(n+s)!}}P_n^s(z),$$

we obtain the following system of algebraic equations in the coefficients a_{nm}:

$$\begin{aligned} a_{nm} &= a_{nm}^0 + \sum_{\nu=0}^{\infty}\sum_{\mu=-\nu}^{\nu} G_{nm,\nu\mu}a_{\nu\mu}, \\ &|m| \le n, \quad n = 0, 1, \ldots. \end{aligned} \tag{14}$$

Here,

$$\begin{aligned} G_{nm,\nu\mu} &= i^{n-\nu}(2n+1)\frac{(n-m)!}{(n+m)!}\frac{i}{4\pi} \\ &\times \int_0^{2\pi}\int_0^{\pi}\Big[k^2R^2(\theta, \varphi)h_\nu^{(2)\prime}(kR)P_\nu^\mu(\cos\theta)\sin\theta \\ &- h_\nu^{(2)}(kR)(\sin\theta)kR_\theta' P_\nu^\mu(\cos\theta) \\ &- i\mu\frac{kR_\varphi'}{\sin\theta}h_\nu^{(2)}(kR)P_\nu^\mu(\cos\theta)\Big]\Big\{j_n(kR)P_n^m(\cos\theta) \\ &- \frac{iW}{\chi(\theta, \varphi)}\Big[-iR(\theta, \varphi)(\sin\theta)j_n'(kR)P_n^m(\cos\theta) \\ &+ \frac{iR_\theta'}{kR}j_n(kR)(\sin\theta)\frac{d}{d\theta}P_n^m(\cos\theta) \\ &+ \frac{mR_\varphi'}{kR\sin\theta}j_n(kR)P_n^m(\cos\theta)\Big]\Big\}e^{i(\mu-m)\varphi}d\theta d\varphi. \end{aligned} \tag{15}$$

The free terms a_{nm}^0 are the expansion coefficients of the known function $g^0(\alpha, \beta)$:

$$\begin{aligned} a_{nm}^0 &= i^n(2n+1)\frac{(n-m)!}{(n+m)!} \\ &\times \int_0^{2\pi}\int_0^{\pi} v^0(\theta, \varphi)j_n(kR)P_n^m(\cos\theta)e^{-im\varphi}d\theta d\varphi. \end{aligned}$$

An important advantage of system (14) is the fact that its matrix elements, as can be seen from Eq. (15),

are expressed through integrals whose multiplicity is twice as small as those in widely used methods such as the method of integral equations for the field on the body's surface and the method of moments. In addition, as we will see below, the method of reduction, which is used for solving system (14), is characterized by a high degree of convergence, and this degree only slightly depends on the scatterer geometry.

In the cases of $W = 0$ (an acoustically soft body) or $W = \infty$ (an acoustically hard body), the initial boundary-value problem takes the form of a Dirichlet or Neumann problem, respectively. In both cases, the algebraic system retains form (14), and one can show that the following relationships are valid:

$$G^D_{nm,\,\nu\mu} + G^N_{nm,\,\nu\mu} = \delta_{\nu n}\delta_{\mu m}, \qquad a^{0D}_{nm} + a^{0N}_{nm} = 0. \tag{16}$$

The notations are evident. These relationships between the elements of the algebraic systems for the Dirichlet and Neumann boundary-value problems are very convenient from the computational standpoint.

If the scatterer is a body of revolution, i.e., if $R(\theta, \varphi) = R(\theta)$, the algebraic system (14) takes on the form

$$a_{nm} = a^0_{nm} + \sum_{\nu = |m|}^{\infty} G_{nm,\,\nu m} a_{\nu m}, \qquad m = 0, \pm 1, \ldots, \pm n; \quad n = 0, 1, \ldots. \tag{17}$$

In this system,

$$G_{nm,\,\nu m} = i^{n-\nu}(2n+1)\frac{(n-m)!}{(n+m)!}\frac{i}{2}\int_0^{\pi}\left\{ j_n(kR)P_n^m(\cos\theta) - \frac{W}{\chi(\theta)}\left[R(\theta) j_n'(kR)P_n^m(\cos\theta) - \frac{R_\theta'}{kR(\theta)} j_n(kR)\frac{d}{d\theta}P_n^m(\cos\theta)\right]\sin\theta\right\} \tag{18}$$

$$\times\left[k^2R^2(\theta)h_\nu^{(2)'}(kR)P_\nu^m(\cos\theta) - kR_\theta' h_\nu^{(2)}(kR)\frac{d}{d\theta}P_\nu^m(\cos\theta)\right](\sin\theta)\,d\theta.$$

By analogy with paper [8], one can show that

$$|G_{nm,\,\nu m}| \le \text{const}\frac{\sigma_1^n}{n \times n!} \tag{19}$$

for $n \gg \nu$. Here,

$$\sigma_1 = \max_{\theta_0,\,\varphi_0,\,s}\left|\frac{kR(\theta_0, \varphi_0)}{2}e^{is\theta_0}\right|, \tag{20}$$

where θ_0 and φ_0 are the roots of the equations

$$[R_\theta'(\theta, \varphi) + isR(\theta, \varphi)]e^{is\theta} = 0; \qquad s = \pm 1; \quad R_\varphi'(\theta, \varphi) = 0. \tag{21}$$

The maximum in Eq. (20) is sought among the roots of system (21). Upon the change of variable $\varsigma = R(\theta, \varphi)e^{i\theta}$, these roots appear to lie inside the contours C_φ, which are the maps of the surface S sections by the $(\varphi, \varphi + \pi)$ plane onto the plane $z = re^{i\alpha}$. If the surface S has nonanalytic (in θ, φ) points, the search for the maximum in Eq. (20) should include these points as well [12].

In the same way, for $\nu \gg n$, one can find that

$$|G_{nm,\,\nu\mu}| \le \text{const}\frac{\nu!}{\sigma_2^\nu},$$

where

$$\sigma_2 = \min_{\theta_0,\,\varphi_0,\,s}\left|\frac{kR(\theta_0, \varphi_0)}{2}e^{is\theta_0}\right|, \tag{22}$$

and the minimum in this expression is sought among those roots of system (21) that correspond, upon the change $\varsigma = Re^{i\theta}$, to points lying outside the aforementioned contours C_φ in the plane $z = re^{i\alpha}$.

Similarly, one can show that

$$\left|a^0_{nm}\right| \le \text{const}\frac{\sigma^n}{n \cdot n!}, \quad \sigma = \max(\sigma_1, \sigma_0) \tag{23}$$

for $n \gg 1$. Here, $\sigma_0 = \dfrac{kr_0}{2}$ and r_0 is the distance to the point inside S that is most distant from the origin and corresponds to a singular point of the function $v^0(\theta, \varphi)$ after it is analytically continued to the region of complex angles [12]. Note that $\sigma_0 = 0$ if u^0 is the field of a plane wave.

From the above estimates, it follows that the unknown coefficients in system (14) must be replaced according to the formula [8]

$$a_{nm} = \frac{\sigma^n}{n!}x_{nm}. \tag{24}$$

Upon this change of variables, system (14) is transformed to the system

$$x_{nm} = x^0_{nm} = \sum_{\nu=0}^{\infty}\sum_{\mu=-\nu}^{\nu} g_{nm,\,\nu\mu}x_{\nu\mu}, \qquad |m| \le n, \quad n = 0, 1, \ldots, \tag{25}$$

where

$$x^0_{nm} = \frac{n!}{\sigma^n}a_{nm}, \quad g_{nm,\,\nu\mu} = \frac{n!}{\nu!}\sigma^{\nu-n}G_{nm,\,\nu\mu}.$$

System (25) is solvable by the method of reduction under the condition that

$$\sigma_2 > \sigma. \tag{26}$$

Table

	N	9	11	13	15	17
Cylinder ($ka = 2$, $kh = 4$)						
$w = 0$	$g(\pi/2,0)$	7.5025E+00	7.5172E+00	7.5229E+00	7.5200E+00	7.4486E+00
$w = 0$	$g(\pi/2,\pi)$	2.5663E+00	2.5169E+00	2.4979E+00	2.5026E+00	2.5027E+00
$w = 1000$	$g(\pi/2,0)$	3.044E+00	3.0743E+00	3.0838E+00	3.0653E+00	3.0644E+00
$w = 1000$	$g(\pi/2,\pi)$	2.4335+00	2.4788E+00	2.5108E+00	2.5070E+00	2.5066E+00
Spheroid ($ka = 2$, $kc = 4$)						
$w = 0$	$g(\pi/2,0)$	6.5647E+00	6.5649E+00	6.5649E+00	6.5659E+00	6.5653E+00
$w = 0$	$g(\pi/2,\pi)$	2.0405E+00	2.0404E+00	2.0404E+00	2.0413E+00	2.0416E+00
$w = 1000$	$g(\pi/2,0)$	2.6626E+00	2.6615E+00	2.6615E+00	2.6615E+00	2.6615E+00
$w = 1000$	$g(\pi/2,\pi)$	1.9921E+00	1.9919E+00	1.9919E+00	1.9919E+00	1.9918E+00
Spheroid ($ka = 1.005$, $kc = 5.1$)						
$w = 0$	$g(\pi/2,0)$	5.7223E–01	5.7231E–01	5.7005E–01	5.7006E–01	5.7005E–01
$w = 0$	$g(\pi/2,\pi)$	5.7178E–01	5.7186E–01	5.6960E–01	5.6962E–01	5.6961E–01
$w = 1000$	$g(\pi/2,0)$	1.2399E–01	1.2408E–01	1.2368E–01	1.2369E–01	1.2367E–01
$w = 1000$	$g(\pi/2,\pi)$	1.2539E–01	1.2564E–01	1.2524E–01	1.2523E–01	1.2525E–01
Cone ($ka = 2$, $kh = 6$)						
$w = 0$	$g(\pi/2,0)$	6.3459E–01	6.1876E–01	6.0257E–01	6.0523E–01	6.0350E–01
$w = 0$	$g(\pi/2,\pi)$	6.5045E–01	6.9022E–01	6.7486E–01	6.7215E–01	6.7252E–01
$w = 1000$	$g(\pi/2,0)$	9.6439E–01	9.4209E–01	9.2592E–01	9.1410E–01	9.2467E–01
$w = 1000$	$g(\pi/2,\pi)$	7.4507E–01	7.5850E–01	7.6272E–01	7.6862E–01	7.6735E–01

The wave scattering by bodies that violate condition (26), in particular, by significantly nonconvex bodies, can be simulated using several bodies of simpler geometry by combining them in a group whose configuration reproduces the geometry of the initial scatterer [13, 14]. Such a simulation is possible because, in the case of a group of bodies, the degree of convergence of the PEM computational algorithm only slightly depends on the distances between the bodies, down to their contact [14].

RESULTS OF CALCULATIONS

We investigated numerically the wave scattering by axially symmetric bodies, namely, by a prolate spheroid with a long half-axis c (along the z axis) and a short half-axis a; by a circular cylinder with a radius a, and spherically rounded ends of the same radius, and the height of the cylindrical part h; and by a circular cone with a spherical base of radius a equal to the radius of the cone and with the height of the conic part h. The calculations were carried out for three values of the impedance $W = 0$, 1000, and $-i$. The latter case corresponds to the so-called matched impedance [6].

We considered the incidence of a unit plane wave at the angles $\theta_0 = \pi/2$ and $\varphi_0 = 0$ for all bodies under consideration, excluding the cone, for which the direction of incidence was characterized by the angles $\theta_0 = 0$ and $\varphi_0 = 0$. The scattering pattern was computed as a function of the angle θ in the plane $\varphi = 0, \pi$.

All calculations were carried out on the basis of the solution of the finite system of equations

$$x_{nm} = x_{nm}^0 + \sum_{\nu = |\mu|}^{N} g_{nm,\nu m} x_{\nu m},$$
$$|m| \le n, \quad n = 0, 1, \ldots, N$$

[this system can be obtained from the general system (25) in the case of a body of revolution], in which N was set equal to 15, i.e., $N \approx 2kd$, in all calculations (excluding the table).

Figures 1–3 show the scattering patterns of a cylinder of height $kh = 4$ (curves *1*) and a prolate spheroid with half-axes $ka = 2$ and $kc = 4$ (curves *2*), which is inscribed in this cylinder. Figures 1–3 correspond to the impedances $W = 1000$, 0, and $-i$, respectively. It can be seen that the difference between the scattering patterns

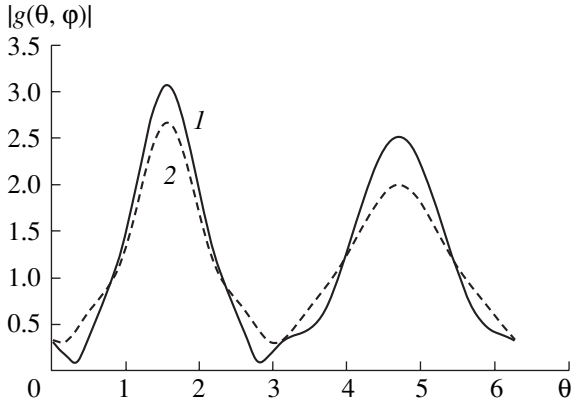

Fig. 1.

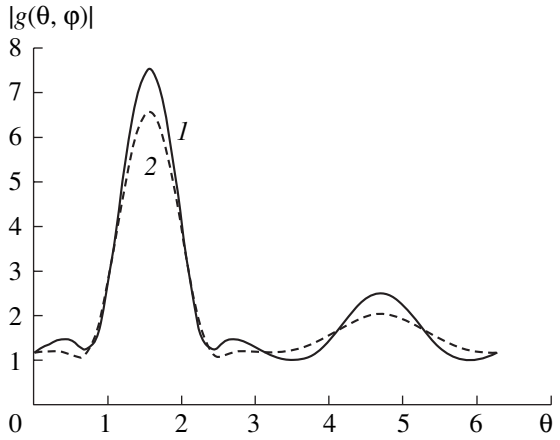

Fig. 2.

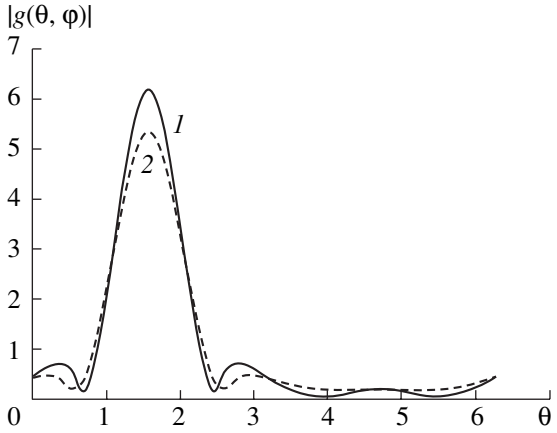

Fig. 3.

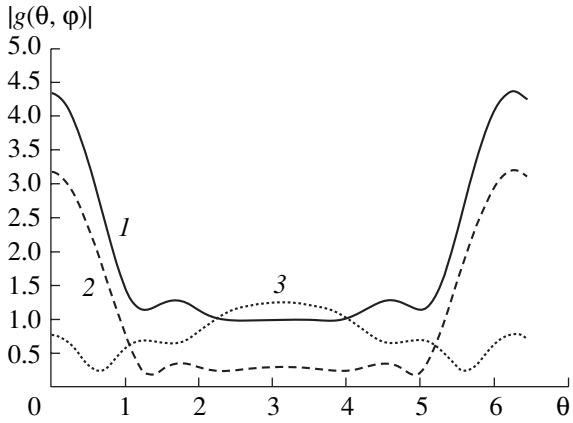

Fig. 4.

is most prominent in the case of an acoustically hard scatterer. The main lobe in the scattering patterns is the shadow lobe, whose width agrees with the geometric optics estimates. However, in the case of an acoustically hard scatterer, the level of the back lobe is quite comparable with the level of the shadow lobe. In the case of the matched impedance, the level of the shadow lobe substantially (by approximately 30 dB) exceeds the level of the back lobe, while this excess measures only about 10 dB in the case of an acoustically soft body. This fact agrees well with the intuitive notion of a perfectly absorbing scatterer.

Figure 4 shows the scattering patterns of a cone characterized by the geometric parameters $ka = 2$ and $kh = 6$ for different values of the surface impedance (curve *1* corresponds to $W = 0$, curve *2*, to $W = -i$, and curve *3*, to $W = 1000$). Here, again, the back lobe of the cone with the matched impedance is smaller than the shadow lobe by about 20 dB. One can see that the scattering pattern is nearly constant over a broad segment (about 90°) corresponding to scattering from the spherical part of the body.

Figure 5 illustrates the results of calculation for the parameter $\frac{2}{ka}|g(\pi/2, \pi)|$, which is the relative radius of the so-called equivalent sphere [6] and characterizes the backscattering cross section of the body. This parameter is represented as a function of ka for the sphere (curve *2*) and the cylinder of height $kh = 0.1$ (i.e., a body that only slightly differs from the sphere) for the impedance $W = 1000$. It can be seen that the difference between these curves is small (less than 2%).

Figure 6 shows the results of a similar calculation of the parameter $\frac{2}{kc}|g(\pi/2, \pi)|$ as a function of kc for the cylinder (curve *1*) and the spheroid (curve *2*) with the same geometric parameters as in Figs. 1–3 for $W = 1000$. Here, the parameter c characterizes half of the body length. It can be seen that both curves vary syn-

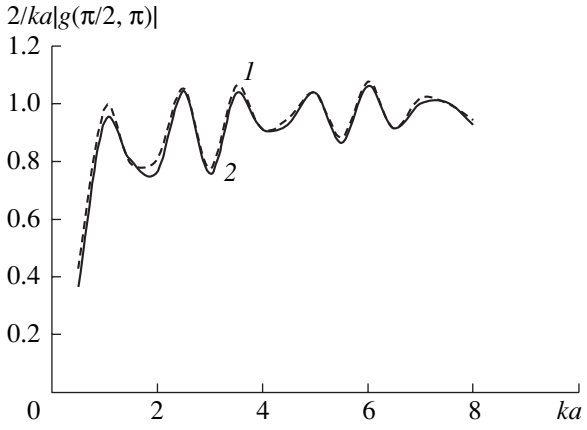

Fig. 5.

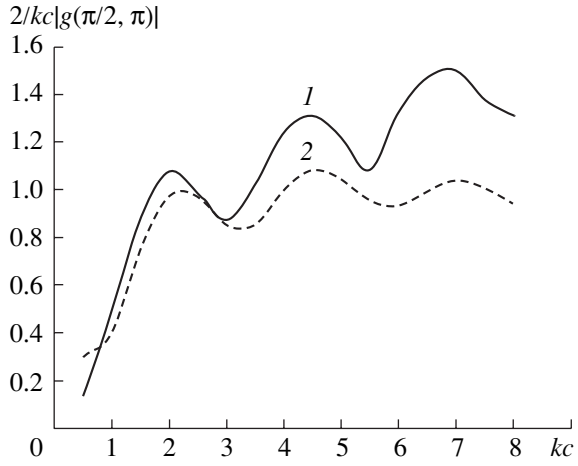

Fig. 6.

chronously; however, the curve for the cylinder goes distinctly higher, which corresponds to Fig. 1 and is explained by the fact that the cylinder has a considerable part of its surface formed by a rectilinear generatrix and oriented normally to the incident wave.

Finally, the table presents the data characterizing the degree of convergence of the computational algorithm used for the cylinder, the spheroid, and the cone. It can be seen that, in the case of the body with an analytical boundary (the spheroid), two correct digits after the decimal point are obtained even with $N \approx kd$. Approximately the same degree of convergence is obtained when solving the problem of wave diffraction by a spheroid using the method of separation of variables and the expansions in spheroidal functions [15]. For bodies with broken boundaries (the cylinder and the cone), one must use $N \approx 2kd$, which is several times (and may be several tens of times) better than the corresponding parameters for the conventional methods.

The numerical results presented above suggest that the pattern equations method is a highly efficient tool for solving the problems of wave diffraction by impedance bodies with a complex geometry, including bodies with edges and conic points. The computational algorithm constructed on the basis of the PEM appears to be very fast. With this method, the calculations of the scattering characteristics of smooth bodies and bodies with singularities (such as edges) are performed using the same algorithm, without taking any special measures.

After this paper was submitted for publication, we became acquainted with paper [16], where the boundary-value problem of wave diffraction by a scatterer of finite size was reduced to an algebraic system of the form of system (14). However, we note that the corresponding algebraic system was obtained in [16] with the use of the diffracted field represented as a series in the spherical wave harmonics, which, in the general case, is correct only for the so-called Rayleigh bodies (see, e.g., [4], Ch. 5 and [12]). In our case, system (14) is rigorously derived from the integro-operator equation (9) solvable under condition (10), which is essentially less restrictive than the Rayleigh body condition [7, 8]. In addition, in our approach, system (14) is only a version of the algebraization of Eq. (9) and is determined by the choice of spherical harmonics as the basis for the representation of the scattering pattern. It is clear that such an algebraization can be realized in many other correct ways.

ACKNOWLEDGMENTS

This work was supported by the Russian Foundation for Basic Research, project no. 00-02-17639.

REFERENCES

1. L. M. Lyamshev, *Sound Reflection from Thin Plates and Shells in Liquid* (Akad. Nauk SSSR, Moscow, 1956).
2. H. Hönl, A. W. Maue, and K. Westpfahl, *Theorie der Beugung* (Springer, Berlin, 1961; Mir, Moscow, 1964).
3. Yu. I. Bobrovnitskiĭ and T. M. Tomilina, Akust. Zh. **36**, 591 (1990) [Sov. Phys. Acoust. **36**, 334 (1990)].
4. *Generalized Multipole Techniques for Electromagnetic and Light Scattering*, Ed. by T. Wriedt (Elsevier, Amsterdam, 1999).
5. A. G. Kyurkchan, Radiotekh. Élektron. (Moscow) **31**, 20 (1986).
6. E. L. Shenderov, *Sound Radiation and Scattering* (Sudostroenie, Leningrad, 1989).
7. A. G. Kyurkchan, Dokl. Akad. Nauk **325**, 273 (1992) [Sov. Phys. Dokl. **37**, 338 (1992)].
8. A. G. Kyurkchan, Dokl. Akad. Nauk **337**, 728 (1994) [Phys.–Dokl. **39**, 546 (1994)].

9. A. G. Kyurkchan and A. I. Kleev, Radiotekh. Élektron. (Moscow) **40**, 897 (1995).
10. A. G. Kyurkchan, Dokl. Akad. Nauk **322**, 686 (1992) [Sov. Phys. Dokl. **37**, 70 (1992)].
11. N. Ya. Vilenkin, *Special Functions and the Theory of Group Representations* (Nauka, Moscow, 1965; Am. Math. Soc., Providence, 1968).
12. A. G. Kyurkchan, B. Yu. Sternin, and V. E. Shatalov, Usp. Fiz. Nauk **166**, 1285 (1996) [Phys.–Usp. **39**, 1221 (1996)].
13. A. G. Kyurkchan, Dokl. Akad. Nauk **348**, 603 (1996).
14. A. G. Kyurkchan and S. A. Manenkov, in *Proceedings of the 4th Conference on Electromagnetic and Light Scattering by Nonspherical Particles. Theory and Applications* (Vigo, Spain, 1999).
15. N. B. Konyukhova and T. V. Pak, *Diffraction of a Plane Sound Wave by a Rigid Prolate Spheroid* (Vych. Tsentr Akad. Nauk SSSR, Moscow, 1985).
16. M. Ochmann, J. Acoust. Soc. Am. **105**, 2574 (1999).

Translated by A. Vinogradov

Acoustical Physics, Vol. 49, No. 1, 2003, pp. 51–61. Translated from Akusticheskiĭ Zhurnal, Vol. 49, No. 1, 2003, pp. 59–70.

In Search of a Noncontact Underwater Acoustic Source

S. V. Egerev

Andreev Acoustics Institute, Russian Academy of Sciences, ul. Shvernika 4, Moscow, 117036 Russia
e-mail: egerev@akin.ru

Received August 5, 2002

Abstract—The history of studies of the photoacoustic effect in liquids and its applications to the development of a "virtual" source of underwater acoustic signals is briefly reviewed. The problem of the efficiency of the photoacoustic conversion is considered. The modes of laser generation of sound, i.e., the thermooptical, nonlinear surface, and nonlinear bulk modes of operation, are discussed taking into account the real features of the marine environment, the most important of them being the surface waves. A review of the publications concerned with the problem of a moving photoacoustic source is presented. Advances in the photoacoustic underwater remote sensing technology are described. © *2003 MAIK "Nauka/Interperiodica".*

The necessity to exploit the resources of the world's seas, monitor meteorological conditions, and solve problems of underwater communications and remote control demands an improvement in the available techniques and devices for acoustic remote sensing of the marine environment. The idea of creating a sound source in a sea medium in a remote manner, without submerging any conventional material transducers, arose almost simultaneously with the development of powerful lasers operating in visual and infrared ranges. It turned out that the region of interaction of laser radiation with the sea medium can play the role of a source of underwater sound. This region has been called the optical underwater acoustic source or a noncontact underwater acoustic source. Its operation was considered to be as follows: a laser source irradiating a preset spot on the sea surface is installed on the deck of a ship or aboard an aircraft, and an acoustic field is generated in the sea medium as a result.

Several decades of studies of the effect and its applications demonstrated that the remoteness of the sound source of laser origin is not its only advantage. Unique characteristics of the field of such a source were revealed, attractive opportunities provided by rapid scanning with the source over the surface were taken into account, and the relative simplicity of creating multiple sources and their synthetic aperture was considered.

Some other special features of noncontact underwater acoustic sources were discovered in the course of further investigation. It turned out that there is no universal approach to creating a noncontact underwater acoustic source. Each problem needs its own definite mode of laser excitation of the sea medium. A certain classification of noncontact underwater acoustic sources has been developed. It distinguishes thermooptical (or linear thermal) noncontact underwater acoustic sources, which radiate sound due to the thermal expansion of the light-absorbing medium volume; combined noncontact underwater acoustic sources, where the major contribution to sound excitation is made by the phase transitions on the water surface while the contribution of thermal expansion remains considerable; and finally, nonlinear bulk noncontact underwater acoustic sources, which are based on the effect of the laser breakdown in the sea medium. This classification generally coincides with the classification adopted in the laboratory applications of photoacoustics.

Systematic studies of the marine applications of the photoacoustic effect started in 1973 on the known initiative by F.V. Bunkin, L.M. Lyamshev, and R.V. Khokhlov, who formulated the program of these studies. At that time, the program was supported by the government.

Recalling the years of fruitful research in this field, L.M. Lyamshev used to say that a retrospective look at the chain of findings, errors, disappointments, and eventually realized diagnostic techniques in the field of marine photoacoustics deserves a special description. It was him who suggested a possible title for such an essay: "In search of a noncontact underwater acoustic source."

The present paper has the same title. It does not pretend to be a comprehensive study but gives an idea of some essential intermediate results obtained by researchers from the leading laboratories of the world in the course of the long-term investigations in this field of research.

BRIEF HISTORY

The significant year was 1962. At that time, White [1] in the USA and Prokhorov *et al*. [2] in the USSR independently discovered effective sound excitation in condensed media under the action of laser pulses. Despite the absence of a clear understanding of the physical phenomena underlying such conversion at that

1063-7710/03/4901-0051$24.00 © 2003 MAIK "Nauka/Interperiodica"

time, underwater acoustics was named one of the possible important applications of the effect. The priority of the patent for a laser-acoustic generator that was filed by Brewer and Rieckhoff [3] refers to 1964. It was this patent that contained the proposal to use the focal region of a powerful laser beam as a pulsed laser source of intense ultrasonic oscillations with a high efficiency of conversion of light energy into sound energy. The record-breaking (at that time) signal level, higher than 0.1 MPa, allowed them to propose this source for both technological applications and oceanic bottom studies.

Starting from the second half of the 1960s, the concept of possible mechanisms of optical sound generation [4–6] and their mutual influence began to form gradually. At first glance, the complexity of the problem manifested itself in the poor reproducibility of experimental data obtained by different researchers. The ratio of the sound amplitudes excited by laser radiation under seemingly identical conditions attained a value of 10^4 and greater. Attempts to resolve this contradiction led to the development of the first rough classification of photoacoustic conversion mechanisms, which retains its significance up to now [7, 8]. The first *in situ* experiments performed in the USA refer to the beginning of the 1970s. The first solutions for the amplitude, spectral, and spatial characteristics of signals were obtained [9, 10].

The studies of the problem of a noncontact underwater acoustic source were performed in the USA at least at three centers in different years: at the Technological Institute in Atlanta (Georgia) [11, 12], at the Laboratory of Applied Research of Texas University, Austin (Texas) [13–15], and at the Laboratory of Naval Weapons in Silver Springs (Maryland) [16]. The so-called sonar ply of the American studies attracts one's attention: the evaluation of the applicability of the method was performed mainly in connection with the possible development of a bistatic "virtual" sonar.

In China, the problems of marine photoacoustics are studied at the Oceanological University (Tsindao) and Institute of Measuring Technology (Dalyan) [17, 18]. In the USSR, optical underwater acoustic studies were carried out at the Andreev Acoustics Institute [19–21], the Physical Institute and General Physics Institute of the Academy of Sciences of the USSR [5–7], at Moscow State University [23], and at the Pacific Oceanological Institute of the Far-East Research Center of the Academy of Sciences of the USSR [24, 25]. Lately, despite considerable cuts in funding of large-scale programs, the support provided by the Russian Foundation for Basic Research made it possible to continue the joint projects of the Andreev Acoustics Institute and Shirshov Oceanology Institute of the Russian Academy of Sciences in optical underwater acoustics [26, 27].

ON THE EFFICIENCY OF A REMOTE CONVERSION OF LIGHT INTO SOUND

Researchers were interested first of all in the problem of the efficiency of conversion of optical energy into sound energy. Other important parameters, such as the spectral-time characteristics of the signal produced by the noncontact underwater acoustic source, its directivity, amplitude, stability to wind waves, the effect of screening of the surface source by a bubble sheet, noise stability, and the classification potential of the signal, were considered as secondary for a long time.

The efficiency of the photoacoustic conversion η can be expressed through the total acoustic energy emitted into the half-space E_{ac} (a pulsed mode of operation):

$$\eta = \frac{E_{ac}}{E_0} = \frac{2\pi r^2}{\rho c E_0}\int_0^{\pi/2}\sin\varphi d\varphi\int_{-\infty}^{\infty}p_\varphi^2(t)dt$$

or the acoustic power W_{ac} (a continuous mode of operation):

$$\eta = \frac{W_{ac}}{W_0} = \frac{2\pi r^2}{\rho c W_0}\int_0^{\pi/2}p_{0\varphi}^2\sin\varphi d\varphi,$$

where φ is the angle that determines the direction to the reception point with respect to the vertical; r is the distance to the reception point; $p_\varphi(t)$ is the pressure pulse at the reception point; $p_0(\varphi)$ is the amplitude of a continuous signal at the reception point; E_0 and W_0 are the energy and power of laser radiation, respectively; ρ is the water density; and c is the sound velocity in water.

Depending on the conditions of sound excitations in water and, mainly, on the conversion mechanisms involved in the process, the value of η varies from 10^{-11} to 0.1.

The smallness of the efficiency of the photoacoustic conversion was embarrassing for the specialists in the field of conventional means of underwater sound generation, because they were used to greater values. For example, it was popular to compare the efficiency of photoacoustic conversion with the efficiency of direct sound transmission into water. Let us imagine a loudspeaker radiating a plane sound wave in air in the direction of the sea surface. With a loudspeaker efficiency of 10^{-1} and a transmission ratio of the sea surface of 10^{-3}, the ratio of conversion of the electromagnetic energy feeding the loudspeaker into underwater sound energy is 10^{-4}, which noticeably exceeds the efficiency of many modes of photoacoustic conversion.

The record-breaking efficiency of photoacoustic conversion (up to 10%) is attained with the help of the laser radiation providing the subsurface breakdown of the sea medium at a depth no smaller than 1 m. In this case, the effect is similar to the effect of sound radiation by an electric discharge and can be evaluated according

to the corresponding models. To develop a general idea of the opportunities provided by a nonlinear noncontact underwater volume sound source, the trotyl equivalent of the optical breakdown of the sea medium was used. Indeed, let us compare the process of breakdown to a microscopic explosion that leads to the rise of an oscillating bubble emitting sound. One can assume that most of the energy evolved in this case is spent on the bubble oscillations. Then, the energy-balance equation can be written in the form

$$\frac{4}{3}\pi p_h R_{max}^3 = E_0,$$

where p_h is the hydrostatic pressure and R_{max} is the maximal radius of the oscillating bubble. Thus, at E_0 = 30 J and p_h = 1 atm, we have R_{max} = 4 cm. Then, we have the following expression for the equivalent mass of the explosive (trotyl equivalent):

$$W_e = \frac{4}{3}\pi\rho_p R_{max}^3,$$

where ρ_p is the density of explosion products when the bubble attains the radius R_{max}. In this case, it is the density of water vapor at $p_h = 0.6 \times 10^{-3}$ g/cm^3, and we finally obtain W_e = 0.15 g. The modest value of W_e should not be disappointing in view of the fact that we are dealing with a bodiless and massless source. Knowing the value of W_e, we can estimate the maximal pressure p_m in a pulse at the distance of 1 m from the breakdown center with the help of the known formulas of the theory of underwater explosions. Estimations give the value $p_m = 2.5 \times 10^5$ Pa. Such an estimate agrees well with experimental data [28]. Despite the high efficiency of conversion, a nonlinear volume source did not find wide application in marine technologies because of the technical difficulties in its implementation.

The signal level in the case of a surface nonlinear photoacoustic (combined) source attains values even greater than that in the previous case (1 MPa m and over at the maximum). However, on the whole, the conversion efficiency is smaller because of the pronounced directivity of the radiation pattern along the normal to the surface, and it reaches only a value of 10^{-2}. The radiation of a combined source is an N-shaped acoustic pulse with a length of 3–10 μs. This mode of photoacoustic conversion is used in various cases of remote sensing of shallow-water regions [27–32]. To excite such a source, powerful ship-based or airborne CO_2 lasers are used [33].

Spectral-time characteristics of a thermooptical source are more varied. A signal can be a narrowband harmonic train (the typical frequencies are 5–25 kHz) or a limited pulse with a total length of 1–3 ms and a carrier frequency of 10–20 kHz, as well as a sequence of short pulses (this so-called quasi-continuous mode was realized for the first time in [34]). A thermooptical source of underwater sound provides an opportunity to control the angular position of the directivity pattern maximum. One should also not forget about additional features of a thermooptical source, which arise when the irradiation spot scans over the surface. The interest in thermooptical noncontact underwater acoustic sources persists [19, 21, 33] despite the small efficiency of conversion. This mode of operation is used successfully to monitor wind waves and the thin subsurface structure of the ocean [21, 35]. Let us examine it in more detail.

A THERMOOPTICAL SOUND SOURCE

Remote radiant heating of a certain region of a sea medium leads to its rapid expansion and to radiation of sound. In the typical case of a harmonic modulation of laser intensity, the frequency of the excited underwater acoustic signal corresponds to the modulation frequency of the laser beam. The wave equation describing the sound field in a medium without losses, which contains thermal sources, was obtained for the first time by U. Ingard in 1958 [36]. The problem of a thermooptical sound source with high directivity was solved in subsequent publications (see, e.g., [4]).

It should be noted that now the studies of thermooptical sound generation are also carried out beyond the framework of underwater acoustics. For example, analytical devices based on the principle of thermal conversion of light energy into sound energy are used widely in biology, medical science, and semiconductor technology.

Let us give a simple estimate of the efficiency of pulsed thermooptical sound generation. Restricting our consideration to the model of rapid heat evolution in a spherical region with the radius R in an infinite liquid, we write down an expression for the pressure increment Δp:

$$\Delta p = \frac{3c^2\beta E_0}{4\pi C_p R^3},$$

where β is the coefficient of thermal expansion of water and C_p is the specific heat. A pressure relief in a spherical region leads to the emission of the so-called N-wave with the peak pressure value p_m at the distance r,

$$p_m = \frac{\Delta p R}{2r},$$

and the length

$$\Delta p = 2R/c,$$

where c is the sound velocity in water.

The total energy in an acoustic pulse is expressed as

$$E_{ac} = \frac{4\pi r^2 p_m \tau}{\rho c} = \frac{9}{8\pi R\rho}\left(\frac{\beta E_0 c}{RC_p}\right)^2,$$

and correspondingly, for the conversion coefficient, we have

$$\eta = \frac{9E_0}{8\pi R\rho}\left(\frac{\beta c}{RC_p}\right)^2.$$

The efficiency turns out to be proportional to the evolved optical energy. For example, at a water temperature of 20°C, $R = 1$ cm, and $E_0 = 1$ J, we have $\eta = 5 \times 10^{-7}$; at $E_0 = 100$ J, η increases up to 5×10^{-5}.

Thermooptical sources are often used to excite sound pulses. However, their important feature is the possibility of obtaining a continuous narrowband sound radiation. The pressure amplitude in the far field at the modulation frequency ω of a continuous laser beam with the Gaussian intensity distribution over the cross section is determined as

$$p_\omega = \frac{\beta W\omega}{\pi C_p r}\frac{\alpha k\cos\varphi}{(\alpha^2 + k^2\cos^2\varphi)}\exp\left[-\left(\frac{ka\sin\varphi}{2}\right)^2\right], \quad (1)$$

where α is the coefficient of light absorption, k is the wave number of sound, and a is the beam radius. When both conditions $ka \ll 1$ and $k > \alpha$ are satisfied (a high-frequency sound radiation by a narrow laser beam, which travels a long distance in the medium), the maximum of the directivity pattern of the acoustic field corresponds to the direction

$$\varphi = \arccos(a/k).$$

The pressure amplitude at the maximum of the directivity pattern does not depend on the coefficient of light absorption:

$$p_m = \frac{\beta W\omega}{4\pi C_p r}.$$

The half-width of the directivity pattern $\Delta\varphi_{0.7} \approx 2\alpha(\sqrt{3})/k$ for $k \gg \alpha$ can be very small. This narrow-beam mode of radiation is realized with the help of blue-green laser radiation. An advantage of laser radiation in the blue-green range is related to the favorable propagation conditions in the atmospheric transparence window and the possibility of focusing from relatively high altitudes.

When $ka \ll 1$ and $k \leq \alpha$ (a low-frequency sound radiation by a narrow laser beam), the maximum of the directivity pattern coincides with the normal to the sea surface. The radiation is inefficient in comparison with the preceding case. In the limiting case $k \ll \alpha$, the directivity pattern exhibits a dipole character.

In the case of sound generation by a wide laser beam ($ka \gg 1$), the pronounced directivity of the field along the normal is realized, as follows from Eq. (1). Formally, this fact is taken into account by the fast decrease in the exponent in Eq. (1) with increasing φ.

Being interested in the transmission of a sound signal along the normal to the surface $\varphi = 0°$, we determine the conditions for obtaining the peak level of pressure in a narrowband signal at a preset depth r. For this purpose, we test Eq. (1) for a maximum by adding the factor $\exp[-\gamma(\omega)r]$, which takes into account the frequency-dependent coefficient of sound absorption in the sea $\gamma(\omega)$, to the right-hand side of this expression. It is evident that the maximal possible level of $p_\omega(r)$ can be realized by varying α and k. The known conditions of the maximum of a function of two variables [in this case, $p_\omega(\alpha, k)$] produce the following optimal values for a preset reception depth and real marine conditions [28]:

$$\alpha_{opt} = k_{opt} = \frac{120}{r_{[m]}^{2/3}}\ [\mathrm{cm}^{-1}].$$

The coefficient of optical absorption depends on the wavelength of laser radiation. It is technically difficult to change the wavelength. A partial optimization is performed at a fixed value of α for the modulation frequency of laser radiation. The presence of the optimum in frequency is connected with the fact that the efficiency of thermooptical conversion in the continuous mode of operation increases with the modulation frequency. However, the propagation conditions in the sea become worse with a frequency increase. For example, in the case of laser radiation with a wavelength of 1.06 μm (which corresponds to $\alpha = 0.18\ \mathrm{cm}^{-1}$), we have a simple engineering formula for the optimal modulation frequency:

$$\omega_{opt} = \frac{9\times 10^4}{r_{[m]}^{1/3}}\ [\mathrm{s}^{-1}].$$

Thus, the optimal modulation frequency of a laser beam decreases slowly with the depth to which the acoustic signal must be transmitted.

An interesting comparative estimate of the intensity of a signal from a harmonic thermooptical sound source at a preset depth r is given in [22]. The comparison was performed with the intensity of the direct signal transmission from a blue-green laser $I_{0.55}$ (an optical radiation with a wavelength of 0.55 μm). The following expression was obtained using Eq. (1):

$$G = \frac{I_{ac}}{I_{0.55}} = 5\times 10^{-12} I_{1.06}\exp\alpha_{0.55}r,$$

where $I_{1.06}$ [W/cm^2] is the intensity of infrared radiation with a wavelength of 1.06 μm, which excites the thermooptical source, and $\alpha_{0.55} = 0.05\ \mathrm{m}^{-1}$ is the coefficient of absorption of the blue-green beam in the sea medium. The estimate shows that, at $I_{1.06} = 100$ W/cm^2, we have $G > 1$ for $r > 400$ m. In other words, starting from a certain depth, the information channel with conversion according to the thermooptical mode turns out to be energetically preferable to the purely optical one.

The first full-scale experiments with thermooptical sources were conducted in 1973 at Travis Lake (Texas)

by a research team from Texas University, Austin [9, 10]. The radiation sources were free-running lasers with neodymium glass (the second harmonic) and ruby. Submerged "virtual" thermoacoustic arrays with a length of up to several meters, which emitted underwater acoustic signals with a duration of 1–2 ms and carrier frequencies from 20 to 50 kHz, were realized with the help of a periscope and changeable onboard systems. The distinctive feature of this configuration is the high vertical directivity of sound radiation. In fact, the half-width of the directivity pattern is $\theta_{1/2} \approx \alpha/k$, which gives several degrees for the case of visual range lasers and indicated frequencies. Later, thermooptical sound sources were used for monitoring surface waves [35] and solving a series of model problems [11]. The endeavors to increase the efficiency of photoacoustic conversion in the thermooptical mode forced researchers to consider the potentialities of sound generation by a moving laser beam.

WHAT CAN BE EXPECTED FROM A MOVING NONCONTACT UNDERWATER ACOUSTIC SOURCE?

The unique feature of the thermooptical conversion mode is the opportunity to create a moving noncontact underwater acoustic source. The first solution to the problem of generation of a shock wave by a laser focus moving in water with a supersonic velocity was obtained in [37]. Studies of moving noncontact sound sources were conducted in the USSR by the research teams of F.V. Bunkin, L.M. Lyamshev, and O.V. Rudenko [7, 23, 38]. It was found that the general efficiency of conversion does not depend on whether the light spot moves along the water surface or remains fixed [38]. However, interest in such a way of photoacoustic conversion persisted, because it offered some additional opportunities for remote control over the sound field in the sea medium. The intrapulse modulation mode is most often used for moving noncontact underwater acoustic sources. The duration of the pulse itself constitutes 1–1.5 ms, and the intrapulse modulation has a frequency of 2–20 kHz. The trajectory of the spot motion along the surface represents a straight line with a length of 5–10 m. Unlike the stationary case, the radiated sound field has a pronounced asymmetry of directivity with respect to the normal to the sea surface. The parameter

$$\tilde{M} = \frac{v}{c}\sin\varphi\cos\theta,$$

where v is the velocity of laser spot scanning and θ is the angle in the horizontal plane between the spot trajectory and the direction to the receiver, plays an important role in the field description.

In the case of the subsonic source motion, $v/c < 1$, the field description is rather simple. The signal represents a pulse compressed by a factor of $(|1 - \overline{M}|)^{-1}$ with the Doppler frequency filling

$$\omega_d = \frac{\omega}{|1 - \tilde{M}|}.$$

At the relative velocity of motion $v/c = 0.9$, the maximum of the directivity pattern occurs in the direction $\varphi = 82°$. Estimation shows that, in this direction, when the sea noise corresponds to waves of Beaufort 4, with an optical pulse energy of 200 J and a modulation frequency of 2 kHz, a signal-to-noise ratio of 20 dB is attained at a distance of 5 km, which is very good for thermal photoacoustic conversion. The Doppler frequency is equal to 20 kHz in this case. Thus, the conversion efficiency does not grow, but the field is redistributed very efficiently.

A continuous spatial structure of the field corresponds to a supersonic scanning by a laser spot along the surface, $v/c > 1$. The analysis of the field structure is performed in the plane of motion of the noncontact underwater acoustic source ($\cos\theta = 1$). A signal at the Doppler frequency is detected in the motion direction, and an inverted tone signal is detected in the opposite direction. The condition $\tilde{M} \cong 1$ corresponds to the Cherenkov direction. In this direction, a signal with an amplitude that is record-breaking for thermooptical sound generation is emitted as the Mach wave. For the peak value of the pressure radiated in the Cherenkov direction, we have the expression [38]

$$P_M = \left(\frac{\alpha c a_0}{2\pi a\cos\varphi}\right)^2 \frac{\beta E_0}{C_p r},$$

where a_0 is the spot aperture and a is the length of the scanning trajectory. The comparison with the radiation level of a stationary noncontact underwater acoustic source with the same energy gives a gain of 20 or more times. The diffraction minima correspond to the values

$$\tilde{M} = 1 \pm \frac{a\omega}{2\pi c}.$$

A broadband pulse (which is typical of the case of scanning by an ordinary focus) and a tone signal can be distinguished according to the signal character in the Cherenkov direction in the conditions of the spatial modulation of the focal spot at the surface by a grid with the step L. In this case, the carrier frequency of the signal is c/L. Such a technique is proposed in [33], where the scheme of its realization is also suggested.

The calculations conducted independently at the Laboratory of Applied Research of the Texas University, Austin [12, 14, 15] confirmed the major features of moving noncontact underwater acoustic sources. The following expression for the upper limit of the effi-

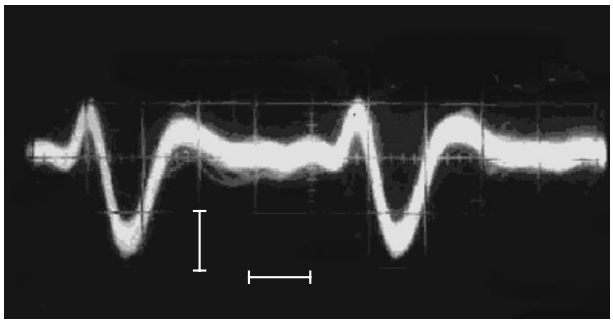

Fig. 1. Oscilloscope pattern of a fragment of the acoustic signal excited in the quasi-continuous mode of operation and detected at a depth of 1 m directly under the light spot in the frequency band from 0.1 Hz to 10 kHz. The repetition rate of the pulses of excitation radiation is 20 kHz, and the average optical power is 20 W. The horizontal scale is 10 μs/division, and the vertical scale is 0.05 Pa/division.

ciency of noncontact underwater acoustic sources in the case of narrowband reception was obtained [14]:

$$\eta < \left(\frac{\beta c}{4\pi C_p}\right)^2 E_0 k^2 4\pi B_a/\rho c,$$

where B_a is the reception bandwidth. Concerning the location applications, from the latter relation it follows that, for a short-range laser-acoustic sonar (the modulation frequency of the beam is 30 kHz and E_0 = 100 J), the value of $\eta = 10^{-6}$ is still acceptable. At the same time, a long-range sonar (a frequency of 3 kHz and E_0 = 100 J) is characterized by small values of $\eta = 10^{-9}$ (even an increase in E_0 by one order of magnitude does not improve the situation).

An unquestionable advantage of moving noncontact underwater acoustic sources consists not in the increase in η but in the possibility of forming a narrow acoustic beam with a record-breaking pressure level in a preset direction, as well as the possibility of providing a reliable targeting due to the frequency character of the probing signal in space.

SURFACE WAVES AND NONCONTACT UNDERWATER ACOUSTIC SOURCES

The influence of surface waves on the parameters of noncontact underwater acoustic sources has widely attracted the attention of researchers [35]. Indeed, the sea surface is always included in the region of photoacoustic conversion. Its linear and angular motions cannot but affect the characteristics of the generated field. Amplitude-phase distortions of a signal and fluctuations of arrival times at a stationary submerged sound receiver were expected. Depending on the problem to be solved, it was necessary either to compensate this influence (for example, in the problems of remote control of underwater vehicles [26, 27]) or, conversely, to stress it (in the problems of monitoring the state of the sea surface).

It is interesting to observe the influence of surface waves on thermooptical sound excitation in the aforementioned quasi-continuous mode. Such a mode was realized in a model experiment in the testing basin of the Andreev Acoustics Institute with the help of an LTI-501 YAG laser. Its radiation was a sequence of pulses with a frequency of 10–20 kHz and a high length-to-period ratio. The laser provided a rather high average power of 20 W, and the characteristic signal level at a depth of 1 m in a broad frequency band was 0.06 Pa. A characteristic oscilloscope pattern for an acoustic signal excited in the case of irradiation of a calm water surface is given in Fig. 1. It is possible to conclude even from the pattern shape that the spectrum of the signal excited in the quasi-continuous mode is enriched with higher harmonics. A spectral analysis in the case of a 7-Hz transmission bandwidth of the filter of a spectrum analyzer provides an opportunity to reveal the fine structure of the components consisting of a set of equidistant lines spaced in frequency at 100 Hz. This can be explained by the fact that the peak optical power was not constant but oscillated with a frequency of 100 Hz and a depth up to 30%. In their turn, these components for the case of higher harmonics are very sensitive to the presence of surface waves.

If controlled waves are produced at the water surface, their influence is more and more noticeable with the growth in the harmonic number. In the model experiment, a wave generator created waves with a period of 2 Hz and an amplitude of 10 cm at the basin surface. The repetition rate of optical pulses was 16 kHz. The influence of waves on the spectral characteristics is barely noticeable for lower harmonics (Figs. 2a, 2b) and becomes essential with the growth of the harmonic number (Figs. 3a, 3b). At constant parameters of surface waves, each line broadens proportionally to the harmonic number. This is connected with the Doppler modulation of the radiation of the source, which moves together with the surface. The level of the spectral density of surface waves correspondingly drops. As one can see from Fig. 3b, the components of the sixth harmonic of the signal are sharply reduced in amplitude. The change in the width of the components of higher harmonics provides an opportunity to evaluate qualitatively the parameters of surface waves.

SURFACE NONLINEAR NONCONTACT UNDERWATER ACOUSTIC SOURCES: APPLICATION TO PROBLEMS OF CLASSIFICATION OF UNDERWATER OBJECTS

A large number of papers, including reviews, are devoted to marine applications of surface nonlinear

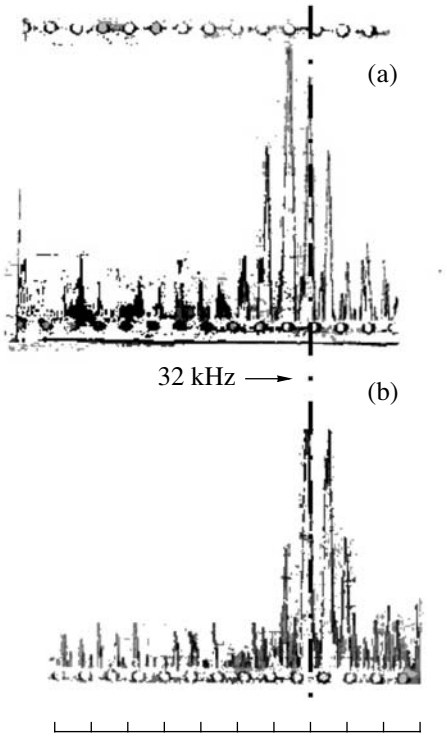

Fig. 2. Fine structure of the second harmonic of the acoustic signal at a depth of 3 m (a) in the absence and (b) in the presence of waves on the surface. The repetition rate of optical pulses is 16 kHz. The horizontal scale is 100 Hz/division.

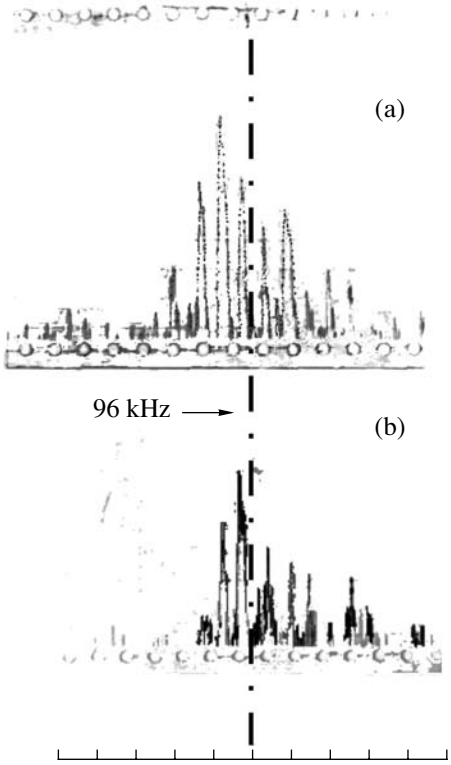

Fig. 3. Fine structure of the sixth harmonic of the acoustic signal at a depth of 3 m (a) in the absence and (b) in the presence of waves on the surface. The repetition rate of optical pulses is 16 kHz. The horizontal scale is 100 Hz/division.

noncontact underwater acoustic sources [21, 30, 31]. Here, we consider one of the applications that is based on bionic analogies. The point is that, as early as in the first experiments with a combined source of sound, it was found that the pulse characteristics are similar to the sounding pulses of cetaceans [39]. Such pulses belong to the class of so-called ultrashort pulses, which seem to be very promising for short-range sonars to provide not only the detection of an underwater target but also its classification. Let us note the important advantages of ultrashort pulses [40]. First, in the case of equal widths of the spectra of ultrashort pulses and conventional narrowband signals (and, therefore, in the case of the same spatial resolution), the ultrashort pulses are less subjected to attenuation and better preserve the initial profile. Second, in the case of a preset resolution determined by the frequency bandwidth, the upper and lower limiting frequencies can be selected in such a way that the signal spectrum will cover the range of natural resonances of the object to be located. In this case, when an ultrashort pulse is reflected, its shape and spectrum will change essentially because of the contribution of the shape and aspect angle of the object and the contribution of its natural resonances (in its turn, this carries information on the elastic and absorptive properties of the object). The shape of narrowerband signals changes inessentially in the case of reflection.

Pulsed signals are characterized by the bandwidth coefficient

$$\Omega = 2(f_{up} + f_{low})/(f_{up} - f_{low}),$$

where f_{up} and f_{low} are the upper and lower limiting frequencies of the spectrum, respectively.

Ultrashort acoustic pulses can be generated not only by dolphins or in the process of photoacoustic conversion. Common transducers and irreversible (explosion or electrical discharge) sources are also used to generate them. However, the property of conventional sound sources is that an ultrashort pulse emitted by them contains additional extraneous oscillations caused by the collapse of cavities in the case of explosions or because of the insufficient bandwidth of the radiating underwater acoustic array [41]. This is the reason why the maximal value of the bandwidth attained in the usual way does not exceed $\Omega = 0.5$. A typical pulse from a combined source that arises due to water irradiation by a pulse of a CO_2 laser provides a value of the bandwidth coefficient close to the record-breaking value of 2. Moreover, an important feature of a photoacoustic source of this type is the absence of sidelobes in the directivity pattern. In fact, the angular distribution of the signal energy in a wide band [or wide band angular

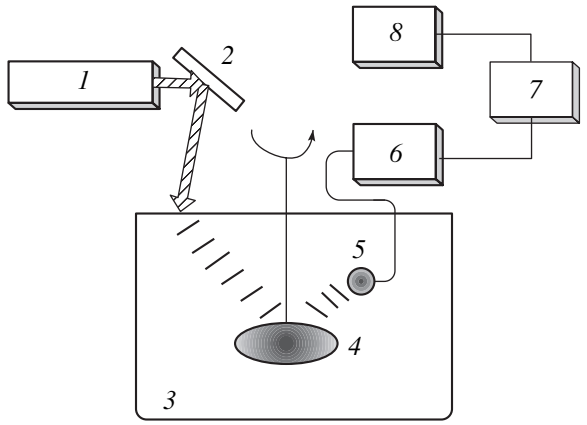

Fig. 4. Block diagram of the model experiment on photoacoustic classification of a submerged object: (*1*) pulsed CO_2 laser, (*2*) rotating mirror, (*3*) test acoustic basin, (*4*) target, (*5*) B&K 8101 hydrophone, (*6*) analog-to-digital converter, and (*7*) computer.

energy distribution (WBEAD) in terms of [42]} has a shape close to Gaussian.

This mode was used in a model experiment on studying the classification potential of ultrashort pulses of photoacoustic origin. In this case, the system of processing of the signal reflected from a target took into account the similarity of the photoacoustic pulse to the sounding pulses of cetaceans, which allow the animals to detect the targets that are interesting to them. Namely, the procedure of pulse segmentation was used.[1] It belongs to the methods of nonlinear filtration and analogous procedures used for speech recognition [43]. In this case, the segmentation algorithm is based on the assumption that the shape of an ultrashort pulse should not change essentially when it is reflected from a smooth target. In the case of additive superposition of the echo signal and interference (noise or reverberation), an interval with time and energy parameters closely corresponding to the initial pulse appears in the record. The selection of intervals with peculiarities from the record and their classification with the echo signal from the target or with the signals of different origin is performed by an adapted interactive expert system based on a computer.

Figure 4 presents a block diagram of the experiment conducted in a laboratory acoustic basin. Metal and polyfoam cylinders with the ends shaped as semispheres were used as targets. The target length was 9 cm and their diameter, 4 cm. The targets were suspended in the horizontal position. In the course of experimenting, the targets were rotated around the vertical axes with an angular step of 10°.

A B&K 8101 hydrophone with a reception frequency bandwidth of 150 kHz was used as a receiver. The bistatic scheme of location was realized; i.e., the receiver position did not coincide with the source position. The pulse repetition rate was 0.5 Hz. The direct signal, the echo signal from the target, and the reverberation signals reflected by the basin walls were detected by the hydrophone, passed through an amplifier and an analog-to-digital converter, and were processed by a computer. Each laser pulse gave rise to a single realization of the echo signal. The upper limit of detectable frequencies was 80 kHz. Records of 190 realizations were obtained for each target.

At the first stage of signal processing, the reverberation signal was separated from the direct and echo signals. Segmentation was performed taking into account the parameters of the sounding signal with a preset confidence interval of possible deviations of the time and energy parameters of the signal reflected from the target.

Further, it was necessary to select, according to the set of spectral-time classification features, from all separated signals precisely the signal that corresponds to the echo signal from the target. All other signals were declared to be a false target and ignored. Finally, after the detection of the echo signal, a conclusion concerning the target material was made according to the same set of features.

Some experimental records are given in Fig. 5 (a polyfoam target) and Fig. 6 (a steel target). Selected intervals are indicated on the time sweeps in the upper parts of the figures, and their spectra are given in the lower parts. In both figures, intervals *1* correspond to the sounding signal, intervals *2* present the echo signals from the targets, intervals *3* show the mirror reflection from the bottom, and interval *4*, the reverberation signal. Naturally, intervals *2* are most interesting from the point of view of analysis. In the case of an acoustically soft target (Fig. 5), intervals *1* and *2* are in antiphase, which is not observed in the case of an acoustically hard target. The spectra of intervals *2* differ noticeably for different targets. It is difficult to take concentrated reflections (intervals *3*) for something else. Intervals *4* corresponding to reverberation signals also have a stable "unique" set of features, and their interfering influence can be easily eliminated.

The dependence of the noise stability of the method and the efficiency of the target material classification on the aspect angle of the target was analyzed in the case of sounding by ultrashort pulses. It turned out that an ultrashort pulse excited in water by laser radiation provides stable parameters for the target classification, these parameters being independent of the aspect angle of sounding. A high efficiency of segmentation of the primary records and the efficiency of analysis of the interval structure were maintained in all realizations. The experiment conducted demonstrated the applicability of the photoacoustic technique to solving the problems of underwater detection and ranging of small targets in shallow-water regions with a high level of reverberation interference.

[1] The segmentation software was provided by S.V. Ryabikov.

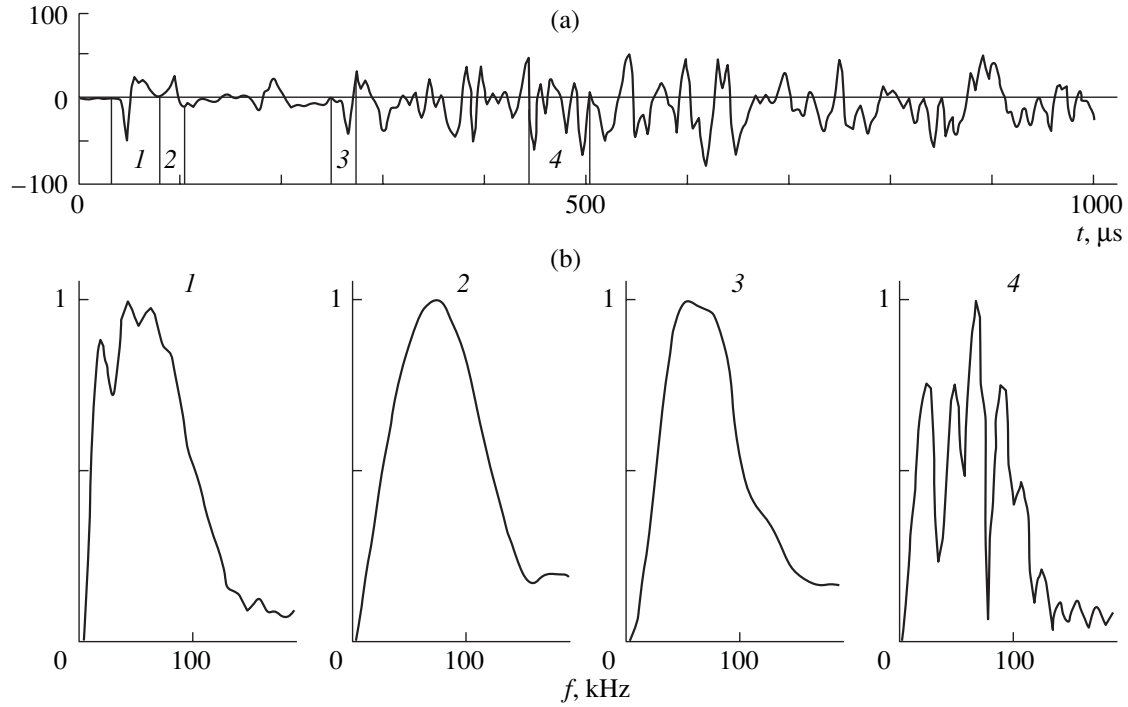

Fig. 5. Records corresponding to a polyfoam target: (a) time sweep for one of the realizations and (b) the spectra of the separated intervals (indicated by numbers).

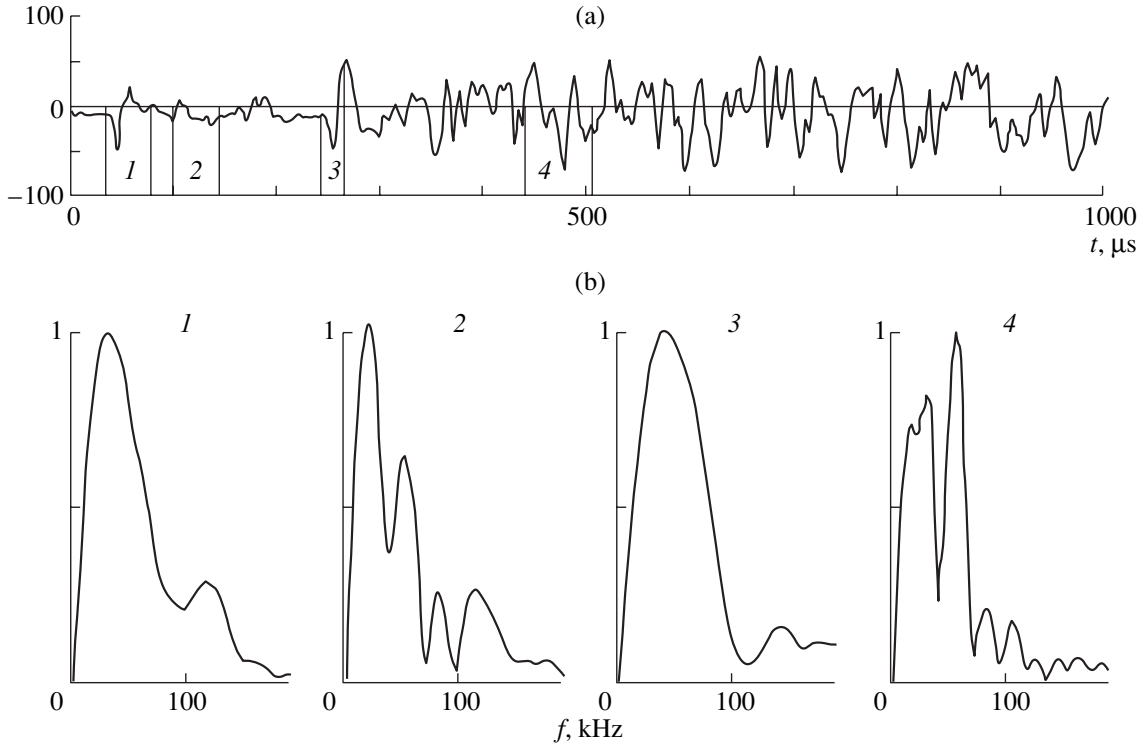

Fig. 6. Records corresponding to a steel target: (a) time sweep for one of the realizations and (b) the spectra of the separated intervals (indicated by numbers).

CONCLUSION

There is already considerable successful experience in full-scale applications of photoacoustic technology. The diagnostics of surface waves [44], bathymetry [30], the analysis of bottom reverberation in shallow-water regions [45], and the diagnostics of the fine surface structure of the sea medium have been mastered. Model studies of sonar applications [11, 13, 16, 46] have been conducted, and ways of identifying small submerged objects and transmitting remote control signals to autonomous oceanographic buoys [27, 28] have been determined. Certain inflated expectations of the first years of photoacoustic underwater investigations, when it was assumed that the source range will be tens of kilometers at least, are more than compensated for by the unexpectedly discovered unique opportunities for the diagnostics of the marine environment on the subkilometer scale.

However, the problem of long-range photoacoustics remains unsolved. In fact, this is a question of the development of laser technology. The development of a new class of reliable powerful lasers is critical for progress in the photoacoustic monitoring of the marine environment [47]. The rapid development of laser technology may make expedient various techniques of realization of noncontact underwater acoustic sources. For example, new excimer lasers emitting short ultraviolet pulses with a small length-to-period ratio provide a high average power. Shifting the radiation wavelength of such lasers on account of stimulated scattering to the range 0.55–1 μm provides an opportunity to maintain the boiling conditions modulated by a frequency of 1–10 kHz in a limited volume of liquid. One can expect that this mode of operation will serve as the basis for a low-frequency noncontact underwater acoustic source with an acoustic power of tens of watts. NH_3 lasers whose power reaches 500 kW and the whole class of chemical lasers with a radiation wavelength of 1.3 μm are promising for the generation of surface nonlinear sources. At the same time, advances in the development of conventional laser technology will in future provide compactness and reliability for the new generation of photoacoustic systems.

ACKNOWLEDGMENTS

I am grateful to O.B. Ovchinnikov and A.E. Pashin for their assistance in model experiments.

REFERENCES

1. R. M. White, J. Appl. Phys. **34**, 3559 (1963).
2. G. A. Askar'yan, A. M. Prokhorov, G. F. Chanturiya, and G. P. Shipulo, Zh. Éksp. Teor. Fiz. **44**, 2180 (1963) [Sov. Phys. JETP **17**, 1463 (1963)].
3. R. G. Brewer and K. E. Rieckhoff, US Patent No. 3,392,368 (9 July 1968).
4. P. J. Westervelt and R. S. Larson, J. Acoust. Soc. Am. **54**, 121 (1973).
5. F. V. Bunkin and V. M. Komissarov, Akust. Zh. **19**, 305 (1973) [Sov. Phys. Acoust. **19**, 203 (1973)].
6. F. V. Bunkin, N. V. Karlov, V. M. Komissarov, and G. P. Kuz'min, Pis'ma Zh. Éksp. Teor. Fiz. **13**, 479 (1971) [JETP Lett. **13**, 341 (1971)].
7. F. V. Bunkin and M. I. Tribel'skiĭ, Usp. Fiz. Nauk **130**, 193 (1980) [Sov. Phys.–Usp. **23**, 105 (1980)].
8. L. M. Lyamshev and K. A. Naugol'nykh, Akust. Zh. **27**, 641 (1981) [Sov. Phys. Acoust. **27**, 357 (1981)].
9. T. G. Muir, J. Acoust. Soc. Am. **54**, 298 (1973).
10. T. G. Muir, C. R. Culbertson, and J. R. Clynch, J. Acoust. Soc. Am. **59**, 735 (1976).
11. Y. H. Berthelot, J. Acoust. Soc. Am. **85**, 1173 (1989).
12. Y. H. Berthelot and I. J. Bush-Vishniac, in *Progress in Underwater Acoustics*, Ed. by Harold M. Merklinger (Plenum, New York, 1987), pp. 603–610.
13. N. P. Chotiros, Proc. SPIE **925**, 255 (1988).
14. N. P. Chotiros, *The Moving Thermoacoustic Array. A Theoretical Feasibility Study* (ARL, Austin, Texas, 1985).
15. Y. H. Berthelot, *Generation of Underwater Sound by a Moving High Power Laser Source* (ARL, Austin, Texas, 1985).
16. R. Cawley, *Linear Propagation Model for Laser Induced Ultrasound in Water* (Silver Spring, Maryland, 1982).
17. Y. R. Qi and D. Y. Zhang, Prog. Nat. Sci. (Suppl.) **6**, S-751 (1996).
18. G. Cui, R. Li, T. Yun, and G. Sang, Prog. Nat. Sci. (Suppl.) **6**, S-755 (1996).
19. L. M. Lyamshev, *Laser Thermooptical Excitation of Sound* (Nauka, Moscow, 1979).
20. K. A. Naugolnykh, S. V. Egerev, I. B. Esipov, and K. A. Matveev, J. Acoust. Soc. Am. **106**, 3135 (1999).
21. S. V. Egerev, in *Progress in Photothermal and Photoacoustic Science and Technology*, Vol. 3: *Life and Earth Sciences*, Ed. by A. Mandelis and P. Hess (SPIE Optical Engineering, Bellingham, 1997), pp. 379–414.
22. A. I. Bozhkov and F. V. Bunkin, Kvantovaya Élektron. (Moscow) **2**, 1763 (1975).
23. B. K. Novikov, O. V. Rudenko, and V. I. Timoshenko, *Nonlinear Underwater Acoustics* (Sudostroenie, Leningrad, 1981; Acoustical Society of America, New York, 1987).
24. O. A. Bukin, V. I. Il'ichev, and V. D. Kiselev, Dokl. Akad. Nauk SSSR **315**, 84 (1990) [Sov. Phys. Dokl. **35**, 940 (1990)].
25. O. A. Bukin, V. I. Il'ichev, and V. D. Kiselev, Pis'ma Zh. Éksp. Teor. Fiz. **52**, 1261 (1990) [JETP Lett. **52**, 681 (1990)].
26. S. V. Egerev, L. M. Lyamshev, A. K. Morozov, and A. E. Pashin, Okeanologiya (Moscow) **36**, 314 (1996).
27. S. V. Egerev, A. K. Morozov, and L. M. Lyamshev, Acta Acust. (2003) (in press).
28. S. V. Egerev, in *Proceedings of the European Conference on Underwater Acoustics*, Ed. by M. Weidert (Elsevier, Luxembourg, 1992), p. 658.
29. L. J. González and I. J. Bush-Vishniak, J. Acoust. Soc. Am. **84**, 1587 (1988).
30. G. D. Hickman and J. R. Edmonds, J. Acoust. Soc. Am. **73**, 840 (1983).

31. B. S. Maccabee, in *Proceedings of Symposium: Ultrasonics-87* (IEEE, New York, 1987), p. 1099.
32. A. D. Pierce and Y. H. Berthelot, J. Acoust. Soc. Am. **85**, 2227 (1989).
33. A. D. Pierce and H. A. Hsieh, in *Progress in Underwater Acoustics,* Ed. by Harold M. Merklinger (Plenum, New York, 1987), pp. 595–602.
34. M. L. Lyamshev, V. G. Mikhalevich, and G. P. Shipulo, Akust. Zh. **26**, 230 (1980) [Sov. Phys. Acoust. **26**, 126 (1980)].
35. S. V. Egerev and A. E. Pashin, Izv. Akad. Nauk SSSR, Fiz. Atmos. Okeana **27**, 259 (1991).
36. P. M. Morse and K. U. Indard, *Theoretical Acoustics* (Princeton Univ. Press, Princeton, 1986).
37. I. B. Esipov, Akust. Zh. **23**, 164 (1977) [Sov. Phys. Acoust. **23**, 92 (1977)].
38. L. M. Lyamshev and L. V. Sedov, Akust. Zh. **26**, 182 (1980) [Sov. Phys. Acoust. **26**, 100 (1980)].
39. V. M. Bel'kovich and N. A. Dubrovskiĭ, *Sensory Basics of Orientation in Cetaceans* (Nauka, Leningrad, 1976).
40. H. F. Harmuth, *Nonsinusoidal Waves for Radar and Radio Communication* (Academic, New York, 1981; Radio i Svyaz', Moscow, 1985).
41. P. Cobo-Parra and R. Carbo-Fite, J. Phys. IV **4** (C5), C5-347 (1994).
42. M. E. Zakharia, presented at *XI All-Union Acoustical Conference* (Moscow, 1991), Separate Issue.
43. J. Mantas, Pattern Recogn. **20** (1), 1 (1987).
44. S. V. Egerev, L. M. Lyamshev, and K. A. Naugol'nykh, Akust. Zh. **36**, 807 (1990) [Sov. Phys. Acoust. **36**, 452 (1990)].
45. S. V. Egerev, A. N. Ivakin, O. B. Ovchinnikov, and A. E. Pashin, J. Phys. IV **4** (C5), C5-351 (1994).
46. X. M. Ren, Y. R. Qi, D. Y. Zhang, and Z. Z. He, Prog. Nat. Sci. (Suppl.) **6**, S-760 (1996).
47. S. V. Egerev, in *Proceedings of IV Russian Scientific and Engineering Conference "Current Status, Problems of Navigation and Oceanography"* (GNINGI, St. Petersburg, 2001), Vol. 2, p. 109.

Translated by M. Lyamshev

Acoustical Physics, Vol. 49, No. 1, 2003, pp. 62–67. Translated from Akusticheskiĭ Zhurnal, Vol. 49, No. 1, 2003, pp. 71–76.

Qualitative Difference between the Signal and the Surface Reverberation in the Active Location with a Coherent Cumulation

V. A. Zverev and P. I. Korotin

Institute of Applied Physics, Russian Academy of Sciences,
ul. Ul'yanova 46, Nizhni Novgorod, 603950 Russia
e-mail: zverev@hydro.appl.sci-nnov.ru

Received December 14, 2001

Abstract—It is shown that outwardly similar (in shapes and levels) pulses reflected from a moving discrete target (the signal) and produced by sound scattering from the waved water surface (the surface reverberation) have a qualitative difference, which manifests itself in a coherent cumulation of signals. The signal and the surface reverberation differently increase as the interval of their coherent summation grows. Quantitatively, this difference consists in the fact that the signal has a much smaller variance of deviations from the linear law of its increase. The effect is observed both in in-field experiments and in numerical simulations. © *2003 MAIK "Nauka/Interperiodica".*

Dedicated to the memory of my friend and colleague L.M. Lyamshev

In the active location, the main interference is reverberation, which cannot be avoided by increasing the power of the probing pulse transmitted into the medium. The bottom reverberation can be noticeably suppressed if the target to be detected moves in such a manner that a Doppler shift occurs in the reflected signal. The frequency shift produced in the reflected signal by the target motion is the qualitative difference between the desired signal and the bottom reverberation. To take advantage of this opportunity, it is sufficient to apply so-called interperiod subtraction, which is widely used in radar for the same purpose [1]. Interperiod subtraction has a frequency characteristic that excludes the zero Doppler frequency, and this feature strongly attenuates the frequencies that are close to zero and suppresses the contribution of the bottom reverberation. Thus, the possibility arises of observing targets whose scattered field has a level that is much lower than that of the bottom reverberation [2–4].

With surface reverberation, which has a wide spectrum in the same frequency band as the Doppler shift of the desired signal, the interperiod processing of the signal becomes less effective. The efficiency can be increased by applying the coherent cumulation of the received pulses. Coherent cumulation consists in the spectral Fourier analysis of a set of samples from the sequence of pulses, which have the same delays relative to the transmitted pulse (the signals of the same range). The spectrum of such a sequence is a frequency decomposition of the Doppler frequency shift (DFS) of the signal. If a discrete target moves uniformly within the entire duration of the spectral decomposition, its DFS spectrum is discrete. If the surface motion were absolutely chaotic, its DFS spectrum would be continuous. Then, the coherent cumulation would lead to the same gain in the signal-to-reverberation ratio as in the spectral detection of a discrete-frequency signal against the background of noise with a continuous spectrum. In reality, the surface motion is not absolutely chaotic. This motion has a spectrum that includes rather narrow maxima. For such a spectrum to considerably reduce the gain of coherent cumulation, it is not necessary that these frequency bands precisely coincide with the DFS of the signal. In the general case, neither the range nor the object speed are known in advance. Therefore, when a signal with a narrow DFS spectrum is observed, one cannot be sure whether this is the reflection from the object or the reverberation. If the sea state, the direction of the waves, and the location direction are such that reverberation signals have narrow maxima in the DFS spectrum, the desired signal can be extracted from this background only if its level is much (as a rule, by 10 dB or more) higher than that of the reverberation. This condition significantly restricts the scattering cross sections for the signals to be reliably detected.

The purpose of this work is to show (based on the experiment) how one can distinguish the signals reflected from the object to be located from the reverberation signals that have a narrow DFS spectrum, are localized in range, and exhibit comparable or even higher levels than the signal. The main idea of this study consists in the fact that regular signals with a dis-

1063-7710/03/4901-0062$24.00 © 2003 MAIK "Nauka/Interperiodica"

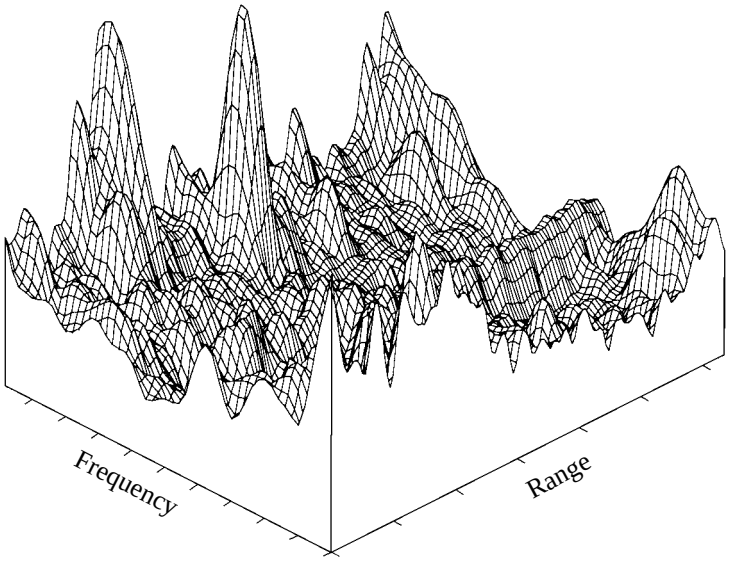

Fig. 1. Pulse pattern in the range–Doppler frequency plane.

crete spectrum are in some aspects quite different from narrowband signals that are random in their nature and are formed by the sound field of a continuous spectrum. It is evident that the signal with a discrete spectrum can be synchronized with the sampling rate in such a way that its Fourier spectrum will occupy a single or several frequency readings, with zeros at other frequencies. No synchronization will lead to the same result if the signal is represented by a narrow spectral line formed by a continuous spectrum: a narrowband noise can have a zero level in no finite frequency band. Unfortunately, the aforementioned feature of the discrete signal cannot be widely used in detecting the signal against the reverberation background, because too strong requirements are imposed on the signal coherence in this case.

We use another difference that does not impose such strict constraints on the coherence. It is known that, if a narrowband signal is coherently cumulated at its own frequency, its level increases proportionally to the cumulation time until its coherence time is reached. After that, the increase terminates. The signal and the reverberation response can have different coherence times. This difference can be quantitatively estimated by measuring the variance in the amplitude deviation from the linear law at the output of the filter that is tuned so as to obtain the maximal response at the maximal time of cumulation. The earlier the beginning of the deviation from the linear law, the higher the variance of the deviations is. For the experimental data, it is shown that the variances of the signal and the reverberation (the latter varying in the same manner as the signal in the range–frequency plane when the time of coherent cumulation increases) can differ by a factor of 7–8 for a cumulation time of several seconds.

Let us begin with considering the experiment. The experiment was performed at the Gor'ki storage lake. The depth of the lake was 7–8 m at the experimental site. A bistatic location scheme was used. The duration of the transmitted pulse was 2 ms. The repetition rate was 400 ms, and the transmitted frequency was 2 kHz. For signal reception, a linear horizontal array was used that consisted of 32 separate hydrophones and was 6 m in length. The signals received by each single hydrophone of the array were recorded in a broad frequency band. So, the array could be phased to select any desired direction of reception. The object of location was represented by a hollow cylindrical tube with a ballast 8 m in length and 0.6 m in diameter. The tube was towed by a rowing boat at a depth of 3 m, with a constant speed of about 0.5 m/s, in different directions and at different distances from the sound source and the receiving array.

As a result of the signal processing, which consisted of array phasing, interperiod subtraction, and coherently cumulation, the signal scattered by the object was reliably detected against all types of reverberation background. The processing procedure yields a high (about 10 dB) excess of the response level over all peaks of the interfering noise in the range–azimuth plane at all possible values of the DFS. The signal can be traced within nearly the entire tack. The coordinates of the scattered pulses form a sequence that fully agrees with the trajectory of the object.

To carry out the experiment under discussion, we had to roughen the signal processing to make the signal and reverberation equal in level. For this purpose, it was sufficient to give up the array phasing and sum up the processed signals from all array hydrophones in their absolute values (incoherently). The resulting pattern in the range–DFS plane is shown in Fig. 1. From this pattern, we determined the Doppler frequencies and the ranges for the two most pronounced pulses. One of

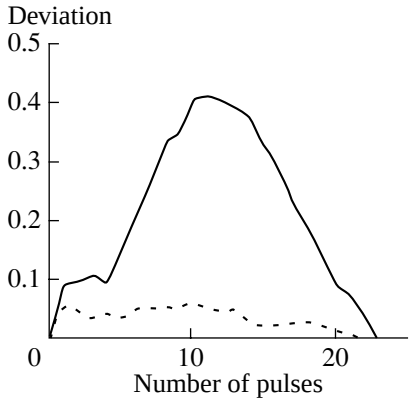

Fig. 2. Deviation of the pulse amplitude growth with increasing number of cumulated pulses from the linear law. Data of the in-field experiment. Signal and reverberation are shown by dashed and solid lines, respectively.

them, namely, the pulse whose coordinates precisely coincided with those of the highest pulse in the coherent summation of the signals received by the array hydrophones, was the desired signal.

To determine the variance in the deviation from the linear law for the signal increase with increasing time of coherent cumulation, we processed the signal in the following way. A function

$$F(n, m) = [f[m, r, n+1] - f(m, r, n)]\exp(i2\pi nw) \quad (1)$$

was formed, where n is the ordinal number of the transmitted pulse, m is that of the receiving hydrophone, f is the complex signal from the mth hydrophone within the time of the nth pulse transmission, r is the range coordinate for the pulse at hand, and w is the Doppler shift of this pulse. The square-bracketed difference in Eq. (1) produces the algorithm of interperiod subtraction, and the exponential serves for the subsequent coherent cumulation of the signal at the detected Doppler frequency shift (w).

Further signal processing consists in the summation of Eq. (1) over n with a variable upper limit t. This procedure follows the formula

$$S(m, t) = \sum_{n=0}^{n=t} F(n, m). \quad (2)$$

At the next stage, we perform the incoherent summation of the signals from all receiving hydrophones of the array:

$$U(t) = \sum_{m} |S(m, t)|. \quad (3)$$

The function represented by Eq. (3) linearly increases within the limits of the signal coherence. The task is to estimate the variance in the deviations from the linear growth. This can be done by using a function, which we call "deviation":

$$Q(t) = \frac{U(t)}{\max(U(t))} - \frac{t}{N}. \quad (4)$$

Here, N is the maximal value of the upper limit of summation in Eq. (2), or the maximal value of t. The concluding procedure consists in calculating the variance of the deviation:

$$D = \sqrt{\sum_{t} (Q(t) - \langle Q(t)\rangle)^2}. \quad (5)$$

The deviation function of Eq. (4) is shown in Fig. 2 for the two selected pulses of Fig. 1. The following values of deviation variances were obtained: $D = 0.136$ for reverberation and $D = 0.019$ for the desired signal. The ratio of the deviation variances of the reverberation and signal is equal to 7. This value is quite high in view of the fact that both pulses of Fig. 1 have the same shapes.

To clear up the physical origin of the difference observed in the deviations, we performed a numerical simulation. The task of such a simulation is similar to that considered in [5, 6]. We had to construct a mathematical model providing the values of the deviations and deviation variances that are close to those observed in the experiment. In the mathematical modeling, the signal and the reverberation were formed from a continuous signal $A(v)$. We selected different forms of the function $A(v)$ for the signal and the interference, while the rest of the procedures of forming these signals were the same.

For the signal, the function $A(v)$ was specified as

$$S(v) = \exp\left(i\frac{2\pi}{768}4v\right)MS(v). \quad (6)$$

For the reverberation, this function had the form

$$R(v) = \exp\left(i\frac{2\pi}{768}8v\right)MR(v). \quad (7)$$

The exponentials with complex arguments lead to different Doppler frequencies for the signal and the reverberation. The modulating functions determine the shape of the spectrum. These functions were as follows:

$$MS(v) = \exp(-0.0006v), \quad (8)$$

$$MR(v) = \cos\left(\pi\frac{v}{960}\right) \quad \text{for} \quad v < 480, \quad (9)$$

$$MR(v) = 0 \quad \text{for} \quad v \geq 480. \quad (10)$$

For the signal, the modulating function was specified as a decaying exponential. Thus, an exponentially decaying harmonic signal served as a model for the desired signal. Such a model agrees well with the experimental data. However, this model cannot be used for the reverberation no matter what the signal decay:

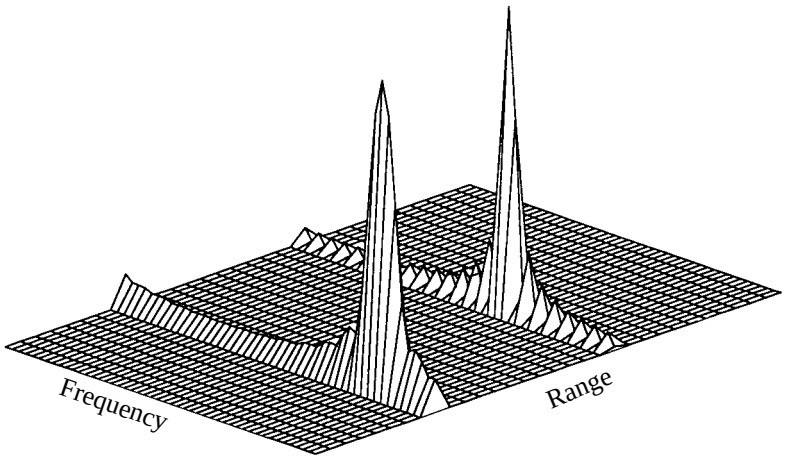

Fig. 3. Pulse pattern in the range–Doppler frequency plane in the numerical experiment.

the corresponding shape of the deviation curve given by Eq. (4) is quite different from that shown in Fig. 2. The statistical model that was constructed in [5, 6] on the basis of a random function with a narrowband spectrum cannot be accepted as well. Satisfactory results were obtained with the signal modeled as a single train of harmonic oscillations of a finite duration. With such a model, the deviation function of Eq. (4) has the shape of a triangle, which seems to be similar to the experimental curve of Fig. 2. If one applies a smooth envelope (according to the cosine law) to the finite train, the resulting dependence will be close to the experimental reverberation curve of Fig. 2 in all aspects. Functions (9) and (10) correspond to this model.

From the whole set of data containing $v = 768$ digits, a matrix $B(\xi, n)$ that had 32 columns with ordinal numbers ξ and 24 rows with ordinal numbers n was constructed. The variable ξ means the range, and the variable n has the same meaning as above: the ordinal number of the pulse. The matrix was formed according to the formula

$$B(\xi, n) = A(\xi + 32n). \quad (11)$$

From the matrix $B(\xi, n)$, a pulsed signal was formed by assigning a value of 1 to the matrix member corresponding to a single value of the variable ξ. The specified values were $\xi = 20$ for the signal and $\xi = 8$ for the reverberation. After that, the matrices of the signal and the reverberation were combined (multiplying the reverberation matrix by 2) and Fourier-transformed (i.e., coherently cumulated) over 24 values of n.

By using the aforementioned procedure, the pulses were formed from the harmonic signals with different amplitude modulation. These pulses are shown in Fig. 3 in the range–DFS plane. Figure 4 shows the laws of amplitude modulation for pulses (8), (9), and (10). In this figure, the values v divided by 32 are plotted along the horizontal axis.

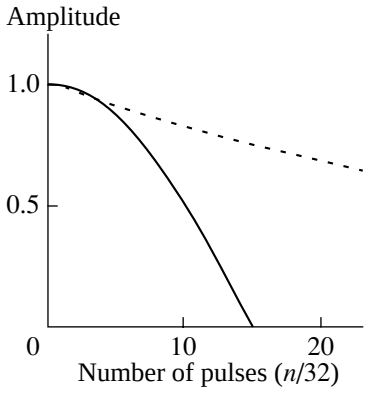

Fig. 4. Decay of the signal amplitude with increasing number of cumulated pulses in the numerical experiment. The functions $MR(v)$ given by Eqs. (9) and (10) are shown by the solid line, and the function $MS(v)$ given by Eq. (8), by the dashed line.

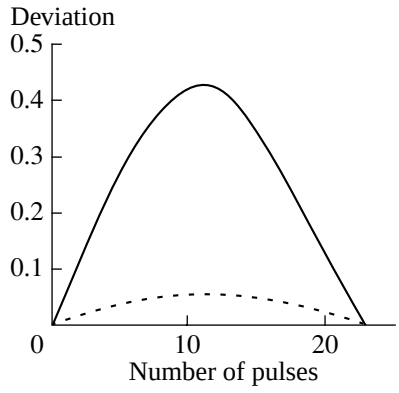

Fig. 5. Deviation of the pulse amplitude growth with increasing number of cumulated pulses from the linear law. Data of the numerical experiment. Signal and reverberation are shown by dashed and solid lines, respectively.

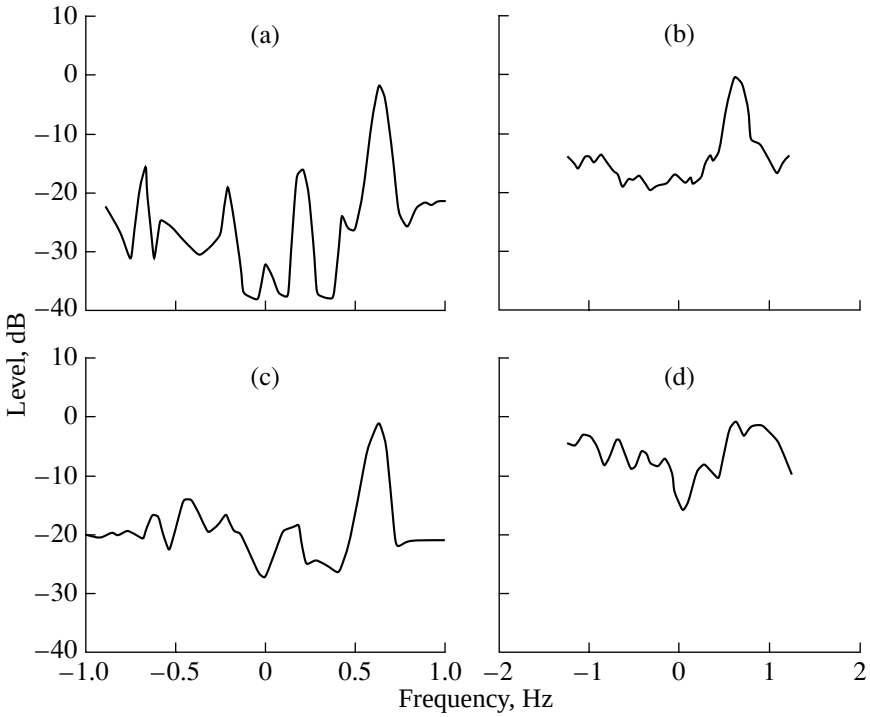

Fig. 6. Variances of deviations and maxima of the pulse amplitudes in the range–azimuth plane versus the DFS. The deviation variances are plotted with the opposite sign for the instants (a) 225 and (c) 300 s. The amplitude maxima are shown for the instants (b) 225 and (d) 300 s.

To determine the deviation function in the model experiment, we used the procedure given by Eq. (4), where the function $F(n, m)$ of Eq. (1) had the following form for the reverberation:

$$FR(n) = B(8, n)\exp(i2\pi n w_R). \quad (12)$$

For the signal, the same function was specified as

$$FS(n) = B(20, n)\exp(i2\pi n w_S), \quad (13)$$

where w_R and w_S were the frequencies maximizing the responses of Fig. 3 for the reverberation and the signal, respectively.

Figure 5 shows the deviation functions for the model signals. The variances of deviations were $D = 0.142$ and $D = 0.018$ for the numerically modeled reverberation and signal, respectively. The ratio of these values is close to 8.

Figure 6 illustrates the effect of using the deviation variance in extracting the signal from reverberation. The plot presents the results of processing the received signals for two time intervals of about 4 s in duration. The beginnings of the intervals correspond to (A) 225 and (B) 300 s after the object of location began to move. The signals were processed by a coherent summation of the outputs of all hydrophones of the array for all 24 pulses.

Figure 6 was obtained in the following way: in the range–azimuth plane, the maximal signal was found at a single fixed value of the DFS; for this signal, its absolute level and variance of deviations were determined; after that, the DFS value was slightly changed, and the signal maximum was again found for the whole range–azimuth plane. The data thus obtained were plotted in Fig. 6. The scattering cross section of the object of location was much greater at instant A than at instant B. Therefore, the signal level is rather high in Fig. 6b. At instant B, the scattering cross section is so small that the signal is undetectable in level. However, at instant B, the signal is reliably detected by using its deviation variance.

Thus, the difference in coherence between the reverberation and the signal can be used to reduce the threshold of detection and extraction of the signal against the reverberation background. This difference can be explained by the fact that reverberation produces a pulse that is outwardly similar to the signal because of the shorter train of coherent pulses. Therefore, to reliably distinguish between the reverberation and the desired signal by the aforementioned method, one should make the time of coherent cumulation longer than the duration of the reverberation train; it is also preferable that the object to be located move uniformly along a straight line. The proposed method seems to be original and promising, as compared to those described in other recent publications (see, e.g., [8]).

ACKNOWLEDGMENTS

We are grateful to B.M. Salin, A.L. Matveev, and V.I. Turchin for useful discussions. This work was supported by the Russian Foundation for Basic Research, project nos. 00-15-96741, 99-02-16401, and 02-02-17056.

REFERENCES

1. R. S. Berkowitz, *Modern Radar: Analysis, Evaluation, and System Design* (Wiley, New York, 1965; Sovetskoe Radio, Moscow, 1969).
2. V. A. Zverev, Akust. Zh. **46**, 75 (2000) [Acoust. Phys. **46**, 62 (2000)].
3. V. A. Zverev, P. I. Korotin, A. L. Matveev, *et al.*, Akust. Zh. **46**, 650 (2000) [Acoust. Phys. **46**, 569 (2000)].
4. V. A. Zverev, P. I. Korotin, A. L. Matveev, *et al.*, Akust. Zh. **47**, 227 (2001) [Acoust. Phys. **47**, 184 (2001)].
5. R. A. Stephen, J. Acoust. Soc. Am. **100**, 2070 (1996).
6. V. A. Zverev, Akust. Zh. **46**, 770 (2000) [Acoust. Phys. **46**, 676 (2000)].
7. V. A. Zverev and N. V. Litvak, Akust. Zh. **45**, 807 (1999) [Acoust. Phys. **45**, 727 (1999)].
8. N. C. Makris and P. Ratilal, J. Acoust. Soc. Am. **109**, 909 (2001).

Translated by E. Kopyl

Acoustical Physics, Vol. 49, No. 1, 2003, pp. 68–74. Translated from Akusticheskiĭ Zhurnal, Vol. 49, No. 1, 2003, pp. 77–84.

Sound Scattering by a Body in a Planar Layered Waveguide

V. M. Kuz'kin

Wave Research Center, General Physics Institute, Russian Academy of Sciences, ul. Vavilova 38, Moscow, 119991 Russia

e-mail: gera@kapella.gpi.ru

Received December 25, 2001

Abstract—In the framework of the theory of integral equations, the problem of sound diffraction by pressure-release and acoustically stiff inhomogeneities of an oceanic waveguide is considered. The iteration method is used to obtain recurrent relations for the surface currents. The relations describe the diffraction process as a sequence of interactions between the body and the waveguide boundaries (multiple reflections). The validity condition for the zero-order approximation, which ignores multiple reflections, is formulated and physically justified. © *2003 MAIK "Nauka/Interperiodica".*

The rigorous theory of diffraction is known to be based on the Huygens principle combined with integral equations that determine the boundary-value problem. However, the current status of the theory of diffraction by bodies in a waveguide does not allow one to obtain rigorous explicit solutions to the boundary-value problem in a closed form [1, 2]. In the majority of acoustic problems, one deals with the Green's functions, for which the solutions to the integral equations can be found by nothing but numerical calculations. Although fast and reliable computer codes exist for calculating the diffracted fields, it is often advantageous to use approximate analytical approaches that allow one to obtain the characteristics of the scattering process in a simple and easy-to-grasp way. By now, the approximate methods [3–6] for calculating the diffraction structure of the sound field in waveguides, which are based on specific physical considerations, are exclusively limited to the situation when one can neglect the effects of multiple reflections from the body and the waveguide boundaries. At the same time, it is obvious that, if the body is located near one of the waveguide surfaces, the multiple scattering effects can be significant. The wide variety of such problems are concerned with the phenomena related to the effect of the interfaces between media on the diffracted field [7–9]. In this connection, it is important to obtain an approximate solution that allows one to consider and estimate the effects of multiple scattering. Such problems are impeded by the fact that the sound fields must satisfy the boundary conditions at the boundaries of the waveguide and the body, which have different geometric shapes and acoustic properties. In such situations, it is most advantageous to expand the external fields into the eigenfunctions of the waveguide and to solve the diffraction problem on the basis of the wave equation in its integral form. The advantage of this approach consists in the fact that the solutions of the integral equations automatically satisfy the boundary conditions at the interface between two media.

This paper presents the method of successive approximations (iterations) for solving the integral equations that describe the sound diffraction by a body with uniform Dirichlet and Neumann conditions in a plane-layered waveguide of the oceanic type. The validity conditions for the zero-order approximation, which ignores multiple reflections, are formulated and physically justified.

STATEMENT OF THE DIFFRACTION PROBLEM

Let us consider the problem of sound diffraction by acoustically soft (the *p*-case) and acoustically stiff (the *s*-case) bodies in a uniform plane-layered waveguide. For this purpose, we use the method of integral equations. A waveguide with thickness H and sound speed profile $c(z)$ has the upper boundary at $z = 0$ and the lower boundary at $z = H$. Let a point source of unit-amplitude harmonic waves be located at a point $Q_0(\mathbf{R}_0)$ with the coordinates $\mathbf{r} = (0, 0)$, $z = z_0$. The coordinates of the geometric center $Q_s(\mathbf{R}_s)$ of the body are $\mathbf{r}_s = (x_s, y_s)$, $z = z_s$, and the reception point $Q(\mathbf{R})$ has the coordinates $\mathbf{r} = (x, y)$, $z = z$. Here, $\mathbf{R} = \mathbf{r} + \mathbf{a}_z z$, $\mathbf{r} = \mathbf{a}_x x + \mathbf{a}_y y$ is the radius vector in the horizontal plane (x, y); and $\mathbf{a}_x$, $\mathbf{a}_y$, and $\mathbf{a}_z$ are the unit vectors. We introduce a Cartesian coordinate system whose origin coincides with the point Q_s. With this coordinate system, an arbitrary point of the medium is determined by its radius vector $\hat{\mathbf{R}} = \hat{\mathbf{r}} + \hat{\mathbf{a}}_z \hat{z}$, where $\hat{\mathbf{r}} = \hat{\mathbf{a}}_x \hat{x} + \hat{\mathbf{a}}_y \hat{y}$ is the radius vector in the horizontal plane and $\hat{\mathbf{a}}_x$, $\hat{\mathbf{a}}_y$, and $\hat{\mathbf{a}}_z$ are the unit vectors. Evidently, the following relation holds: $\mathbf{R} = \mathbf{R}_s + \hat{\mathbf{R}}$.

1063-7710/03/4901-0068$24.00 © 2003 MAIK "Nauka/Interperiodica"

As a result of diffraction, at the observation point $Q(\mathbf{R})$, the total field p is a superposition of the incident u and scattered w fields: $p(\mathbf{R}) = u(\mathbf{R}) + w(\mathbf{R})$. The incident monochromatic field u produced by the point source of frequency ω (i.e., the Green's function G) is determined by the wave equation

$$[\Delta + k^2(z)]u(\mathbf{R}) = -\delta(\mathbf{R} - \mathbf{R}_0) \tag{1}$$

and satisfies the corresponding boundary conditions at the upper ($z = 0$) and lower ($z = H$) surfaces of the waveguide, as well as the radiation condition at infinity. Here, $k(z) = \omega/c(z)$ is the wave number at the horizon z. Let us restrict our consideration to the cylindrically symmetric problem and assume that the solution to Eq. (1) is known [10]:

$$u(\mathbf{R}) = G(\mathbf{R}) = \frac{i}{4}\sum_m \psi_m(z_0)\psi_m(z)H_0^{(1)}(h_m r)\exp(-\kappa_m r), \tag{2}$$

where $H_0^{(1)}$ is the Hankel function of the first kind; h_m, ψ_m, and κ_m are the propagation constant, normalized eigenfunction, and attenuation coefficient of the mth mode, respectively; and $r = |\mathbf{r}|$ is the horizontal distance from the source to the observation point. By using the Huygens principle, we can represent the scattered field in the form [11]

(a) for the p-case [$p = 0$ at the surface (S)],

$$w(\mathbf{R}) = -\oint_S \varphi(\hat{\mathbf{R}}')G(\mathbf{R}, \mathbf{R}_s + \hat{\mathbf{R}}')d\hat{\mathbf{R}}', \tag{3a}$$

(b) for the s-case [$\partial p/\partial n = 0$ at the surface (S)],

$$w(\mathbf{R}) = \oint_S \vartheta(\hat{\mathbf{R}}')\frac{\partial}{\partial n'}G(\mathbf{R}, \mathbf{R}_s + \hat{\mathbf{R}}')d\hat{\mathbf{R}}', \tag{3b}$$

where φ and ϑ are the surface densities of the ordinary and dipole sources, respectively; $\partial/\partial n$ is the derivative in the direction of the outer normal to the surface (S); and $d\hat{\mathbf{R}}'$ is the element of the body's surface (S) in the vicinity of the point $\hat{\mathbf{R}}'$. The integration is performed over the surface (S) of the body. Here and below, the primes label all quantities and operators associated with the integration point. Expressions (3a) and (3b) satisfy the boundary conditions of the Helmholtz equation (1), so it remains for us to satisfy the boundary conditions at (S). From the boundary condition at the body's surface, we obtain the Fredholm equation of the second kind for the unknown functions φ and ϑ [11]:

(a) for the p-case,

$$\varphi(\hat{\mathbf{R}}) = 2\frac{\partial u(\hat{\mathbf{R}})}{\partial n} - 2\oint_S \varphi(\hat{\mathbf{R}}')\frac{\partial}{\partial n}G(\hat{\mathbf{R}}, \hat{\mathbf{R}}')d\hat{\mathbf{R}}', \quad \hat{\mathbf{R}} \in (S), \tag{4a}$$

(b) for the s-case,

$$\vartheta(\hat{\mathbf{R}}) = 2u(\hat{\mathbf{R}}) + 2\oint_S \vartheta(\hat{\mathbf{R}}')\frac{\partial}{\partial n'}G(\hat{\mathbf{R}}, \hat{\mathbf{R}}')d\hat{\mathbf{R}}', \quad \hat{\mathbf{R}} \in (S). \tag{4b}$$

The surface densities φ and ϑ are determined by both the incident field and the secondary field produced by all elements of the surface. Equation (4b) determining ϑ is the integral equation of the same type as Eq. (4a) determining φ. These equations differ in the first terms on their right-hand side and in their kernels, because they involve normals to the surface at different points, namely: $n = n(\hat{\mathbf{R}})$ and $n' = n(\hat{\mathbf{R}}')$. The kernels are asymmetric, and the following expression is valid for the "transposed" kernels:

$$\frac{\partial}{\partial n}G(\hat{\mathbf{R}}', \hat{\mathbf{R}}) = -\frac{\partial}{\partial n'}G(\hat{\mathbf{R}}, \hat{\mathbf{R}}'). \tag{5}$$

In general, Eqs. (1)–(4) solve the problem of sound diffraction by a body in the waveguide, because their solutions satisfy the boundary conditions at the surfaces of the body and the waveguide together with the radiation condition.

To rigorously derive Eqs. (3) and (4), it is sufficient to apply the known derivation procedure of the Helmholtz equation to Eq. (1) and then to perform the conversion to the surface currents. This procedure does not differ in any way from the case of free space [11]. We omit the computation details but make the following remark. The resultant expressions are in fact the consequence of the generalized Helmholtz equation whose integrand involves the free-space Green's function $G_0(\mathbf{R}, \mathbf{R}_0)$. Such a generalization is based on the known property of the solution to the wave equation: at a regular point, the wave function can be represented as an integral over an arbitrary closed surface encircling this point, the form of the Green's function $G(\mathbf{R}, \mathbf{R}_0)$ being immaterial. Really, Eqs. (3) and (4) correspond to the Huygens principle and also satisfy the boundary conditions at the body's surface when $G(\mathbf{R}, \mathbf{R}_0)$ is treated as an arbitrary function that satisfies the wave equation (1) and fits the physical conditions of the problem. In free space, the only such condition is the radiation condition at infinity. Therefore, the Green's function is specified in the form $G(\mathbf{R}, \mathbf{R}_0) = \exp(ik|\mathbf{R} - \mathbf{R}_0|)/4\pi|\mathbf{R} - \mathbf{R}_0|$. For the problem of sound scattering in the waveguide, the Green's function $G(\mathbf{R}, \mathbf{R}_0)$ should be treated as the solution to Eq. (1) that determines the fields satisfying

the boundary conditions at the waveguide surfaces. In our case, such a solution is given by Eq. (2).

Let us apply Eqs. (1)–(4) to the calculation of the Fraunhofer fields in the waveguide. Assuming that the horizontal distance between the body and the source is long enough, we expand the source field (2) into plane waves. Using the asymptotic form of the Hankel function, we reduce the incident field at the body's surface to the form

$$u(\mathbf{R}_s + \hat{\mathbf{R}}) = \sum_m [u_m^+(\mathbf{R}_s + \hat{\mathbf{R}}) + u_m^-(\mathbf{R}_s + \hat{\mathbf{R}})], \quad (\mathbf{R}_s + \hat{\mathbf{R}}) \in (S), \tag{6}$$

where

$$u_m^\pm(\mathbf{R}_s + \hat{\mathbf{R}}) = u_m(\mathbf{R}_s)[a_m^\pm(z_s)\exp(i\mathbf{k}_m^\pm\hat{\mathbf{R}})], \quad \hat{\mathbf{R}} \in (S) \tag{7}$$

are the partial plane waves corresponding to the mth mode,

$$u_m(\mathbf{R}_s) = \sqrt{\frac{i}{8\pi}}\frac{\psi_m(z_0)\psi_m(z_s)}{\sqrt{h_m r_s}}\exp(ih_m r_s - \kappa_m i_s) \tag{8}$$

is the field of the mth mode at the body's center, and

$$a_m^\pm(z_s) = \frac{1}{2} \pm \frac{\psi_m'(z_s)}{2ig_m(z_s)\psi_m(z_s)}. \tag{9}$$

Here, $\mathbf{k}_m^\pm = (\mathbf{h}_m \pm \mathbf{g}_m)$ are the local wave vectors of the Brillouin rays of the incident field with the horizontal $\mathbf{h}_m$ and vertical $\pm\mathbf{g}_m$ components, $\mathbf{h}_m = (\mathbf{r}_s/r_s)h_m$, $\mathbf{g}_m = \hat{\mathbf{a}}_z g_m$, $g_m(z_s) = \sqrt{k^2(z_s) - h_m^2}$, and $r_s = |\mathbf{r}_s|$ is the horizontal distance between the source and the body's center. In deriving Eq. (6), we used the expansion of the eigenfunction $\psi_m(z)$ in the vicinity of the reference point z_s:

$$\psi_m(z_s + \hat{z}) = \psi_m(z_s)[a_m^+\exp(ig_m\hat{z}) + a_m^-\exp(-ig_m\hat{z})], \tag{10}$$

which is admissible in the approximation of a locally homogeneous medium [12]. The latter means that the inhomogeneous medium is close to a homogeneous one within the characteristic vertical size of the body.

Let the partial plane waves $u_m^\pm$ induce surface currents with the densities $\varphi_m^\pm$ (the p-case) or $\vartheta_m^\pm$ (the s-case) on the body's surface. These currents generate secondary diffraction fields. Then, for the diffracted field (3a) or (3b) in the far-field zone, Eqs. (2) and (10) yield

$$w(\mathbf{R}) = \sqrt{\frac{i}{8\pi}}\sum_\mu T_\mu\psi_\mu(z_s)\psi_\mu(z) \times \frac{\exp(ih_\mu|\mathbf{r} - \mathbf{r}_s| - \kappa_\mu|\mathbf{r} - \mathbf{r}_s|)}{\sqrt{h_\mu|\mathbf{r} - \mathbf{r}_s|}}, \tag{11}$$

where function T_μ takes the form

(a) in the p-case,

$$T_\mu = -\sum_m \left\{ a_\mu^+ \oint_S \varphi_m^+(\hat{\mathbf{R}}')\exp(-i\mathbf{k}_\mu^-\hat{\mathbf{R}}')d\hat{\mathbf{R}}' + a_\mu^+ \oint_S \varphi_m^-(\hat{\mathbf{R}}')\exp(-i\mathbf{k}_\mu^-\hat{\mathbf{R}}')d\hat{\mathbf{R}}' + a_\mu^- \oint_S \varphi_m^+(\hat{\mathbf{R}}')\exp(-i\mathbf{k}_\mu^+\hat{\mathbf{R}}')d\hat{\mathbf{R}}' + a_\mu^- \oint_S \varphi_m^-(\hat{\mathbf{R}}')\exp(-i\mathbf{k}_\mu^+\hat{\mathbf{R}}')d\hat{\mathbf{R}}' \right\}, \tag{12a}$$

(b) in the s-case,

$$T_\mu = \sum_m \left\{ a_\mu^+ \oint_S \vartheta_m^+(\hat{\mathbf{R}}')\frac{\partial\exp(-i\mathbf{k}_\mu^-\hat{\mathbf{R}}')}{\partial n'}d\hat{\mathbf{R}}' + a_\mu^+ \oint_S \vartheta_m^-(\hat{\mathbf{R}}')\frac{\partial\exp(-i\mathbf{k}_\mu^-\hat{\mathbf{R}}')}{\partial n'}d\hat{\mathbf{R}}' + a_\mu^- \oint_S \vartheta_m^+(\hat{\mathbf{R}}')\frac{\partial\exp(-i\mathbf{k}_\mu^+\hat{\mathbf{R}}')}{\partial n'}d\hat{\mathbf{R}}' + a_\mu^- \oint_S \vartheta_m^-(\hat{\mathbf{R}}')\frac{\partial\exp(-i\mathbf{k}_\mu^+\hat{\mathbf{R}}')}{\partial n'}d\hat{\mathbf{R}}' \right\}. \tag{12b}$$

Here, $\mathbf{k}_\mu^\pm = \mathbf{h}_\mu \pm \mathbf{g}_\mu$ are the local wave vectors of the Brillouin rays of the diffracted field, $\mathbf{h}_\mu = [(\mathbf{r} - \mathbf{r}_s)/|\mathbf{r} - \mathbf{r}_s|]h_\mu$, and the vectors $\pm\mathbf{g}_\mu$ and factors $a_\mu^\pm$ are similar to $\pm\mathbf{g}_m$ and $a_m^\pm$ of Eq. (9). Here and further, we use Greek symbols (μ, ν, …) and Latin ones (m, n, …) for enumerating the modes of the scattered and primary fields, respectively. The integrands on the right-hand side of Eq. (12b) are equal to

$$\vartheta_m^\pm(\hat{\mathbf{R}}')\frac{\partial\exp(-i\mathbf{k}_\mu^\pm\hat{\mathbf{R}}')}{\partial n'} = -i\vartheta_m^\pm(\hat{\mathbf{R}}')(\mathbf{k}_\mu^\pm, \mathbf{n}')\exp(-i\mathbf{k}_\mu^\pm\hat{\mathbf{R}}'). \tag{13}$$

In view of Eq. (13), the integrals of Eqs. (12a) and (12b) mean the Fourier transforms for the surface density of the sources. According to the reciprocity theorem [13], they describe the angular distribution of the Fraunhofer partial field diffracted in the direction of the wave vector $\mathbf{k}_\mu^\pm$ when a plane wave propagating in the direction of $\mathbf{k}_m^\pm$ is incident on the body. The quantity $F(\mathbf{k}_m^\pm, \mathbf{k}_\mu^\pm)$ is given by the following expressions

(a) in the *p*-case,

$$F(\mathbf{k}_m^\pm, \mathbf{k}_\mu^\pm) = \frac{1}{a_m^\pm u_m(\mathbf{R}_s)} \oint_S \varphi_m^\pm(\hat{\mathbf{R}}') \exp(-i\mathbf{k}_\mu^\pm \hat{\mathbf{R}}') d\hat{\mathbf{R}}', \quad (14a)$$

(b) in the *s*-case,

$$F(\mathbf{k}_m^\pm, \mathbf{k}_\mu^\pm) = \frac{-i}{a_m^\pm u_m(\mathbf{R}_s)} \oint_S \vartheta_m^\pm(\hat{\mathbf{R}}')(\mathbf{k}_\mu^\pm \mathbf{n}') \exp(-i\mathbf{k}_\mu^\pm \hat{\mathbf{R}}') d\hat{\mathbf{R}}'. \quad (14b)$$

This quantity has a dimensionality of meters and can be treated as a generalization of the concept of the scattering amplitude to the case of the waveguide propagation. On the right-hand side of Eqs. (14a) and (14b), the factor $(1/a_m^\pm u_m(\mathbf{R}_s))$ multiplying the integral serves to normalize the amplitude of the plane wave of the *m*th mode. According to Eqs. (4a) and (4b), the surface density is determined from the integral equations

(a) in the *p*-case,

$$\varphi_m^\pm(\hat{\mathbf{R}}) = 2\frac{\partial u_m^\pm(\hat{\mathbf{R}})}{\partial n} - 2\oint_S \varphi_m^\pm(\hat{\mathbf{R}}') \frac{\partial}{\partial n} G(\hat{\mathbf{R}}, \hat{\mathbf{R}}') d\hat{\mathbf{R}}', \quad \hat{\mathbf{R}} \in (S), \quad (15a)$$

(b) in the *s*-case,

$$\vartheta_m^\pm(\hat{\mathbf{R}}) = 2u_m^\pm(\hat{\mathbf{R}}) + 2\oint_S \vartheta_m^\pm(\hat{\mathbf{R}}') \frac{\partial}{\partial n'} G(\hat{\mathbf{R}}, \hat{\mathbf{R}}') d\hat{\mathbf{R}}', \quad \hat{\mathbf{R}} \in (S), \quad (15b)$$

where the quantities $G(\hat{\mathbf{R}}, \hat{\mathbf{R}}')$ and $u_m^\pm(\hat{\mathbf{R}})$ are given by Eqs. (2) and (7). In view of the definitions of Eqs. (8), (14a), and (14b), the diffracted field of Eq. (11) can be expressed as

$$w(\mathbf{R}) = -\sqrt{\frac{i}{8\pi}} \sum_\mu \sum_m S_{\mu m}(z_s) u_m(\mathbf{R}_s) \psi_\mu(z_s) \psi_\mu(z) \times \frac{\exp(ih_\mu|\mathbf{r} - \mathbf{r}_s| - \kappa_\mu|\mathbf{r} - \mathbf{r}_s|)}{\sqrt{h_\mu|\mathbf{r} - \mathbf{r}_s|}}, \quad (16)$$

where the scattering matrix of the guided modes has the form

$$S_{\mu m} = a_m^+ a_\mu^+ F(\mathbf{k}_m^+, \mathbf{k}_\mu^-) + a_m^- a_\mu^- F(\mathbf{k}_m^-, \mathbf{k}_\mu^+) + a_m^+ a_\mu^- F(\mathbf{k}_m^+, \mathbf{k}_\mu^+) + a_m^- a_\mu^+ F(\mathbf{k}_m^-, \mathbf{k}_\mu^-). \quad (17)$$

Expression (16) agrees well with the common apprehension that, in the far-field zone, the diffracted field is a superposition of plane waves emitted by individual elements of the body's surface in the directions $\mathbf{k}_\mu^\pm$. As a result, the task is to determine the unknown functions $\varphi_m^\pm(\hat{\mathbf{R}})$ and $\vartheta_m^\pm(\hat{\mathbf{R}})$. A rigorous solution to Eqs. (15a) and (15b) can be found for a limited range of problems associated with the use of the Green's function $G_0(\mathbf{R})$ of a homogeneous space. This situation is caused by the fact that the mathematics of the diffraction theory is based on the use of the homogeneous-space Green's function [11, 14], and a replacement of this function by another (the waveguide Green's function $G(\mathbf{R})$) requires a total modification of the methods of solving the integral equations. Thus, in considering the sound propagation in the waveguide, we have to use approximate methods.

ITERATIVE METHOD

To find approximate solutions $\varphi_m^\pm(\hat{\mathbf{R}})$ and $\vartheta_m^\pm(\hat{\mathbf{R}})$ to integral equations (15a) and (15b), we use the method of successive approximations. The method of iterations is especially advantageous when the problem to be solved is close to a problem that can be solved exactly. In this case, it is assumed that the differences in the two solutions are not singular; i.e., the exact solution can be transformed to the approximate one in a continuous manner. Explicitly, it means that the perturbation should be a continuous function of the parameter that determines the value of the perturbation. As the zero-order approximation, we use the quantities $\varphi_m^{\pm(0)}$ and $\vartheta_m^{\pm(0)}$ that are the solutions to Eqs. (15a) and (15b) with the kernel in the form of the homogeneous-space Green's function $G_0(\hat{\mathbf{R}}, \hat{\mathbf{R}}') = \exp(ik|\hat{\mathbf{R}} - \hat{\mathbf{R}}'|)/4\pi|\hat{\mathbf{R}} - \hat{\mathbf{R}}'|$; these solutions are assumed to be known. By substituting the known functions $\varphi_m^{\pm(0)}$ and $\vartheta_m^{\pm(0)}$ into the integrals on the right-hand side of Eqs. (15a) and (15b), we find the first approximations in the form of the sum of two terms: $\varphi_m^{\pm[1]} = \varphi_m^{\pm(0)} + \varphi_m^{\pm(1)}$ and $\vartheta_m^{\pm[1]} = \vartheta_m^{\pm(0)} + \vartheta_m^{\pm(1)}$.

In the *p*-case, we have

$$\varphi_m^{\pm(1)}(\hat{\mathbf{R}}) = 2\oint_S \varphi_m^{\pm(0)}(\hat{\mathbf{R}}') \frac{\partial}{\partial n} [G_0(\hat{\mathbf{R}}, \hat{\mathbf{R}}') - G(\hat{\mathbf{R}}, \hat{\mathbf{R}}')] d\hat{\mathbf{R}}', \quad \hat{\mathbf{R}} \in (S), \quad (18a)$$

and in the *s*-case,

$$\vartheta_m^{\pm(1)}(\hat{\mathbf{R}}) = 2\oint_S \vartheta_m^{\pm(0)}(\hat{\mathbf{R}}')\frac{\partial}{\partial n'}[G(\hat{\mathbf{R}}, \hat{\mathbf{R}}') - G_0(\hat{\mathbf{R}}, \hat{\mathbf{R}}')]d\hat{\mathbf{R}}', \quad \hat{\mathbf{R}} \in (S). \tag{18b}$$

If, on the right-hand side of integral expressions (15a) and (15b), the unknown functions are replaced by their first approximations, $\varphi_m^{\pm[1]}$ and $\vartheta_m^{\pm[1]}$, we can find the second approximations for $\varphi_m^{\pm[2]}$ and $\vartheta_m^{\pm[2]}$ as sums of three terms: $\varphi_m^{\pm[2]} = \varphi_m^{\pm(0)} + \varphi_m^{\pm(1)} + \varphi_m^{\pm(2)}$ and $\vartheta_m^{\pm[2]} = \vartheta_m^{\pm(0)} + \vartheta_m^{\pm(1)} + \vartheta_m^{\pm(2)}$.

Then, in the *p*-case, we have

$$\varphi_m^{\pm(2)}(\hat{\mathbf{R}}) = -2\oint_S \varphi_m^{\pm(1)}(\hat{\mathbf{R}}')\frac{\partial}{\partial n}G(\hat{\mathbf{R}}, \hat{\mathbf{R}}')d\hat{\mathbf{R}}', \quad \hat{\mathbf{R}} \in (S), \tag{19a}$$

and in the *s*-case,

$$\vartheta_m^{\pm(2)}(\hat{\mathbf{R}}) = 2\oint_S \vartheta_m^{\pm(1)}(\hat{\mathbf{R}}')\frac{\partial}{\partial n'}G(\hat{\mathbf{R}}, \hat{\mathbf{R}}')d\hat{\mathbf{R}}', \quad \hat{\mathbf{R}} \in (S). \tag{19b}$$

In Eqs. (19a) and (19b), the quantities $\varphi_m^{\pm(1)}$ and $\vartheta_m^{\pm(1)}$ are given by Eqs. (18a) and (18b). By repeating these iterative procedures many times, we obtain a sequence of functions $\varphi_m^{\pm(n)}(\hat{\mathbf{R}})$ and $\vartheta_m^{\pm(n)}(\hat{\mathbf{R}})$ whose sum tends to the exact solutions $\varphi_m^{\pm}(\hat{\mathbf{R}})$ and $\vartheta_m^{\pm}(\hat{\mathbf{R}})$:

$$\varphi_m^{\pm}(\hat{\mathbf{R}}) = \sum_{n=0}^{\infty} \varphi_m^{\pm(n)}(\hat{\mathbf{R}}), \quad \vartheta_m^{\pm}(\hat{\mathbf{R}}) = \sum_{n=0}^{\infty} \vartheta_m^{\pm(n)}(\hat{\mathbf{R}}), \tag{20}$$

because the surface densities of sources are finite for physical reasons. The *n*th steps of iterations for $\varphi_m^{\pm(n)}$ and $\vartheta_m^{\pm(n)}$ follow the recurrent relations

(a) in the *p*-case,

$$\varphi_m^{\pm(n)}(\hat{\mathbf{R}}) = -2\oint_S \varphi_m^{\pm(n-1)}(\hat{\mathbf{R}}')\frac{\partial}{\partial n}G(\hat{\mathbf{R}}, \hat{\mathbf{R}}')d\hat{\mathbf{R}}', \quad \hat{\mathbf{R}} \in (S), \quad n \geq 2, \tag{21a}$$

(b) in the *s*-case,

$$\vartheta_m^{\pm(n)}(\hat{\mathbf{R}}) = 2\oint_S \vartheta_m^{\pm(n-1)}(\hat{\mathbf{R}}')\frac{\partial}{\partial n'}G(\hat{\mathbf{R}}, \hat{\mathbf{R}}')d\hat{\mathbf{R}}', \quad \hat{\mathbf{R}} \in (S), \quad n \geq 2. \tag{21b}$$

Note that, according to Eq. (5), the approximations $\varphi_m^{\pm(n)}$ and $\vartheta_m^{\pm(n)}$, $n \geq 1$, which are given by Eqs. (18a), (18b), (21a), and (21b), follow the same functional dependence. The quantities $\varphi_m^{\pm(n)}$ and $\vartheta_m^{\pm(n)}$ from the perturbation series (20) can be interpreted as follows: the zero-order terms $\varphi_m^{\pm(0)}$ and $\vartheta_m^{\pm(0)}$ determine the diffracted field without accounting for multiple reflections between the body and the waveguide boundaries, and the higher terms $\varphi_m^{\pm(n)}$ and $\vartheta_m^{\pm(n)}$, $n \geq 1$ can be understood as the surface densities governed by the *n*-fold interaction of the body and the waveguide boundaries. Then, the first terms given by Eqs. (18a) and (18b) are nothing but the well-known Born approximation. Thus, with the use of representation (20), which is the solution to integral equations (15a) and (15b), the process of diffraction in the waveguide is represented as a sequence of interactions between the body and the waveguide boundaries (multiple reflections). The aforementioned considerations allow one to determine in which case several initial approximations lead to a good result. After the determination of the solutions to integral equations (15a) and (15b) in the form of series (20), the quantity $F(\mathbf{k}_m^{\pm}, \mathbf{k}_\mu^{\pm})$, which determines the scattering matrix for the waveguide modes $S_{\mu m}$ (17), can be found from Eqs. (14a) and (14b).

Similarly, a theory of perturbations can be developed for the problem of sound diffraction by a body with an impedance surface in a regular plane-layered waveguide.

VALIDITY OF THE FIRST-ORDER APPROXIMATION

Let us consider the conditions when the first-order approximation is justified. In this case, according to Eqs. (14a), (14b), (15a), and (15b), the scattering matrix $S_{\mu m}$ (17) of the waveguide modes is determined by the scattering amplitude in a homogeneous medium. This fact was proved earlier in [3, 12].

Evidently, in order for the first-order approximation to be valid, the residue of the perturbation series (20) should be much smaller in its absolute value than the zero-order term. In the general case of arbitrary functions $\varphi_m^{\pm(0)}$ and $\vartheta_m^{\pm(0)}$, the estimation of the infinite sum of the omitted terms is rather complicated. Therefore, the usual practice is to restrict the problem to considering the first terms $\varphi_m^{\pm(1)}$ and $\vartheta_m^{\pm(1)}$ and to find the conditions when the following inequalities hold:

$$|\varphi_m^{\pm(1)}(\hat{\mathbf{R}})| \ll |\varphi_m^{\pm(0)}(\hat{\mathbf{R}})|, \quad |\vartheta_m^{\pm(1)}(\hat{\mathbf{R}})| \ll |\vartheta_m^{\pm(0)}(\hat{\mathbf{R}})|. \tag{22}$$

Strictly speaking, this validity criterion of the zero-order approximation works only when expansions (20) converge and have an alternating sign. This is precisely the case under consideration. The first inequality is met because of the physical understanding of the finiteness of the surface density of sources, and the second ine-

quality is justified by Eqs. (21a) and (21b). Hence, conditions (22) are necessary and sufficient for the zero-order approximation to be valid. By using Eqs. (5), (18a), and (18b), we can rewrite conditions (22) as follows:

(a) in the *p*-case,

$$2\left|\oint_S \varphi_m^{\pm(0)}(\hat{\mathbf{R}}')\frac{\partial}{\partial n}[G_0(\hat{\mathbf{R}},\hat{\mathbf{R}}')-G(\hat{\mathbf{R}},\hat{\mathbf{R}}')]d\hat{\mathbf{R}}'\right| \ll \left|\varphi_m^{\pm(0)}(\hat{\mathbf{R}})\right|, \quad \hat{\mathbf{R}}\in(S), \tag{23a}$$

(b) in the *s*-case,

$$2\left|\oint_S \vartheta_m^{\pm(0)}(\hat{\mathbf{R}}')\frac{\partial}{\partial n}[G_0(\hat{\mathbf{R}}',\hat{\mathbf{R}})-G(\hat{\mathbf{R}}',\hat{\mathbf{R}})]d\hat{\mathbf{R}}'\right| \ll \left|\vartheta_m^{\pm(0)}(\hat{\mathbf{R}})\right|, \quad \hat{\mathbf{R}}\in(S). \tag{23b}$$

In general, inequalities (23a) and (23b) are too complicated to be directly analyzed. Let us simplify the problem to extract simple and easy-to-grasp estimates from expressions (23).

Suppose that the body is close to one of the waveguide boundaries: the free water surface at $z = 0$, for instance. Let the characteristic vertical size d of the body be much smaller than the waveguide thickness H, $d \ll H$, and the medium be locally homogeneous within the layer of thickness $z_s + d$ near the boundary (see [12]). Then, in the first approximation, the Green's function of the waveguide can be replaced by that of a half-space with a pressure-release surface. Thereby, the problem is reduced to that of sound scattering by two bodies (real and imaginary) that are mirror symmetric with respect to the plane $z = 0$. In this case, the function $G(\hat{\mathbf{R}}, \hat{\mathbf{R}}')$ involved in expressions (23a) and (23b) takes the form [11]:

$$G(\hat{\mathbf{R}},\hat{\mathbf{R}}') = \frac{\exp(ik|\hat{\mathbf{R}}-\hat{\mathbf{R}}_1'|)}{4\pi|\hat{\mathbf{R}}-\hat{\mathbf{R}}_1'|} - \frac{\exp(ik|\hat{\mathbf{R}}-\hat{\mathbf{R}}_1'+\mathbf{a}|)}{4\pi|\hat{\mathbf{R}}-\hat{\mathbf{R}}_1'+\mathbf{a}|}, \quad \hat{\mathbf{R}},\hat{\mathbf{R}}_1'\in(S_1). \tag{24}$$

Here, (S_1) is the surface of the real body with the geometric center at the point $Q_s(\mathbf{R}_s)$, $\mathbf{a}$ is the vector connecting two mirror-symmetric points $\hat{\mathbf{R}}_2'$ and $\hat{\mathbf{R}}_1'$ of the surfaces (S_2) and (S_1), (S_2) is the surface of the imaginary body with the geometric center at the point $Q_s^*(\mathbf{R}_s^*)$, and $\mathbf{R}_s^* = \mathbf{R}_s - 2\hat{\mathbf{a}}_z z_s$. By substituting Eq. (24) into expressions (23a) and (23b), we obtain the inequalities

(a) in the *p*-case,

$$\frac{1}{2\pi}\left|\oint_{S_1}\varphi_m^{\pm(0)}(\hat{\mathbf{R}}_1')K(\hat{\mathbf{R}},\hat{\mathbf{R}}_1')d\hat{\mathbf{R}}_1'\right| \ll \left|\varphi_m^{\pm(0)}(\hat{\mathbf{R}})\right|, \quad \hat{\mathbf{R}}\in(S_1), \tag{25a}$$

(b) in the *s*-case,

$$\frac{1}{2\pi}\left|\oint_{S_1}\vartheta_m^{\pm(0)}(\hat{\mathbf{R}}_1')K(\hat{\mathbf{R}},\hat{\mathbf{R}}_1')d\hat{\mathbf{R}}_1'\right| \ll \left|\vartheta_m^{\pm(0)}(\hat{\mathbf{R}})\right|, \quad \hat{\mathbf{R}}\in(S_1), \tag{25b}$$

where the kernel $K(\hat{\mathbf{R}}, \hat{\mathbf{R}}_1')$ is given by the expression

$$K(\hat{\mathbf{R}},\hat{\mathbf{R}}_1') = \frac{(\mathbf{n},\mathbf{b})}{b^3}(ikb-1)\exp(ikb), \quad \mathbf{b} = \hat{\mathbf{R}}-\hat{\mathbf{R}}_1'+\mathbf{a}, \quad b = |\mathbf{b}|. \tag{26}$$

For each specific case, the validation of approximations (25a) and (25b) is not difficult, and we do not particularize it here.

To obtain a rough estimate for the domain of validity of the zero-order approximation (25a) and (25b), we proceed as follows. Let us specify $\varphi_m^{\pm(0)}$ = const and $\vartheta_m^{\pm(0)}$ = const in expressions (25a) and (25b) and make use of the mean-value theorem for a triple integral. In doing so, we keep in mind that the modulus of the integral is not greater than the integral of the modulus of the integrand. To simplify inequalities (25a) and (25b), we specify $(\mathbf{n}, \mathbf{b}) = b$ in Eq. (26). The quantity b involved in these inequalities is no smaller than the least distance and no greater than the maximal one between two points, one of which lies on the surface (S_1) and the other lies on (S_2). As a characteristic value of the quantity b, we accept the distance $2z_s$ between the geometric centers of the bodies: $b = 2z_s$. As a result, we obtain

$$S\sqrt{1+(2kz_s)^2}/8\pi z_s^2 \ll 1, \tag{27}$$

where S is the area of the body's surface. In two limiting cases of short and long waves, we find from Eq. (27)

(a) for short waves, $(2kz_s)^2 \gg 1$,

$$S/2\lambda z_s \ll 1, \tag{28a}$$

(b) for long waves, $(2kz_s)^2 \ll 1$,

$$S/8\pi z_s^2 \ll 1. \tag{28b}$$

Hence, if the sound wavelength λ is much smaller than the distance z_s from the body to the water surface at $z = 0$, it is sufficient that the surface area be small relative to the quantity $2\lambda z_s$ for the zero-order approximation to be valid. If the wavelength is much longer than this distance, the first term of the perturbation series can be

omitted when the surface area is small relative to the quantity $8\pi z_s^2$. The estimating conditions (28a) and (28b) agree well with the data of numerical modeling [15–17]. For example, in considering the sound scattering by two spheres in [17], it was shown that the effect of the secondary scattered fields is does not exceed 10% if the radius of the sphere meets the condition $r \le 2z_s/5$. According to expression (28b), we obtain $z_s \ge 2.2r$.

Thus, in the framework of the theory of integral equations, the problem of sound diffraction by pressure-release and acoustically stiff bodies in a plane-layered waveguide of oceanic type is formulated. The possibility of applying the theory of perturbations to solving the integral equations is considered. A recurrent method for calculating the corrections to the scattering parameters with allowance for the multiple reflections of waves by the body and the waveguide boundaries is proposed. The conditions for the multiple reflections to be neglected (the zero-order approximation) are discussed. In the zero-order approximation, the scattering matrix of the waveguide modes is shown to be determined by the scattering amplitude in a homogeneous space.

ACKNOWLEDGMENTS

This work was supported by the Russian Foundation for Basic Research (project nos. 99-02-17671 and 00-15-96636) and the Federal Special-Purpose Program "Integration of Science and Higher Education in Russia for 2002–2006" (project no. J04-10).

REFERENCES

1. S. M. Gorskiĭ, V. A. Zverev, and A. I. Khil'ko, in *Formation of Acoustic Fields in Oceanic Waveguides*, Ed. by V. A. Zverev (Inst. Prikl. Fiz., Akad. Nauk SSSR, Nizhni Novgorod, 1991), pp. 82–114.
2. A. Sarkissian, J. Acoust. Soc. Am. **102**, 825 (1997).
3. Yu. A. Kravtsov, V. M. Kuz'kin, and V. G. Petnikov, Akust. Zh. **30**, 339 (1984) [Sov. Phys. Acoust. **30**, 199 (1984)].
4. N. V. Gorskaya, S. M. Gorskiĭ, V. A. Zverev, *et al.*, Akust. Zh. **34**, 55 (1988) [Sov. Phys. Acoust. **34**, 29 (1988)].
5. V. N. Nemtsova and M. V. Fedoryuk, Akust. Zh. **32**, 131 (1986) [Sov. Phys. Acoust. **32**, 81 (1986)].
6. A. Sarkissan, J. Acoust. Soc. Am. **95**, 2340 (1994).
7. S. A. Yang, J. Acoust. Soc. Am. **105**, 93 (1999).
8. M. Ochmann, J. Acoust. Soc. Am. **105**, 2574 (1999).
9. A. V. Zatserkovnyĭ, V. A. Sergeev, and B. P. Sharfarets, Akust. Zh. **47**, 650 (2001) [Acoust. Phys. **47**, 565 (2001)].
10. L. M. Brekhovskikh and Yu. P. Lysanov, *Fundamentals of Ocean Acoustics* (Gidrometeoizdat, Leningrad, 1982; Springer, New York, 1991).
11. H. Hönl, A. W. Maue, and K. Westpfahl, *Theorie der Beugung* (Springer, Berlin, 1961; Mir, Moscow, 1964).
12. V. M. Kuz'kin, Akust. Zh. **47**, 483 (2001) [Acoust. Phys. **47**, 591 (2001)].
13. L. M. Lyamshev, Dokl. Akad. Nauk SSSR **125**, 1231 (1959) [Sov. Phys. Dokl. **4**, 406 (1959)].
14. M. V. Fedoryuk, Izv. Akad. Nauk SSSR, Ser. Mat. **49**, 160 (1985).
15. A. A. Kleshchev, *Underwater Acoustic Scatterers: A Handbook* (Sudostroenie, St. Petersburg, 1992).
16. V. V. Varadan and V. K. Varadan, J. Acoust. Soc. Am. **70**, 213 (1981).
17. S. O. Kvyatkovskiĭ, in *Problems of the Ocean and Ship Acoustics* (LKI, Leningrad, 1986), pp. 43–50.

Translated by E. Kopyl

Acoustical Physics, Vol. 49, No. 1, 2003, pp. 75–80. Translated from Akusticheskiĭ Zhurnal, Vol. 49, No. 1, 2003, pp. 85–91.

Admittance of a Groove on a Rigid Surface under a Grazing Flow

A. D. Lapin and M. A. Mironov

Andreev Acoustics Institute, Russian Academy of Sciences, ul. Shvernika 4, Moscow, 117036 Russia

e-mail: mironov@akin.ru

Received May 18, 2002

Abstract—The problem of sound diffraction by a groove on a rigid surface in the presence of a grazing flow is considered. The input admittance of the groove is calculated, and its real part is shown to be negative. © *2003 MAIK "Nauka/Interperiodica".*

The effect of the average shear of the flow on the acoustic admittance of holes in a screen separating stationary and moving media is of interest for the design and analysis of silencers operating in a moving medium. It has been proven experimentally that the tangential discontinuity spanning the throat of a Helmholtz resonator changes both its resonance frequency and its loss coefficient [1]. The admittance of an isolated hole in a screen was investigated in detail in [2]. A rigorous analytical method for calculating the effect of the tangential discontinuity on the acoustics of a hole in a screen was suggested in papers [3, 4]. A numerical difference procedure for solving the Navier–Stokes equation was used in paper [5] (which presents an exhaustive list of publications concerning the effect of a flow on the acoustics of cavities). In this paper, we extend the method suggested in papers [3, 4] to the problem of a rigid plane with a groove spanned by a tangential discontinuity. The main difference in the formulations of the problems on the diffraction by holes without and with a tangential discontinuity consists in different boundary conditions on the front edge. In the absence of a tangential discontinuity, the conditions on both edges are formulated as zero-valued energy flux in the edge direction. If a tangential discontinuity is present, the Kutta–Zhukovski condition is formulated on the front edge: the displacement and the slope of the tangential discontinuity vanish at the edge. Papers [3, 4] showed that the problem of the diffraction by a hole spanned by a tangential discontinuity can be reduced to two problems that are solved sequentially. The first problem is that of the diffraction by a hole in the absence of the flow. After this problem is solved, the solution to the problem with the tangential discontinuity can be obtained from the solution to the first problem by using certain operator transformation that can be represented explicitly in an analytical form. The extension suggested in this paper offers a possibility to extend this procedure to the situations in which the Green's functions are different on the different sides of the tangential discontinuity.

Consider the diffraction of sound by a rectangular groove in a rigid surface (Fig. 1). The density and the sound velocity in the groove coincide with those in the half-space and are denoted as ρ and c, respectively. The medium in the half-space $y > 0$ moves along the x axis with a velocity U, and the medium in the groove is at rest. Under the action of the sound field, the interface between the moving and stationary media—the tangential discontinuity—is displaced. Denote by $\eta(x, t)$ the deviation of this interface from the plane $y = 0$. Let the harmonic sound field in the moving medium be known in the case of a closed groove ($\eta \equiv 0$). We denote the sound pressure in this field by $p_0(x, y)$ [we omit the temporal factor $\exp(-i\omega t)$]. The problem consists in finding the displacement $\eta(x)$ of the tangential discontinuity over an open groove. From this displacement, we can determine the sound pressure field in both the groove and the half-space.

Denote by Φ_1 and Φ_2 the sound potentials of the scattered fields in the stationary and moving media, respectively. The sound pressures and the y-components of velocities and displacements are related to these potentials as follows:

$$p_1 = i\omega\rho\Phi_1, \quad p_2 = i\omega\rho\left[1 + \frac{U}{-i\omega}\frac{\partial}{\partial x}\right]\Phi_2, \tag{1}$$

$$\begin{aligned} v_{1y} &= \frac{\partial\Phi_1}{\partial y} = -i\omega\eta_1(x, y), \\ v_{2y} &= \frac{\partial\Phi_2}{\partial y} = -i\omega\left[1 + \frac{U}{-i\omega}\frac{\partial}{\partial x}\right]\eta_2(x, y). \end{aligned} \tag{2}$$

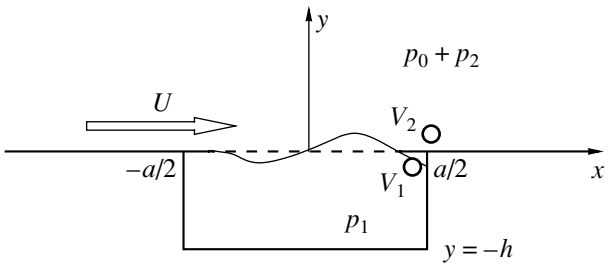

Fig. 1. Groove on a rigid plane with a grazing flow over it.

The total field must satisfy the condition of the pressure continuity in the hole

$$p_1(x, 0) = p_2(x, 0) + p_0(x, 0), \quad |x| < a/2, \tag{3}$$

the displacement continuity in the hole

$$\eta_1(x, 0) = \eta_2(x, 0) = \eta(x), \quad |x| < a/2, \tag{4}$$

and the Kutta–Zhukovski condition on the front edge

$$\eta\left(-\frac{a}{2}\right) = 0, \quad \left.\frac{d\eta}{dx}\right|_{x = -a/2} = 0. \tag{5}$$

We represent the fields p_1 and p_2 in the form

$$p_1 = p_{1r} + p_{1l}, \quad p_2 = p_{2r} + p_{2l},$$

where p_{1r} and p_{2r} are the fields produced by the normal displacements of the tangential discontinuity in the stationary and moving media and p_{1l} and p_{2l} are the fields produced in the stationary and moving media by the end sources resulting from the discontinuous flow around the right-hand edge of the groove. We note that the fields p_{1l} and p_{2l} are calculated for a closed groove ($\eta \equiv 0$). Let us write the integral relationships relating the fields p_{1r}, p_{2r}, p_{1l}, and p_{2l} to the displacement $\eta(x)$ and then substitute these expressions into the boundary condition (3). The resulting expression will be the desired equation in $\eta(x)$. In accordance with Eqs. (1), (2), and (4), we can assume that the fields p_{1r} and p_{2r} are produced by the respective sources of volume velocity,

$$f_1 = +i\omega\eta(x), \quad f_2 = -i\omega\left[1 + \frac{U}{-i\omega}\frac{\partial}{\partial x}\right]\eta(x),$$

which are distributed over the plane $y = 0$ in the interval $|x| < a/2$. Using the Fourier method, we obtain the following expressions for the fields p_{1r} and p_{2r}:

$$p_{1r}(x, y) = \sum_{n = 0}^{n = \infty} \frac{\omega^2 \rho b_n}{\sqrt{k_n^2 - k^2}\sinh[\sqrt{k_n^2 - k^2}h]} \times \cos\left[k_n\left(\frac{a}{2} + x\right)\right]\cosh[\sqrt{k_n^2 - k^2}(h + y)], \tag{6}$$

$$p_{2r}(x, y) = -\rho\omega^2 \int_{-\infty}^{+\infty} g(\alpha)\frac{\left(1 - \frac{U}{\omega}\alpha\right)^2}{\sqrt{\alpha^2 - (k - M\alpha)^2}} \times \exp[i\alpha x - \sqrt{\alpha^2 - (k - M\alpha)^2}\, y]d\alpha, \tag{7}$$

where $k_n = \pi n/a$, $k = \omega/c$, $M = U/c$, and it is assumed that $\mathrm{Re}\sqrt{\alpha^2 - (k - M\alpha)^2} > 0$ for $\mathrm{Im}\, k > 0$. The coefficients b_n and $g(\alpha)$ are the amplitudes of the Fourier components in the expansion of the displacement $\eta(x)$ in the Fourier series and in the Fourier integral, respectively:

$$\eta(x) = \sum_{n = 0}^{\infty} b_n \cos\left[k_n\left(\frac{a}{2} + x\right)\right] = \int_{-\infty}^{\infty} g(\alpha)e^{i\alpha x}d\alpha,$$

$$b_n = \frac{2}{a\varepsilon_n}\int_{-a/2}^{a/2} \eta(x)\cos\left[k_n\left(\frac{a}{2} + x\right)\right]dx, \tag{8}$$

$$g(\alpha) = \frac{1}{2\pi}\int_{-a/2}^{a/2} \eta(x)e^{-i\alpha x}dx,$$

where $\varepsilon_0 = 2$ and $\varepsilon_n = 1$ for $n \neq 0$. These coefficients are related as follows:

$$b_n = \frac{2\pi}{a\varepsilon_n}\left\{g(-k_n)\exp\left(ik_n\frac{a}{2}\right) + g(k_n)\exp\left(-ik_n\frac{a}{2}\right)\right\}, \tag{9}$$

$$g(\alpha) = \frac{1}{2\pi}\sum_{n = 0}^{\infty} G_n(\alpha)b_n,$$

where

$$G_n(\alpha) = \int_{-a/2}^{a/2} \cos\left[k_n\left(\frac{a}{2} + x\right)\right]e^{-i\alpha x}dx$$

$$= \frac{\alpha}{(\alpha^2 - k_n^2)}\left\{[(-1)^n + 1]\sin\left(\frac{\alpha a}{2}\right) + i[(-1)^n - 1]\cos\left(\frac{\alpha a}{2}\right)\right\}.$$

To obtain the parameters of the end sources, we use the following physical speculations. In the case of the negative deviation of the tangential discontinuity at the point $x = a/2$, the moving medium finds its way into the groove. This inflow can be described as the action of a volume velocity source located near (below) the right-hand side of the groove. The amplitude of the harmonic component of this volume velocity is approximately $V_1 = -\beta_1 U\eta\left(\frac{a}{2}\right)$, where the coefficient β_1 measures about 0.5. In the case of the positive deviation of the tangential discontinuity at the point $x = \frac{a}{2}$, the medium between this discontinuity and the plane $y = 0$ becomes stationary. This stop can be described as the action of a volume velocity source located near (above) the right-hand side of the groove. The amplitude of the harmonic component of this volume velocity is approximately $V_2 = -\beta_2 U\eta\left(\frac{a}{2}\right)$, where the coefficient β_2 measures

again about 0.5. For a closed groove ($\eta \equiv 0$), these monopole end sources create the fields

$$p_{1l}(x, y) = -i\omega\rho \sum_{n=0}^{n=\infty} \frac{(-1)^n 2V_1}{a\varepsilon_n \sqrt{k_n^2 - k^2} \sinh[\sqrt{k_n^2 - k^2} h]} \times \cos\left[k_n\left(\frac{a}{2} + x\right)\right] \cosh[\sqrt{k_n^2 - k^2}(h + y)], \quad (10)$$

$$p_{2l}(x, y) = -i\omega\rho \frac{V_2}{2\pi} \int_{-\infty}^{+\infty} \frac{\left(1 - \frac{U}{\omega}\alpha\right)}{\sqrt{\alpha^2 - (k - M\alpha)^2}} \times \exp\left[i\alpha\left(x - \frac{a}{2}\right) - \sqrt{\alpha^2 - (k - M\alpha)^2}\, y\right] d\alpha. \quad (11)$$

The fields $p_1 = p_{1r} + p_{1l}$ and $p_2 = p_{2r} + p_{2l}$, where p_{1r}, p_{2r}, p_{1l}, and p_{2l} are determined by formulas (6), (7), (10), and (11), satisfy boundary condition (4). Let us make them satisfy boundary condition (3). For this purpose, we expand the fields $p_{1r}(x, 0)$ and $p_{1l}(x, 0)$ in the Fourier integrals; by virtue of Eqs. (9), we obtain the expansions

$$p_{1r}(x, 0) = \rho\omega^2 \int_{-\infty}^{\infty} g(\alpha) \frac{\coth[\sqrt{\alpha^2 - k^2} h]}{\sqrt{\alpha^2 - k^2}} e^{i\alpha x} d\alpha, \quad (12)$$

$$p_{1l}(x, 0) = -i\omega\rho \frac{V_1}{2\pi} \int_{-\infty}^{\infty} \frac{\coth[\sqrt{\alpha^2 - k^2} h]}{\sqrt{\alpha^2 - k^2}} e^{i\alpha(x - a/2)} d\alpha. \quad (13)$$

Substituting Eqs. (7), (11), (12), and (13) into boundary condition (3), we obtain the integral equation in $g(\alpha)$:

$$\int_{-\infty}^{\infty} g(\alpha) \left\{ \frac{\left(1 - \frac{U}{\omega}\alpha\right)^2}{\sqrt{\alpha^2 - (k - M\alpha)^2}} + \frac{\coth[\sqrt{\alpha^2 - k^2} h]}{\sqrt{\alpha^2 - k^2}} \right\} e^{i\alpha x} d\alpha = \frac{1}{\rho\omega^2}[p_0(x, 0) + p_l(x, 0)], \quad |x| < \frac{a}{2}, \quad (14)$$

where

$$p_l(x, 0) = p_{2l}(x, 0) - p_{1l}(x, 0) = \frac{i\omega\rho}{2\pi} U\eta\left(\frac{a}{2}\right) \int_{-\infty}^{\infty} \left\{ \beta_2 \frac{1 - \frac{U}{\omega}\alpha}{\sqrt{\alpha^2 - (k - M\alpha)^2}} - \beta_1 \frac{\coth[\sqrt{\alpha^2 - k^2} h]}{\sqrt{\alpha^2 - k^2}} \right\} e^{i\alpha(x - a/2)} d\alpha. \quad (15)$$

For a given pressure drop at the hole $P(x) \equiv p_0(x, 0) + p_l(x, 0)$, the displacement of the boundary at $U \neq 0$ can be expressed through the displacement at $U = 0$. Denote the solution of Eq. (14) at $U = 0$ as $g_0(\alpha)$. Then, the solution for $U \neq 0$ (for the same pressure drop at the hole $P(x)$) will be

$$g(\alpha) = g_0(\alpha) \frac{\left\{ \frac{\left(1 - \frac{U}{\omega}\alpha\right)^2}{\sqrt{\alpha^2 - (k - M\alpha)^2}} + \frac{\coth[\sqrt{\alpha^2 - k^2} h]}{\sqrt{\alpha^2 - k^2}} \right\}_{U=0}}{\left\{ \frac{\left(1 - \frac{U}{\omega}\alpha\right)^2}{\sqrt{\alpha^2 - (k - M\alpha)^2}} + \frac{\coth[\sqrt{\alpha^2 - k^2} h]}{\sqrt{\alpha^2 - k^2}} \right\}}.$$

The displacement can be obtained by the formula

$$\eta(x) = \int_{-\infty}^{\infty} g(\alpha) e^{i\alpha x} d\alpha = \frac{1}{2\pi} \int_{-\infty}^{\infty} \int_{-a/2}^{a/2} \eta_0(x_0) \frac{1}{W(\alpha)} \times \exp[i\alpha(x - x_0) + \sqrt{\alpha^2 - k^2} h] dx_0 d\alpha, \quad (16)$$

where

$$W(\alpha) = \left(1 - \frac{U}{\omega}\alpha\right)^2 \frac{\sqrt{\alpha^2 - k^2}}{\sqrt{\alpha^2 - (k - M\alpha)^2}} \sinh[\sqrt{\alpha^2 - k^2} h] + \cosh[\sqrt{\alpha^2 - k^2} h] \quad (17)$$

and $\eta_0(x) = \int_{-\infty}^{\infty} g_0(\alpha) e^{i\alpha x} d\alpha$ is the boundary displacement at $U = 0$.

The integral with respect to α in Eq. (16) can be calculated with the use of the residue theory. The poles of the integrand are the roots of the equation $W(\alpha) = 0$. This equation has two physical roots, $\alpha = \alpha_1$ and $\alpha = \alpha_2$, that determine the wave numbers of free hydrodynamic waves. Performing the corresponding calculations and satisfying boundary conditions (15) on the edge by adding free hydrodynamic waves to the solution, we obtain the desired displacement

$$\eta(x) = \frac{R(\alpha_1) + R(\alpha_2)}{\alpha_2 - \alpha_1} \eta_0(-a/2)[e^{i\alpha_1(x + a/2)} - e^{i\alpha_2(x + a/2)}] + iR(\alpha_1) \int_{-a/2}^{x} \eta_0(x_0) e^{-i\alpha_1 x_0} dx_0 e^{i\alpha_1 x} + iR(\alpha_2) \int_{-a/2}^{x} \eta_0(x_0) e^{-i\alpha_2 x_0} dx_0 e^{i\alpha_2 x}, \quad (18)$$

where

$$R(\alpha) = \frac{1}{\frac{d}{d\alpha}W(\alpha)}\exp(\sqrt{\alpha^2 - k^2}h),$$

$$\left\{\frac{d}{d\alpha}W(\alpha)\right\}_{\alpha = \alpha_{1,2}} = \sinh[\sqrt{\alpha_{1,2}^2 - k^2}h]$$

$$\times\left\{-2\frac{U}{\omega}\left(1 - \frac{U}{\omega}\alpha\right)\frac{\sqrt{\alpha^2 - k^2}}{\sqrt{\alpha^2 - (k - M\alpha)^2}}\right.$$

$$+\left(1 - \frac{U}{\omega}\alpha\right)^2 M\frac{k\alpha^2(1 - M) + k^3}{\sqrt{\alpha^2 - k^2}[\alpha^2 - (k - M\alpha)^2]^{3/2}}$$

$$\left.-\frac{\alpha h}{\sqrt{\alpha^2 - k^2}\sinh^2[\sqrt{\alpha^2 - k^2}h]}\right\}_{\alpha = \alpha_{1,2}}.$$

The limiting values of the roots for the case of an incompressible medium ($c = \infty$) are

$$\alpha_{1,2} = \frac{\omega}{U}(1 \pm i), \quad h \longrightarrow \infty;$$

$$\alpha_{1,2} = \frac{\omega}{U}\left(\frac{U}{\omega h}\right)^{1/3}\frac{1 \pm i\sqrt{3}}{2}, \quad h \longrightarrow 0.$$

Thus, the calculation of the displacement $\eta(x)$ for $U \neq 0$ requires knowledge of the displacement $\eta_0(x)$ at $U = 0$ (for the same pressure drop on the hole). The latter can be obtained as follows. Substitute the fields $p_1 = p_{1r} + p_{1l}$ and $p_2 = p_{2r} + p_{2l}$, where p_{1r} and p_{2r} are determined by Eqs. (6) and (7) at $U = 0$, into boundary condition (3); then, multiply both sides of the resulting relationship by $\cos\left[k_m\left(\frac{a}{2} + x\right)\right]$ and integrate the result with respect to x over the interval $|x| < a/2$. By virtue of Eqs. (9), we obtain a system of algebraic equations in the amplitudes b_n:

$$b_m\frac{\varepsilon_m a}{2}\frac{\coth[\sqrt{k_m^2 - k^2}h]}{\sqrt{k_m^2 - k^2}} + \sum_{n=0}^{\infty}\frac{b_n}{2\pi}\int_{-\infty}^{\infty}\frac{G_n(\alpha)G_m^*(\alpha)}{\sqrt{a^2 - k^2}}d\alpha$$

$$= \frac{1}{\rho\omega^2}\int_{-a/2}^{a/2}P(x)\cos\left[k_m\left(\frac{a}{2} + x\right)\right]dx.$$

With these amplitudes, we obtain the displacement $\eta_0(x)$ by the formula

$$\eta_0(x) = \sum_{n=0}^{\infty}b_n\cos\left[k_n\left(\frac{a}{2} + x\right)\right]. \tag{19}$$

Represent the displacement $\eta_0(x)$ in the form

$$\eta_0(x) = \eta_0^{(0)}(x) + \eta\left(\frac{a}{2}\right)\zeta(x), \tag{20}$$

where $\eta_0^{(0)}(x)$ is the displacement caused by pressure $p_0(x, 0)$ and $\eta\left(\frac{a}{2}\right)\zeta(x)$ is the displacement caused by pressure $p_l(x, 0)$ (in the absence of the flow). Using Eqs. (18) and (20), we obtain an expression for $\eta\left(\frac{a}{2}\right)$:

$$\eta\left(\frac{a}{2}\right) = -\left\{\frac{[R(\alpha_1) + R(\alpha_2)]}{\alpha_2 - \alpha_1}\eta_0^{(0)}\left(-\frac{a}{2}\right)[e^{i\alpha_1 a} - e^{i\alpha_2 a}]\right.$$

$$+ iR(\alpha_1)\int_{-a/2}^{a/2}\eta_0^{(0)}(x_0)e^{-i\alpha_1 x_0}dx_0 e^{i\alpha_1 a/2}$$

$$\left.+ iR(\alpha_2)\int_{-a/2}^{a/2}\eta_0^{(0)}(x_0)e^{-i\alpha_2 x_0}dx_0 e^{i\alpha_2 a/2}\right\}$$

$$\times\left\{\frac{[R(\alpha_1) + R(\alpha_2)]}{\alpha_2 - \alpha_1}\zeta\left(-\frac{a}{2}\right)[e^{i\alpha_1 a} - e^{i\alpha_2 a}]\right. \tag{21}$$

$$+ iR(\alpha_1)\int_{-a/2}^{a/2}\zeta(x_0)e^{-i\alpha_1 x_0}dx_0 e^{i\alpha_1 a/2}$$

$$\left.+ iR(\alpha_2)\int_{-a/2}^{a/2}\zeta(x_0)e^{-i\alpha_2 x_0}dx_0 e^{i\alpha_2 a/2} - 1\right\}^{-1}.$$

Formulas (18), (20), and (21) form the solution to the problem of the motion of the tangential discontinuity in a hole. Consider briefly the structure of the solution. According to Eq. (18), the displacement of the tangential discontinuity is the sum of two hydrodynamic waves, one of which exponentially increases and the other exponentially decreases. These waves are excited by the sources represented by the vertical displacements of particles in the hole that coincide with those appearing in the upper half-space under the action of the pressure fields $p_0(x, 0)$ and $p_l(x, 0)$ in the absence of the flow in the upper half-space. The field p_l realizes the feedback between the displacements of the tangential discontinuity on edge $x = a/2$ and the displacements over the entire hole.

The solution obtained above can be used, in particular, to calculate the input admittance of the groove, if its length is small in comparison with the wavelength of

the incident wave. The input admittance is determined by the formula

$$Y = V/\int_{-a/2}^{a/2} p_0(x,0)dx, \tag{22}$$

where

$$V = -\int_{-a/2}^{a/2} (-i\omega)\eta(x)dx - \beta_1 U\eta\left(\frac{a}{2}\right) \tag{23}$$

is the volume velocity of the medium passing through the hole. In Eq. (23), the first term is related to the displacement flow of the medium under the lateral motion of the tangential discontinuity, and the second term is related to the penetration of a jet of the moving medium into the stationary medium filling the groove.

The algorithm suggested for the calculation is closed and exact but cumbersome. The main calculation difficulty, unrelated to the presence of the tangential discontinuity, consists in solving the system of equations in the coefficients b_n. To obtain a qualitatively correct estimate of the behavior of the tangential discontinuity and acoustic admittance of the groove, we can consider the problem in a simplified formulation. Namely, assume that displacement $\eta_0(x)$ is a purely piston displacement. In other words, we retain only the first term in the Fourier series (19). It should be emphasized that the displacement of the tangential discontinuity calculated by Eq. (18) is not assumed to be a piston displacement. We simplify only the auxiliary problem concerning the calculation of the displacement field on the hole in the absence of the flow. The same procedure was used in paper [1].

Thus, we assume that both sources—the pressure in the external field $p_0(x)$ and the pressure $p_l(x)$ of the end sources of the volume velocity—act on a weightless rigid piston closing the groove. The problem consists in finding the piston displacement under the action of these two sources. To additionally simplify the problem, we assume that the medium is weakly compressible, so that the wavelength of sound is much longer than the size of the groove. In this case, the displacement $\eta_0^{(0)}$ caused by the action of the external field is expressed as (this displacement is proportional to the medium compressibility in the groove volume)

$$\eta_0^{(0)} = -\frac{h}{\rho c^2}p_0,$$

and the parameter ζ, which is determined as the proportionality coefficient between the displacement of the tangential discontinuity on the rear edge $\eta\left(\frac{a}{2}\right)$ and η_0 (assuming that the medium in the groove is incompressible, this coefficient is calculated by equating the volume displacement of the end source to the volume displacement of the piston), has the form

$$\zeta = \frac{-\beta_1 U}{-i\omega a}.$$

The integrals appearing in Eq. (21) are calculated analytically, and the displacement $\eta\left(\frac{a}{2}\right)$ is found to be

$$\eta\left(\frac{a}{2}\right) = -\frac{\dfrac{R(\alpha_1)+R(\alpha_2)}{\alpha_1-\alpha_2}(e^{i\alpha_1 a}-e^{i\alpha_2 a}) + \dfrac{iR(\alpha_1)}{-i\alpha_1}(1-e^{i\alpha_1 a}) + \dfrac{iR(\alpha_2)}{-i\alpha_2}(1-e^{i\alpha_2 a})}{\zeta\left[\dfrac{R(\alpha_1)+R(\alpha_2)}{\alpha_1-\alpha_2}(e^{i\alpha_1 a}-e^{i\alpha_2 a}) + \dfrac{iR(\alpha_1)}{-i\alpha_1}(1-e^{i\alpha_1 a}) + \dfrac{iR(\alpha_2)}{-i\alpha_2}(1-e^{i\alpha_2 a})\right]-1}\eta_0^{(0)}.$$

Then, we determine the displacement η_0 in the auxiliary problem:

$$\eta_0 = \eta_0^{(0)}\left\{1-\zeta\frac{\dfrac{R(\alpha_1)+R(\alpha_2)}{\alpha_1-\alpha_2}(e^{i\alpha_1 a}-e^{i\alpha_2 a}) + \dfrac{iR(\alpha_1)}{-i\alpha_1}(1-e^{i\alpha_1 a}) + \dfrac{iR(\alpha_2)}{-i\alpha_2}(1-e^{i\alpha_2 a})}{\zeta\left[\dfrac{R(\alpha_1)+R(\alpha_2)}{\alpha_1-\alpha_2}(e^{i\alpha_1 a}-e^{i\alpha_2 a}) + \dfrac{iR(\alpha_1)}{-i\alpha_1}(1-e^{i\alpha_1 a}) + \dfrac{iR(\alpha_2)}{-i\alpha_2}(1-e^{i\alpha_2 a})\right]-1}\right\}.$$

Rearranging this expression, we obtain

$$\eta_0 = \eta_0^{(0)}\left\{\frac{-1}{\zeta\left[\dfrac{R(\alpha_1)+R(\alpha_2)}{\alpha_1-\alpha_2}(e^{i\alpha_1 a}-e^{i\alpha_2 a}) + \dfrac{iR(\alpha_1)}{-i\alpha_1}(1-e^{i\alpha_1 a}) + \dfrac{iR(\alpha_2)}{-i\alpha_2}(1-e^{i\alpha_2 a})\right]-1}\right\}.$$

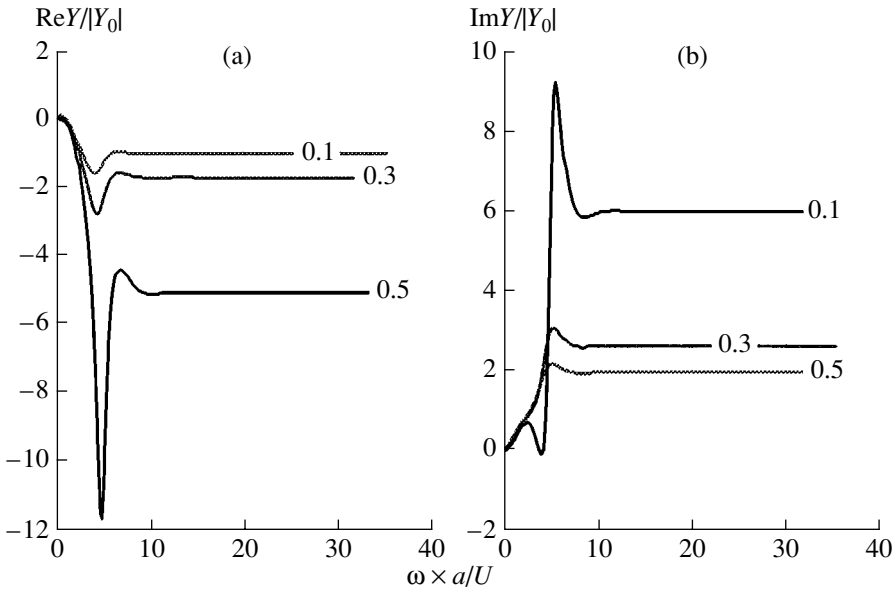

Fig. 2. (a) Real and (b) imaginary parts of the groove admittance as functions of frequency. The abscissa axis represents the dimensionless frequency and the ordinate axis, the dimensionless admittance normalized by the absolute value of the groove admittance in the absence of flow, $Y_0 = i\omega h/\rho c^2$. Different curves correspond to different values of the parameter β_1 (the values are indicated near the curves). The dimensional parameters are $h = 0.005$ m, $a = 0.005$ m, and $U = 17$ m.

We calculate the displacement of the tangential discontinuity by Eq. (18):

$$\eta(x) = \eta_0\left\{-\left(\frac{R(\alpha_1)}{\alpha_1} + \frac{R(\alpha_2)}{\alpha_2}\right)\right.$$

$$+ e^{i\alpha_1\left(x+\frac{a}{2}\right)}\left[\frac{R(\alpha_1) + R(\alpha_2)}{\alpha_1 - \alpha_2} + \frac{R(\alpha_1)}{\alpha_1}\right]$$

$$\left. - e^{i\alpha_2\left(x+\frac{a}{2}\right)}\left[\frac{R(\alpha_1) + R(\alpha_2)}{\alpha_1 - \alpha_2} + \frac{R(\alpha_2)}{\alpha_2}\right]\right\}.$$

This expression satisfies the Kutta–Zhukovski condition. Now, we can calculate the effective admittance of the groove. The volume velocity is

$$V = -(-i\omega)\eta_0\left[-\left(\frac{R(\alpha_1)}{\alpha_1} + \frac{R(\alpha_2)}{\alpha_2}\right)a\right.$$

$$+\left(\frac{R(\alpha_1) + R(\alpha_2)}{\alpha_1 - \alpha_2} + \frac{R(\alpha_1)}{\alpha_1}\right)\frac{1}{i\alpha_1}(e^{i\alpha_1 a} - 1)$$

$$\left. -\left(\frac{R(\alpha_1) + R(\alpha_2)}{\alpha_1 - \alpha_2} - \frac{R(\alpha_2)}{\alpha_2}\right)\frac{1}{i\alpha_1}(e^{i\alpha_2 a} - 1)\right] - \beta_1 U\eta\left(\frac{a}{2}\right).$$

All quantities appearing in this expression were calculated above. Ultimately, they are all expressed through $\eta_0^{(0)}$. The admittance of the groove is

$$Y = V/ap_0.$$

Figure 2 shows the calculated real and imaginary parts of the admittance normalized by the absolute value of the elastic admittance of the groove in the absence of flow, $Y_0 = i\omega h/\rho c^2$. Different curves correspond to different coefficients β_1. The real part of the admittance is negative. This means that work is performed on the acoustic field, so that the total power of the field increases.

We dedicate this work to the memory of L.M. Lyamshev who greatly contributed to the study of aeroacoustic interactions (see, e.g., [6]).

REFERENCES

1. A. S. Hersh, B. Walker, and M. Bucka, AIAA Pap., No. 78-1125 (1978).
2. D. Ronnenberger, J. Sound Vibr. **24** (1), 133 (1972).
3. M. S. Howe, J. Fluid Mech. **330**, 61 (1997).
4. M. A. Mironov, Akust. Zh. **28**, 528 (1982) [Sov. Phys. Acoust. **28**, 310 (1982)].
5. P. M. Radavich, A. Selamet, and J. M. Novak, J. Acoust. Soc. Am. **109**, 1343 (2001).
6. L. M. Lyamshev, Akust. Zh. **8**, 91 (1962) [Sov. Phys. Acoust. **8**, 66 (1962)].

Translated by A. Vinogradov

Acoustical Physics, Vol. 49, No. 1, 2003, pp. 81–87. Translated from Akusticheskiĭ Zhurnal, Vol. 49, No. 1, 2003, pp. 92–99.

Resonant Acoustic Spectroscopy at Low *Q* Factors

A. V. Lebedev[1], L. A. Ostrovskiĭ[1, 2], A. M. Sutin[1, 3], I. A. Soustova[1], and P. A. Johnson[4]

[1] *Institute of Applied Physics, Russian Academy of Sciences, ul. Ul'yanova 46, Nizhni Novgorod, 603950 Russia*
e-mail: soustova@hydro.appl.sci-nnov.ru

[2] *Zel Technologies/NOAA Environmental Technology Laboratory, 325 Broadway, Boulder, Colorado 80305, USA*

[3] *Davidson Laboratory, Stevens Institute of Technology, 711 Hudson Street, Hoboken, NJ 07030, USA*

[4] *Los Alamos National Laboratory, Los Alamos, New Mexico 87501, USA*

Received August 26, 2002

Abstract—The application of resonant acoustic spectroscopy to rock, building materials, and materials with cracks is hindered by the substantial mechanical losses in these materials and by the overlapping of the individual resonance responses. The paper describes a method for the determination of the resonance frequencies in low-*Q* materials in the presence of a strong overlapping of resonances. The effect of cracks on the values of the resonance frequencies and *Q* factors is studied experimentally. *© 2003 MAIK "Nauka/Interperiodica".*

Resonant acoustic spectroscopy (RAS) has received wide acceptance as a method for measuring the elasticity tensors of various samples [1]. A detailed description of RAS methods along with examples of their application can be found in [1–3]. The high accuracy of this technique has made it a popular instrument for solving a wide variety of problems. For example, RAS is used for analyzing such effects and parameters as dissipation mechanisms in solids [4], phase transitions in superconducting materials [5], the mobility of dislocations in a crystal lattice [6], the structures of polycrystalline bodies [7] and composites [8], the effect of the treatment of a material on its microstructure [9], and the elastic moduli of the third order [10]; RAS is also used for estimating the grain size in a structurally inhomogeneous medium [11]. One of the most important areas of application of RAS is the nondestructive testing of materials [12–14].

Initially, RAS methods were developed for measuring the properties of crystals, e.g., for the determination of the specific heat of crystals or the detection of phase transitions in them. Such samples are almost free of internal defects, and, hence, the mechanical losses in them are small. Each resonance observed on these samples manifests itself as a sharp peak. The position of each peak in the frequency spectrum of the response determines a resonance frequency, and the width of the peak indicates the *Q* factor. This method of measuring the resonance frequencies and the *Q* factors enjoys wide application [1].

As for the resonant acoustic spectroscopy of composite and structurally inhomogeneous materials, the main obstacle here is the overlapping of individual resonance responses, which hinders the resolution of resonances and makes it impossible to obtain the required accuracy when using this method for nondestructive testing [15]. Unlike crystals, the composites and structurally inhomogeneous media (such as rock or building materials) are characterized by great numbers of internal defects and, hence, by high mechanical losses. As a result, the resonances do not manifest themselves as separate peaks, and the measurement of the resonance frequencies and *Q* factors by the conventional RAS technique is rather difficult. In the recent publication [16] (by one of the authors of this paper), the matched-filter processing of the experimental data was proposed as a method to determine the resonance frequencies and the *Q* factors in acoustic spectroscopy. In another publication [17], this method was shown to provide a high accuracy in measuring the elastic constants, including the cases when the conventional technique (the identification of the peaks) fails.

In the present paper, matched-filter processing is used to determine the resonance frequencies and the *Q* factors for materials with high concentrations of internal defects and to estimate the effect of cracks on the values of the resonance frequencies and *Q* factors at fracture. The first section briefly describes (on the basis of [16]) the method of the determination of the resonance frequencies and the *Q* factors of the samples; the second section describes the experimental setup and the scheme of measurements; and the third section discusses the results.

RESOLUTION OF OVERLAPPING RESONANCES

For the methods under consideration, the usual approach is the minimization of the mean square deviation of the measurement data from some selected physical model whose parameters are to be determined. In analyzing the linear response of a mechanical vibratory system with many degrees of freedom (modes), it is natural to choose a model in the form of the superposition of individual resonances. Then, the complex

1063-7710/03/4901-0081$24.00

transfer function (TF) being defined as $\mathrm{TF}(\omega) = A_{\mathrm{out}}(\omega)/A_{\mathrm{inp}}(\omega)$, where $A_{\mathrm{inp}}(\omega)$ and $A_{\mathrm{out}}(\omega)$ are the complex amplitudes of the input and output signals proportional to the force and the displacement, respectively, should be represented in the form

$$\mathrm{TF}(p) = \sum_{l=1}^{M} A_l G(p, \delta_l, \omega_l). \quad (1)$$

Here, M is the number of resonances in the frequency range under consideration ($\omega_{\min} < \omega < \omega_{\max}$), $p = i\omega$, $G(p, \delta_l, \omega_l) = \dfrac{1}{p^2 + 2\delta_l p + \omega_l^2}$ is the response for the lth resonance, δ_l is the corresponding loss factor, and ω_l is the corresponding frequency. Function (1) describes the response of an arbitrary linear vibratory system in the frequency domain [18]. Let us assume that we know N values of the transfer function at the frequencies $p_n = i(\omega_{\min} + 2\pi\Delta f n/N)$, where $0 \le n \le N$, $\Delta f = (\omega_{\max} - \omega_{\min})/2\pi$ is the frequency range in which the experimental data are given, and $\Delta f/N$ is the frequency resolution of the transfer function. Then, the finite parameters of model (1), i.e., the number of resonances, their frequencies and amplitudes, and the loss factor, should provide the minimal mean square deviation of the measured (or given) values of $\mathrm{TF}_{\mathrm{exp}}(p_n)$ from the results of calculation by Eq. (1). We set the variations of the square magnitude of the corresponding difference with respect to A_l equal to zero to obtain a system of linear equations for the amplitudes of the responses:

$$C_{kl} A_l = D_k, \quad (2)$$

where $C_{kl} = \sum_{j=1}^{N} G^*(p_j, \delta_k, \omega_k) G(p_j, \delta_l, \omega_l)$ and $D_k = \sum_{j=1}^{N} G^*(p_j, \delta_k, \omega_k)\mathrm{TF}(p_j)$.

To determine the resonance frequencies ω_l and the loss factors δ_l in model (1), we use the modified methods of linear prediction in the time domain (see, e.g., [19]). To change from the frequency domain of definition of the transfer function to the time domain (the pulse response), we use a discrete Fourier transform, so that the array of equidistant readings in the frequency domain $\mathrm{TF}(p_n)$ is put in correspondence with an array of the readings ζ_n equidistant in time. The deviation of the predicted value of ζ_n from the measured one ζ_n^{exp} is minimized as follows [19]. We determine a characteristic polynomial $H(z) = 1 + \sum_{k=1}^{L} h_k z^{-k}$ with $z = \exp((-\delta + i\omega)/\Delta f)$. The polynomial coefficients represent the solution to the system of equations

$$a_{jk} h_k + b_j = 0, \quad (3)$$

where $a_{jk} = \zeta_{L-k+j}$, $b_j = \zeta_{L+j}$, $j = 1, 2, \ldots, N-L$, $k = 1, 2, \ldots, L$, and $L \ge M$. The zeros of the polynomial H [$H(z_l) = 0$, $z_l = \exp((-\delta_l + i\omega_l)/\Delta f)$] coincide with the poles of expression (1) (see [16, 19]). As a result, the mean square deviation of the measured data from the data obtained using model (1) with the corresponding set of parameters (ω_l, δ_l) and with the amplitudes A_l satisfying Eq. (2) proves to be minimal.

In the absence of losses ($\delta_l = 0$), the autocorrelation matrix $A = \hat{a}^+ \hat{a}$ [where $\hat{a} = a_{jk}$ is determined from Eqs. (3) and the sign $(\cdot)^+$ denotes Hermitian conjugation] has the dimension $L \times L$ and the rank M. The first M eigenvalues Λ of this matrix are positive ($\Lambda_k > 0$, $k = 1, 2, \ldots, M$), and the remaining $L - M$ eigenvalues are equal to zero: $\Lambda_k = 0$, $k = M+1, M+2, \ldots, L$ [19]. The presence of noise in the experimental data results in that the matrix A has a full rank. According to [19], the experimental data can be separated into the desired signal and the noise component by using the difference in the eigenvalues Λ_k: the small values of Λ_k should be identified with noise.

The presence of loss ($\delta_l \ne 0$) smoothes out the spectrum of the eigenvalues of the matrix A. In this case, the boundary between the desired signal (the contribution of resonances) and noise is assumed to be the break of the spectrum of Λ_k [16]. This allows one to determine the number M of the "true" resonances in model (1). If the signal-to-noise ratio (snr) is known or can be determined independently, the number of resonances can also be determined from the energy considerations (each Λ_k is equal to the power of the corresponding degree of freedom). Namely, for every (mth) physical resonance, the following condition should be met:

$$\mathrm{snr} \times \Lambda_m \ge \sum_{k=1}^{L} \Lambda_k. \quad (4)$$

The number of resonances M is determined as the maximal value of m satisfying inequality (4).

In this study, the number of resonances in the frequency band Δf is performed through the search for singularities in the spectrum of the eigenvalues Λ_k and the search for the maximal value of m in inequality (4). Then, after the value of M is determined, equations (3) and (2) are solved sequentially, and the parameters involved in model (1) are determined. The result of calculating the transfer function by Eq. (1) is compared with the experimental data. If discrepancies are obtained, the whole procedure is repeated with another value of L, which serves as the initial approximation for the number of resonances.

The measurement error for the parameters of model (1) is estimated in the conventional way. The goal function, which represents the sum of the squared magnitudes of the difference between the measured values of the transfer function and the parametric model (1), is represented as a Taylor series up to the

second-order terms for the values of A_l, ω_l, δ_l corresponding to the minimum of the goal function. In this case, the variance of each parameter of model (1) is determined by the ratio of the goal function to the second derivative of the goal function with respect to the corresponding parameter.

The proposed method was used to analyze the results of two series of measurements performed for materials with cracks. One series was performed for polycarbonate samples with the use of a swept signal, as in the case of the standard methods of resonant acoustic spectroscopy. The other series was performed for concrete samples with the use of impulse excitation of natural vibrations in the samples (impulse resonant spectroscopy). Note that no nonlinear effects were observed in the experiments described below.

RESONANT SPECTROSCOPY OF POLYCARBONATES

The polycarbonate samples had the form of rectangular bricks with the dimensions $13 \times 38 \times 132$ mm^3. Each sample had a 12-mm-deep groove. Under a cyclic loading, a visible crack was formed at the groove bottom. Sample no. 1 served as reference and was not subjected to loading, while sample no. 2 under the cyclic loading developed a 6-mm-long crack.

The measuring setup is schematically represented in Fig. 1. Piezoceramic transducers in the form of 2-mm-thick disks, 10 mm in diameter, were glued to the end surfaces of the sample. One of the transducers was used for the excitation of vibrations in the sample and the other served as a receiver. The response was measured by a resonant ultrasound spectroscope (produced by Dynamic Resonance Systems, see http://www.ndtest.com/). The setup made it possible to vary the excitation frequency and to save the data on the hard disk of a computer. The frequency resolution (the step in frequency) was 1 Hz in the frequency band 8–30 kHz and provided the possibility of recording the resonances with a Q factor up to 1000, which far exceeded the measured values of the Q factor.

Figure 2 presents the measured transfer function for a defect-free polycarbonate sample and the corresponding transfer function reconstructed by Eq. (1). One can see that, even for such a sample, the conventional analysis of the power spectral density (the search for peaks) does not allow one to determine all resonance frequencies and Q factors. Specifically, resonances marked in Fig. 2 by the numbers *3*, *7*, *9*, *12–15*, *17*, *18*, *20*, *22*, and *24* do not manifest themselves as peaks. Moreover, neither the amplitude nor the phase dependence of the transfer function on frequency provides the determination of the resonance positions with the use of only the local properties of TF(ω).

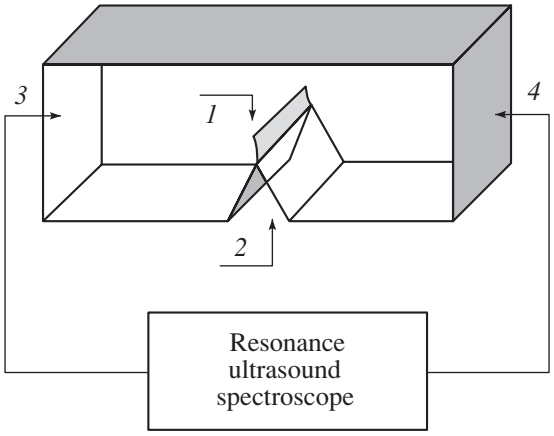

Fig. 1. Measuring setup: (*1*) crack, (*2*) groove, (*3*) position of the driving transducer, and (*4*) position of the receiver.

At the same time, the method discussed above provides the resolution of even noticeably overlapping resonance responses. To determine the number of resonances in the measuring frequency band, we performed the search for singularities (breaks) in the dependence $\Lambda(m)$ by using inequality (4). The value of the snr involved in inequality (4) was estimated as the ratio of the total spectral density (the sum of squared amplitudes) to the noise power in Fig. 2. The noise amplitude at every frequency was estimated as the difference between the measured value and the mean value obtained from the piecewise-linear smoothing approximation of the TF. The horizontal dashed line in Fig. 3 shows the noise power normalized to the total power of the signal. The intersection of this line with the curve corresponding to the eigenvalue spectrum normalized to the total power corresponds to the number of resonances in the measuring frequency band. The number of the resonances was found to be 29 within the frequency band 8–30 kHz. The Q factor of four resonances out of these 29 proved to be less than seven, which was much smaller than the mean value of the Q factor being approximately equal to 50. The appearance of these resonances was caused by the finite width of the measuring frequency band Δf and by the smooth trends arising in the frequency dependence of the TF. One resonance was found to have an amplitude comparable with the noise level and large errors in the measurements of its frequency and Q factor. Thus, the five resonances specified above were excluded from the analysis. The remaining $M = 24$ resonances are shown in Fig. 2. Their parameters were used for calculating the TF by Eq. (1).

It is well known that the presence of cracks mainly leads to a decrease in the Q factor while the propagation velocities of elastic waves vary within fractions of percent [20]. Since, initially, the Q factor values are small even for the defect-free sample, the measurement of the

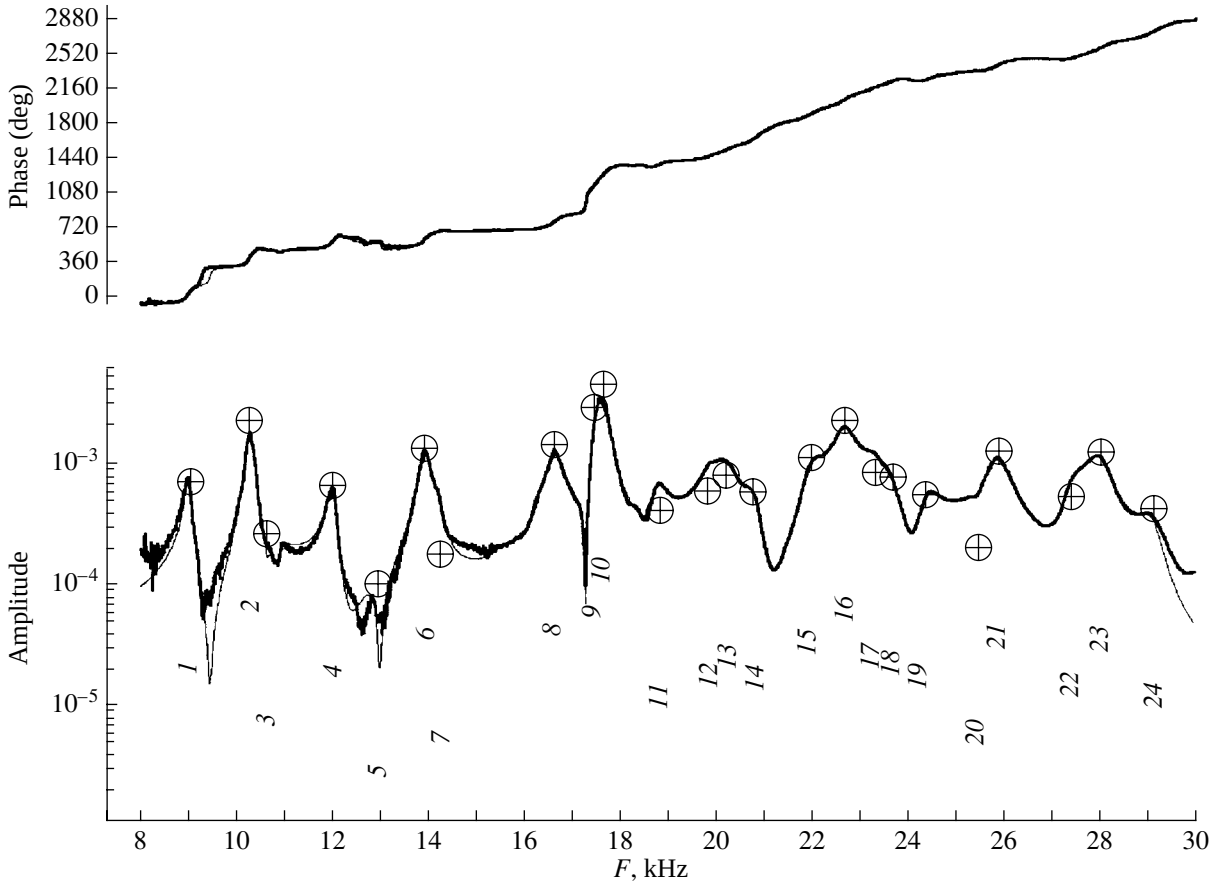

Fig. 2. Result of the reconstruction of the transfer function for sample 1 of polycarbonate (thin lines) and the experimental values of the TF (thick lines). The upper plot shows the phase and the lower plot, the amplitude of the TF.

Q factor variation due to the presence of cracks presents a difficult problem.

Figure 4 shows the resonance frequencies and the Q factors of the first ten resonances for polycarbonate samples 1 and 2. The frequencies were measured to within 1%, and the accuracy of the Q factor measurement was much lower. The maximal measurement errors were observed for the resonances whose amplitudes were comparable with the noise level (*1–3* in Fig. 2) and in the case of a considerable overlapping of the responses (*9* and *10* in Fig. 2). Of all resonances presented in Fig. 4, we can separate three, namely, the resonances marked by arrows (*6–8*) in Fig. 2, for which the measured values of the Q factor are statistically distinguishable (the confidence intervals of the data obtained for samples 1 and 2 do not overlap). The maximal variations in the resonance frequencies occur for the same three resonances *6–8* (Fig. 4). For these resonances, the appearance of the crack is accompanied by a loss increase. The Q factor decreases in the presence of the crack by approximately a factor of 2 with respect to the initial value ($Q_0 \approx 100$). The maximal changes in the Q factor are observed for the mode with the maximal initial Q factor value (mode *6* in Fig. 4).

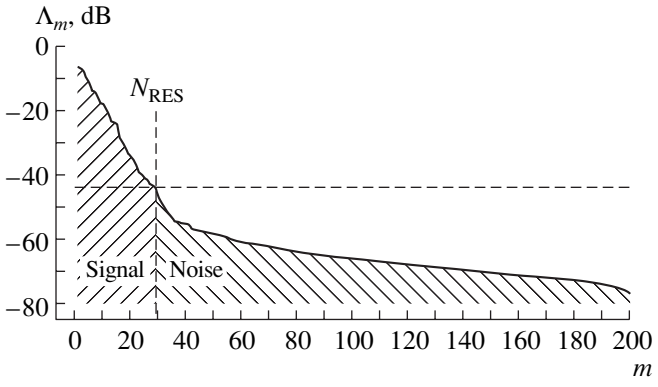

Fig. 3. Spectrum of the eigenvalues of the autocorrelation matrix for sample 1 of polycarbonate; the spectrum is normalized to the total power.

IMPULSE RESONANT SPECTROSCOPY OF CONCRETE SAMPLES

The second series of measurements was performed on two concrete samples. The samples had the form of rectangular bricks with the dimensions $152.4 \times 152.4 \times$

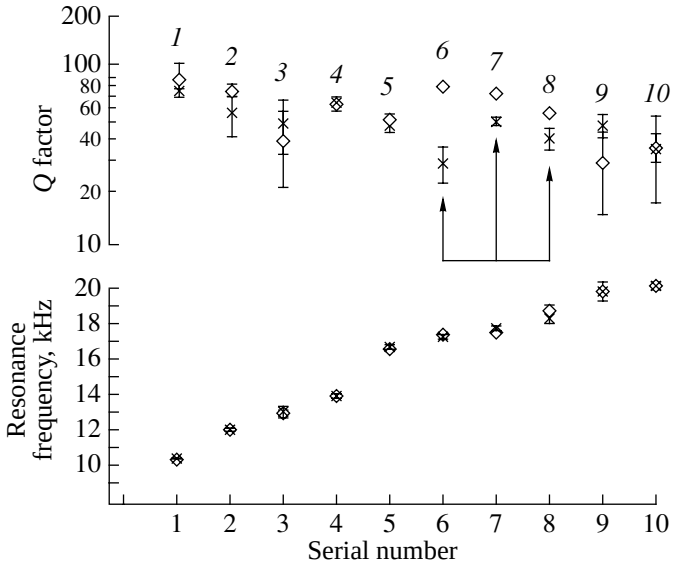

Fig. 4. Variations in the resonance frequencies and *Q* factors for the defect-free polycarbonate sample 1 and for sample 2 with a crack. The serial numbers of resonances correspond to the numbers given in Fig. 2. The measurement errors are shown by vertical segments, which correspond to the 60% confidence intervals under the assumption that the random noise is Gaussian. The diamonds (◇) refer to sample 1, and the crosses (×), to sample 2.

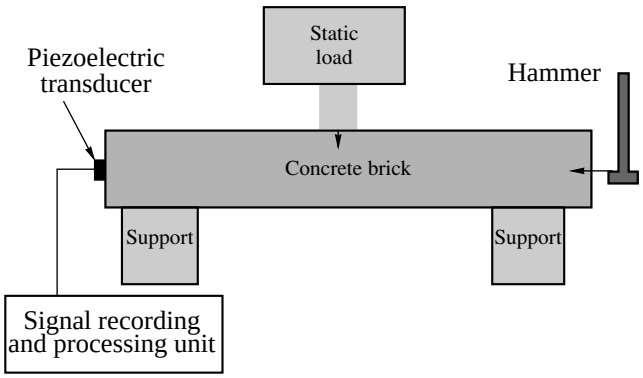

Fig. 5. Experimental setup.

533.4 mm^3 and had no grooves. Both samples initially had no defects and were gradually destroyed by a linearly increasing load until their fracture. The experimental setup is illustrated in Fig. 5.

The natural vibrations of the sample were excited by a small hammer. The latter performed a single stroke, which was controlled by a piezoceramic transducer mounted on the hammer.

Figure 6 presents examples of signal records after the stroke for a defect-free concrete brick and for a brick under the effect of a load causing the formation of microcracks. One can see that, in the brick with cracks, the increased losses lead to a faster damping of the excited vibrations.

The vibration excitation by a hammer stroke along the sample axis mainly resulted in the excitation of longitudinal vibrations. In the reconstruction of the TF for a concrete sample containing no defects, we obtained the peak corresponding to the lowest mode of longitudinal vibrations of the concrete brick (this mode is observed against the minimal noise level). As the sample was gradually destroyed, the peak was split, and the splitting increased with increasing load (Fig. 7).

Figure 8 shows this splitting as a function of the load applied to the sample. The breaking force in Fig. 7 is normalized in such a way that zero corresponds to the absence of load while unity, to the maximal value of the force beyond which the sample fracture takes place. The splitting of the peak is presumably related to the formation of cracks. The cracks were formed in the region of the maximal axial tension under the load (when the force was close to maximal, the cracking could be detected visually). Without discussing the mechanism of the splitting (it will be the subject of our subsequent studies), we note that the appearance of inhomogeneities inside the sample evidently leads to an increase in the number of eigenmodes (longitudinal or flexural), and one of the factors responsible for this effect is the elimination of the degeneracy related to the square cross section of the brick. Figure 9 shows the dependence of the *Q* factor of longitudinal vibrations

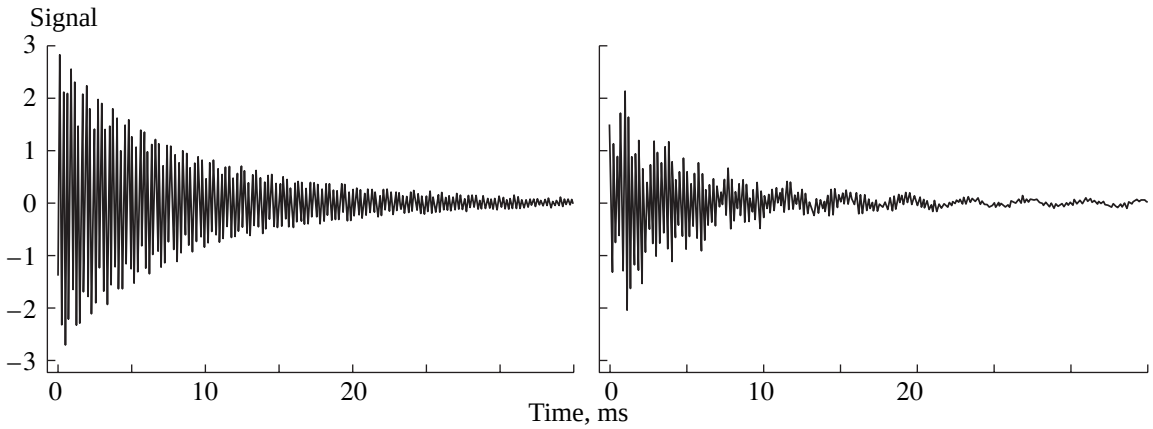

Fig. 6. Responses of concrete samples to a hammer stroke: the left plot refers to the defect-free sample and the right plot, to the sample immediately before fracture.

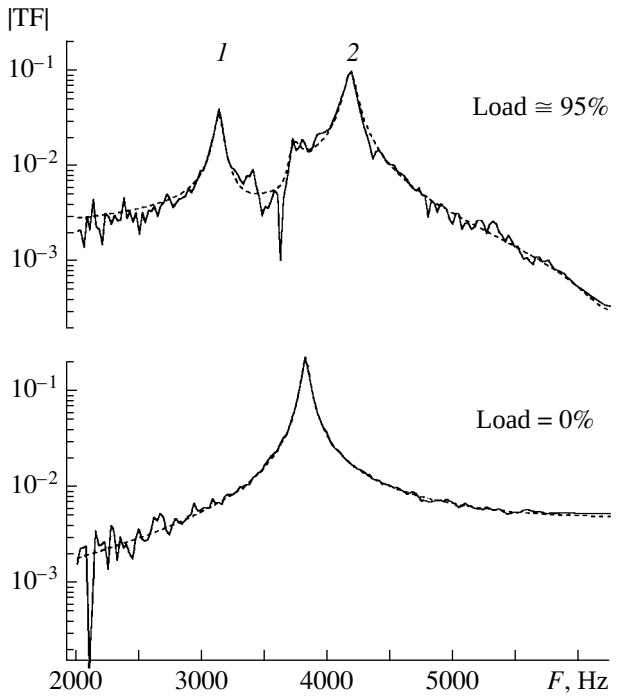

Fig. 7. Splitting of the peak under an increasing load; the peak corresponds to the longitudinal mode. The dashed lines show the result of the reconstruction of the frequency response by Eq. (1). (The peak numbers correspond to those in Fig. 8.)

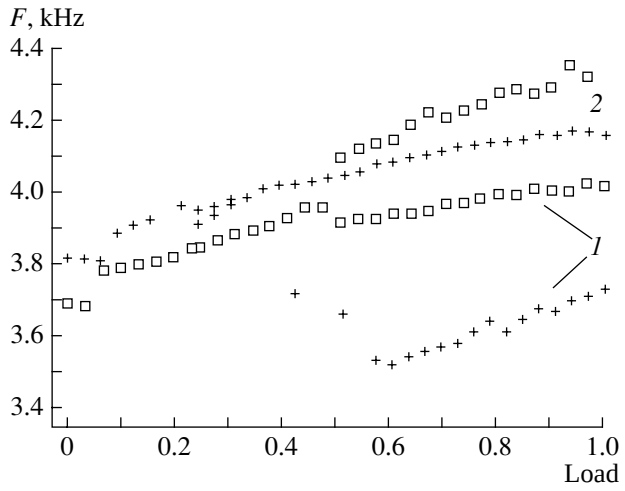

Fig. 8. Dependence of the resonance frequencies on the relative value of the breaking load for two peaks (*1* and *2*). The difference between samples 1 and 2 is determined by the difference in the material parameters of concrete of which they are made. The crosses (+) refer to sample 1 and the squares (□), to sample 2.

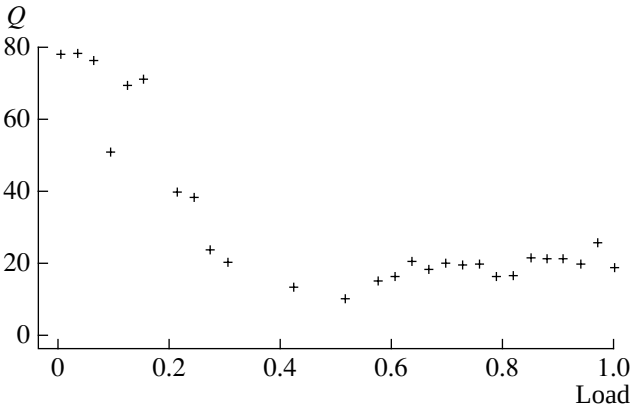

Fig. 9. Dependence of the *Q* factor of longitudinal vibrations on the relative value of the breaking load. The measurement error for the *Q* factor does not exceed 10.

(crosses in Fig. 8 and peak *1* in Fig. 7) on the breaking load. The data presented in Fig. 9 are obtained from the measurements on sample 1, which were performed with the highest accuracy. The data shown in Fig. 9 testify to the rapid decrease in the *Q* factor, starting from loads of about 10–20% of the ultimate load.

In the experiment, we observed a brittle fracture of concrete. It is expedient to compare our results with other data on the brittle fracture of solids. For example, polycrystalline rock, including granite, exhibits brittle fracture [21]. In [22], it was shown that, in granite, microcracks are formed at the initial stage of fracture, when the breaking force does not exceed 20% of the ultimate strength. With further load increase, small cracks coalesce, and the formation of new cracks slows down. Small cracks cause a dissipation increase [20]. As one can see from the data shown in Fig. 9, in our case, the maximal change in the *Q* factor is also observed at the initial stage of fracture (presumably, at the stage of microcrack formation). By contrast, the maximal splitting of the longitudinal and flexural modes is observed under loads of 20% or more (presumably, at the stage corresponding to the microcrack coalescence and the strongest violation of symmetry in the sample).

Thus, the method of matched-filter processing allows one to extend the area of application of resonant acoustic spectroscopy to the case of materials with low *Q* factors. It becomes possible to perform acoustic measurements of viscoelastic characteristics of structurally inhomogeneous media the vibrations of which are characterized by *Q* factors within 10–20. The above results of the experimental study of fracture processes can be considered as the first step in this direction.

ACKNOWLEDGMENTS

We remember with gratitude the numerous fruitful discussions with L.M. Lyamshev. These discussions, in particular, stimulated our interest in the subject studied in this paper.

This study was supported in part by the Interdepartmental Center for Science and Engineering (project no. 1369) and the Russian Foundation for Basic

Research (project nos. 00-05-64252 and 00-15-96741). We are grateful to the Los Alamos National Laboratory (USA) for the technical support of our measurements.

REFERENCES

1. A. Migliori and J. L. Sarrao, *Resonant Ultrasound Spectroscopy: Applications to Physics, Materials Measurements, and Nondestructive Evaluation* (Wiley, New York, 1997).
2. F. Birch, J. Geophys. Res. **80**, 756 (1975).
3. J. Maynard, Phys. Today **27**, 26 (1996).
4. W. P. Mason, K. J. Marfurt, D. N. Beshers, and J. T. Kuo, J. Acoust. Soc. Am. **62**, 1206 (1977).
5. A. Migliori, W. Visscher, S. Brown, *et al.*, Phys. Rev. B **41**, 2098 (1990).
6. G. Cannelli, R. Cantelli, F. Cordero, and F. Trequattrini, Phys. Rev. B **55**, 14865 (1997).
7. P. J. Kielczynski, A. Morean, and J. F. Bussiere, J. Acoust. Soc. Am. **95**, 813 (1994).
8. J. E. Vuorinen, R. B. Schwarz, and C. McCullough, J. Acoust. Soc. Am. **108**, 574 (2000).
9. K. Foster, S. L. Fairburn, R. G. Leisure, *et al.*, J. Acoust. Soc. Am. **105**, 2663 (1999).
10. D. G. Isaak, J. D. Carnes, O. L. Anderson, and H. Oda, J. Acoust. Soc. Am. **104**, 2200 (1998).
11. H. Ogi, M. Hirao, and T. Honda, J. Acoust. Soc. Am. **98**, 458 (1995).
12. P. Heyliger and H. Ledbetter, J. Nondestruct. Eval. **17** (2), 79 (1998).
13. S. H. D. Valdes and C. Soutis, J. Sound Vibr. **228** (1), 1 (1999).
14. H. Ogi, P. Heyliger, H. Ledbetter, and S. Kim, J. Acoust. Soc. Am. **108**, 2829 (2000).
15. T. Lee, R. S. Lakes, and A. Lal, Rev. Sci. Instrum. **71** (7), 2855 (2000).
16. A. V. Lebedev, Akust. Zh. **48**, 381 (2002) [Acoust. Phys. **48**, 339 (2002)].
17. A. V. Lebedev, V. V. Bredikhin, I. A. Soustova, *et al.*, Preprint No. 588, IPF RAN (Nizhni Novgorod Inst. of Applied Physics, Russian Academy of Sciences, 2002).
18. E. Skudrzyk, *Simple and Complex Vibratory Systems* (State U.P., State College, Pennsylvania, 1968).
19. D. W. Tafts and R. Kumaresan, IEEE Trans. **70**, 975 (1982).
20. J. E. White, *Underground Sound, Application of Seismic Waves* (Elsevier, New York, 1983).
21. W. F. Brace, B. W. Paulding, and C. H. Scholtz, J. Geophys. Res. **71**, 3939 (1966).
22. T. Yanagidani, S. Ehara, O. Nishizawa, *et al.*, J. Geophys. Res. **90** (B8), 6840 (1985).

Translated by E. Golyamina

Acoustical Physics, Vol. 49, No. 1, 2003, pp. 88–90. Translated from Akusticheskiĭ Zhurnal, Vol. 49, No. 1, 2003, pp. 100–103.

Sound Generation Due to the Interaction of Surface Waves

K. A. Naugolnikh[1, 2] and S. A. Rybak[2]

[1] *University of Colorado, Zeltech, USA*

[2] *Andreev Acoustics Institute, Russian Academy of Sciences, ul. Shvernika 4, Moscow, 117036 Russia*

e-mail: rybak@akin.ru

Received September 5, 2002

Abstract—Two opposite gravity-capillary waves of equal frequency give rise to the formation of a standing wave on the ocean surface and, thus, in the nonlinear approximation, generate a sound wave of twofold frequency with an amplitude proportional to the squared height of the surface wave [1]. This effect, being caused by the nonlinear interaction of opposite surface waves, can give rise to the radiation of sound waves in both ocean and atmosphere [2]. Opposite waves can appear in the ocean as a result of different ocean–atmosphere interactions and, in particular, as a result of the blocking of capillary waves on the slope of a gravity wave. © *2003 MAIK "Nauka/Interperiodica".*

L.M. Lyamshev contributed to research in acoustic hydrodynamic phenomena while he was interested in Aeolian tones, turbulent flow noise, and nonlinear sound generation. This paper deals with the latter problem. In the nonlinear approximation, a standing surface wave in the ocean is accompanied by the appearance of a continuous sound wave with a twofold frequency and an amplitude proportional to the squared height of the surface wave [1]. Being caused by the nonlinear interaction of opposite gravity-capillary waves, this effect gives rise to the generation of sound waves [2] that propagate both upwards, in the atmosphere, and downwards, in the ocean.

The interaction between the surface waves and the sound wave is best described in terms of a three-wave interaction [3]. Consider the interaction between the surface waves and sound that satisfy the conditions of synchronism:

$$\omega_1 + \omega_2 = \omega, \tag{1}$$

$$k_1 + k_2 = q_\rho, \tag{2}$$

where ω_i and k_i are the frequencies and the wave numbers of opposite gravity-capillary waves and ω and q_ρ are the frequency and the horizontal component of the wave number of sound. The flow of liquid caused by the surface waves can be considered as potential:

$$\Delta\varphi = 0, \tag{3}$$

where φ is the velocity potential. The boundary conditions on the free surface of the liquid are formulated as the equality of the vertical velocity component to the derivative of the velocity potential with respect to the vertical coordinate z (the kinematical boundary condition),

$$\frac{\partial\zeta}{\partial t} + \frac{\partial\zeta}{\partial x_i}\frac{\partial\varphi}{\partial x_i} = \frac{\partial\varphi}{\partial z}, \tag{4}$$

and the balance of pressures at the free surface of the liquid (the dynamic boundary condition),

$$\frac{\partial\varphi}{\partial t} + \frac{1}{2}(\nabla\varphi)^2 - gz + \gamma\Delta\zeta = 0. \tag{5}$$

Here, ζ is the elevation of the surface of liquid, $\gamma = \alpha/\rho$, α is the surface tension, and ρ is the density of the liquid. In the problem under consideration, the nonlinearity is mainly determined by the boundary conditions. Therefore, the propagation of sound can be described by the linear wave equation

$$\frac{\partial^2\varphi}{\partial t^2} - c^2\Delta\varphi = 0, \tag{6}$$

where c is the velocity of sound.

Indeed, the nonlinear terms in the equation for sound are smaller than the nonlinear terms in hydrodynamic equations by a factor equal to the ratio of the velocity of surface waves to the velocity of sound [3].

Let the vertical coordinate z increase in the upward direction and the plane $z = 0$ coincide with the free surface of the liquid. Then, gravity-capillary waves traveling along the x axis can be represented in the form

$$\varphi_{gi} = \varphi_i e^{ik_{ix}x - k_{iz}z - i\omega_i t}, \quad i = 1, 2. \tag{7}$$

We assume that the sound wave travels downwards in the vertical direction:

$$\varphi_s = \varphi_0 e^{iq_z z - i\omega t}, \quad q_z = \omega/c. \tag{8}$$

Consider the interaction of opposite surface waves ($k_1 + k_2 = 0$) and a sound wave traveling downwards ($q_\rho = 0$) under the condition that they satisfy synchronism condition (1) (see figure). If we substitute expressions (6) and (7) into Eqs. (3) and (4) and retain only bilinear terms, then, following [3], in the approximation of slowly varying amplitudes, we obtain

$$\frac{\partial \varphi_1}{\partial t} = -i2q_z k\varphi_0\varphi_2^+, \quad (9)$$

$$\frac{\partial \varphi_2}{\partial t} = -i2q_z k\varphi_0\varphi_1^+, \quad (10)$$

$$\varphi_0 = i4(k^2/\omega)\varphi_1\varphi_2. \quad (11)$$

As was shown in paper [4], the consideration of higher approximations makes no difference. Taking into account the relationship between the potential of the surface wave velocity and the surface displacement, $\varphi_i = (\omega/k)\zeta_i$, we obtain an expression for the amplitude of the sound wave produced by the interaction of opposite surface waves of amplitude ζ_a:

$$\left\|\frac{p_s}{p_g}\right\| = \left\|\frac{\varphi_0}{\varphi_1}\right\| = 4k\zeta_a. \quad (12)$$

This expression means that the ratio of pressure amplitudes of the sound and surface waves is proportional to the slope of the surface wave. The excess pressure caused by the elevation of the surface to a height ζ is $p_g = \rho g\zeta$, where g is the gravity acceleration. Then, assuming that $\zeta_a = 10^{-2}$ cm and $4k\zeta_a = 0.1$, we obtain $p_s \sim 10^{-1}$ Pa. Note that this estimate corresponds to the noise level experimentally measured in the ocean in the 10-Hz range [5]. The generation of sound by the broadband field of surface waves is described by the relationship derived by Brekhovskikh [2]:

$$P^2(\omega) = \frac{\pi\rho^2}{4c^2}\omega^2(5\omega^2 - kg)^2\Phi^2(\omega)\left(k\frac{dk}{d\omega}\right)^{-1}. \quad (13)$$

Here, $P(\omega)$ is the spectral density of pressure in the sound wave, ρ is the density of the liquid, and $\Phi(\omega)$ is the one-dimensional spectral density of wind waves. To obtain quantitative estimates, we will represent the angular spectrum of wind waves by the empirical expression suggested by Toba [6]:

$$S(k) = Bk^{-9/2}u_*, \quad (14)$$

where $B = 0.03/T^{0.5}$, $u_* = 0.04U^W$, and U^W is the wind speed. The corresponding frequency spectrum has the form

$$\Phi(\omega) = \frac{00.9}{\omega^{8/3}}u_*\gamma^{4/3}. \quad (15)$$

From this formula, for example, it follows that the spectral density $\Phi(\omega)$ measures 10^{-2} cm^2/s at a frequency of 10 Hz. Hence, the spectral density of the sound field generated by wind waves at frequencies of about 10 Hz measures $P(\omega) = 10^{-2}$ Pa Hz$^{-1/2}$, and the pressure amplitude in the 10-Hz frequency band measures $p_s = 10^{-1}$ Pa, which agrees with the experimental data on internal sea noise under moderate winds.

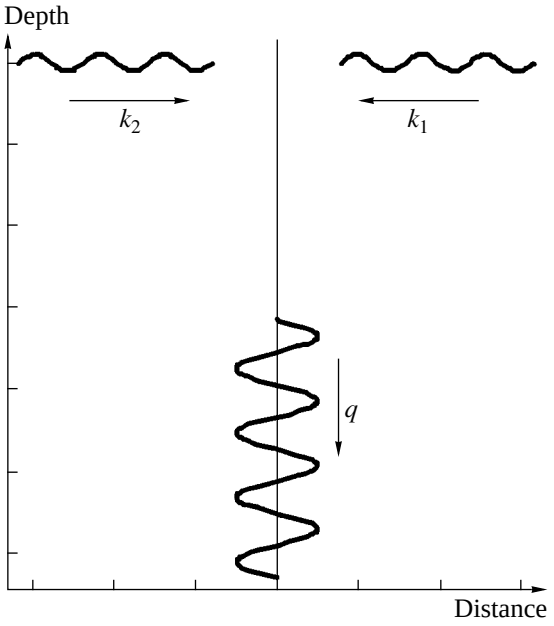

Opposite gravity-capillary waves with wave vectors k_1 and k_2 generate a sound wave with a wave vector q.

In this context, the question arises of what the conditions are under which opposite surface waves appear. It is clear that opposite waves appear under local disturbances of the ocean–atmosphere interface, such as cyclones. The disturbances produced on the sea surface by a cyclone traveling over it interact with the wind waves, and this interaction may result in the formation of standing waves. Long standing waves generate infrasound in the atmosphere and globally propagating microseisms in the ocean bottom. In particular, paper [7] presents data on the infrasonic disturbances generated by Pacific cyclones and detected at the Badar observatory (near Irkutsk), as well as on the corresponding microseisms received at the Petropavlovsk-Kamchatskiĭ seismic station.

The analysis of radar angular spectra argues, generally, for the complexity of the sea surface structure and, in particular, for the presence of waves traveling in the direction against the main wind waves [8]. The generation of gravity waves traveling against the wind was observed in the scattering of signals of high-frequency radars. It was assumed that this effect could be explained by the nonlinear interaction of gravity waves, which was described in terms of the radiation flux [9] or four-wave interaction [10]. Conversely, for capillary waves, a possible mechanism for the generation of opposite waves can be related to the effect of blocking.

An inhomogeneous flow caused by the orbital flow of liquid in a gravity wave affects the propagation of the capillary ripples on the slope of the gravity wave and causes their modulation and blocking. The capillary wave cannot traverse the zone where its group velocity becomes equal to the phase velocity of the carrier gravity wave (with allowance for the orbital velocity). Hence, a caustic is formed, and this caustic corresponds to the appearance of an opposite capillary wave. Mathematically, this effect can be explained using Lamb's problem on the disturbances caused by the action of pressure on the surface of a homogeneous flow of liquid moving with velocity U [11]. The action of pressure specified by the function $P\delta(x)$ causes disturbances on the surface of the flow, and these disturbances propagate in the form of two waves: a short wave in the direction against the flow and a long wave in the flow direction:

$$\begin{aligned} \varsigma(x) &= \frac{-2P}{\Delta^{1/2}}\begin{Bmatrix} \sin k_1 x, & x \le 0 \\ \sin k_2 x, & x \ge 0 \end{Bmatrix}, \\ \Delta &= U^4 - 4g\gamma, \\ k_1, k_2 &= \frac{1}{2\gamma}(U^2 \pm (U^4 - 4g\gamma)^{1/2}). \end{aligned} \tag{16}$$

Two cases can be distinguished: $\Delta \le 0$ and $\Delta \ge 0$ [11], which are arbitrarily called the resonance and out-of-resonance cases, respectively. In the resonance case, the wave number is real-valued, and a apropagating wave exists. In the out-of-resonance case, no real-valued solution exists. At $\Delta = 0$, the blocking conditions take place, and the expression for the disturbance diverges. A more accurate calculation procedure shows that the wave near the caustic is described by the Airy function and the above divergence disappears. In the ocean, an inhomogeneous flow appears, for example, on the slope of a gravity wave and blocks the capillary ripples traveling along the slope. At the blocking point, the long wave component arriving at the caustic is reflected and transformed into the short wave component. At the caustic, where $\Delta = 0$, we have $k_1 = -k_2 = k$, i.e., two opposite waves appear with wave numbers equal in magnitude but different in sign. The magnitude of the wave number k is determined from the blocking condition $\Delta = 0$. Using this condition, from Eq. (16) we obtain

$$k = \frac{U^2}{2\gamma}, \tag{17}$$

where $U = (4g\gamma)^{1/4}$.

Thus, we approximately have $k = 3.8$ cm^{-1}, which makes it possible to determine the frequency of the generated sound: it proves to be about 10^2 Hz. However, the condition $k_1 + k_2 = q_\rho = 0$ is satisfied only at the caustic and is violated when the distance from the caustic increases because of the increase in the difference between the wave numbers. The interaction of opposite waves with $q_\pi \ne 0$ results in the generation of a sound wave whose wave vector has the vertical component $q_z = \sqrt{\left(\frac{\omega}{c}\right)^2 - q_\rho^2}$. In the latter formula, ω is the frequency determined according to the synchronism condition (1) as the sum of frequencies of interacting opposite waves, and $q_\rho = k_1 + k_2$.

If $\omega/c \le q_\rho$ the vertical component of the wave vector q_z is imaginary and the sound wave becomes inhomogeneous. However, taking into account the fact that the generated sound wave frequency determined by the frequencies of the opposite surface waves is low, we can conclude that the inhomogeneous wavelength is long, measuring hundreds of meters in characteristic cases. For this reason, the long-wave inhomogeneous sound waves generated due to the blocking of surface waves can contribute to the noise of the surface layer of the ocean.

ACKNOWLEDGMENTS

This work was supported in part by the NATO Collaborative Linkage Grant EST.CLG.977.890, the Support Program for Scientific Schools (project no. 00-15-96678), and the Russian Foundation for Basic Research (project no. 02-02-17325).

REFERENCES

1. M. S. Longuet-Higgins, Philos. Trans. R. Soc. London, Ser. A **243**, 1 (1950).
2. L. M. Brekhovskikh, Sov. Phys. Acoust. **12**, 323 (1967).
3. V. V. Goncharov, K. A. Naugol'nykh, and S. A. Rybak, Izv. Akad. Nauk SSSR, Fiz. Atmos. Okeana, No. 4, 431 (1977).
4. A. C. Kibblewhite and C. Y. Wu, J. Acoust. Soc. Am. **85**, 1935 (1989).
5. C. Clay and H. Medwin, *Acoustical Oceanography* (Wiley, New York, 1977).
6. Y. Toba, J. Oceanogr. Soc. Jpn. **29**, 209 (1973).
7. V. N. Tabulevich, E. A. Ponomarev, A. G. Sorokin, and N. N. Drennova, Izv., Atmos. Ocean. Phys. **37**, 218 (2001).
8. R. H. Stewart and C. C. Teague, J. Phys. Oceanogr. **10**, 128 (1980).
9. D. D. Cromble, K. Hasselman, and W. Sell, Boundary-Layer Meteorol. **13**, 45 (1978).
10. K. I. Volyak, *Nonlinear Wave Processes* (Nauka, Moscow, 1989), pp. 72–110.
11. H. Lamb, *Hydrodynamics*, 6th ed. (Cambridge Univ. Press, Cambridge, 1932; Gostekhizdat, Moscow, 1947).

Translated by A. Vinogradov

Acoustical Physics, Vol. 49, No. 1, 2003, pp. 91–96. Translated from Akusticheskiĭ Zhurnal, Vol. 49, No. 1, 2003, pp. 104–109.

Acoustic Characteristics of a Multichannel Transmission Line of Longitudinal–Flexural Type

V. V. Tyutekin

Andreev Acoustics Institute, Russian Academy of Sciences, ul. Shvernika 4, 117036 Russia

e-mail: Tyutekin@akin.ru

Received August 20, 2002

Abstract—The properties of a multichannel transmission line of longitudinal–flexural type are considered. Analytical formulas are obtained for the principal acoustic characteristics of a symmetric multichannel transmission line, such as the input impedance matrix and the vectors of the reflection and transmission factors, in the case of an arbitrary number and arbitrary parameters of single lines with simultaneous longitudinal and flexural oscillations. *© 2003 MAIK "Nauka/Interperiodica".*

Dedicated to L.M. Lyamshev, with whom the author was lucky to collaborate for more than 50 years.

The problem of sound and vibration absorption and insulation remains topical from both theoretical and practical points of view. Along with the progress in the so-called active methods [1–6], the conventional methods of wave absorption and insulation also continue to be developed (see, e.g., [7]). One such method is described in [8, 9], which investigate the characteristics of new acoustic objects, namely, the so-called multichannel transmission lines (MTL), in the cases of purely longitudinal [8] and purely flexural [9] waves.

In the present paper, the MTL method is generalized to the case of longitudinal and flexural waves simultaneously propagating in such a line. As in [8, 9], the following acoustic characteristics of longitudinal–flexural MTL are calculated: the input impedance and the reflection and transmission factors of flexural waves.

We assume that a longitudinal–flexural MTL consists of a number of single transmission lines in the form of parallel flat bars (strips) that can perform both longitudinal and flexural vibrations at a frequency ω. Each line is characterized by the following parameters: l is its length (the same for all lines); $m_j = \rho_j h_j$ is the linear mass (it is assumed that the bar width is much smaller than the wavelength of the flexural wave); ρ_j is the density; h_j is the thickness; $G_j = \dfrac{E_j h_j^3}{12}$ and $g_j = E_j h_j$ are the flexural and longitudinal rigidities, respectively; E_j is Young's modulus; $j = -N$ to N is the bar number; and H_j is the distance between the jth bar and the "middle" plane of the MTL. It is assumed that the latter is a structure symmetric with respect to this plane; i.e., all the parameters of the jth bar coincide with the respective parameters of the $-j$th one. For example, $G_j = G_{-j}$, $\rho_j = \rho_{-j}$, etc. In addition, for convenience, we assume that $H_j = -H_{-j}$ and the middle planes of the bar corresponding to $j = 0$ and the MTL coincide.

The MTL model under consideration implies that the left ends of all lines ($x = 0$) are connected with each other, as well as the right ends ($x = l$) (Fig. 1a), by weightless perfectly rigid plates that can shift and rotate as a whole with respect to the middle plane, so that the transverse displacements w_j and the rotations w_j' of each end are the same for all the lines.

According to the chosen model, we believe that the transverse displacements w_j and the longitudinal ones u_j in each of the single lines satisfy the equations for the flexural and longitudinal vibrations of a bar, respectively:

$$\frac{d^4 w_j}{dx^4} - k_j^4 w_j = 0, \tag{1}$$

$$\frac{d^2 u_j}{dx^2} + k_{1j} u_j = 0. \tag{2}$$

In Eqs. (1) and (2), $k_j^4 = \dfrac{m_j \omega^2}{G_j}$, $k_{1j}^2 = \dfrac{m_j \omega^2}{g_j}$, and k_j and k_{1j} are the wave numbers of longitudinal and flexural waves in the jth line.

The general solutions to Eqs. (1), (2) can be taken as

$$w_j = a_j \cos k_j x + b_j \cosh k_j x + c_j \sin k_j x + d_j \sinh k_j x, \tag{3}$$

$$u_j = A_j \cos k_{1j} x + B_j \sin k_{1j} x. \tag{4}$$

1063-7710/03/4901-0091$24.00 © 2003 MAIK "Nauka/Interperiodica"

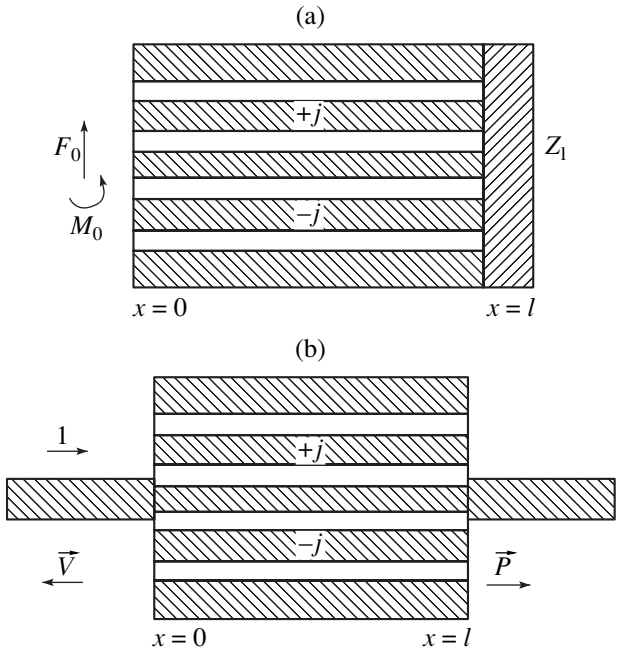

Fig. 1. Illustration of the derivation of equations for the acoustic characteristics of the longitudinal–flexural MTL.

The boundary conditions can be written as

$$w_j(0, l) = w_{0, l}, \tag{5}$$

$$w_j'(0, l) = w_{0, l}', \tag{6}$$

$$\sum_{j=-N}^{N} F_j(0, l) + F_{0, l} = 0, \tag{7}$$

$$\sum_{j=-N}^{N} [M_j(0, l) + M_{1l}(0, l)] + M_{0, l} = 0, \tag{8}$$

$$u_j(0, l) = H_j w_{0, l}', \tag{9}$$

$$M_{1, j}(0, l) = H_j N_j(0, l). \tag{10}$$

Here, $w_{0, l}$ and $w_{0, l}'$ are unknown displacements and rotations at $x = 0$ and $x = l$; F_j and M_j are cutting forces and bending moments, respectively; N_j are longitudinal forces; M_{1j} are "additional" moments emerging due to the longitudinal forces; and $F_{0, l}$ and $M_{0, l}$ are predetermined transverse forces and rotational moments applied to the connecting plates. Equations (5)–(7) correspond to the flexural vibrations, while Eqs. (8)–(10) refer to the longitudinal ones.

The quantities F_j, M_j, and N_j are expressed through the generalized displacements by the well-known formulas

$$F_j = -G_j \frac{d^3 w_j}{dx^3}, \quad M_j = -G_j \frac{d^2 w_j}{dx^2}, \quad N_j = -g_j \frac{du_j}{dx}. \tag{11}$$

We introduce the relative forces

$$f_j = \frac{F_j}{G_j k_j^3}, \quad m_j = \frac{M_j}{G_j k_j^2}, \quad n_j = \frac{N_j}{g_j k_{1j}}. \tag{12}$$

Using solutions (3) and (4) along with formulas (11) and (12), we can express the unknown constants through the values of functions at the point $x = 0$:

$$a_j = \frac{1}{2}\left[\frac{w_j'(0)}{k_j} - f_j(0)\right], \quad b_j = \frac{1}{2}\left[\frac{w_j'(0)}{k_j} + f_j(0)\right],$$

$$c_j = \frac{1}{2}[w_j(0) - m_j(0)], \quad d_j = \frac{1}{2}[w_j(0) + m_j(0)],$$

$$A_j = -n_j(0), \quad B_j = u_j(0).$$

Substituting these values into Eqs. (3), (4), and (12) at $x = l$, and introducing the vector of generalized forces and displacements for each end of a single line

$$\vec{Q}_j(0, l) = [m_j(0, l), f_j(0, l)]^T,$$

$$\vec{U}_j(0, l) = \left[w_j(0, l), \frac{w_j'(0, l)}{k_j}\right]^T,$$

we obtain a system of equations for the flexural component of oscillations:

$$2\vec{U}_j(l) = P_j \vec{U}_j(0) + R_j \vec{Q}_j(0), \tag{13}$$

$$2\vec{Q}_j(l) = R_j \vec{U}_j(0) + P_j \vec{Q}_j(0). \tag{14}$$

Here, P_j and R_j are 2×2 matrices of the form

$$P_j = \begin{pmatrix} C_j^+ & S_j^+ \\ S_j^- & C_j^+ \end{pmatrix}, \quad R_j = \begin{pmatrix} C_j^- & S_j^- \\ S_j^+ & C_j^- \end{pmatrix},$$

whose constituent functions are

$$C_j^{\pm} = \cosh\varphi_j \pm \cos\varphi_j, \quad S_j^{\pm} = \sinh\varphi_j \pm \sin\varphi_j,$$
$$\varphi_j = k_j l.$$

For the longitudinal component, we similarly obtain

$$n_j(0) = \frac{u_j(l)}{\sin\varphi_{1j}} - u_j(0)\cot\varphi_{1j},$$
$$n_j(l) = u_j(l)\cot\varphi_{1j} - \frac{u_j(0)}{\sin\varphi_{1j}}, \quad \varphi_{1j} = k_{1j} l. \tag{15}$$

It is the latter equations that were used in the previous paper [8] to obtain its main results. Using boundary conditions (5), (6), and (9), we represent formulas (13)–(15) as

$$2\vec{U}_j(l) = R_j \vec{U}_0 + P_j \vec{Q}_j(0), \tag{16}$$

$$2\vec{Q}_j(l) = R_j \vec{U}_0 + P_j \vec{Q}_j(0), \tag{17}$$

$$n_j(0) = H_j\left(\frac{w_l'}{\sin\varphi_{1j}} - w_0'\cot\varphi_{1j}\right),$$
$$n_j(l) = H_j\left(w_l'\cot\varphi_{1j} - \frac{w_0'}{\sin\varphi_{1j}}\right). \quad (18)$$

Here, $\vec{U}_0 = \left(w_0, \frac{w_0'}{k_j}\right)^T$ and $\vec{U}_l = \left(w_l, \frac{w_l'}{k_j}\right)^T$.

To be able to apply boundary conditions (7) and (8), we should obtain $\vec{Q}_j(0)$ and $\vec{Q}_j(l)$ from Eqs. (16) and (17) as explicit functions of $\vec{U}_0$ and $\vec{U}_l$. To make further transformations easier, it is expedient to return to the element-by-element representation of vectors. From Eqs. (16) and (17), after some (simple, but time consuming) transformations with matrix multiplication we obtain:

$$m_j(0) = \left(-p_j w_0 - T_j^- \frac{w_0'}{k_j} + C_j^- w_l - S_j^- \frac{w_l'}{k_j}\right)\Delta_j^{-1}, \quad (19)$$

$$f_j(0) = \left(T_j^+ w_0 + p_j \frac{w_0'}{k_j} - S_j^+ w_l + C_j^- \frac{w_l'}{k_j}\right)\Delta_j^{-1}, \quad (20)$$

$$m_j(l) = \left(C_j^- w_0 + S_j^- \frac{w_0'}{k_j} - p_j w_l + T_j^- \frac{w_l'}{k_j}\right)\Delta_j^{-1}, \quad (21)$$

$$f_j(l) = \left(S_j^+ w_0 + C_j^- \frac{w_0'}{k_j} - T_j^+ w_l + p_j \frac{w_l'}{k_j}\right)\Delta_j^{-1}. \quad (22)$$

The latter formulas contain some additional constants:

$$p_j = \sinh\varphi_j \sin\varphi_j,$$
$$T_j^{\pm} = \sin\varphi_j \cosh\varphi_j \pm \cos\varphi_j \sinh\varphi_j,$$
$$\Delta_j = 1 - \cos\varphi_j \cosh\varphi_j.$$

For the sake of convenience, we introduce the parameters G^0, k^0 and g^0, k_1^0 of a certain "comparison" line along with the dimensionless quantities

$$\Psi_j = \frac{G_j}{G^0}, \quad \xi_j = \frac{k_j}{k^0}, \quad \Psi_{1j} = \frac{g_j}{G^0}, \quad \xi_{1j} = \frac{k_{1j}}{k^0}. \quad (23)$$

With allowance for Eq. (23), the expressions for the renormalized generalized forces can be transformed into

$$m_j(0) = \frac{\Psi_j \xi_j^2}{\Delta_j}\left(-p_j w_0 - T_j^- \xi_j^{-1}\frac{w_0'}{k^0} + C_j^- w_l - S_j^- \xi_j^{-1}\frac{w_l'}{k^0}\right), \quad (24)$$

$$f_j(0) = \frac{\Psi_j \xi_j^3}{\Delta_j}\left(T_j^+ w_0 + p_j \xi_j^{-1}\frac{w_0'}{k^0} - S_j^+ w_l + C_j^- \xi_j^{-1}\frac{w_l'}{k^0}\right), \quad (25)$$

$$m_j(l) = \frac{\Psi_j \xi_j^2}{\Delta_j}\left(C_j^- w_0 + S_j^- \xi_j^{-1}\frac{w_0'}{k^0} - p_j w_l + T_j^- \xi_j^{-1}\frac{w_l'}{k^0}\right), \quad (26)$$

$$f_j(l) = \frac{\Psi_j \xi_j^3}{\Delta_j}\left(S_j^+ w_0 + C_j^- \xi_j^{-1}\frac{w_0'}{k^0} - T_j^+ w_l + p_j \xi_j^{-1}\frac{w_l'}{k^0}\right), \quad (27)$$

$$m_{1j}(0) = \Psi_{1j}\xi_{1j} H_j^2\left(\frac{w_l'}{k^0}\frac{1}{\sin\varphi_{1j}} - \frac{w_0'}{k^0}\cot\varphi_{1j}\right), \quad (28)$$

$$m_{1j}(l) = \Psi_{1j}\xi_{1j} H_j^2\left(\frac{w_l'}{k^0}\cot\varphi_{1j} - \frac{w_0'}{k^0}\frac{1}{\sin\varphi_{1j}}\right). \quad (29)$$

Without considering the longitudinal components, we can write the desired quantities by introducing the impedance matrices

$$\vec{Q}(0) = Z^{00}\vec{U}_0 + Z^{0l}\vec{U}_l, \quad (30)$$

$$\vec{Q}(l) = Z^{l0}\vec{U}_0 + Z^{ll}\vec{U}_l. \quad (31)$$

Here, $\vec{U}_0 = \left(w_0, \frac{w_0'}{k^0}\right)^T$, $\vec{U}_l = \left(w_l, \frac{w_l'}{k^0}\right)^T$, and the 2×2 matrices Z^{ik} have the elements

$$Z_{11}^{00} = -Z_{22}^{00} = Z_{11}^{ll} = -Z_{22}^{ll} = -\sum_{j=-N}^{N}\frac{\Psi_j \xi_j^2}{\Delta_j} p_j;$$

$$Z_{12}^{00} = -Z_{12}^{ll} = -\sum_{j=-N}^{N}\frac{\Psi_j \xi_j}{\Delta_j} T_j^-;$$

$$Z_{21}^{00} = -Z_{21}^{ll} = -\sum_{j=-N}^{N}\frac{\Psi_j \xi_j^3}{\Delta_j} T_j^+;$$

$$Z_{11}^{0l} = Z_{22}^{0l} = Z_{11}^{l0} = Z_{22}^{l0} = \sum_{j=-N}^{N}\frac{\Psi_j \xi_j^2}{\Delta_j} C_j^-;$$

$$Z_{12}^{0l} = Z_{12}^{l0} = -\sum_{j=-N}^{N}\frac{\Psi_j \xi_j}{\Delta_j} S_j^-;$$

$$Z_{21}^{0l} = Z_{21}^{l0} = -\sum_{j=-N}^{N}\frac{\Psi_j \xi_j^3}{\Delta_j} S_j^+.$$

One can see from these formulas that flexural vibrations of the MTL are described by six independent matrix elements. To take into account the longitudinal vibrations, the matrix elements corresponding to the effect of longitudinal forces should be added. Since the latter affect only the moment component of the generalized forces and only through the "rotational" component of the generalized displacements, the additional moments can be represented as

$$m_1(0) = z_{12}^{00}\frac{w_0'}{k^0} + z_{12}^{0l}\frac{w_l'}{k^0}; \quad m_1(l) = z_{12}^{l0}\frac{w_0'}{k^0} + z_{12}^{ll}\frac{w_l'}{k^0}.$$

Here, the matrix elements, on the basis of Eqs. (28) and (29), have the form

$$z_{12}^{00} = -z_{12}^{ll} = \sum_{j=-N}^{N} \Psi_{1j}\xi_{1j}H_j^2\cot\varphi_{1j};$$

$$z_{12}^{0l} = -z_{12}^{l0} = \sum_{j=-N}^{N} \frac{\Psi_{1j}\xi_{1j}}{\sin\varphi_{1j}}H_j^2.$$

These elements should be added to the respective matrix elements of flexural impedances. In this case, Eqs. (30) and (31) can be rewritten as

$$\vec{Q}(0) = Z_{00}\vec{U}_0 + Z_{0l}\vec{U}_l, \tag{30a}$$

$$\vec{Q}(l) = Z_{l0}\vec{U}_0 + Z_{ll}\vec{U}_l. \tag{31a}$$

Here, the renamed impedances Z_{ik} take into account both flexural and longitudinal components and can be represented in the form

$$Z_{ll} = \begin{pmatrix} Z_{11}^{00} & -(Z_{12}^{00} + z_{12}^{00}) \\ -Z_{21}^{00} & -Z_{11}^{00} \end{pmatrix};$$

$$Z_{l0} = \begin{pmatrix} Z_{11}^{0l} & Z_{12}^{0l} - z_{12}^{0l} \\ -Z_{21}^{0l} & Z_{11}^{0l} \end{pmatrix}; \tag{32}$$

$$Z_{00} = \begin{pmatrix} Z_{11}^{00} & Z_{12}^{00} + z_{12}^{00} \\ Z_{21}^{00} & -Z_{11}^{00} \end{pmatrix}; \quad Z_{0l} = \begin{pmatrix} Z_{11}^{0l} & Z_{12}^{0l} + z_{12}^{0l} \\ Z_{21}^{0l} & Z_{11}^{0l} \end{pmatrix}.$$

From Eqs. (30a) and (31a), one can easily obtain the input impedance matrix of the MTL. For this purpose, we represent the generalized forces as

$$\vec{Q}(0) = Z_{\text{in}}\vec{U}_0; \quad \vec{Q}(l) = Z_{\text{l}}\vec{U}_l. \tag{33}$$

Here Z_{in} and Z_{l} are the input impedance matrix and the loading matrix, respectively. Substituting Eq. (33) into Eqs. (30a) and (31a), we obtain

$$(Z_{00} - Z_{\text{in}})\vec{U}_0 + Z_{0l}\vec{U}_l = 0, \tag{34}$$

$$Z_{l0}\vec{U}_0 + (Z_{ll} - Z_{\text{l}})\vec{U}_l = 0. \tag{35}$$

Eliminating the arbitrary vector $\vec{U}_0$ (or $\vec{U}_l$) from Eqs. (34) and (35), we obtain the mutual relations between the matrices Z_{in} and Z_{l}:

$$Z_{\text{in}} = Z_{00} - Z_{0l}(Z_{ll} - Z_{\text{l}})^{-1}Z_{l0}, \tag{36}$$

$$Z_{\text{l}} = Z_{ll} - Z_{l0}(Z_{00} - Z_{\text{in}})^{-1}Z_{0l}. \tag{37}$$

From formulas (36) and (37), we obtain such acoustic characteristics of the MTL as the reflection and transmission factors of flexural waves. The model used for calculation is presented in Fig. 1b. A single transmission line is connected to the MTL on the left and right. To describe its parameters, we use the quantities G^0 and k^0 introduced earlier. (Structurally, this line can pass through the multichannel line so as to represent the line with the number j =0.) A harmonic wave of unit amplitude propagates along this line from left to right:

$$w = \exp(ik^0x).$$

This wave generates two reflected waves, one being uniform and the other nonuniform with its amplitude decreasing with $x \longrightarrow -\infty$:

$$w_1 = R\exp(-ik^0x) + E\exp(k^0x).$$

Upon propagation through the MTL, similar waves emerge at its output:

$$w_2 = D\exp(ik^0(x-l)) + F\exp(-k^0(x-l)). \tag{38}$$

Here, R and D are the desired reflection and transmission factors of the flexural wave.

Using the above notation, we can write the components of the generalized displacement at $x = 0$ as

$$w_0 = 1 + R + E; \quad \frac{w_0'}{k^0} = i - iR + E.$$

Similarly, the components of the generalized force are

$$\frac{M_0}{G^0(k^0)^2} = m_0 = 1 + R + E,$$

$$\frac{F_0}{G^0(k^0)^3} = f_0 = i - iR - E.$$

Introducing the vectors

$$\vec{U}_0 = \left(w_0, \frac{w_0'}{k^0}\right)^T, \quad \vec{Q}_0 = (m_0, f_0)^T,$$

$$\vec{V} = (R, E)^T, \quad \text{and} \quad \vec{A}_0 = (1, i)^T,$$

the above relations can be written in matrix form:

$$\vec{U}_0 = S_1\vec{V} + \vec{A}_0, \quad \vec{Q}_0 = S_2\vec{V} + \vec{A}_0. \tag{39}$$

Here, the matrices S_1 and S_2 are

$$S_1 = \begin{pmatrix} 1 & 1 \\ -i & 1 \end{pmatrix}, \quad S_2 = \begin{pmatrix} 1 & -1 \\ -i & -1 \end{pmatrix}.$$

Let us introduce, as above, the input impedance matrix, which now will be related to the incident and reflected waves:

$$\vec{Q}_0 = -Z_{\text{in}}^0\vec{U}_0. \tag{40}$$

Substituting Eq. (40) into Eq. (39) and eliminating $\vec{U}_0$, we obtain the vector of the reflection factors

$$\vec{V} = -(Z_{\text{in}}^0 S_1 + S_2)^{-1}(I + Z_{\text{in}}^0)\vec{A}_0. \tag{41}$$

In Eq. (41), I is the unitary matrix.

Since from Eqs. (7) and (8) it follows that

$$Z_{\text{in}} = -Z_{\text{in}}^0,$$

the final formula for the vector of the reflection factors of the MTL takes the form

$$\vec{V} = (Z_{\text{in}}S_1 - S_2)^{-1}(I - Z_{\text{in}})\vec{A}_0\,. \tag{42}$$

The quantity Z_l involved in Eq. (36) for Z_{in} will be defined below.

In a similar way, we can find the vector of the transmission factors of the MTL. Starting from formula (38) for the transmitted waves, we find

$$w_l = D + F; \quad \frac{w_1'}{k^0} = iD - F;$$

$$\frac{M_l}{G^0(k^0)^2} = m_l = D - F, \quad \frac{F_l}{G^0(k^0)^3} = f_l = iD + F\,.$$

Introducing, as above, the vectors

$$\vec{U}_l = \left(w_l, \frac{w_l'}{k^0}\right)^T, \quad \vec{Q}_1 = (m_l, f_l)^T, \quad \vec{P} = (D, F)^T,$$

we can write the expressions

$$\vec{U}_l = q_1\vec{P}; \quad \vec{Q}_l = q_2\vec{P};$$

where the matrices q_1 and q_2 have the form

$$q_1 = \begin{pmatrix} 1 & 1 \\ i & -1 \end{pmatrix}, \quad q_2 = \begin{pmatrix} 1 & -1 \\ i & 1 \end{pmatrix}.$$

Writing the obvious chain of equalities

$$\vec{Q}_l = Z_l\vec{U}_l = Z_l q_1\vec{P} = q_2\vec{P},$$

for Z_l, we obtain

$$Z_l = q_2 q_1^{-1}. \tag{43}$$

We can determine the vector $\vec{P}$ of the transmission factors of a flexural wave by Eq. (34) [or (35)], which can be rewritten as

$$\vec{U}_l = Z_{0l}^{-1}(Z_{\text{in}} - Z_{00})\vec{U}_0. \tag{44}$$

Substituting the expressions for $\vec{U}_l$ and $\vec{U}_0$ from the above formulas, we obtain a formula for the desired vector, which is expressed through the quantities defined earlier:

$$\vec{P} = q_1^{-1}Z_{0l}^{-1}(Z_{\text{in}} - Z_{00})(S_1\vec{V} + \vec{A}_0)\,. \tag{45}$$

Note that since, according to Eq. (41), vector $\vec{V}$ is proportional to vector $\vec{A}_0$, vector $\vec{P}$ is also proportional to it.

Thus, the principal acoustic characteristics of the MTL of the flexural–longitudinal type are obtained: the input impedance, along with the reflection and transmission factors, in the case of its excitation by a flexural wave propagating along the single line connected to the MTL in its middle plane, which is its plane of symmetry. Note that the symmetric structure and the way of connection described do not lead to the appearance of longitudinal waves in the reflected and transmitted fields. Similarly, when a longitudinal wave is incident on the MTL, no flexural waves appear. In this case, the situation is completely described in the previous paper [8], and its results can be used in solving the latter problem.

REFERENCES

1. V. V. Tyutekin, Akust. Zh. **43**, 238 (1997) [Acoust. Phys. **43**, 202 (1997)].

2. A. I. Boĭko and V. V. Tyutekin, Akust. Zh. **45**, 454 (1999) [Acoust. Phys. **45**, 402 (1999)].
3. J. Guo, J. Pan, and C. Bao, J. Acoust. Soc. Am. **101**, 1492 (1997).
4. K. Wicker and E. Arens, Acustica (Suppl. 1) **85**, S47 (1999).
5. C. R. Fuller and P. E. Cambou, Acustica (Suppl. 1) **85**, S102 (1999).
6. E. V. Korotaev and V. V. Tyutekin, Akust. Zh. **46**, 84 (2000) [Acoust. Phys. **46**, 71 (2000)].
7. *Acoustics Handbook*, Ed. by Malcolm J. Crocker (Wiley, New York, 1997).
8. V. V. Tyutekin, Akust. Zh. **46**, 809 (2000) [Acoust. Phys. **46**, 710 (2000)].
9. V. V. Tyutekin, Akust. Zh. **47**, 706 (2001) [Acoust. Phys. **47**, 618 (2001)].

Translated by A. Kruglov

Acoustical Physics, Vol. 49, No. 1, 2003, pp. 97–108. Translated from Akusticheskiĭ Zhurnal, Vol. 49, No. 1, 2003, pp. 110–122.

Sequences from Number Theory for Physics, Signal Processing, and Art[1, 2]

Manfred R. Schroeder

Drittes Physikalisches Institut, University of Göttingen, Germany, and AT&T Bell Laboratories (ret.), USA

Received August 27, 2002

Abstract—In this article I discuss numerical sequences of potential interest to physicists, engineers, and artists. Foremost among these are the maximum-length or "Galois" sequences, based on the prime number 2 and larger primes, which have found wide use in physics, including acoustics, and engineering:

—the measurement of impulse responses in concert halls, radar echoes from planets (to check the General Theory of Relativity), and travel times in the deep-ocean sound channel (to monitor water temperature and global warming);

—the spatial diffusion of sound waves, coherent (laser) light, and electromagnetic waves;

—algebraic error-correcting codes (Simplex and Hamming codes);

—minimizing peak-factors for radar and sonar signals, synthetic speech, and computer music;

—the formation of X-ray images with 2D masks (in X-ray astronomy).

Other sequences include

—quadratic-residue sequences for the construction of wide-band diffusing reflection-phase-gratings in one and two dimensions;

—the Morse–Thue sequence, the Fibonacci and "rabbit" sequences and their musical potential; and

—certain self-similar sequences from number theory that engender attractive visual patterns, rhythms, and melodies.

INTRODUCTION

Number theory has been considered since time immemorial to be the very paradigm of pure—some would say useless—mathematics. Number theory is the queen of mathematics, according to Carl Friedrich Gauss, the lifelong wunderkind of arithmetic. What could be more beautiful than a deep satisfying relationship between whole numbers. (One is almost tempted to call them wholesome numbers.) In fact, it is hard to come up with a more appropriate designation than their learned name: integers—meaning the "untouched ones." How high they rank in the realm of pure thought and aesthetics above their lesser brethren, real and complex numbers.

Yet, as we shall see here, number theory can provide totally unexpected answers to real-world problems. Specifically, I will focus on the application of sequences of numbers that have found wide use in concert hall acoustics, deep ocean monitoring of global warming, precise radar ranging of interplanetary distances for checking Einstein's Theory of General Relativity, error-correcting codes for the Internet, X-ray astronomy, speech synthesis, and the creation of musical rhythms and melodies.

GALOIS FIELDS

A pure, continuous sine wave has a power spectrum with a single frequency component, but its envelope is constant in time. By contrast, a sharp impulse has a power spectrum with many frequencies, but of course its envelope is limited to a short-time interval. Thus, for a given maximum amplitude, the sharp pulse does not pack much energy. Are there waveforms that contain many frequencies, i.e., broadband signals whose energy is more evenly distributed in time, allowing higher energies to be transmitted (by an active long-range radar or sonar, for example)? This is one of the most fundamental and pervasive questions in modern signal design. The answer to this question is a resounding "yes." In fact, there exist periodic broadband signals whose discrete spectral frequency components have constant magnitude and whose amplitudes in time also have constant magnitude, say ±1. This sounds almost to good to be true. But a little number theory shows that this can indeed be accomplished.

The branch of number theory that guarantees this astounding result is called finite-field theory. (In languages other than English, the word *field* is often replaced by a word derived from the Latin word *corpus*

[1] The article is based on the author's *Number Theory in Science and Communication*, 3rd ed. (Springer 1997).

[2] The article was submitted at the request of L.M. Lyamshev after he got acquainted with this work by the author of the well-known book on fractals and saw a relation to acoustics. The article was submitted by the author in English.

1063-7710/03/4901-0097$24.00 © 2003 MAIK "Nauka/Interperiodica"

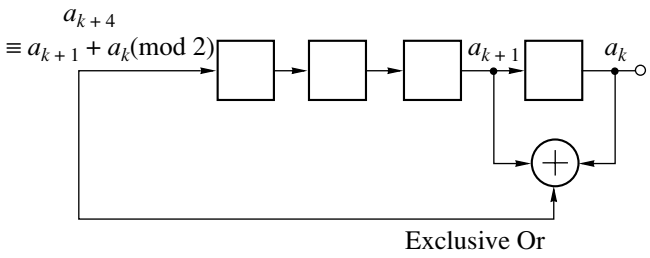

Fig. 1. Four-stage linear shift register with feedback connection using an "exclusive or" gate.

(body), as in the German *Zahlkörper*.) Finite fields, also called Galois fields, abbreviated GF, (after the French mathematician Evariste Galois (1811–1832)) that are of interest here are based on prime numbers p and their powers p^m. A finite field based on the prime number 5, for example, has 5 elements: 0, 1, 2, 3, 4, and all arithmetic operations are performed modulo 5; i.e., only the remainders modulo 5 are considered. Thus, 3 + 4 does not equal 7, as in ordinary arithmetic, but 3 + 4 equals 2, the remainder when 7 is divided by 5. Similarly, for multiplication, 2×4 equals 3 modulo 5 and, for division, 2/4 also equals 3 (because 4×3 equals 2 modulo 5). Here is a list of reciprocals in GF(5): $\frac{1}{2} = 3$, $\frac{1}{3} = 2$, $\frac{1}{4} = 4$.

Finite fields based on prime powers p^m are usually represented by "vectors" in m dimensions, each vector component being one of the elements $0, \ldots, p-1$. Thus, the finite field GF(2^2) consists of the following two-dimensional binary vectors: 00, 01, 10, 11. Addition proceeds place by place (without carries) modulo p. Thus, for example, 01 + 11 = 10.

For purposes of multiplication, the vectors are represented by polynomials. Thus, the polynomial $x + 1$ corresponds to the vector 10, etc. To multiply two vectors, their polynomials are multiplied modulo a primitive polynomial, which thus plays the role of a prime number. For GF(2^2), a primitive polynomial is $x^2 + x + 1$. Setting it equal to zero ($x^2 + x + 1 = 0$ or $x^2 = x + 1$) means identifying x^2 with $x + 1$.

Thus, for example, 10×1 written as a product of two polynomials becomes $x(x + 1) = x^2 + x = x + 1 + x = 2x + 1 = 1$ (note that 2 = 0, and –1 = +1, in fields based on the prime number 2). The "polynomial" 1 corresponds to the vector 01. Therefore, finally, $10 \times 11 = 01$. This looks funny, but it's true and consistent!

GALOIS SEQUENCES

The primary use of primitive polynomials in finite fields GF(p^m) is the generation of Galois sequences, also known as maximum-length sequences, i.e., periodic sequences with period length $p^m - 1$ such that their DFT (discrete Fourier transform) has constant magnitude (is "flat") while—in the case of $p = 2$—the amplitude values of the sequences are restricted to the two values {0, 1} or, after a simple transformation, {+1, –1} [1].

Let us study the generation of a Galois sequence and its properties for the case of $p = 2$ and $m = 3$, i.e., GF(2^3). A primitive polynomial for GF(2^3) is $p(x) = x^3 + x + 1$. Next let us look at the reciprocal of $p(x)$, because the preferred method of generating Galois sequences, namely by linear recursion, corresponds to taking reciprocals:

$$\frac{1}{p(x)} = (x^4 + x^2 + x + 1)(1 + x^7 + x^{14} + \ldots).$$

Written as a binary sequence, the first factor is 0010111. (Note that in GF(2^3) vectors have $2^3 - 1 = 7$ dimensions. Hence the two 0s to the left of 10111, reflecting the fact that the terms x^5 and x^6 in the first factor are missing, i.e., have zero coefficients.) The second factor $(1 + x^7 + x^{14} + \ldots)$ means that the sequence 0010111 is repeated periodically with a period length of 7:

$$a_k = 0010111, 0010111, 001\ldots. \quad (1)$$

Note that the a_k obey the following recursion:

$$a_{k+3} = a_{k+1} + a_k, \quad (2)$$

which stems directly from the "generating" polynomial $p(x)$ set equal to zero:

$$x^3 + x + 1 = 0$$

or

$$x^3 = x + 1$$

(note again that –1 equals +1 for $p = 2$).

The recursion formula (2) for the Galois sequence (1) leads directly to its electronic realization by a shift register with linear feedback (see Fig. 1). Galois sequences are therefore also called "shift-register sequences" [2].

For generating the Galois sequence by computer program, we start with some initial conditions (not all 0), say 001, and then generate the next term by adding (modulo 2) the two leftmost terms (0 0), resulting in

0 0 1 0.

Next, we add the next two left terms (0 1), giving

0 0 1 0 1.

By repeating this process of adding (modulo 2) successive pairs of terms, we get

0 0 1 0 1 1
0 0 1 0 1 1 1
0 0 1 0 1 1 1 0
0 0 1 0 1 1 1 0 0
0 0 1 0 1 1 1 0 0 1,
etc.

The resulting sequence repeats after $2^3 - 1 = 7$ steps, as it must: a three-stage shift register can at most hold $2^3 = 8$ different binary triplets, all of which, except the {0, 0, 0} triplet, occur exactly once (if $p(x)$ is primitive!). As a consequence, the number of 1s per period equals 2^{m-1} or, for $m = 3, 4$. (The number of 0s equals $2^{m-1} - 1$ or 3.)

Instead of the {0, 1} alphabet, the {+1, –1} alphabet is preferred in many applications. Thus, instead of generating a pulse (1) or no pulse (0), a positive pulse (+1) or a negative pulse (–1) is used. The general formula to convert a one-sided alphabet $a = \{0, \ldots, p-1\}$ into a symmetric alphabet b is

$$b = \exp\left(\frac{2\pi i a}{p}\right).$$

Thus, for the binary alphabet ($p = 2$) $a = 0$ is mapped into +1 and $a = 1$ goes into $\exp(\pi i) = -1$. (The b are known in mathematics as pth roots of unity; they are located on the unit circle in the complex plane.)

The above sequence $a_k = 0010111, 001\ldots$ is thus converted to $b_k = + + - + - - -, + + -\ldots$, where "+" stands for +1 and "–" stands for –1.

For the b_k, the addition in the recursion (2) turns into multiplication,

$$b_{k+3} = b_{k+1} b_k,$$

or, equivalently,

$$b_k = b_{k-2} b_{k-3}. \quad (3)$$

Note that the number of +1s per period is one less than the number of –1s. Thus the sum of the b_k over one period equals exactly –1.

Now let us look at the circular correlation sequence of the b_k, defined by

$$c_n = \sum_{k=0}^{2^m-2} b_k b_{k+n}. \quad (4)$$

For $n = 0$, we get, trivially, $c_0 = 2^m - 1$. For $n \neq 0$, it is easy to show that the product $b_k b_{k+1}$ equals a simple shift, say by s, of the b_k:

$$b_k b_{k+n} = b_{k+s}.$$

Thus, the correlations are given by a sum of the b_k over one period,

$$c_n = \sum_{k=0}^{2^m-2} b_{k+s},$$

or considering that b_k is periodic with period $2^m - 1$:

$$c_n = \sum_{k=0}^{2^m-2} b_k,$$

which equals –1. Thus, the autocorrelation sequence c_n of the b_k has exactly two values:

$$c_0 = 2^m - 1,$$

$$c_n = -1$$

for $n = 1, \ldots, 2^m - 2$.

The DFT of such a two-valued sequence has itself only two distinct values. In fact, the power spectrum $||B_n|^2$ is "flat":

$$|B_0|^2 = 1$$

and

$$|B_n|^2 = 2^m$$

for $n = 1, \ldots, 2^m - 2$.

Thus, except for the "dc" component $|B_0|^2$, all $2^m - 2$ "ac" power spectral lines have the same power: 2^m.

CONCERT HALLS, OCEANS, AND VENUS

Galois sequences have been used for precision measurements of impulse responses of a wide variety of "linear systems" under the most adverse circumstances, including the determination of concert hall acoustics during an actual music performance. Thus, the testing of acoustic performance spaces in the presence of a live audience has become a real possibility!

One of the remarkable applications of Galois sequences has been the measurement of ocean temperatures (for monitoring global warming) by measuring sound transmission delays between Heard Island in the Indian Ocean and Greenland, a distance exceeding 10000 km (see Fig. 2) [3]. The fact that sound waves can travel over such large distances is due to the trapping of sound energy in a waveguidelike channel at a (moderate) depth corresponding to the minimum sound velocity (see Fig. 3 for a computer ray simulation) [4].

Perhaps the most spectacular application of Galois sequences has been the measurement of interplanetary distances such as that between Earth and Venus when the latter is hiding behind the Sun (upper conjunction). In this application the Galois sequence is used to switch the phase of a CW (continuous wave) radar pulse between 0° and 180° at zero crossings of the sinusoidal radar signal (see Fig. 4 for the sequence + + + – – + –). Such a radar signal has a broad frequency spectrum around the carrier frequency, which is conducive to precision time measurements by the Uncertainty Principle. With a peak-power limitation of the radar signal, the maximum average power (300 kW) can be radiated into space. But with Venus in upper conjunction, only 10^{-27} of the outgoing energy, or less than 10^{-21} W, is reflected to Earth! Results of such measurement by I. Shapiro [5] are illustrated in Fig. 5, showing the extra delay, of up to about 180 μs, over that if the speed of light was constant along the entire return path of the radar signal. But when Venus is in upper conjunction, the radar signal is

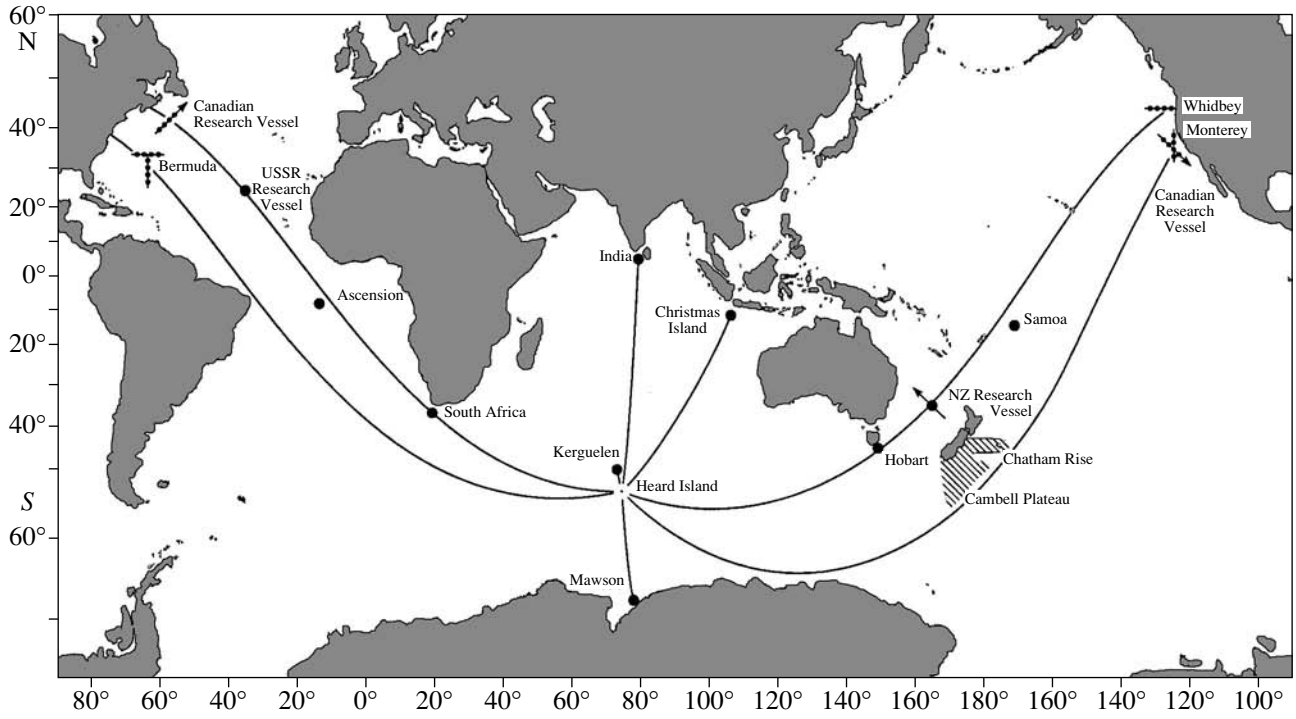

Fig. 2. Long-range ocean monitoring (courtesy of Munk).

skirting the Sun and, according to Einstein's Theory of General Relativity, slowed down by the Sun's gravitational field. The solid curve shows Einstein's prediction of the delay. The measurements thus confirm his theory, as opposed to several other competing theories. (This was the fourth crucial test of General Relativity, the three earlier ones being the perihel motion of Mercury, the bending of star light grazing the sun (first observed during an eclipse in 1919), and the frequency shift of light emitted in a gravitational field.)

The Galois sequence used by Shapiro in these astounding measurements had a period length of $2^6 - 1 = 63$. In the meantime, even the extremely small "Shapiro" time delay caused by the relatively weak gravitational field of the Earth (compared to the sun) has been measured and found to be in agreement with General Relativity (order of magnitude: 10^{-10} s).

CONCERT HALL ACOUSTICS

One area in which Galois sequences have made a difference, as already mentioned, is concert hall acoustics. Here the high signal-to-noise ratio (SNR) obtainable with Galois sequences allows precision measure-

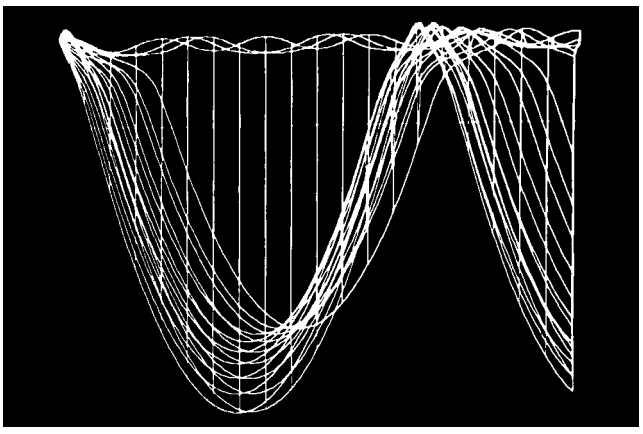

Fig. 3. Computer ray tracing of sound in ocean with surface channel (courtesy of M.M. Sondhi).

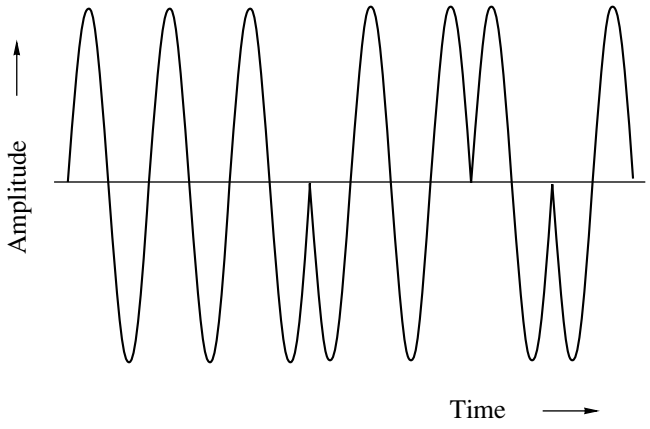

Fig. 4. Phase-switched radar signal.

ments in the presence of a noisy audience (most halls are measured—unrealistically—without an audience) and even during an actual musical performance! (Here the amplitude of the Galois sequence is adjusted to such a low level as to be masked by the music and thus inaudible.) The high temporal resolution has allowed the pinpointing of disturbing echoes in Philharmonic Hall in New York (now Avery Fisher Hall) and the discovery of the culprit for the low-frequency deficiencies (the overhead reflecting panels, called—perhaps appropriately—"clouds"). The measurement (see Fig, 6), revealed a 20-dB loss along the center aisle of the hall between 750 and 125 Hz. By contrast, upper balcony seat A-15 showed only a 3-dB spread. (This seat was included in the measurement program, because the ushers, students of the Juliard School of Music, named that seat as the best in Philharmonic Hall [16]).

Galois sequences have also been used in psychophysics and neurophysiology, for example, to measure brain-stem responses [7]. Other applications are in atmospheric physics [8] and numerous other fields.

For all these applications, fast computational algorithms are crucial [9, 10].

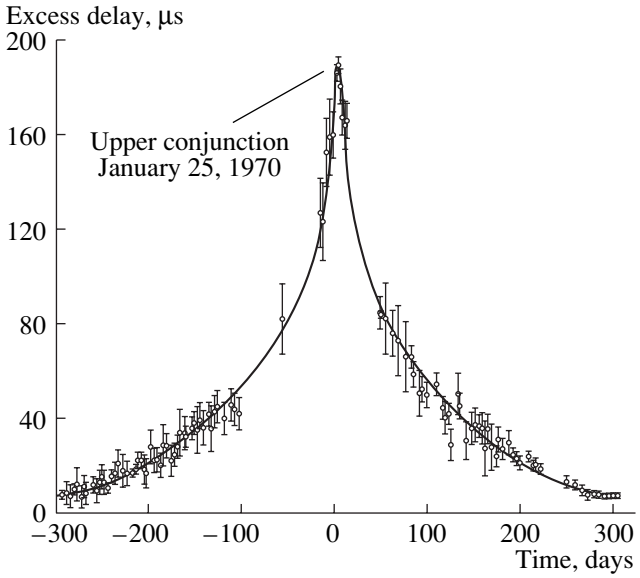

Fig. 5. Excess round-trip radar delay Earth–Venus during upper conjunction (Venus behind the Sun). Solid line: prediction by Einstein's Theory of General Relativity (after I. Shapiro).

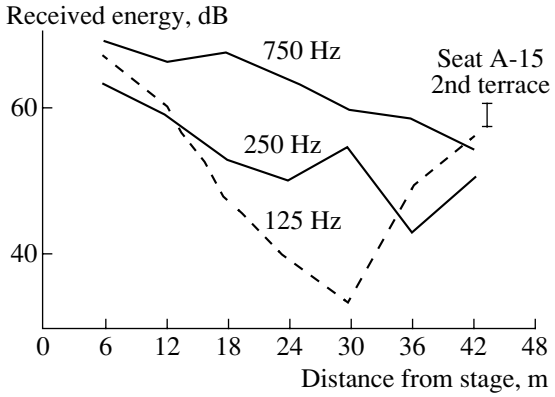

Fig. 6. Sound energy in three different frequency bands along the center aisle of Philharmonic Hall (New York). Note the sharp drop at 125 Hz and the small variation for a seat in the upper balcony (A-15).

PEAK FACTORS

Voiced speech sounds are electronically synchronized by filtering a quasiperiodic train of pulses consisting of, say, 31 in-phase harmonics (see Fig. 7, upper waveform), which leads to a "raucous" sound of the synthetic speech signal.

By replacing the all-zero phases in the 31-term Fourier-cosine series by the 31 signs (±1) of a Galois sequence from GF(2^5), i.e., a +1 corresponds to a zero phase angle and a –1 corresponds to a phase angle equal to π, the peak factor can be appreciably lowered (see Fig. 7, lower waveform, plotted to the same scale as the upper waveform [1]). The two waveforms shown in Fig. 7 have the same total power and the same (flat) power spectrum, yet they sound very different, the lower peak factor giving rise to a "smoother" sound and more pleasant sounding synthetic speech. The reason for this surprising effect of Galois phase can be understood as follows. Instead of minimizing the amplitude range of the waveform $s(t)$ for a given power, we can ask for the minimum of the fourth moment of the ("Hilbert") envelope of the waveform

$$\int |\sigma(t)|^4 dt,$$

where $\sigma(t)$ is the "analytic signal" corresponding to $s(t)$, defined by

$$\sigma(t) := \sqrt{s^2(t) + \mathbb{G}^2(t)},$$

and $\in(t)$ is the so-called Hilbert transform of $s(t)$ [11]. As is well known, the analytic signal has a nonvanishing Fourier transform only for positive frequencies. Its absolute square, the square envelope $|\sigma|^2$, is of course the autocorrelation of that spectrum. Thus, $|\sigma|^4$ measures the power in the squared envelope. The smaller this power, the more constant, i.e., less "peaky" $|\sigma|^2$ will be.

ERROR CORRECTING CODES

Another important application of Galois sequences occurs in digital error correcting [12]. As we saw above, Galois sequences in the finite field GF(p^m) are generated by a linear recursion modulo p.

For $p = 2$ (the most frequent case) and $m = 3$, say, one such recursion is

$$a_{k+3} = a_{k+1} + a_k (\mathrm{mod}\ 2).$$

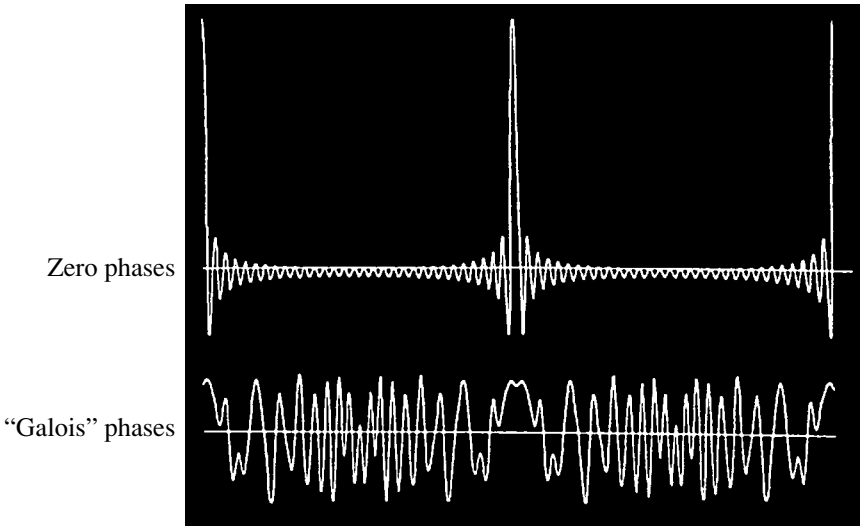

Fig. 7. Peak factor reduction of periodic pulse (upper waveform). By using Galois phases, the peak amplitude range can be lowered nearly threefold. (Both waveforms are drawn to the same scale.)

With the initial condition 1 1 1, say, the rest of one period of the sequence is 0 0 1 0. In the context of error correcting codes, we now consider the initial condition (1 1 1), the information bits, and the remaining bits (0 0 1 0) the check bits. This is the simplex code (of length 7), so called because the geometric representation of the code words is a simplex (for example, a tetrahedron in three dimensions). The general binary simplex code has length $2^m - 1$, with m information bits (i.e., 2^m code words) and $2^m - 1 - m$ check bits. Thus its relative rate of information transmission is only $m/(2^m - 1)$. But the code words have a mutual Hamming distance of 2^{m-1}, which allows the detection of 2^{m-2} errors and the correction of $2^{m-2} - 1$ errors, or, for large m, almost 25%. This remarkable capability, a result of the relatively large Hamming distance of 2^{m-1}, is directly related to the low autocorrelation of the corresponding ± 1 sequence: a small correlation corresponds to a large Hamming distance.

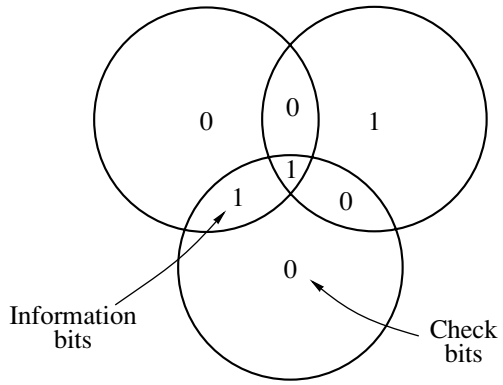

Fig. 8. Venn diagram illustrating the working of a length-7 Hamming code. The inner 4 bits (fat) are the information bits. The other 3 bits (thin) are the check bits determined to make the parity (sum of bits modulo 2) in each of the 3 circles zero. It is easily seen that reversing any of the 7 bits will violate the proper parity in one or more circles, thereby uniquely identifying its location.

The simplex code is the basis of several other powerful error correcting codes that are used in computers, compact discs, and interplanetary space exploration. The "dual" of the simplex codes are the famous Hamming codes in which the roles of information and check bits are reversed. Thus the Hamming code of length 7 has 4 information and only 3 check bits, enough to correct one error in any of the 7 bits—or to indicate that there is no error. To distinguish between these 8 cases is, in fact, the most 3 binary check bits could accomplish. Hamming codes are therefore called perfect codes. (All binary perfect codes are, in fact, Hamming codes.) Figure 8 illustrates the error correction of the length-7 Hamming code by means of a Venn diagram.

Hamming codes, as they are perfect codes, are also perfect covering codes [14]. A covering code is a selection of points in a space such that "unit balls" will cover all other points of the space. An optimum covering code has the smallest possible number of points. Good covering codes are needed for quantizing analog or digital signals into the smallest number of representative points for a given maximal error. They are also good for solving certain "hat color" puzzles.

X-RAY ASTRONOMY

X rays are difficult to focus. Fresnel zone plates are highly wavelength dependent. But number theory offers a method of X ray imaging applicable in X-ray astronomy that avoids these difficulties [15]. The methods depends on a two-dimensional (2D) "Galois array" obtained by laying down a Galois sequence on a rectan-

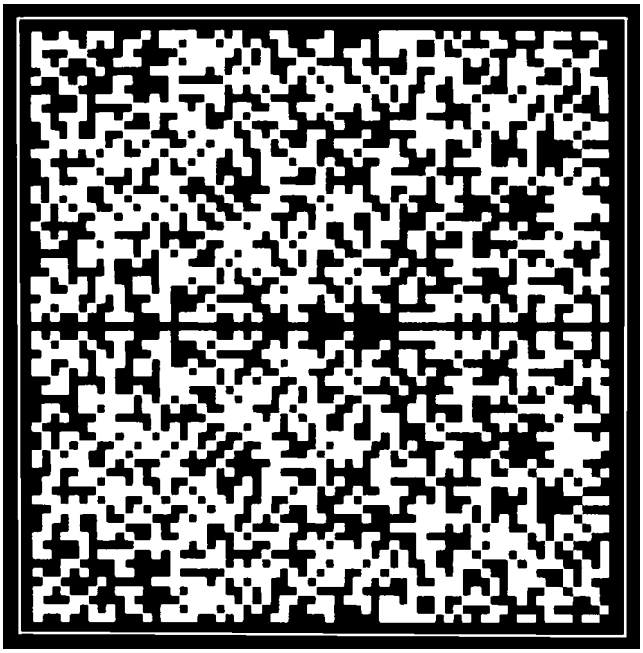

Fig. 9. Two-dimensional Galois array.

gular grid in a diagonal way, a "1" corresponding to a little square-shaped transparent hole and a "0" to a little square area blocking X-rays. For this method to work, the length of the sequence $L = 2^m - 1$ must be factorable into two coprime factors. (Thus L must not be a Mersenne prime.)

For example, for $m = 12$, $L = 4095 = 63 \times 65$. The corresponding 2D array is shown in Fig. 9. The X-ray shadow from this mask is scanned into a computer where it is deconvolved with the same 63×65 array, giving the image shown in Fig. 10 (revealing two X-ray sources).

DIFFUSORS

One of the widest applications of Galois sequences and arrays is to wave diffusion (sound, microwaves, light) by means of gratings. For this purpose the Galois sequence (in the ± 1 form) is realized as a sequence of reflection factors (see Fig. 11). A normally incident plane wave is diffracted with nearly equal energies into the different diffraction orders [13] (see Fig. 12). Of course, for twice the design frequency (half the wavelength), the troughs have a depth of $\lambda/2$. Thus, there is no round trip phase shift and the grating acts much like a plane mirror! To broaden the frequency range, the prime number 2 used in the design of the grating has to be replaced by a larger prime p, giving a grating of length $p^m - 1$ and useful for $p - 1$ frequencies (1, 2, 3, …, $p - 1$). (For noninteger multiples of the design frequency, say 1.5, the scattering is still very good.)

QUADRATIC-RESIDUE DIFFUSORS

Another approach to constructing broadband diffusors is based on the quadratic residues of a prime number p. For $p = 7$, for example, the quadratic residues of the integer 0, 1, 2, 3, 4, 5, 6, 7, … are 0, 1, 4, 2, 2, 4, 1, 0 …, a sequence repeating with period $p = 7$. A reflection phase grating based on the quadratic residues of the prime $p = 17$ is illustrated in Fig. 13. The depths of the individual troughs are given by

$$d_n = \frac{\lambda_0}{2p}(n^2) \bmod p,$$

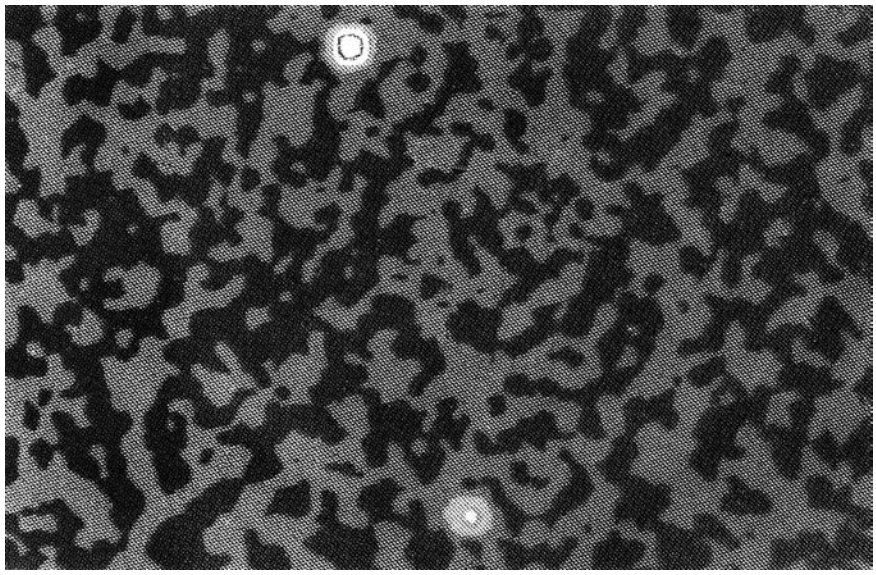

Fig. 10. X-ray image constructed with the array of Fig. 9 revealing two X-ray sources.

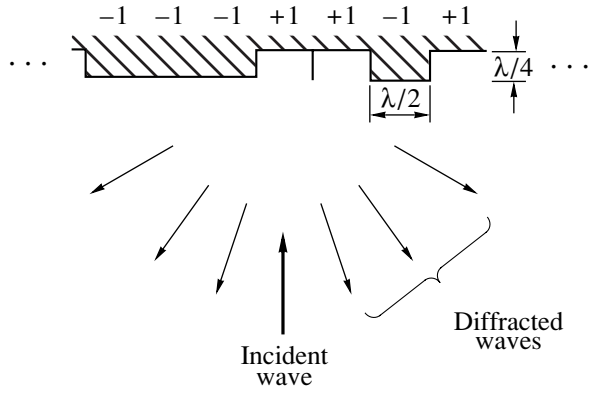

Fig. 11. Reflection phase grating based on Galois sequence of length 7.

Fig. 12. Backscatter from a metallic Galois reflection phase grating shown in Fig. 11. (The measurements were made with 3-cm microwaves.)

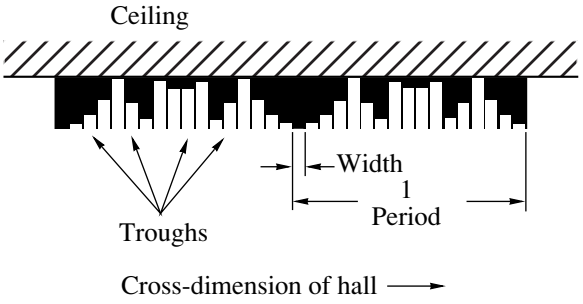

Fig. 13. Reflection phase grating based on the quadratic residues of the prime number 17.

where λ_0 is the fundamental (longest) wavelength. It is easy to show that the sequence of reflection coefficients

$$r_n = \exp(2\pi i dn/\lambda_0)$$

has a vanishing autocorrelation sequence (except for a shift congruent to zero modulo p). Thus, the corresponding power spectrum is flat and the scattering pattern is uniform [1].

The resulting broad scattering is shown in Fig. 14. Again, such a grating works well for $p - 1$ frequencies, i.e., almost four musical octaves for $p = 17$.

THE RABBIT SEQUENCE

One of the most interesting binary sequences is the rabbit sequence [16]: 1 0 1 1 0 1 0 1 …, generated by the transformation 0 ⟶ 1 and 1 ⟶ 1 0. Starting with a simple 0, the sequence of "generations" is thus

n	Rabbits	F_n
0	0	1
1	1	1
2	1 0	2
3	1 0 1	3
4	1 0 1 1 0	5
…		

Each generation is the last-but-one generation appended to the last generation. The number of bits in generation n is thus the nth Fibonacci number F_n, which obeys the recursion $F_n = F_{n-1} + F_{n-2}$ starting with $F_0 = F_1 = 1$. The number of 1s in generation n equals F_{n-1} and the number of zeros is F_{n-2}. The ratio of 1s to 0s therefore tends to the "golden mean" $g = (\sqrt{5} + 1)/2 = 1.618$. In fact, the golden mean is useful in generating the entire rabbit sequence r_n without recourse to recursion:

$$r_n = \lfloor (n+1)g \rfloor - \lfloor ng \rfloor,$$

where $\lfloor x \rfloor$ stands for largest integer not exceeding x. The name "rabbit sequence" stems from the fact that the mapping 0 ⟶ 1 and 1 ⟶ 1 0 is the one considered by Fibonacci [17] for procreating rabbits: Immature rabbits become mature (0 ⟶ 1) and mature rabbits survive and get (immature) children (1 ⟶ 1 0). One of the important properties of the rabbit sequence is its self-similarity illustrated with the help of the rabbit lattice ("lettuce") (see Fig. 15). The scaling factor equals $(\sqrt{5} + 1)/2 = g$.

QUASICRYSTALS

When an alloy, obtained by rapid cooling of a 1 : 6 mixture of manganese and aluminum, Al_6Mn, is exposed to a beam of electrons, the resulting diffraction pattern shows bright spots and a fivefold symmetry (see Fig. 16) [18]. The diffraction pattern shows also self-similarity: there are numerous regular pentagons of different sizes, with a scale factor of g or $g^2 = 1 + g = 2.618\ldots$. Now, a fivefold symmetry of any periodic lattice is forbidden by fundamental geometry. Yet the light spots seem to imply a periodic crystal. Thus, something must be wrong. The resolution of the puzzle comes, of all things, from Fibonacci's rabbits. There, we encountered a 1D structure (see Fig. 15), which is self-similar and scales with a factor g. Can we find a 3D analog? Figure 17 illustrates a projection method that generates the 1D rabbit lattice from a square lattice [19]. This method can be generalized to 2D and 3D rabbit lattices. To generate a 2D rabbit lattice, one starts from a five-

dimensional hypercubic lattice and projects down to an appropriately inclined plane (see Fig. 18). When this computer-generated aperiodic lattice is positioned in a laser beam, the diffraction pattern shown in Fig. 19 results, showing exactly the right scaling and fivefold symmetry! (Courtesy of H.W. Strube and H. Henze.)

THE MORSE–THUE SEQUENCE

Another important mathematical sequence for physics is the Morse–Thue sequence. Like the rabbit sequence, it is self-generating, obeying the mapping rules 0 ⟶ 01 and 0 ⟶ 1 0. Starting with a simple 0, we get the following sequence of generations:

n	m_n	Number of bits
0	0	1
1	0 1	2
2	0 1 1 0	4
3	0 1 1 0 1 0 0 1	8
…		

In other words, the Morse–Thue sequence is generated by the simple rule "copy and append the complement." This rule is "inherited" in the sense that the nth generation is obtained by copying the $(n-1)$th generation and appending its complement.

There is also a direct formula for the kth term of the sequence: m_k is the sum of the digits modulo 2 of the binary representation of k. For example, the 7th term (counting from zero) equals 1 because 7 € 1 1 1 and 1 + 1 + 1 = 1 modulo 2. The Morse–Thue sequence is self-similar in the sense that $m_{2k} = m_k$. It got its name from Axel Thue [20], who used it in mathematical linguistics and Marston Morse [21], who discovered its importance in chaotic dynamics.

SYMBOLIC DYNAMICS

Consider a simple example of a discrete nonlinear dynamical system, the iterated quadratic map

$$x_{n+1} = f(x_n) = rx_n(1 - x_n).$$

For $x = \left(1 - \frac{1}{r}\right)$, the map has a fixed point and for $r = 2$, the fixed point is "super stable" [$f(x)$ has a zero derivative]. The initial value of $x = \frac{1}{2}$ will stay at $x_0 = \frac{1}{2}$, called the "orbit." Symbolically, we denote this orbit by

$$C\ C\ C\ \ldots \text{ (period length 1)},$$

where C stands for "center" $\left(x = \frac{1}{2}\right)$.

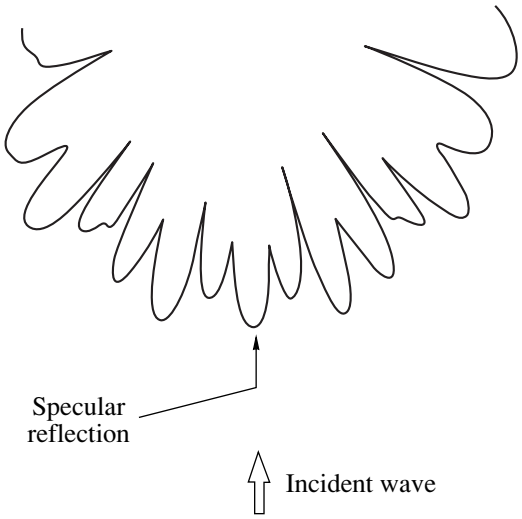

Fig. 14. Reflection pattern of the grating shown in Fig. 13.

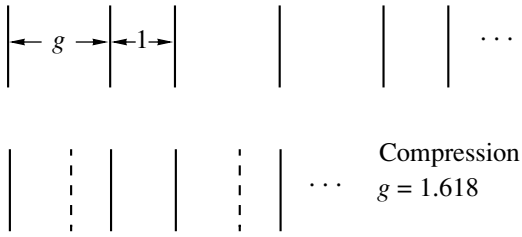

Fig. 15. A one-dimensional rabbit lattice ("lettuce") and its self-similarity. When compressed by a factor g each "atom" of the original lattice is directly above an atom of the compressed lattice. Each 1 in the rabbit sequence corresponds to an "interatomic" distance proportional to g, and each 0 corresponds to a distance of 1.

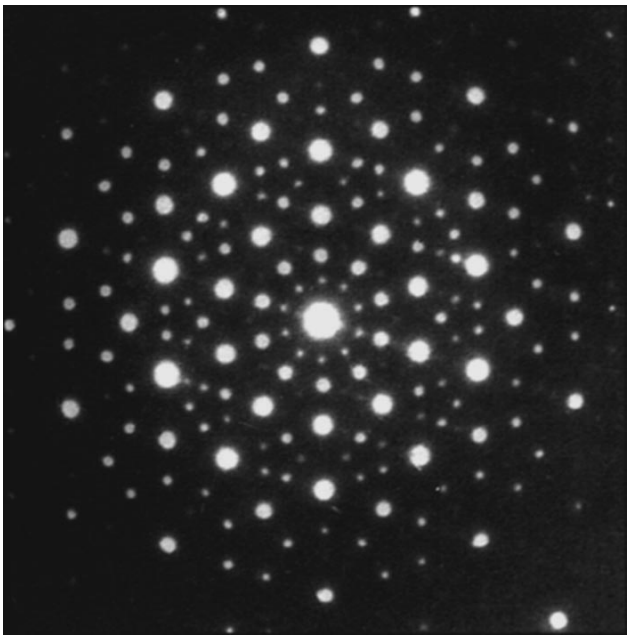

Fig. 16. Electron diffraction pattern of a quasicrystal with fivefold forbidden symmetry (from [18]).

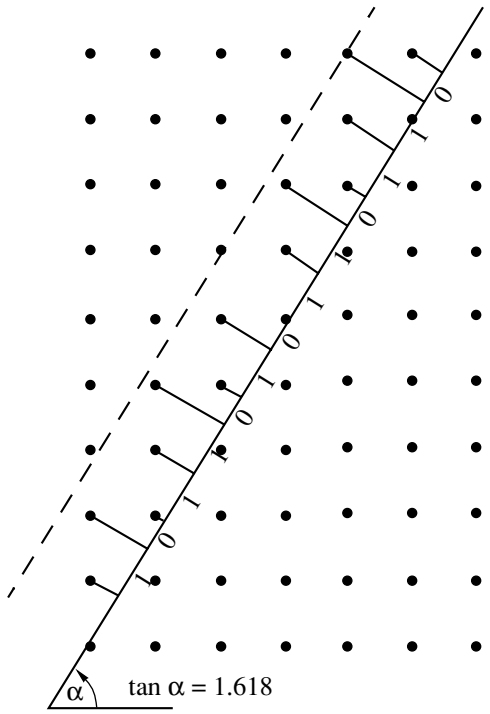

Fig. 17. Projection method for generating the 1D quasiperiodic "rabbit lattice" illustrated in Fig. 15.

For $r = 1 + \sqrt{5} = 3.236\ldots$, the map has a super stable orbit of period length 2. Starting with $x_0 = \frac{1}{2}$, we get $x_1 = 0.809\ldots x_3 = \frac{1}{2}, \ldots$. Symbolically: *C R C R C R* … (period length 2). Here, *R* stands for "right" because x_1 is to the right of (greater than) x_0.

For subsequent values of *r*, we obtain super stable orbits of period lengths 4, 8, 16, etc., the so-called period-doubling cascade. The symbolic dynamics are, respectively,

C … (period length 1)

C R … (period length 2)

C R L R … (period length 4)

C R L R R R L R … (period length 8).

Is there a simple rule to go from one symbolic dynamics to the next? Yes, there is: we copy the orbit once and change the second *C* alternately to *R* and *L* [16]. The orbit can also be described by a binary sequence by writing 1 instead of *R* and 0 for *C* or *L*:

0

0 1

0 1 0 1

0 1 0 1 1 1 0 1

….

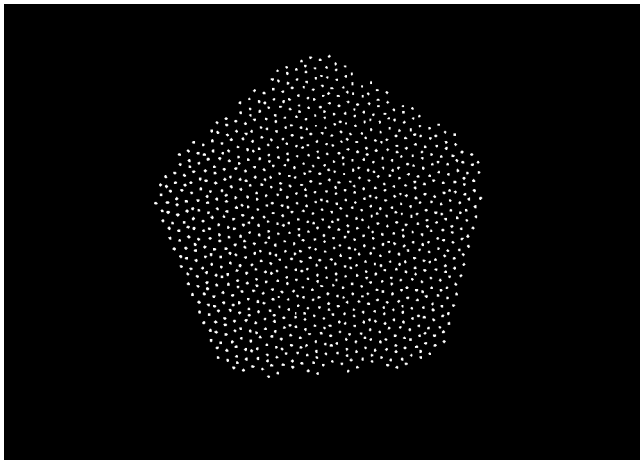

Fig. 18. A computer-generated 2D rabbit lattice obtained by projecting a five-dimensional hypercubic lattice onto an appropriately inclined plane.

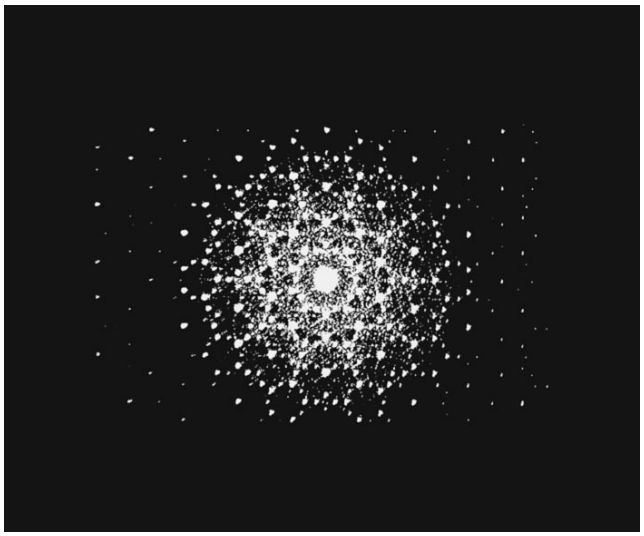

Fig. 19. Diffraction pattern from quasiperiodic lattice shown in Fig. 18.

There is a deep connection between the symbolic dynamics of the quadratic map and the Morse–Thue sequence:

0 1 1 0 1 0 0 1….

Taking first differences modulo 2 yields

1 0 1 1 1 0 1…,

which, except for the initial 0, are the symbolic dynamics of the quadratic map at its super stable orbits at the end of the period doubling cascade! Thus, an intriguing connection is revealed between a case of nonlinear dynamics and number theory (see [16] for more details).

	1	2	3	4	5	6	7	8	9	10	11	12	13	14	15	...
Binary:	1	10	11	100	101	110	111	1000	1001	1010	1011	1100	1101	1110	1111	...
Number of 1's:	1	1	2	1	2	2	3	1	2	2	3	2	3	3	4	...
C Major:	C	C	D	C	D	D	E	C	D	D	E	C	E	E	F	...
Every 3d note:			D			D			D			C			F	...
Melody:			D									C			F	...

Fig. 20. The baroque integer sequence converted to sound in the C-major scale by identifying 1 with C, 2 with D, etc. Repeated notes are not repeated but held for a longer time, thereby imparting a rhythm.

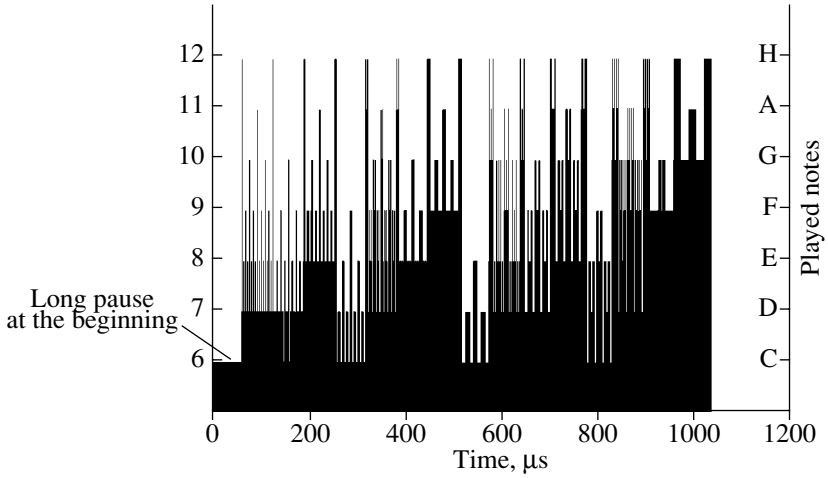

Fig. 21. Computer-generated "baroque" melody. This and other melodies are available on the Internet [22, 23].

BAROQUE INTEGERS

Let us consider yet another rule for generating interesting sequences, namely "copy, add 1, and append." Thus, starting with a single 0, we obtain

0

0 1

0 1 1 2

0 1 1 2 1 2 2 3.

The *n*th term of the sequence signifies the number of 1s in the binary notation of *n*. This follows directly from the generating rule and the initial condition (b_0 = 0, see Fig. 20). Taking the b_n modulo 2 gives the already mentioned Morse–Thue sequence.

Like so many other objects generated by iteration, the baroque integers [16] sequence is self-similar: Taking all even numbered terms, b_n, reproduces the infinite sequence b_n (because n and $2n$ have the same number of 1s in binary notation). Taking however, every third term, b_{3m}, produces an interesting new sequence whose partial sums show a noteworthy fractal growth property. Such decimated baroque-integer sequences, converted to sound (see Fig. 20), can also produce melodies [22, 23] reminiscent of baroque composition (hence my designation). This is particularly true when every 63rd term is taken (see Fig. 21), which is said to sound like one of the Scarlattis.

REFERENCES

1. M. R. Schroeder, *Number Theory in Science and Communication*, 3rd ed. (Springer, Berlin, 1997).
2. S. W. Golomb, *Shift Register Sequences* (Aegean Park, Laguna Hills, Calif., 1982).
3. W. Munk, J. Fluid Mech. **173**, 43 (1986).
4. M. M. Sondhi, personal communication.
5. I. Shapiro, Phys. Rev. Lett. **13**, 789 (1964).
6. M. R. Schroeder, B. S. Atal, G. M. Sessler, and J. E. West, J. Acoust. Soc. Am. **40**, 434 (1966).
7. U. Eysholdt and C. E. Schreiner, Audiology **21**, 242 (1982).
8. D. K. Wilson and D. W. Thomson, Atmos. Oceanic Technol. **11**, 751 (1994).

9. M. Cohn and A. Lempel, IEEE Trans. Inf. Theory **23**, 135 (1977).
10. H. Alrutz and M. R. Schroeder, in *Proceedings of 11th Conference on Acoustics* (Paris, 1983), p. 235.
11. M. R. Schroeder, *Computer Speech: Recognition, Compression, Synthesis* (Springer, Berlin, 1999).
12. F. J. MacWilliams and N. J. F. Sloane, *The Theory of Error-Correcting Codes* (North-Holland, Amsterdam, 1977).
13. *Physical Acoustics*, Ed. by M. R. Schroeder and R. N. Thurston (Academic, New York, 1988), Vol. 18, pp. 1–20.
14. D. Slepian, *Key Papers in the Development of Information Theory* (IEEE Press, New York, 1974).
15. N. J. A. Sloane and M. Harwitt, Appl. Opt. **15**, 107 (1976).
16. M. R. Schroeder, *Fractals Chaos, Power Laws* (Freeman, New York, 1992).
17. L. Fibonacci, *Liber Abaci* (Pisa, 1202).
18. D. Shechtman, I. Blech, D. Gratias, and J. W. Cahn, Phys. Rev. Lett. **53**, 1951 (1984).
19. V. Elsner, Phys. Rev. B **32**, 4892 (1985).
20. A. Thue, K. Nord. Vid. Skrifter I Math. Nat. (Oslo) **7**, 1 (1906).
21. M. Morse, Trans. Am. Math. Soc. **22**, 84 (1921).
22. L. Kindermann, http://reglos.de/musinum/
23. M. R. Schroeder, in *141st Meeting of Acoustical Society of America*, http://www.acoustics.org/press/141st/schroeder.html